Nanomechanical Investigation of Soft Biological Cell Adhesion using Atomic Force Microscopy

Eleftherios Siamantouras

A thesis submitted for the degree of Doctor of Philosophy
in the University of Warwick

School of Engineering, University of Warwick
January 2014

Biomedical Engineering
School of Engineering
University of Warwick
Coventry
CV4 7AL

Table of Contents

Chapter 2. AFM Single Cell Force Spectroscopy

List of Figures

Figure 1.8 The adherens junction and the cadherin-catenin complex is crucial for cell-cell adhesion and facilitates cell communication via gap-junctions. Gap-junctions permit the direct transfer of small molecules and ions between coupled cells and their formation depends on E-cadherin based cell-cell adhesion. The pro-fibrotic cytokine TGF-β1 is associated with elevated glucose and it is important in many tubulointerstitial diseases where disassembly of the adherens junction (AJ) represents the initial overt change in epithelial organisation ahead of cellular migration associated with EMT.

Figure 2.1 Schematic diagram of the vertical tip movement during the approach and retract process in force spectroscopy for the measurement of F-d curves. As the probe approaches within a few tens of nanometers, it comes into a regime of an attractive van der Waals forces. The probe is weakly attracted toward the sample surface and as it approaches closer to the sample, it enters in the repulsive realm of Lennard-Jones potential, where the probe is strongly repelled from the surface. As the cantilever is retracted from the sample, the tip remains in contact with the surface due to interaction forces, and the cantilever is deflected downwards. At some point of retraction, the force required to disrupt the adhesion is reached. The attractive or repulsive forces can be measured by spring stiffness.

Figure 2.2 A schematic illustration of a single cell indentation and a representation of a F-d curve obtained from a single cell. Various elements of the cell are contributing to the overall determination of the E modulus. Special considerations regarding the depth of indentation and the fitting of the curve to a mechanical model needs to be taken into account according to the purpose of investigation i.e. whole cell elasticity, membrane or CSK elasticity etc.

Figure 2.3 Schematic of an AFM head capable of long range displacement pulling (100μm) to facilitate long distance force spectroscopy i.e. complete separation of adherent cells during cell-to-cell adhesion experiments. The cantilever is mounted on the inclined part of the glass block holder using a spring. The incline of 10 degrees ensures that any contact between the sample and the holder will be prevented. The glass block remains locked on the AFM head during experiments.

Figure 2.4 A photo of the instrument set-up showing the AFM head and stage mounted on a inverted microscope. A CCD camera was mounted on the left-side port on the microscope to monitor the experiments. The cantilever glass holder is positioned on place by lifting up the AFM head prior the experiments. Once the cantilever is mourned on the head the alignment of laser can take place. After calibration of the cantilever the head must not be lifted nor the alignment of laser should be changed.

Figure 2.5 A schematic diagram showing the optical path of the laser. Initially the laser must be adjusted to get reflected from the end of the cantilever with the aid of the optical microscope. Then by adjusting both the mirror and the photodetector the laser spot must be adjusted to reach the centre of the photodetector to achieve maximum sensitivity.

Figure 2.6 An optical image showing proper alignment of the infrared laser spot on a tipless functionalised cantilever. Any residuals left from the chemical modification will affect the sum value of the detector. As it can be seen from the photo soft cantilevers used for contact mode are relatively transparent.

Figure 2.7 An Arrow series rectangular tipless cantilever with a triangular free end, made from monolithic silicon for special applications, i.e. they can be used for attaching cells or spheres to the free end of the cantilever. The wide part of silicon is usually referred as 'chip', while the main of the cantilever has thickness: 1.0μm, width: 100μm and length: 500μm. At the end of the cantilever the tip can be seen where a cell or a microbead can be attached (Nanoworld Arrow™ TL1).

Figure 2.8 Measurement of force curve on a hard substrate (clean petri dish) in PBS solution for calibration. The linear part of the curve is chosen for the calculation of the gradient of the line. Here, the sensitivity is 55.3nm/V.

Figure 2.9 Free fluctuations are plotted against frequency for the thermal noise measurement of an Arrow TL-1 contact mode cantilever in fluid. Three resonant peaks, corresponding to the resonance at around 1kHz, are shown. Both phase and amplitude are reduced with comparison to the spectrum in air. The second peak was

used to determine the spring constant by the use of a correction factor. The calculated value was 0.0206N/m, whilst the nominal value provided by the manufacturer is 0.03N/m.

Figure 2.10 Schematic design of the elements functionalising a tipless cantilever. The surface of the cantilever is first coated with PLL (25μg/ml in PBS, 30min in RT), which promotes the attachment of Fn molecules. The cantilever was next incubated in Fn solution (20μg/ml in PBS, 2h at 37°C), and finally brought in contact with the membrane of a suspended cell. Molecules in the surface of the cell that are involved in adhesion readily attach to Fn in the extracellular domain, while in the intracellular domain they are connected with actin filaments through adherens junction.

Figure 2.11 Phase contrast images of a single HK2 (a) and MIN6 (b) cell attached to a TL1 arrow tipless cantilever. The cantilever-cell was brought in contact with a substrate cell and a predefined contact time it was retracted to investigate functional tethering between two cells. Width of the cantilever (rectangular part): 100μm. Note the laser spot (purple) used for measuring the deflection of the cantilever.

Figure 2.12 A force distance curve of two MIN6 cells that are brought in contact.Initially the cells are bounded into a cantilever and the substrate (phase 1). Then they are approached to each other, and after a short period of contact the two cells are attached. During this time bonding is formed (phase 2). Next, the cantilever is retracted and force versus displacement is measured (phase 3) until they are completely detached (phase 4). Based on the F-d retraction curve adhesion parameters can be determined including maximum force of detachment from the highest negative deflection of the cantilever, work of removal from the area under the curve and distance of complete separation from maximum pulling range before separation. In addition unbinding steps that correspond to ligation rupture can be determined. Steps in the initial part of the curve, such as in 's' area, are followed after a bond rupture while 't' steps are followed after a deformation of membrane tethering.

Figure 2.13 Schematic diagram of a single cell indentation experiment. (a) The displacement z of the piezo-actuator includes both the indentation height δ and the deflection of the cantilever x. (b)The deflection of the cantilever x, must be subtracted

from the z height measured during AFM indentation. The corrected tip-sample-separation curve represents the actual F-d curve that can be used for calculation of elasticity.

Figure 2.14 Single and clusters of Polystyrene microbeads on a glass coverslip. The mean diameter of the bead is10μm with coefficient of variance ≤10%.

Figure 2.15 A spherical polystyrene microbead of 10μm in diameter attached on the very end of an Arrow TL-1 tipless cantilever. (a) An optical image showing the side view of the microsphere attached to the tip of the sensor. (b) An optical image showing the top view of the cantilever-bead and KH2 cells on the substrate.

Figure 2.16 Indentation of a single cell using spherical indenter, where δ is the indentation depth, α is the radius of the contact area between the probe and the plasma membrane, R is the radius of the probe and F the loading force.

Figure 2.17 Schematic design of the surface of a probe and the sample. Dotted line represent the theoretical assumption, while continuous line is a representation of the actual micro-environment. Roughness at molecular level contributes to the uncertainty of the determination of initial contact point and contact area during indentation. Various membrane extensions such as long chain molecules on the surface of the cell can cause a force jump indicating a false contact point.

Figure 2.18 Optical image demonstrating the determination of cell height prior indentation experiments. The target cell is marked with a circle while arrows show the points of clean substrate area that can be used as a reference point. A low set-point force of 0.2nN was used for the cantilever to touch a point in a clean area next to a measuring cell and the surface of the cell. Their displacement difference was used to determine the height of the cell and subsequently the indentation depth. When a single test within a cluster was tested one reference point was used for measuring the height of the cell (a). For cells in smaller cluster or individuals the reference values were obtained by measuring the area surrounding the cell. Single cell have more reference points (b & c).

Figure 2.19 Elasticity can be determined by fitting the model to the F-d curves in the range of 5-10% of indentation. The spherical probe has large area of contact and it is important to take under consideration the effects of the substrate.

Figure 2.20 AFM indentation using force-controlled and height-controlled displacement of a cell with thickness 3.5μm. Hertz theory assumptions require that the depth of indentation depth δ is maximum 10% of the cell height. As shown in the F-d curves, the contact point was determined by a positive ramp of the force sensor. In (a), a set-point force of 4.5nN was used to indent the sample resulting in a displacement of approximately1500nm. As δ was increased the value of E modulus was increased significantly, suggesting that stiffer elements (e.g. nucleus or substrate) are contributing to the calculation of elasticity. In (b) a set-point force of 100pN was used to determine sample thickness with regards to the reference substrate and indentation depth δ is fixed for the specific position on the cell. The procedure was repeated for each testing cell.

Figure 2.21 Processing of cell-to-cell adhesion force curves. In (a) a raw F-d curve, as measured by AFM-SCFS, is shown. After applying the following functions: (1) smoothing, (2) set the x-axis Baseline, (3) detect the Contact point, (4) detect the Minimum Force value, (5) determine the Area under the curve and (6) Step fitting, the F-d retraction curve of (b) is resulted. As illustrated the determination of the point at which the cells are completely separated is the most important step, since the x-axis baseline acts as a reference for further analysis. F_{max} is the difference between the minimum force value and the baseline, while W_D (grey region) is the integral of the continuous area under the baseline. In addition, d_s can be determined by the difference between F_{max} and the point of complete separation. Zooming in the x-axis displays detection of early unbinding events.

Figure 2.22 Processing of indentation force curves. In (a) a raw F-d curve, as measured by AFM-FS, is shown. After applying the following functions on the approach curve: (1) smoothing, (2) substract the Baseline to set the zero force level, (3) detect the Contact point, (4) correct the height of the cantilever bending and (5) apply the Hertz model, the F-d extension curve of (b) is resulted. In order to calculate the elasticity of a cell, an F-d curve was analysed as shown. Fitting in incremental and vari-

ous parts of displacement confirmed that the experimental procedure was robust. A contact point of 118nm resulted in better fit of the data.

Figure 3.1 The morphology of MIN6 cells cultured in low extracellular calcium (0.5mM). In (a), an optical image of MIN6 cells in monolayers demonstrates that cells are organised in low proximity between each others, forming clusters that enable cell-to-cell coupling and communication. In (b), a fluorescence microscopy image of a single cell illustrates the cobblestone morphology that is maintained by the CSK (stained in red colour). The nucleus of the cell, occupying a large area of the cytoplasm, is clearly shown (purple colour).

Figure 3.2 Phase microscopy image showing a β-cell-to-β-cell SCFS adhesion experiment. No morphological nor phenotypical changes between the samples were observed by optical images. The suspended cell was attached on the functionalised cantilever and then was brought in contact with a single substrate cell (within a cluster of cells) for 5secs, while force versus displacement were measured simultaneously. In (a), an optical image showing MIN6 cells incubated for 48 hours in 0.5mM Ca^{2+} (Control) while in (b) cells were incubated in 0.5mM Ca^{2+} +R568.

Figure 3.3 The effects of CaSR activation, followed by treatment with the calcimimetic R568, on E-cadherin mediated cell-to-cell adhesion were examined using AFM-SCFS. F_{max} is the difference between the minimum force value and the point of complete detachment, W_D (grey region) is the integral of the continuous area under the baseline of complete separation and d_s is the difference between F_{max} and the point of complete separation. Set-point force of 0.8nN, contact time of 5sec and pulling speed of 5μm/sec were remained constant throughout the experiments. Alterations of adhesion parameters such as F_{max}, W_D and d_s provide an important insight about functional cell-to-cell adhesion. In (a) F_{max} is 0.9nN, W_D is 6.7 fJoule and d_s is 34.6μm while in (b) F_{max} is 1.3nN, W_D is 16.9fJoule and d_s is 54.2μm.

Figure 3.4 Retraction force-distance curves obtained by MIN6 cell-to-cell adhesion measurements, showing the effects of CaSR activation on the tether rupture events. Unbinding of ligations that occur during the early pulling phase (10μm after the minimum force value) are preceded by a force ramp ('j' events). As the pulling distance

increases an area is reached where the rupture events are preceded by a displacement plateau as well ('t' events) due to the deformation of the cell. In (a) the number of TREs is 39, whilst most of the unbinding events occurred in the first 11μm of pulling range, corresponding to the area of 'j' and mixed 'j' and 't' events. In (b) the number of TREs is 61, whilst most of the 'j' events occurred in the first 3.2μm. The arrows illustrating the displacement plateau combined with the fact that the initiation of 't' events occurred much earlier as shown in (b) indicates that MIN6 cells became more deformable after treatment with the calcimimetic.

Figure 3.5 Histograms of control cells showing (a) distribution of frequencies of maximum unbinding forces and (b) distribution of frequencies of work of detachment.

Figure 3.6 The effects of the calcimimetic R568 (1μM) on (b) the maximum unbinding force (increased by 30%), (c) the number of tethering rupture events (increased by 48%), (d) the work of detachment (increased by 39%) and (e) the distance to complete separation (increased by 72%) are shown. Data are expressed as mean ±SEM of more than 30 cells from 4 separate experiments, where key significances are shown, ***$p<0.001$.

Figure 3.7 Phase microscopy image showing a β cell indentation experiment. The cantilever was modified using a 10μm polystyrene microbead cell to enable indentation of a single substrate cell (within a cluster of cells), while force versus displacement were measured simultaneously. In (a), an optical image showing MIN6 cells incubated for 48 hours in 0.5mM Ca^{2+} (Control) while in (b) cells were incubated in 0.5mM Ca^{2+} +R568.

Figure 3.8 The effects of CaSR activation, followed by treatment with the calcimimetic R568, on E modulus as determined using AFM-FS indentation. For a cell of 4.5 μm in height the depth of indentation was 450nm. The contact point for each cell was identified by fitting various parts of the extension F-d curve with Hertz model. A contact point at approximately 0.1nN was used for the calculation of E modulus. The extension speed of 5μm/sec was remained constant throughout the experiments. (a)

glucose media. Note that the substrate cells were elongated and were not organised in clusters.

Figure 4.3 The effects of the cytokine TGF-β1 on E-cadherin mediated cell-to-cell adhesion of HK2 cells were examined using AFM-SCFS. F_{max} is the difference between the minimum force value and the point of complete detachment, W_D (grey region) is the integral of the continuous area under the baseline of complete separation and d_s is the difference between F_{max} and the point of complete separation. Set-point force of 1.0nN, contact time of 10sec and pulling speed of 5μm/sec were remained constant throughout the experiments. Alterations of adhesion parameters such as F_{max}, W_D and d_s provide an important insight about functional cell-to-cell adhesion. In (a) F_{max} is 0.9nN, W_D is 8.6 fJoule and d_s is 61.7μm while in (b) F_{max} is 0.68nN, W_D is 2.7fJoule and d_s is 28.2μm.

Figure 4.4 Retraction force-distance curves obtained by HK2 cell-to-cell adhesion measurements, showing the effects of TGF-β1 on the tether rupture events. Unbinding of ligations that occur during the early pulling phase (approximately 5μm after the minimum force value) are preceded by a force ramp ('j' events). As the pulling distance increases an area is reached where the rupture events are preceded by a displacement plateau as well ('t' events) due to the deformation of the cell. In (a) the number of TREs is 73, whilst most of the unbinding events occurred in the first 8.2μm of pulling range, corresponding to the area of 'j' and mixed 'j' and 't' events. After that point and until the complete detachment of the cells extended separation displacements occurred ('t' events), owing to the deformation of the cell. In (b) the number of TREs is 51, whilst most of the unbinding events occurred in the first 3.85μm, and were not preceded by a displacement plateau.

Figure 4.5 Histograms of control cells showing (a) distribution of frequencies of maximum unbinding forces and (b) distribution of frequencies of work of detachment.

Figure 4.6 The effects of the cytokine TGF-β1(48h/10ng/ml) on (a) the maximum unbinding force (decreased by 19%), (b) the number of tethering rupture events (decreased by358%), (c) the work of detachment (decreased by 53%) and (d) the distance to complete separation (decreased by 46%) are shown. Data are expressed as

mean ±SEM of more than 40 cells from 5 separate experiments, where key significances are shown, ***p<0.001.

Figure 4.7 Phase microscopy images showing HK2 cells indentation experiment. The cantilever was modified using a 10μm polystyrene microbead probe to enable indentation of a single substrate cell (within a cluster of cells for control group), while force versus displacement were measured simultaneously. In (a), an optical image showing normal HK2 cells (control) while in (b) cells that were treated for 48 hours with TGF-β1 are shown.

Figure 4.8 The effects of TGF-β1 treatment on E modulus as determined by the extension F-d curves acquired using AFM-FS indentation.

Figure 4.9 Histograms of control cells showing distribution of frequencies of E modulus (a) in control cells and (b) in TGF-β1 treated cells.

Figure 4.10 The effects of the cytokine TGF-β1 (10ng/ml) on the E modulus of HK2 cells. Treated cells showed an increase of 71% compare to the untreated group. Data are expressed as mean ±SEM of more than 30 cells from 3 separate experiments, where key significances are shown, ***p<0.001.

Figure 4.11 Fluorescence microscopy images showing the effects of TGF-β1 on both cell morphology and cytoskeletal reorganisation. The changes in the arrangement of the cytoskeleton (red) mainly affected the cell architecture. The nucleus of each cell is shown in purple. is In (a), normal cells are shown that were grown in low glucose (5mM) alone, while in (b) cell treated with TGF-β1 (10ng/ml) are shown.

Figure 4.12 Retraction F-d curves acquired by adhesion measurements of control HK2 cells with incremental pulling speed are shown. The effects of increasing pulling speed on adhesion characteristics are clearly represented by the changes in the work of detachment. Further, for speeds higher than 5μm/sec partial separation was observed. The levels of incomplete separation were increasing with the increase of pulling speed resulting in the complete rejection of measurements with pulling speed of 12.5μm/sec due to the limitation of 100μm in displacement range.

Figure 4.13 Effects of increased pulling speed on cell-to-cell adhesion parameters as acquired by SCFS retraction F-d curves of HK2 cells. Data are expressed as mean ± SD and the effects of increasing pulling speed on (a) maximum unbinding force, (b) work of detachment and (c) number of tethering rupture events are illustrated.

Figure 4.14 Cell-to-cell adhesion process of HK2 cells showing the changes in surface molecular binding and re-arrangement of the cytoskeleton into the periphery upon treatment with TGF-β1. During phase 1 the cells are in contact with each other and E-cadherin ligation is formed. In (a), a schematic of control cells is shown while in (b), a schematic of cells after treatment with TGF-β1 is shown. In phase 2 the separation process between the two cells is illustrated. In (c), increased distance of separation due to cell deformation, corresponded to higher work of detachment for normal cells while in (d) cells became more rigid due to cytoskeletal reorganisation into the periphery after TGF-β1 resulting in decreased distance of separation inevitably leading to a dramatic reduction of work of detachment. All in all, surface binding affinity was partially responsible for the changes in work of detachment that was mainly influenced by changes in the elastic properties of each cell.

List of Tables

Table 4.6 Table presenting the differences in E modulus between control and TGF-β1 treated cells using paired wise t-test.

Table 4.7 A table showing the number of tested MIN6 cells and number of processed or rejected retraction F-d curves obtained by SCFS adhesion experiment with incremental retraction velocities. As shown, more than 1/2 of the curves of 10 and 12.5 μm/sec were rejected, while no cells at 15μm/sec were accepted for processing.

Acknowledgments

I would like to express my gratitude to my supervisor, Dr Isaac Kuo-Kang Liu, for all his support and guidance he offered throughout this research project. Also, I would like to thanks our collaborator Dr Paul Squires for highlighting the biological importance of this research project. In addition, I would like to thanks Dr Claire Hills for preparing the cell samples and providing the fluorescence microscopy images for this work.

Moreover, I would like to thanks JPK instruments for the free installation of the CellHesion200 system in our laboratory over a period of 6 months. Thereby, I would also like to thanks Dr Torsten Muller and Dr Alex Winkel for the seminar on AFM force spectroscopy.

This PhD was fully funded by the School of Engineering and I would like to express my gratitude for this financial support.

Last but not least, I would like to thanks Pythagora Chatziandreou for his valuable help on photoshop, Dr Aikaterini Kassavou and Constantino Andreou for their valuable help on the statistics of biosamples, Dr Charoula Tzanakou and Theofilo Karantzali for helping me to sort out an inspiring place for the writing of the thesis, Dr Emmanuel Alvizo for his suggestions on the thesis, Dr Soroush Abolfathi for his valuable comments on the analysis of the data, Dr Lena Alkhudairy for her great input on the background of diabetes and any future reader of this document.

Declaration

I hereby declare that the work on this thesis, submitted in partial fulfilment of the requirements for the degree of Doctor of Philosophy at The University of Warwick, presents my own work and has not been previously submitted to any other institution for any degree, diploma or other qualification. The contribution of collaborative work has been specifically acknowledged. All sources of information have been acknowledged by means of references and bibliography. Published work is contained in the Appendix.

Parts of this thesis have been published by the author:

Siamantouras, E., Hills, C.E., Younis, M.Y.G., Squires, P.E., Liu, K-K. (2014). 'Quantitative investigation of calcimimetic R568 on beta cell adhesion and mechanics using AFM single cell force spectroscopy' *FEBS Letters*, **588**, 1178-1183.

Hills C.E., Jin T., Siamantouras E., Liu K-K., Jefferson K.P., Squires P.E. (2013). 'Special k" and a loss of cell-to-cell adhesion in proximal tubule-derived epithelial cells: modulation of the adherens junction complex by ketamine' *PLos One*, **8** (8), e71819–e71819.

Hills C.E., Younis M.Y.G., Bennett J., Siamantouras E., Liu K-K., Squires P.E. (2012). 'Calcium-Sensing receptor activation increases cell-cell adhesion and β-cell function' *Cellular Physiology and Biochemistry* **30** (3), 575 – 586.

Hills C.E., Siamantouras E., Smith S.W., Cockwell P., Liu K-K., Squires P.E. (2012). 'TGFβ Modulates cell-cell communication in early epithelial-to-mesenchymal transition' *Diabetologia* **55**,812 - 824.

Parts of this thesis has been presented in:

Siamantouras E., Liu K-K., Claire C.E., Squires P.E. 'Quantitative investigation of calcium-sensing receptor activation on β-cell adhesion and mechanics'. In: Diabetes UK Professional Conference, Liverpool, March 2014.

Siamantouras E., Mustafa M.Y.G., Claire C.E., Squires P.E., Liu K-K. 'New quantitative Study of Intricate interplay between cell adhesion and cytomechanics'. In: International Conference on Scanning Probe Microscopy on Soft and Polymeric Materials, Netherlands, 23-26 September 2012.

Siamantouras E., Mustafa M.Y.G., Claire C.E., Liu K-K., Squires P.E. 'Activation of the extracellular calcium-sensing receptor increases functional tethering between pancreatic beta-cells'. In: Diabetes UK Professional Conference, Glasgow, March 2012.

Claire C.E., Siamantouras E., Liu K-K., Squires P.E. 'TGFβ-modulates cell-cell-communication in early epithelial-to-mesenchymal transition'. In: Diabetes UK Professional Conference, Glasgow, March 2012.

Abstract

Cell-to-cell adhesion is critically important for the improved secretory function of endocrine pancreatic beta (β)-cells and for the progression of fibrosis in the renal proximal tubule in Diabetic Nephropathy. In this research project the effects of specific biochemical treatment on functional cell-to-cell adhesion and single cell mechanics were systematically investigated. Atomic Force Microscopy (AFM) Single Cell Force Spectroscopy was applied to quantitatively characterise E-cadherin mediated surface ligation and cytoskeletal reorganisation in the pancreatic mouse insulinoma MIN6 and human kidney proximal tubule HK2 cell model. AFM tipless cantilevers were functionalised with a single cell or a spherical microbead for performing cell-to-cell adhesion and single cell indentation experiments respectively. The impact of elastic deformation of single cells into cell-to-cell adhesion was examined by performing adhesion experiments at various retraction speeds. The results illustrate that both adhesive and mechanical properties of single cells constitute important underlying factors of the physiological and pathological conditions under investigation since they were significantly affected by biochemical changes. More specifically, it is suggested that the enhanced secretory function of MIN6 cells upon calcium-sensing receptor activation is owned to a combination of increased E-cadherin mediated cell-to-cell adhesion and decreased elastic (*E*)-modulus of single cells. In addition, it was shown that treatment of HK2 with the cytokine TGF-β1 decreased E-cadherin mediated cell-to-cell adhesion and increased *E* modulus of single cells, suggesting a mechanism that initiates early fibrotic changes in the tubular epithelia. Overall, both studies demonstrate that alterations of biological states evoke complex interactions between E-cadherin and actin cytoskeleton as manifested by the interplay between the mechanistic behaviour and surface binding of the cells. Therefore single cell mechanics have profound effects on cell-to-cell adhesion characterisation, particularly when physiological versus pathological states are to be investigated.

Abbreviations

AFM	Atomic Force Microscopy
AJ	Adherens Junction
ANOVA	Analysis of Variance
BFP	Biomembrane Force Probe
CAM	Cell Adhesion Molecules
CCD	Charged-Coupled Device
ConA	Concanavalin A
CSK	Cytoskeleton
DMEM	Dulbecco's Modified Eagle Medium
d_s	Distance of Complete Separation
E modulus	Elastic modulus
E-cadherin	Epithelial (E) Cadherin
ECM	Extracellular Matrix
EDTA	Ethylenediaminetetraacetic acid
EMT	Epithelial-to-Mesenchymal Transition
F	Force
F-d	Force-displacement Curve
F_{max}	Maximum Unbinding Force
Fn	Fibronectin
FS	Force Spectoscopy
GJ	Gap Junction
Hz	Hertz
HK2	Human Kidney Cell Line 2
ICAM-1	Intercellular Adhesion Molecule 1
LFA-1	Lymphocyte Function-associated Antigen 1
LPA	Lysophosphatidic acid

MA	Micropipette Aspiration
MIN6	Mouse Insulinoma Cell Line 6
MTC	Magnetic Twisting Cytometry
N	Newton
NI	Nano-indentation
OT	Optical Tweezers
PBS	Phosphate Buffered Saline
PLL	Poly-L-lysine
pN	Pico-Newton
R_s	Radius of Probe
RBC	Red Blood Cells
RGD	Arginine-Glycine-Aspartic Acid
SCFS	Single Cell Force Spectroscopy
SD	Standard Deviation
SEM	Standard Error of Mean
TGF-β1	Transforming Growth Factor beta 1
TREs	Tether Rupture Events
TRITC	Tetramethylrhodamine
UV	Ultra Violet
W_D	Work of Detachment
α	Radius of contact area
δ	Indentation Depth
3D	3 Dimensional

Chapter 1

Nanomechanics in Cellular Biology

1. Nanomechanics in Cellular Biology

1.1 Introduction

Understanding of the fundamental mechanisms for the development and progression of chronic diseases, such as diabetic nephropathy, was and still is directed by the advances of novel techniques that allow structural and functional investigation of living cells. Moreover, advances in tissue engineering and organs replacement heavily depend on the understanding of how cells interact with each other and respond to their microenvironment. Besides, relation of the cellular adhesion to the abnormal growth and metastases of cancer cell necessitate the advancements of novel experimental techniques in molecular biology (Cooper & Hausman, 2009). In addition, the adhesive behaviour of cell with other surfaces is crucial for the biocompatibility of implants (Elter et al., 2011). However, as a living system, the cell represents a highly complex organisational architecture that exhibits complicated mechanical and adhesive behavior. Inevitably, for the past three decades, engineered materials, such as commercial polymers and metals, have been widely used in medical devices and implants, primarily owing to their well characterized mechanical and adhesive properties. However, recent advancements in cell biology and tissue engineering necessitate the development of novel materials with mechanical properties that will resemble those of soft parts of biological structures (Scott et al., 2004; Ikai, 2008). Unlike classical mechanics, several special considerations need to be taken into account in the characterization of the mechanical properties of biological cells, since they show a complex 3-D structure, and they are distinguished by their compex mechanical and interfacial behavior (Scott et al., 2004). For example, the cell cytoskeleton has a fibre-like structure with a diameter less than 25nm, and is normally subjected to complex chemical and mechanical environment, including cell-cell and cell-extracellular

matrix (ECM) interactions. Therefore, the cytoskeleton is the principal factor that determines the deformation behaviour of a single cell (Bao & Suresh, 2003). In addition, the deformation behavior of cells and tissues is a result of integrated interaction between cytoplasmic elements such as the cytoskeleton (CSK) and the ECM. Therefore, mechanical and adhesive properties are affected simultaneously both at local and whole cell scale (Puech et al., 2006; Bao et al., 2009). Accurate determination of such complex material behaviour necessitates an understanding of the fundamental deformation behaviour in the nanoscale. Hence, nanomechanical characterization is critical for materials such as soft biological cells and tissues (Haque & Saif, 2002).

1.2 General Background

The cell is the basic building block of multicellular organisms, such as human tissue and organs. It is responsible for performing all the necessary functions of life including metabolism, homeostasis, growth and reproduction. Although eukaryotic cells vary between organs and tissues in size, shape and function they all have similar structures. Typically their structure include the plasma membrane and various cytoplasmic organelles such as the CSK and the nucleus. A diagram showing the main structure of a cell is depicted in Figure 1.1. Genetic information is contained inside the nucleus, which is the largest subcellular element with a diameter of approximately 5μm. However, red blood cells have a biconcave disk shape with no nucleus since they are constantly subjected into mechanical deformation while moving into narrow capillaries (Scanlon & Sanders, 2002; Cooper & Hausman, 2009; Pocock & Richards, 2009).

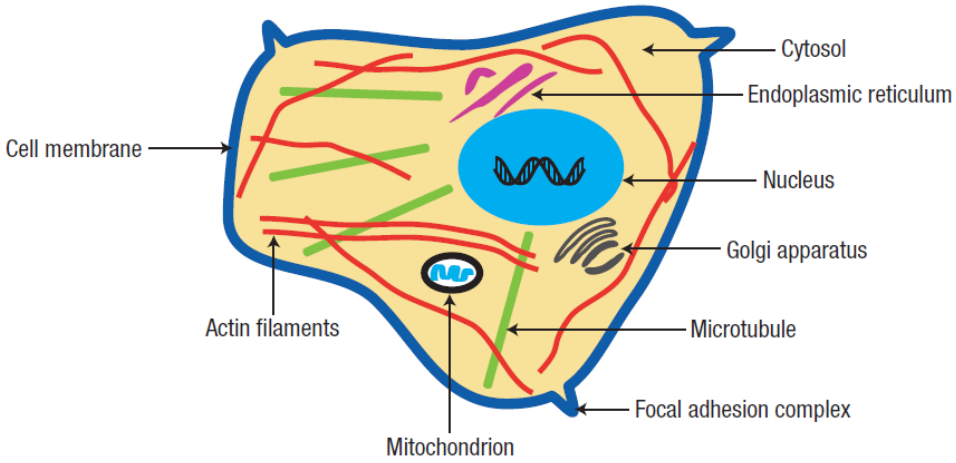

Figure 1.1 The cell membrane forms an outer boundary of the cell and is essentially a double layer of lipid molecules that regulates the passage of substances in and out of the cell as well as its response to chemical signals such as hormones. Focal adhesion points are high protein concentration points on the membrane, which are associated with the microfilament network in the inside and cell surface receptors or extracellular matrix on the outer side of the cell. The cytoplasm is a fluidic like media which forms a suspension for the organelles, including a network of protein filaments that maintains the shape called the cytoskeleton. Image adopted from Bao & Suresh, (2003).

The cell is a dynamic system that interacts continuously with its external environment, that is either other cells or extracellular matrix. This dynamic interaction is controlled by the plasma membrane that surrounds the cell and serves as a barrier between cells with which they can interact via cell adhesion molecules (CAMs). CAM proteins however, are not simply involved in the formation of tethering between cells but they also respond to any changes in the extracellular microenvironment, affecting the intracellular domain as well. Essentially, CAMs are transmembrane molecules that are linked to cytoskeletal filaments at the adherens junction. The connection of

the extracellular domain to the cytoskeleton results in an intricate interplay of the mechanical and adhesive properties of the cell, which may lead to alterations in the elastic deformation of whole cell (Puech et al., 2006). Puech et al. (2005) measured the adhesive properties of single zebrafish cells to coated substrates and concluded that extracellular binding affects intracellular signalling. In addition, Bershadsky et al. (2003) highlighted that focal adhesion points act as mechanosensors responsible for the signalling cascade within the cell. Thus, it is no doubt that cell adhesion events are important in controlling various cellular functions such as differentiation, wound healing, cancer proliferation and metastasis (Chaudhuri et al., 2009; Puech et al., 2006).

As a living unit the cell adapts continuously to its microenviroment in an attempt to maintain an overall healthy state. In fact, living cells in the human body are constantly subjected to mechanical stimulation throughout life. The changes of a cell in response to the environment can be of biochemical as well as biomechanical nature. The stresses and strains can arise from both the external environment and internal physiological conditions. Depending on the characteristics of the mechanical stimuli, cells will respond in a variety of ways altering their structure and consequently their functions. For example mechanical compression of chondrocytes modulates proteoglycan synthesis, strongly suggesting that the structure and function of many living cells depend directly on their global and local mechanical environment
(Van Vliet et al., 2003; Lim et al., 2006; Kuznetsova et al., 2007). Ingber (2002) investigated the transduction of chemical signals to mechanical cues through focal adhesion complexes in endothelial cells and highlighted the importance of mechanical control to variety of cell processes including growth, differentiation, motility and apop-

tosis. Likewise, forces generated within the cell, for example during cytokinesis, have a biological implication. Although the importance of mechanical forces in biology is not a new concept, it is currently attracting more recognition for its contributing in several emerging biomedical fields, such as molecular biology and nanobioengineering (Pelling & Horton, 2008). Recent advancements in technology allow the detection of these forces, yet we are only in the first steps of decoupling forces of specific interest from such a complex mechanochemical environment. Nevertheless, it is evident that mechanical cues are equally important for performing major cellular tasks, such as motility, division, intracellular secretion etc, as the biochemical cues (Bao et al., 2009). In addition the cell responds to the biochemical environment by continuously changing its structure and morphology. Changes in deformation provide important information about the normal and diseased states of the cell (Bao & Suresh, 2003). Any changes of the resistance of the cell to elastic deformation can be measured and expressed as changes in the Elastic modulus *E* or Young's modulus. Hence, measurements of single cell mechanical properties can form the base for a correlation between morphological/structural defects with physio/pathological states.

Furthermore, determination of the mechanical properties of soft tissues and cells has attracted significant scientific and commercial attention due to their importance in future progress of biomedicine, including drug delivery, cell repair, wound healing etc (Sirghi et al., 2008). Studies of whole cell populations under mechanical stimulation, investigate how biomechanics regulate the structure and function of tissues and subsequently organs. Besides, mechanical stimulation that exerts at the tissue level is transmitted to single cells, influencing their physiological function (Lim et al., 2006). However, the fact that most cells respond heterogeneously is a major challenge of

such studies. This is due to the difficulty in decoupling the response of a single cell from the response of the complete cell population, tissue or organ (Van Vliet et al., 2003). After all, the structural integrity of tissues or entire organs arises from the mechanochemical interactions between the cells and the ECM (Lim et al., 2006). Therefore, elasticity and responses of single cells to external forces, as well as adhesion forces between cells, have attracted tremendous attention in the modern bioengineering research (Lulevich et al., 2006). Figure 1.2 shows an overview of Young's modulus for different biological materials.

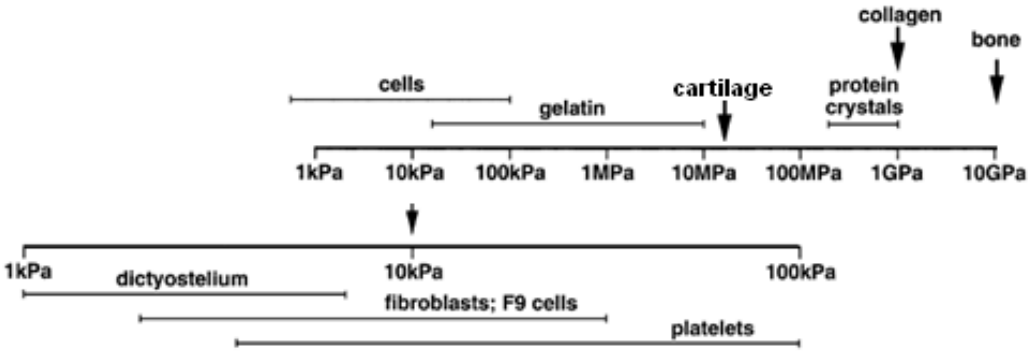

Figure 1.2 The Young's (elastic) moduli of different biological materials, image adopted from Alonso & Goldmann, (2003).

In addition, well known examples such as muscle atrophy and bone resorption indicate the importance of the mechanical stimulus, which has been implicated at the cellular level in terms of processes including adhesion, motility and differentiation. However the intricate coupling between the biochemical and mechanical processes of the cells is still poorly understood. Particularly, application of external mechanical stimuli can induce biochemical reactions, and likewise changes in chemical stimuli can alter the structure and mechanical integrity of the cell, even in the absence of mechanical stimuli (Van Vliet et al., 2003; Kasas & Dietler, 2008). Specific chemical agents can influence the interfacial and mechanical properties of living cells. This

may be useful for possible applications in clinical diagnostics or even therapy of certain types of diseases (Lim et al., 2006). Puech et al (2005) measured the unbinding forces of melanoma cells (Wistar Melanoma 115) from a fibronectin coated surface using atomic force microscopy to investigate the effect of the arginine-glycine-aspartic acid (RGD) blocking agent, suggesting that chemical agents have an impact on the adhesive cell-substrate properties.

A fact of great significance is the competence of cells to recognise mechanical stimulation, which is translated into a biological response (mechanotransduction). Investigation of cell-to-cell adhesion is important as a mediator of mechanotransduction (Ingber, 2006). However, adhesion between cells is related to the mechanical deformation, through CAMs. As the cell responds continuously to external environment by altering its structure, for instance during cell migration where contractile forces are produced inside the cell in order for the cell body to become motile (Bao & Suresh, 2003; Bao et al., 2010), the mechanotransduction process between cells is affected by changes in their mechanical properties. Furthermore, a variety of biological processes, such as cell growth, proliferation and even apoptosis are influenced by changes in cell shape and cellular adhesion (Lim et al., 2006; Chaudhuri et al., 2009). In fact, any deviation in the structural and mechanical properties of cells can result in a breakdown of the physiological processes and may possibly lead to diseases (Lim et al., 2006). For example, endothelial cells can maintain a healthy endothelium or lead to vascular diseases, such as thrombosis and atherosclerosis, when they sense a change in the magnitude, mode, type and duration of applied shear stress (Van Vliet et al., 2003; Bao et al., 2010). An additional important phenomenon in cell mechanics is that mechanical forces and deformation of a single cell can lead

to the guidance and regulation of major cellular functions, including motility and differentiation (Zhu et al., 2000; Bao et al., 2009; Kam & Roy, 2010).

Finally, of significant importance is the direct connection of the mechanical and adhesive response of individual cells to certain pathologies. As biological information is transferred mechanically, mechanical forces not only induce biological responses in cells, but they also alter cell structure and function. Moreover, the mechanical properties of cells appear to be affected by transitions between healthy and diseased states. Mechanical detection of these states may indeed be a key for future progress in Nanomedicine (Figure 1.3) (Pelling et al., 2008). In support of that, Hoh and Schoenenberger (1994) used AFM to monitor the increase in stiffness in kidney cells under chemical influences (Kasas & Dietler, 2008). Recent experiments performed using optical tweezers have shown that when the malaria parasite plasmodium falciparum intestates human erythrocytes, the shear modulus of the cell membrane can be increased up to tenfold as the disease state progresses (Van Vliet et al., 2003).

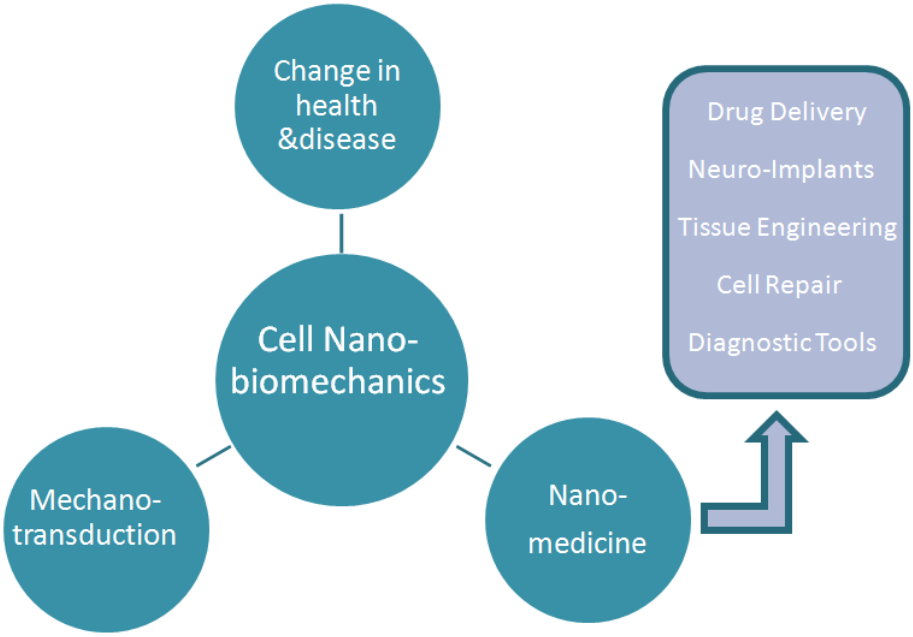

Figure 1.3 A systematic sketch of cell nano-biomechanics associated with physiological and pathological processes, which are important for the future progress in nanomedicine.

Subsequently, the mechanical properties of individual cells can determine the structural integrity of whole tissues arising from the mechanical interactions between cells and the surrounding ECM. Likewise, mechanical loads exerted at the tissue level are transmitted to individual cells influencing their physiological functions (Lim et al., 2006). Conclusively, the investigation of single cell mechanics is essential for the characterization and control of the mechanical properties and functions of reconstituted tissues, an important task for the practical application of tissue engineering (Lulevich et al., 2006).

1.3 Mini-Review of Nanomechanical Tools

To date, there exist a variety of testing techniques and associated models in the field of experimental nanomechanics of single cells. As well described in several comprehensive reviews in the literature (Bao & Suresh, 2003; Van Vliet et al., 2003; Lim et al., 2006; Liu, 2006), these techniques include optical tweezers (OT), and its variation optical stretcher (OS), atomic force microscopy (AFM), nanoindentation (NI), micropipette aspiration (MA), magnetic tweezers (MT) and its variation magnetic twisting cytometry (MTC) and biomembrane force probe (BFP). Although the fundamental principal of these techniques is to measure the deformation of biological cells under an applied force, the developed instruments vary in their operating principles, cell manipulation, force and displacement maximum resolutions, and amount of deformation (Van Vliet et al., 2003). Figure 1.4 shows the force range of important cellular processes with respect to the range of common nanomechanical instruments, while in Figure 1.5 the schematics of common experimental techniques are represented.

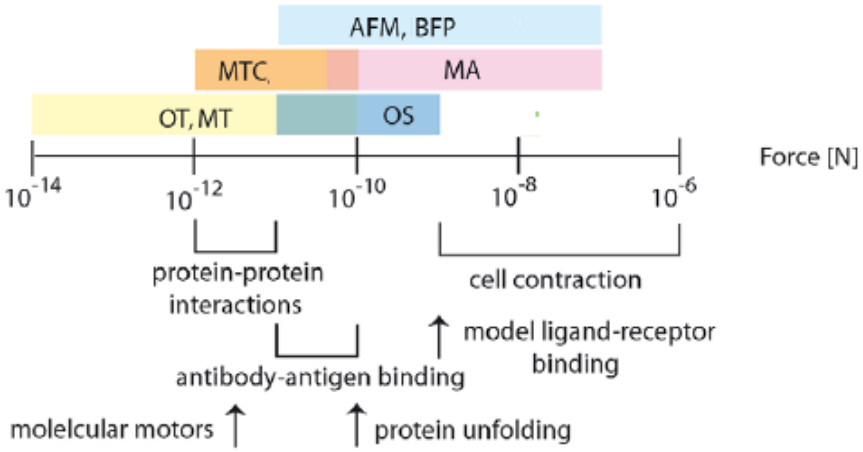

Figure 1.4 Diagram showing the force range of force common nanomechanical testing instruments, in relation to the range of major biological structures/processes. Image adopted from Van Vliet et al. (2003).

In OT an attraction force is created between a dielectric bead of a higher refractive index than the suspending medium and a highly focused laser beam that attracts the bead towards the focal point of the trap. In a widely used version of OT, two microbeads are attached to the opposite ends of a cell (Figure 1.5a). OT has been effectively used for stretching, rotation and folding, as well as calculating the relaxation time of RBCs (Van Vliet et al., 2003, Zhang & Liu, 2008). Operating an AFM in force spectroscopy (AFM-FS) mode and with suitable cantilever tips, AFM can be used to indent specific points on the cell surface (Figure 1.5b) (Franz & Puech, 2008). The elastic modulus of a single cell can be calculated by fitting the indentation curve with an appropriate theoretical model.

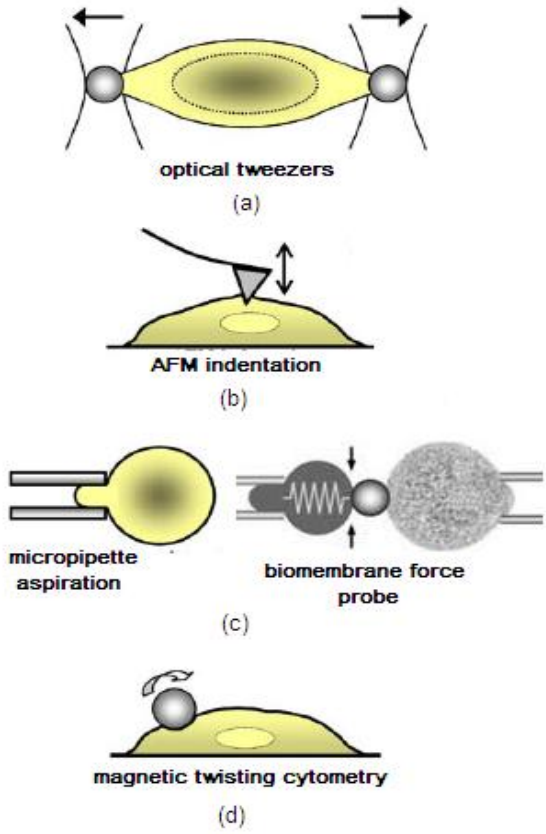

Figure 1.5 Schematics of common Nanomechanical testing techniques. Image adopted from Lim et al. (2006).

Kasas & Dietler (2008) have reviewed the application of AFM indentation for measuring the mechanical properties of numerous cell types. In MA (Figure 1.5c), a micropipetter is used for drawing a part of the cell into a capillary under the application of negative pressure, while the length of membrane sucked into the micropipette is recorded optically (Bao et al., 2003). MA has been used to study elastic properties of soft cells, such as neutrophils and red cells, as well as harder cells such as tenocytes (Hochmuth, 2000; Qi et al., 2006). BFP is a related technique in which a bead is attached to the sucked cell that serves as the soft spring of a force transducer (Figure 1.5c) (Van Vliet et al., 2003). In MTC a magnetic bead that is attached to the surface of the cell, is twisted under the influence of a magnetic field causing deformation of the cell (Figure 1.5d). By measuring the rotational frictional coefficient of the bead, viscoelastic properties of the cytoskeleton and cell's surface have been examined (Bao et al., 2003; Van Vliet et al., 2003).

Despite the variation of the means by which mechanical properties are examined, the fundamental principle among them is similar, that is to determine cell deformation under an applied load. However, direct comparison of the mechanical properties of the tested samples, as determined by the different techniques, is often scarce. This is mainly due to the diversion in assumptions during experimental procedures, sample preparation as well as the dependency of certain geometrical parameters of each technique, e.g. the contact area between the sample and the loading medium. Therefore, the most suitable for each individual experiment will be determined by the requirements of a situation, the type of application and the budget.

Today, AFM based Force Spectroscopy (AFM-FS) has been recognized as one of the most versatile high-end instruments for studying biomechanics at the cellular

level. In addition by specific chemical modification of the AFM tip, the instrument can be effectively used for studying cell-to-cell/substrate adhesion. A significant advantage over the other methods is that it allows high resolution force measurements (~pN) over a large dynamic range (~5pN to ~100nN) for displacements up to 100μm. Therefore, it can be effectively used in cellular adhesion studies to resolve the unbinding events between single ligand-receptor interactions, while providing sufficient force and displacement ranges to ensure detection of maximum unbinding forces and complete cell-cell and cell-substrate separation (Chaudhuri et al., 2009; Friedrichs et al., 2010). Moreover, the AFM tip can be fitted with either a sharp or spherical tip, depending on the measurement of local or whole cell elasticity. Since a spherical probe indents a much larger area of the sample than the sharp tip does, thereby Young's modulus of single cells can be calculated from the force-displacement curves under spherical indentation. In this report the focus will be on the application of AFM based force spectroscopy to experimentally characterise physiological and pathological phenomena of biological cells, by quantifying adhesion forces and elasticity of single cells.

1.4 Atomic Force Microscopy

The AFM belongs to the category of the scanning probe microscopes that has been in use since 1980. Although, it was introduced as a method to overcome the drawbacks of the common scanning tunnelling microscope, AFM is one of the major techniques widely used in the nanotechnology research today.

1.4.1 AFM Basics

Binning et al. (1986) first developed the AFM introducing a powerful tool that could provide 3-D images of the surface topography of biological samples in both liquid and gaseous environment. Soon, AFM emerged as a powerful tool to quantify the mechanical and interfacial properties of cells and to date it is commonly used in modern bioengineering research as a high-end instrument for measuring a relatively wide range of biological forces, from pN to nN (Binning et al., 1986; Lulevich et al., 2006; Franz & Puech, 2008; Ikai, 2008; Chaudhuri et al., 2009).

The AFM comprises of the following major components: a probe, a microfabricated cantilever, a piezo base scanner, a laser source, a photodetector diode, the sample, and a computer that processes that output reading and providing feedback control to the piezo scanner (Figure 1.6). The microfabricated cantilever tip is usually made from silicon and silicon nitride and can be of various number of geometrical shapes. A pyramidal shape cantilever tip is commonly used for imaging because of its low mechanical resistance to vertical deflection and high resistance to lateral torsion. However, with certain modification of the cantilever tip, AFM can be configured as a nanoindentation system or a cell-to-cell adhesion assay. For example, the tip of the instrument can be fitted with either a sharp or spherical tips of various diameters, in order to characterise local or whole cell elasticity. When the probe is brought into close proximity of the specimen surface, the force between the probe and the sample results into a deflection of the cantilever. This force is measured by the reflected laser spot from the back of the cantilever beam that is collected in the photodetector diode, as illustrated in Figure 1.6.

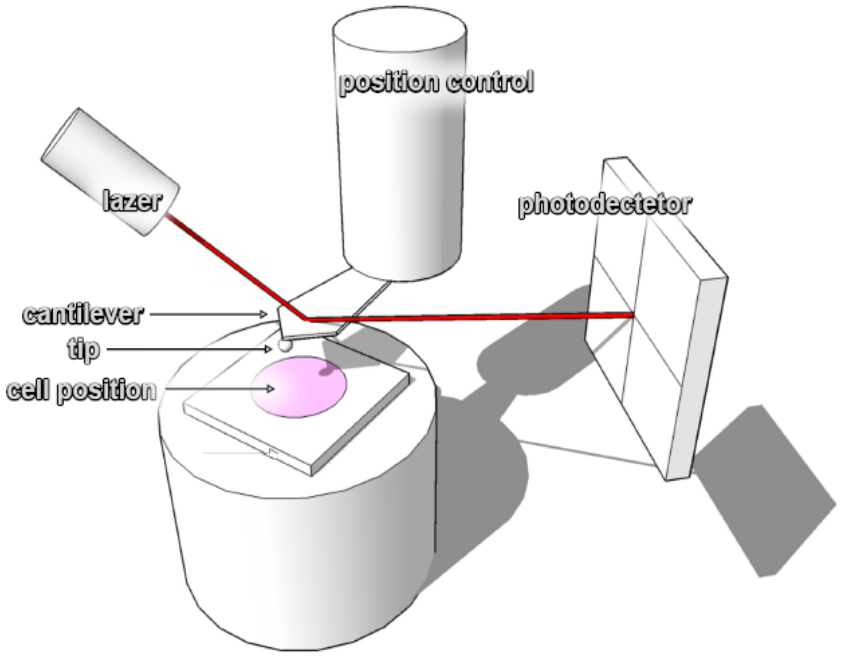

Figure 1.6 Basic components of AFM. During force spectroscopy experiments the cantilever is stationary in x-y direction but ramped at a given position in z-direction. A laser is used to read on a diode the deflection of a very soft cantilever equipped with a sharp tip. Mechanical contact is controlled via feedback between the piezo and the photodiode (Franz & Puech, 2008; Van Vliet et al., 2003).

1.4.2 Force Spectroscopy in Biology

Cell mechanics of living cells are dynamic due to the fact that forces are generated within the cell during cellular processes including cytokinesis, differentiation and migration. Furthermore, changes in the biochemistry induce changes in the mechanics of biological cells. Characterisation of the alteration of the mechanical properties contributes to the understanding of the fundamental mechanisms regulating cell morphology and function (Franz & Puech, 2008). Young's modulus of a single cell can be calculated by fitting the indentation curve with an appropriate theoretical model. A mechanical model that is widely used for the determination of elasticity is

the Hertz model, although it is valid for small indentation depths (Carl & Schillers, 2008). Kasas & Dietler (2008) have reviewed the application of AFM indentation for measuring the mechanical properties of numerous cell types, such as cardiocytes, osteoblasts, fibroblasts, erythrocytes and cochlear hair cells. However, determination of Young's modulus absolute values is still very challenging as there is no appropriate theoretical model to accurately describe the complexity of biological samples. Moreover, the effects of adhesion force on the tip/indenter must be taken into account in AFM force-displacement curves. An indentation model that takes into account the effect of tip-cell adhesion force in nanoscale indentation when using pyramidal tips has been recently proposed (Kasas & Dietler, 2008; Sirghi et al., 2008). Wojcikiewicz et al. (2004) studied the compliance of 3A9 clonal T-cells (10μm in diameter) assuming that the cell is an isotropic elastic solid and the AFM tip is a rigid cone, while Young's modulus was calculated in accordance with a modification of the Hertz model proposed by Love and Hertz.

Furthermore, AFM is a valuable tool to measure the mechanical forces between adhesive cells (Kuznetsova et al., 2007). The predictive, diagnostic and therapeutic role of adhesion molecules, such as CAMs, in cardiovascular (Jaitovich & Etcheverry, 2004) and Alzheimer's disease (Wennstrom & Nielsen, 2012) has been addressed. Chaudhuri et al (2009) studied leukocyte to endothelial cell adhesion using AFM combined with side-view fluorescent imaging, which performs *in-situ* imaging of cellular deformation on the loading axis. The major advantage of AFM lies in its capacity that it allows studying the mechanical properties of biological materials under both physiological-like and artificially (experimentally-induced) conditions with high spatial

and force resolutions. This made possible by introducing an optical deflection system and a fluid cell chamber into the AFM instrumentation (Franz & Puech, 2008).

1.4.3 Application of AFM on Single Cell Elasticity

Over the past twenty years, determination of the mechanical properties of cells during cellular processes and diseased states has attracted remarkable attention. The increasing research interest is mainly due to the demands of novel tissue engineering materials and for the therapeutic interventions in cell biology. In AFM indentation a force-distance curve is recorded as a function of the deflection of the cantilever versus the height (indentation) of the cell. Elasticity can be then extracted by applying the Hertz contact theorem and its variations such as Sneddon, JKR and Tatara theories for elastic indentation (Radmacher, 2002; Liu, 2006; Franz & Puech, 2008; Ikai, 2008). However, the extraction (measurement and interpretation) of the elastic properties of the cell is challenging due to the complex nature of the testing material and undefined experimental parameters. The precise tip geometry, tip-sample contact point, contact area and indentation depth, as well as the Poisson ratio of the sample are factors that influence the calculation of elastic properties, and induce errors in the absolute determination of elasticity. Variations of elastic modulus, *E*, of different cell types measured by AFM indentation are in the range from <1kPa to several 100kPa. This has serious implications when trying to produce comparable values between physiological and pathological states, since the differences in *E* between normal and malignant tissue may coincide in this range. Kuznetsova et al. (2007) reviewed the elastic modulus of living cells measured by AFM probing concluding that the values ranging widely from 0.2kPa (for leukocytes) up to 200kPa (for cardiocytes). The effects of sample preparation processes in the large scattering of

the *E* values were also underlined in the study. One such issue is the chemical immobilisation of the substrate, since firm contact between cells and substrate is required. However, chemical changes in the environment affect the mechanical properties of living cells. A method to overcome this difficulty, by providing mechanical immobilisation by placing the cells into microwells, was suggested by Rosenbluth et al. (2006). In this study the deformability of lymphoid leukemia cells was investigated. To test the effect of deformation rate during experiments, commercial pyramidal AFM tips and an indenter fitted with a 10μm diameter spherical bead were used at various piezo extension rates. The size of the cells was significantly smaller from the microwells, to avoid constrains by the walls during mechanical testing. The data were analysed using Hertz and liquid droplet models to investigate which model describes best the sample cell lines. The results showed that the Hertz model fit the data significantly better than the liquid droplet model at low deformation rates when testing leukemia cells.

Kiss et al. (2011) investigated the difference in elasticity of human embryonic stem cells (hESCs) during differentiation that were indented by a pyramidal AFM tip. During the experiments, researchers measured force-indentation curves at different locations on the surface of the hESCs using a sharp pyramidal tip. The results suggested that the elasticity of the hESCs varied significantly at different developmental states, with range of Young's modulus between 0.05Pa and 10kPa. The authors also demonstrated the variation of the elasticity across the surface of the cell, owing to the contributions of the underlying structures. Harris et al. (2011) used AFM indentation to test if there is a source of error to elasticity measurements on kidney cells when using pyramidal and spherical tipped cantilevers. Indentation measurements

were performed by using a standard unmodified pyramidal cantilever (0.05N/m), and by using the same cantilever modified with a spherical tip. The results suggested that measurements with the spherical tipped cantilever characterised the elasticity more correctly than measurements with pyramidal tipped cantilevers that provided an overestimation of the measured elasticity. Given such drawbacks in the determination of single cell elasticity, A-Hassan et al. (1998) discussed whether absolute values of elastic modulus can be acquired by AFM indentation experiments. They have examined epithelial madine-darby canine kidney (MDCK) cells cultured in monolayers, addressed the issues of tip-sample contact point and geometry, and suggested an approach for analyses of AFM force displacement (*F-d*) curves to overcome these experimental uncertainties. Essentially, they performed *F-d* curves across a single cell and calculated relative variations of *E*, by assuming a relationship between the indentation work for a predetermined indentation force and the elastic constants along the indentation points (force integration to equal limits). In addition, the ability of AFM to generate reproducible *F-d* the curves at scan rated <25μm/s, as long as the measurements are performed at the same position of the cell, was demonstrated. Besides, scanning of the surface of a cell using the AFM either in contact or tapping mode provides information about local surface elasticity at each point of contact. The differences of cantilever oscillation can produce a map of the relative *E* of cell surface.

Another major challenge in the mechanical characterisation of soft biological cells is the fitting of the acquired data to an appropriate mathematical model (Kasas & Dietler, 2008). Ohashi et al. (2002) determined the elastic modulus of bovine endothelial cells exposed to shear stress using both experimental and numerical meth-

ods. Although that the values for control and sheared cell calculated by finite element modelling were higher in comparison to Hertz fitting, the tendency of the *E* modulus between control and sheared cells was the same. More importantly, this shows that *E* modulus can be used as a relative indicator/parameter in comparison experiments and since AFM measurements can be performed in near physiological conditions, this tool is useful to study a variety of biological phenomena including physiological versus pathological conditions of cells.

Li et al. (2008) used AFM to investigate the elastic properties of benign and cancerous human breast epithelial cells. During the experiments the researchers employed different loading rates from 0.03 to 1 Hz and used Hertz's contact model, at a physiological temperature of 37ºC in order to determine the mechanical characteristics of the sample cells. The AFM images showed that healthy cells have more well-defined stress fibers network than cancerous epithelial cells, with Young modulus being significantly lower (1.4-1.8 times) for diseased cells. These findings have considerable implication on diagnosis and treatment of cancer metastasis. Furthermore, Li et al. (2009) investigated the elasticity changes in individual breast cancer cells. Specifically, they quantified and compared the elasticity of non-malignant (MCF-10A) and malignant (MCF-7) human breast epithelial cells using spherical AFM nanoindentation. They also investigated the influence of the different temperatures and different loading rates. During the study indentation was performed using loading rates from 0.03 to 1 Hz, with constant indentation force (0.2nN) at temperatures of 24ºC and 37 ºC. The Hertz model was used for small deformations and the results showed that higher values of the apparent elastic modulus were associated with increase loading rate for both MCF-7 and MCF-10A cells. Furthermore, the results showed that elastic

modulus is smaller at a higher temperature. The authors concluded that both loading rates and temperature need to be considered when performing mechanical tests of single cells using AFM. Cross et al. (2007) studied the stiffness variations of metastatic lung cancer cells, obtained from pleural effusions of patients with metastatic ademocarcinoma, using AFM. Measurements were performed at 27ºC using a constant speed. The results suggested that metastatic cancer cells were 70% softer than normal cells, when compared to other pleural effusions from patients with different clinical histories.

Rotsch et al. (2000) investigated the importance of actin network for the mechanical stability of living cells by using drugs (Cytochalasin B and D, Latrunculin A) to dissemble the structure of the cell. During drug action, AFM-based elasticity measurements were performed by recording time series of force maps on the cells and the force-displacement curve data were analysed off-line. The results proved that disaggregation of F-actin resulted in a loss of cell rigidity but treatment with drugs that impacted microtubules had no effect on elasticity. Finally, the authors concluded that the actin network is primarily responsible for the elastic properties of living cells.

All in all, it is clear that there are a few factors that need to be considered in order to obtain meaningful results from AFM indentation. Sample preparation may ease or optimize the experiment, but it should not be performed in the cost of loss of physiological characteristics of the cell. Another factor is the heterogeneity of the cell causing variations of the elastic modulus in different cell region. Therefore, probing of the cell should always be monitored during the experiments, to ensure that testing is performed in the same location on the cell's surface. Indentation depth largely depends

on the mechanical model for *E* determination and should be carefully defined before the experiments or during analysis of *F-d* curves. In addition, changes in elasticity indicate CSK reorganisation, a phenomena that plays a significant role in cell signalling, cell-to-cell adhesion and various cell processes such as motility, division and mitosis.

1.4.4 Application of AFM on cellular adhesion

AFM-FS was primarily used as an assay to quantify the molecular forces between single isolated receptor - ligand binding (Friedrichs et al., 2010). However, since the functions of surface receptors in isolation were different from their *in vivo* equivalent, AFM was applied as a single cell force spectroscopy (SCFS) tool to quantify surface ligation between living cells. AFM-SCFS allows different experimental set-ups, most commonly including

(a) Adhesion of a tipless-, bead-coated cantilever to an immobilised substrate cell,

(b) Adhesion of a cantilever-attached cell to a coated surface, and

(c) Adhesion of a cantilever-attached cell to an immobilised substrate cell.

Although set-up (a) has the advantage that a specific type of functionalisation can be tested sequentially on various types of cells within an experiment, contamination of the functionalised tip after continuing cell contacts could finally result in only a few reliable measurements. Since characterisation of the adhesion process necessitates the measurement of manifold Force vs distance (*F-d*) curves, this configuration is not an option for long or strong tip-cell contacts (Friedrichs et al., 2013). Grandbois et al. (2000) applied this approach to produce affinity images of RBCs by measuring the rupture force of adhesion events using a Helix pomatia lectin functionalised tip. Their

study suggested that the chemical wearing out of the cantilever was minimised for contact forces less than 40pN. Another major drawback of this method is the spreading of receptor or ligand of interest across the surface of the cantilever, affecting strongly the local ligand-receptor binding density and can lead to data scattering over time (Friedrichs et al., 2013).

Type (b) set-up, in which a single cell is attached on the cantilever, overcomes the problem of contamination as long as it is established that the suspended cells are not affected prior attachment. Nevertheless, the possibility of substrate's contamination still remains, hence it is suggested to probe different spots on the same surface in cell-to-ECM adhesion studies (Friedrichs et al., 2013). Friedrichs et al. (2010) developed an SCFS assay to investigate cell adhesion to ECM in physiological conditions. The study involved integrin-mediated adhesion of HeLa cells, attached on concanavalin (Con) A coated cantilevers, to collagen I substrate. The study demonstrated that cell-substrate unbinding force decreased significantly when integrins on the cell surface were inhibited by ethylenediaminetetraacetic acid *(*EDTA), and described a protocol that can be applied to other cell lines. Zhang et al. (2002) investigated the mechanical binding between the leukocyte function-associated integrin-1 (LFA-1), expressed on the T cell hybrid cell line 3A9, and its cognate ligand intercellular adhesion molecule-1 (ICAM-1). In order for the cell to be attached on the cantilever, it was first chemically activated (functionalised) using ConA. To study the individual ligand-receptor complex contact duration and contact force were minimised (~50msec, <0.5nN). This study confirmed that the adhesion was mediated by LFA-1 and ICAM-1 and that unbinding forces were increased with loading rate, demonstrating the viscoelastic nature of integrins' ligation.

Type (c) configuration, which is considered a special application of (b) (Friedrichs et al., 2013), was the most challenging set-up in terms of sample preparation and experimental procedure. However, since the adhesion molecules are functioning *in situ*, this method is considered as the most promising method to generate results in near physiological conditions. In addition, since the local geometry of both contact surfaces is of the same nature, differences in spread area between the cantilever-attached system and substrate-cell are eliminated. Nevertheless, continuous observation of the morphology of the cantilever-attached cell is required. A drawback of this configuration is the procedure for immobilisation of a cell to the cantilever, since suspended cells tend to stick to the substrate cells than the cantilever. To overcome this difficulty, parts of the substrate can be coated with trypsin, an enzyme used for harvesting of cells. Furthermore, although single cell-to-cell adhesion measurements provide information about receptor-ligand interactions in their natural environment, this type of set-up has the disadvantage of being time consuming since only one individual substrate cell can be characterised at each time. In addition, long cell-to-cell contact times should be avoided (<20mins), due to the thermal drift of the AFM (Friedrichs et al., 2010).

In general the most challenging task in cell-to-cell adhesion is the specificity of surface molecular interactions, arising from the heterogeneous nature of the sample (Zhang et al., 2002). Therefore localisation of the binding protein of interest as well as its distribution must be well established prior SCFS experiments. In a recent study by Hills et al. (2013), a concentration-dependent progression of proximal kidney fibrosis under cytotoxic doses of ketamine was reported. Homegeneity of adhesion experiments was assured by using an established model cell line for human epithe-

lial cells of the proximal tubule human kidney cell line (HK2). Localisation and distribution of E-cadherin was assessed by analytical techniques prior to SCFS experiments. A single suspended cell was attached to the end of a tipless cantilever using poly-l-lysine (25μg/ml) and fibronectin (20μg/ml) and subsequently brought into contact with a substrate cell using consistent values for contact force and time (1nN, 10sces) throughout the experimental series. Changes in whole cell morphology and CSK re-organisation indicated the interplay between adhesion and mechanics.

Furthermore, various studies demonstrate the competence and versatility of SCFS in investigating several aspects of cell-to-cell adhesion including severe pathological conditions, such as cancer. Hoffman et al. (2011) investigated interactions between jurkat T-cell and the breast cancer cells MCF7 that were induced by a bispecific antibody (bsAb HEA125xOKT3). A single cell was captured and attached to a Cell-Tak coated cantilever with a force of 0.8 nN for 10 sec. The attached cells was allowed to rest and establish contact to the cantilever for 10 min. Cell-to-cell contact time was varied (30secs-5mins), demonstrating the capability of SCFS to detect changes in specific adhesion molecules in early stages. Steffen et al. (2011) studied cell-to-cell adhesion of red blood cells treated with lysophosphatidic acid (LPA). It was reported that Cell-Tak was the most effective adhesive for attaching a single RBC to a cantilever. The results indicated a significant difference in adhesion behaviour between control and LPA-stimulated red blood cells. Mean value of the maximum unbinding force of control RBCs was 28.8±8.9 pN, whereas in the LPA induced experiments a significantly higher value of 100±84 pN was observed. In addition the study showed that the effective pulling range for complete unbinding increased with cell-to-cell contact time.

1.5 Diabetes Mellitus

This section covers the essentials of pancreatic physiology and provides a basic background of physiological versus pathological conditions of diabetes and diabetic nephropathy. The biological context for the research questions associated with the secretion function of β-cells and the fibrotic changes of renal proximal tubule in chronic kidney disease is also covered.

1.5.1 Pathophysiology of the Endocrine Pancreas

Situated behind the stomach in the higher left quadrant of the abdominal cavity, pancreas is a glandular organ that performs both exocrine (digestive) and endocrine (hormone) functions (Scanlon & Sanders, 2002). However, since this study is mainly focused on the hormones secreting cells only the endocrine function will be discussed. The cells in the endocrine pancreas that synthesise and release hormones reside within the islet of Langerhans or pancreatic islets. The main function of the islet is to regulate and maintain glucose homeostasis (Bilous & Donnelly, 2010). A microscopic section view of a healthy pancreas in which the islets can be distinguished by their discrete islet like morphology is presented in Figure 1.7. Although a normal human pancreas has ~1 million islets, they constitute only 2-3% of the gland's mass (Bilous & Donelly, 2010; Castano & Eisenbarth, 1990). The islet of Langerhans is composed by several endocrine islet cell types (Shih et al., 2002), and while another cell type expression has been reported (Wierup et al., 2004), β-cell type is the most abundant, constituting approximately 60-70% of the islet mass (Bilous & Donelly, 2010).

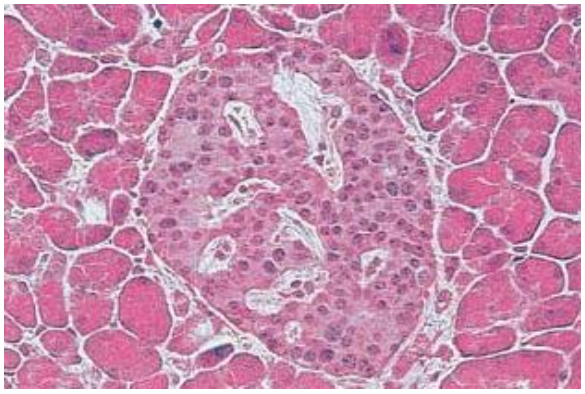

Figure 1.7 A microscopic section of normal pancreas. Lighter staining cells, compare to exocrine tissue, in the centre are identified as the 'islet of Langerhans'(original magnification x350). Image from Bilous & Donelly (2010).

The metabolism and other energy-requiring processes of the cells are basically relying on receiving a continuous supply of carbohydrates, such as glucose, which will get oxidised (burned) inside the cell (Pocock & Richards, 2009; Cohen & Wood, 2000). Therefore, it is essential that the amount of glucose in liquid blood (plasma glucose), is maintained within the normal range (4-8 mmol/l). Hormones produced by the pancreas, such as insulin and glucagon, provide minute-to-minute regulation of glucose requirements. However, insulin is essentially the only hormone that acts to reduce the concentration of blood glucose (Pocock & Richards, 2009). As anticipated insulin impairment inevitably leads to elevated glucose concentrations in the blood-stream (hyperglycamia) and sugar excretion in the urine (glycosuria) (Cohen & Wood, 2000; Bilous & Donelly, 2010).

Diabetes mellitus, or plainly diabetes is the most common endocrine disorder (Yoon & Jun, 2005; Cohen & Wood, 2000) associated with chronic hyperglycaemia due to a deficiency in insulin secretion or insulin resistance (Sakuraba et al., 2002; Bilous &

Donelly, 2010). Based on the aetiology of diabetes can be classified into two major categories: Type 1 diabetes, also called insulin dependent, is characterised by β cell destruction resulting in complete insulin deficiency, and Type 2 diabetes, or non-insulin dependent, in which reduced secretion and loss of insulin sensitivity/response is observed (Zimmet et al., 2001; Pocock & Richards, 2009; Bilous & Donnelly, 2010).

Type 1 is less common (5-10% of diabetic population), but it is considered to be more severe (Cohen & Wood, 2000; Shaw et al., 2010; Zhang et al., 2010). Type 1 diabetes can be classified into two main types: 1a or autoimmune and 1b or idiopathic (Bilous & Donnelly, 2010). The islet fails to secrete normal amounts of insulin because of the progressive destruction of the β cells by autoreactive T cells (Yoon & Jun, 2005). It occurs by the age of 30-40 years old (Pocock & Richards, 2009; Cohen & Wood, 2000) and especially in children (Scanlon & Sanders, 2002), while the onset of the disease is connected to genetic predisposition (Castano & Eisenbarth, 1990).

Type 2 diabetes is becoming a serious healthcare issue in the 21th century as it accounts for approximately 90% of the diabetic population (Zimmet et al., 2001). It develops progressively due to a deterioration of β islet cells that results in reduced insulin secretion and/or insulin resistance. Despite the fact that genetic tendency and obesity are potential risk factors, the exact disease causation is still poorly understood (Pocock & Richards, 2009; Bilous & Donnelly, 2010). Dysfunction of β cell is already ~50% in recently diagnosed patients and keeps on declining rapidly despite of the therapy. In addition, although the mass of β islet cells decreased by only 20-

40%, a >80% reduction in insulin is observed (Bilous & Donnelly, 2010). Additional functional defects such as decreased communication via surface ligation should be investigated.

1.5.2 Historical Background & Implications

Even though diabetes was ignored in Europe in the past, Thomas Willis, an English physician, noted the effects of diabetes in the urine in the 17th century. Later on, in 1889, Minkowski and Mering from Strasbourg connected the cause of this disorder with pancreas, by removing the organ from a dog. The description of a pancreas as small clusters of cells was completed by Paul Langerhans in Berlin. The function of the cells was still unknown until Edouard Laguesse in France (1893) suggested that the islet cells were endocrine tissue of the pancreas that produced an hormone for glucose regulation and called the cells 'islets of Langerhans'. Insulin was discovered by Banting and Best in 1921 at University of Toronto. This discovery led immediately on the treatment of the first diabetic patient in 1922 by extracting and purifying insulin from pancreas. Today, human insulin can be produced by modern genetic engineering techniques and drugs that stimulate both insulin secretion and sensitivity are being developed. Indeed, there is intensive interest in converting research into therapies for diabetes mainly due to the serious implications of the disease (Luft, 1989; Bilous & Donnelly, 2010).

The total number of people with diabetes worldwide has been increased from 170 million in 2000 to 220 millions in 2010, and projected to increase to more than 300 million by 2030 (Zimmet et al., 2001; Bilous & Donnelly, 2010). In addition there are complicated relapses associated with diabetes, that make the disease a major health

concern with serious socioeconomical consequences. Mortality caused by ketoacidosis and coma due to absolute deficiency of insulin is high in UK and other developed countries. Long-term micro-vascular implications include diabetic retinopathy, diabetic nephropathy and dry gangrene. Diabetes is the most common cause of blindness in those of working age and the most common single cause of end-stage renal failure worldwide (Scanlon & Sanders, 2002; Bilous & Donnelly, 2010).

At the moment diagnosis of diabetes is accomplished by detecting chronic hyperglycaemia. However, new methods for early diagnosis are absolutely necessary since approximately 20% of new patients with type 2 diabetes have already presented vascular implications. This means that the exact onset of the disease occurred almost 5-6 years before the serious implications of the disease have started to develop (Bilous & Donnelly, 2010). Cardiovascular complications due to uninhibited glucose fluctuations may increase 3 to 8 fold (Norhammar et al., 2002). Such important clinical problems necessitate the development of novel therapies for the treatment of disease and/or prevention of its implications.

1.5.3 Physiological Secretory Function & Islet Architecture

Insulin is a vital hormone. It is synthesised in and secreted from the β cells within the islet of Langerhans in the pancreas. Although insulin secretion is the mainly stimulated by glucose, its modulation is also associated with co-released factors including nutrients, such as amino- & fatty-acids, hormones and neurotransmitters (Sharp, 1996; MacDonald et al., 2005).

Insulin is responsible for the transport of glucose through the plasma membranes inside the cell in order to be metabolised for energy. The rate at which excess glucose is changed into fatty acids by the liver can also be increased by insulin. By performing these actions, as well as by promoting the use of glucose for energy production in the bloodstream, insulin manages to reduce the concentration of sugar in the blood. In addition, by increasing the uptake of amino acids into cells and by converting them into proteins, insulin contributes to the metabolic function of the cell (Cohen & Wood, 2000).

Adjacent β cells are coupled by gap junctions that allow the direct passage of molecules and electrical currents. Gap junctions are formed by transmembrane proteins and are important in cell-to-cell communication pathways for the coordination of insulin secretion in the pancreatic islet (Benninger et al., 2011). Since cell-to-cell adhesion leads the formation of gap junctions, enhanced cellular adhesion may improve cell communication and secretion responsiveness within the islet.

E-cadherin is a surface adhesion molecule involved in the tethering of adjacent cells, which substantially contributes in maintaining the 3-dimensional structure of the pancreatic islets (Dahl et al., 1996). E-cadherin ligation mediates β-cell-to-β-cell coupling and regulates intercellular communication within islets (Brereton et al., 2006). A study by Rogers et al. (2007) suggested that E-cadherin mediated cell adhesion contributes to the enhanced secretory function of β cell clusters. Moreover, knock down of E-cadherin expression during islet dispersion reduced glucose-evoked insulin release (Halban et al., 1988; Meda, 2003). Recently, it has been shown that neutralisation of E-cadherin reduced glucose-evoked synchronicity in calcium signals between

adjacent cells apart from causing considerable reduction in insulin secretion (Rogers et al., 2007). Alteration of the pseudoislet architecture was substantial and was accompanied by a loss of the adhesive properties as indicated by the attenuation of dye transfer between adjacent cells. Their results suggested that there is a strong functional consequence in regulating intercellular communication via gap-junctions following neutralisation of E-cadherin. Thus, it may be implied that E-cadherin mediated cell adhesion has important repercussions for the islet function in terms of glucose responsiveness and insulin secretion. It is therefore important to develop an experimental protocol to determine quantitatively the changes in adhesion forces between β cell-to-cell adhesion and elucidate if an increase in E-cadherin improves the function of the islet by enhancing cell-to-cell communication.

It is well reported that the higher glucose-evoked insulin secretion of mouse insulinoma MIN6 cells when organised as pseudoislets, is mediated by enhanced cell-to-cell interactions and/or elevated expression of gap-junction proteins, such as E-cadherin (Hauge-Evans et al., 1999; Calabrese et al., 2003; Brereton et al., 2006; Kelly et al., 2010). An appropriate model that resembles function of β islet cells along with a switch to increase E-cadherin expression were identified for the purpose of this study.

1.5.4 The MIN6 Model Islet

Primary human tissue is considered as the touchstone to investigate endocrine secretory functions. However, human islets constitute a precious sample material with complex heterotypic interactions between islet cells; hence, it is not considered to be appropriate for the investigation of basic mechanisms by which cell-to-cell interac-

tions occur. In contrast, a well established cell line for resolving mechanisms of glucose-evoked insulin secretion characteristics, such as the mouse insulinoma cell line (MIN6) (Ishihara et al., 1993), offer a continuous supply of unlimited growth homogeneous sample material. In addition, cell lines offer an animal-free opportunity for experimental manipulation without ethical concerns and therefore have the added advantage of being subjected to pathophysiological treatment. Moreover, the major advantage of using a clonal cell line is the ability to control the consistency and reproducibility of experiments (Skelin et al., 2010). However, special cell culturing skills are required to guarantee the proper preservation of the cell line structure and function. In fact, the disadvantage of being amenable to changes of their characteristics is derived from their own ability to grow continuously (Skelin et al., 2010).

Although MIN6 cells morphologically resemble primary islets, they do show differences in the insulin secretion response when compared to primary β cell. Kelly et al. (2010) reported enhanced response to glucose when treated as pseudoislets. In addition, the glucose-evoked secretory response of MIN6 cells is higher when they are cultured as pseudoislets rather than monolayers in a culturing substrate (Hauge-Evans et al., 1999). In this project MIN6 cells were cultured in monolayers due to the experimental requirements of AFM-SCFS.

1.5.5 The Extracellular Calcium-Sensing Receptor (CaSR)

CaSR is involved in local paracrine signalling with great repercussions in insulin secretion. Brown et al. (1993) was the first to identify and clone the CaSR in the bovine parathyroid gland. The role of this cationic ion binding receptor in the systemic circulation is to sense local changes in extracellular Ca^{2+} from one cell and evoke appro-

priate counter-regulatory responses into a neighbouring cell to regain Ca^{2+}-homeostasis (normocalcaemia). This is accomplished by regulating the secretion of parathyroid hormone and urinary calcium concentration (Brown, 2007). Since CaSR is directly involved with the propagation of signals, the receptor has an significant function in cell-to-cell coupling and communication.

The functional link between the receptor and regulation of systemic calculation in normal physiology and disease has been extensively studied (Brown, 2007). However, CaSR expression is not restricted to the cells involved in the control of systemic Ca^{2+} (Brown & MacLeod, 2001). It has been reported previously that CaSR is found on tissues not associated with normocalcaemia, such as oesophageal (Justinich et al., 2008), colonic epithelia (Cheng et al., 2004), the cardiovascular system (Smajilovic et al., 2011) and pancreatic β islets (Rasschaert et al., 1999; Squires et al., 2000; Gray et al., 2006). Kato et al. (1997) in a study using insulinoma cells that were extracted from primary culture by surgery, suggested that insulin release was elevated when the level of Ca^{2+} was increase and that CaSR mediates calcium-evoked insulin secretion. The expression of the receptor in pancreatic islets was confirmed by Bruce et al. (1999) and suggested that the receptor controls physiological function of insulin secretion. However, in their study the receptor was not localised to β cells, and it was Rasschaert & Malaisse (1999) who showed that the receptor was present in insulin-secreting β cells and suggested that CaSR mediates calcium-evoked insulin secretion. Increase secretion of insulin in human islets upon CaSR activation was also suggested by Gray et al. (2006).

The role of CaSR in improving function of β islet cells by synchronisation of insulin release within the islet is achieved through enhanced cell-to-cell communication (Hauge-Evans et al., 1999; Jones et al., 2007; Kitsou-Mylona et al., 2008; Hills et al., 2012b). It is firmly established that CaSR is expressed in pancreatic β cells where it is thought to improve the functional responsiveness of the β cells, by enhancing cell-to-cell communication, and promote insulin secretion. In a study using MIN6 cells, Rogers et al. (2007) suggested that apart from playing an important role in the formation of pseudoislets, E-cadherin facilitates their function by increasing gap junction communication. These data imply that E-cadherin mediated cell adhesion has important repercussions for the islet function in terms of glucose responsiveness and insulin secretion. However, the association between cell-to-cell communication and cell-cell contact or adhesion remained unclear (Hills et al., 2012b). The functional mechanism underlying intercellular communication between β cells through E-cadherin upon CaSR activation has been investigated in this research project.

1.5.6 CaSR Activation

Activation of the receptor initiates calcium-evoked insulin release in human pancreatic islets (Gray et al., 2006). Since CaSR activation has an impact on β cell function, it is expected that changes in receptor expession/function are connected to the response of insulin secretion. Secretion of insulin that was evoked by glucose was inhibited after knocking out the gene KCJN15 and inactivating the CaSR simultaneously (Okamoto et al., 2012). In addition, in diabetic cardiomyopathy it is suggested that expression of CaSR is decreasing with the progression of disease (Bai et al., 2012).

Although various ligands activate CaSR, the Ca^{2+} remains the main agonist of the receptor (Brown & MacLeod, 2001). Activation of the receptor using a phenylalkylamine agonist (calcimimetic) is accomplished by increasing the affinity of its ligands for Ca^{2+}, having the advantage of avoiding the high number of non-specific events (Hills et al., 2012b). Activation of CaSR using calcimimetics was reviewed by Trivedi et al. (2008), while the enhanced insulin secretion functions was suggested by Gray et al. (2006). Direct measurements of extracellular spaces surrounding β cells using Ca^{2+}-sensitive microelectrodes (Gerbino et al., 2012), support the concept that local 'hot spots' of extracellular Ca^{2+} activate the CaSR on neighbouring cells (Hills et al., 2012b). In addition, calcimimetics were used to increase the secretory response of glucose up to a maximum level in pancreatic of rats (Straub et al., 2000). The use of calcimimetics for CaSR activation in the pancreas results in a transient increase of insulin secretion without the need for stimulation by certain glucose concentration. The fact that insulin release is rising in the absence of prestimulus activation by glucose, highlights that CaSR may has a key role in the secretory function of primary β cell islets (Gray et al., 2006).

1.6 Diabetic Nephropathy

Disease complications in diabetes has been identified as one of the most pressing global challenges of the developed world. The proximal tubule area of the human renal system is a complex system with active metabolic functions. In addition, proximal tubule plays an important role of internal homeostasis, since it acts as a regulator. Damage of the renal tubule after diagnoses of diabetes and in the absense of other obvious symptoms, is the main cause of acute dysfunction of the kidneys (Racusen et al., 1996).

Diabetic nephropathy (DN) accounts for approximately 50% of those patients presenting an end stage renal failure and is the most common cause of entry into the renal replacement therapy programme. While multiple structural and functional changes are associated with DN, it is as well characterised by an accumulation of ECM in both the glomerular mesangium and tubular interstitium. Continuous accumulation of excessive fibrotic deposition, eventually leads to a reduced function of renal excretion. Renal fibrosis can be identified by the activation of phenotypical transformations. The phenotypical fibrotic change of tubulointerstitial fibrosis is the crucial pathology underlying progressive chronic kidney disease in diabetes. Central to this process is epithelial-to-mesenchymal transition (EMT) or the transdifferentiation of tubular epithelial cells into myofibroblasts (Hills et al., 2012a). Understanding early signals that control deposition of fibrotic material in the interstitium is essential for the development of therapies that could alleviate the malignant transformation of epithelial cells to fibroblasts.

1.6.1 Molecular Mediators of Renal Fibrosis in DN: TGF-β1

Transforming Growth Factor-beta (TGF-β) is a pro-sclerotic cytokine of a family of polypeptide growth factors that can cause differentiation of various cell types (Cooper & Hausman, 2009). In addition, it is suggested that this cytokine acts as a molecular mediator for the fibrotic changes observed in DN (Sharma & Ziyadeh, 1995; Kanwar et al., 2008). In diabetic conditions, increased levels of glucose stimulate the production of TGF-β1 in the renal proximal tubule (Oldfield et al., 2001; Qi et al., 2007). Since the production of epithelial cell recognition and organisational proteins is regulated by TGF-β1, stimulation of the cytokine by glucose contributes to the reciprocal loss of tubular epithelial cells and accumulation of interstitial fibroblasts,

phenomena that are associated with reduced kidney excretory function (Zeisberg & Kalluri, 2004). Fibrosis involves an excess accumulation of ECM and usually results in loss of function as the normal tissue is replaced with scar tissue (Ban & Twigg, 2008). All patients with chronic renal diseases subsequently show a progressive decline in renal function. The process is largely irreversible and ultimately results to an end-stage renal failure.

1.6.2 EMT & E-Cadherin in DN

Upregulation of TGF-β1 in diseased renal states plays an important role during the EMT of renal proximal tubular cells (Hills et al., 2012b). The loss of epithelial characteristics in this process, such as the epithelia adhesion protein E-cadherin, is concurred with the acquirement of proteins that are associated with a mesenchymal phenotype. In addition, this process is culminated by reorganistation of the CSK and disruption of the tubular basement membrane. Loss of cell-to-cell adhesion, associated with reduced E-cadherin levels, represents a critical step in the early phenotypical and morphological changes of epithelial proximal tubule cells to fibroblasts (Zheng et al., 2009). Cadherins are adhesion proteins that have an important role in forming the multi-protein adherens junction (AJ) that links the extracellular domain to the actin cytoskeleton and other downstream signalling molecules, such as the phosphoinositide 3-kinase PI3K (Vaezi et al., 2002; Moreno et al., 2005). The extracellular domain mediates ligation with E-cadherin on adjacent cells, while the cytoplasmic domain binds to β-catenin, linking cadherin to the actin cytoskeleton via the catenins (Figure 1.8). Interaction of cadherin with F-actin not only increases the adhesive strength of the junction, but also acts as a signalling ‘hub’ for proteins that influence adhesiveness and/or initiate intracellular signalling. Co-localised with E-

cadherin and β-catenin at the sites of cell-to-cell contact, connexins are transmembrane proteins that connect the cytoplasm of adjoining cells and form gap junctions (GJs). Since intercellular adhesion precedes GJ formation and inhibition of cadherin-based cell adhesion is known to inhibit GJ assembly, it is reasonable to hypothesise that glucose-evoked increases in TGF-β would compromise cell communication and function in the proximal tubule (Hills et al., 2012a).

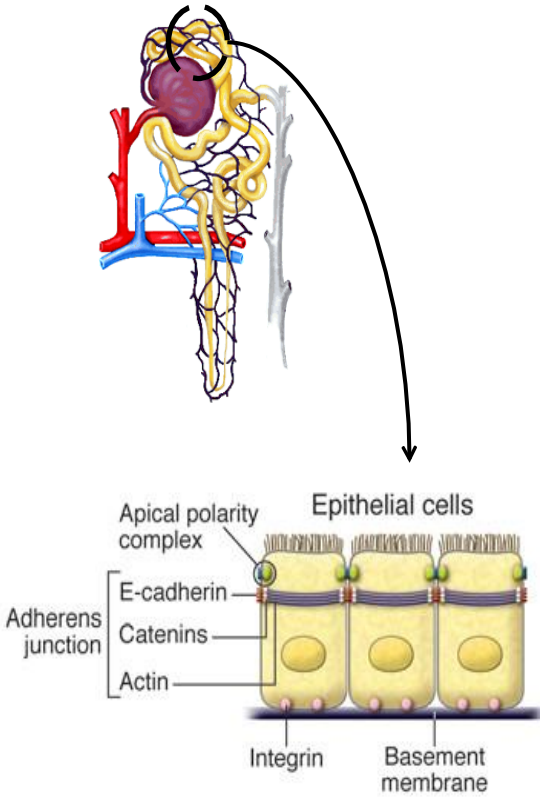

Figure 1.8 The adherens junction and the cadherin-catenin complex is crucial for cell-cell adhesion and facilitates cell communication via gap-junctions. Gap-junctions permit the direct transfer of small molecules and ions between coupled cells and their formation depends on E-cadherin based cell-cell adhesion. The pro-fibrotic cytokine TGF-β1 is associated with elevated glucose and it is important in many tubulointerstitial diseases where disassembly of the AJ represents the initial overt change

in epithelial organisation ahead of cellular migration associated with EMT. Image adopted from Hills, DUK 2012.

1.6.3 Renal Proximal Tubule Cells: The Human Kidney Cell Line (HK)2

The advantages and disadvantages of using a clonal cell line instead of primary tissue were discussed earlier (Skelin et al., 2010). HK2 cells retain functional characteristics of proximal tubular epithelium (Ryan et al., 1994). This cell line is an established model for studying diabetic nephropathy (Racusen et al., 1996). Panchapakesan et al. (2013) used the HK2 cell line to study diabetic drugs. Han et al. (2006) used HK2 cells to study the role of high glucose and angiotensin-II in the early progression of glomelular scleroses in DN. Tian et al. (2007) studied the effects of various growth factors, including TGF-β1, on HK2 cell migration following EMT. Slattery et al. (2005) investigated the complication of renal tubulointerstitial fibrosis after successful transplantation by stimulating the release of TGF-β1 in HK2 cells using cyclosporine A. Hills et al. (2009) studied reversed morphological changes of HK2 cells by blocking the fibrotic effects of TGF-β1 aiming to identify new therapy agents. In this project HK2 cells were cultured in monolayers and preserved at physiological temperature during AFM-SCFS experiments.

1.7 Aims & Objectives

Primary aim of this research project was to examine the biomechanical characteristics of soft biological cells, such as HK2 and MIN6 cells, in a quantitative manner. More specifically, the study will be focused on the application and development of AFM-SCFS technique to characterise cell-to-cell adhesion and single cell mechan-

ics, under chemical treatments that are associated with physiological and pathological biological phenomena. The main objectives were as follows:

- To perform AFM-SCFS experiments to examine cell-to-cell adhesion and single cell elasticity in two cell lines (MIN6 and HK2).
- To characterise E-cadherin mediated cell-to-cell adhesion in order to investigate the role of communication pathways, such as gap junctions, in (a) the coordination of insulin secretion of the endocrine cells, (b) the excessive concentration of fibrotic material in the proximal tubule.
- To characterise single cell elasticity in order to correlate differences in Young's modulus with the physiological/pathological conditions and elucidate the effects of elastic deformation, upon cytoskeletal reorganisation, on cell-to-cell adhesion.
- To investigate the effects of increasing pulling velocities and hence the effects of viscoelastic deformation on maximum unbinding forces and work or energy of detachment.

Chapter 2

AFM Single Cell Force Spectroscopy

2. AFM Single Cell Force Spectroscopy

The complex response of cells to a biochemical stimulus is a result of an integrated interplay between mechanical and adhesive properties. In this chapter the methodology of characterising single cell mechanics and cell-to-cell adhesion is described.

2.1 Introduction to Force Spectroscopy in Biology

Based on AFM technology, AFM Force Spectroscopy is a powerful tool for high resolution single cell force measurements. In general, AFM operates on the principle of mechanical interactions between the probe and the sample surface. Briefly, a piezo actuator moves the base of a cantilever towards the surface of the sample in the vertical direction and then retracts it again, while the deflection of the cantilever is measured continuously (Ikai, 2008). Typically, the dimensions of a tip for scanning a sample are in the nanoscale (tip radius 5-50nm), which results in extremely small tip-sample interaction forces (pN). A simple way to understand force spectroscopy measurements is to consider the movement of a cantilever, in contact mode, on a hard, incompressible surface in air. The schematic of this process is represented in Figure 2.1, in which the vertical tip movement during the approach and retract process for the measurement of *F-d* or simply force curves is illustrated. A force curve is the result of mechanical interaction between the tip of the cantilever and the surface of the sample. When the tip reaches the distance of a few tens of nanometers, the attractive forces due to the van der Waals forces between the tip and the sample, cause a weak attraction of the probe towards the surface of the sample. The cantilever is deflected downwards resulting in a small 'jump to contact' peak. As the distance between tip and sample decreases further, a stage is reached where the tip

touches the surface causing the cantilever to deflect upwards, resulting in an increase of the repulsive contact forces. When the cantilever is retracted from the sample the phenomena of adhesion occurs, in which the cantilever is still in contact with the sample. During this process the cantilever is deflected downwards, and adhesion can be detected in a force curve by a negative force peak. As the cantilever is further retracted from the surface, adhesion forces will be disrupted and the tip will be completely separated from the sample. Using spring stiffness the deflection of the cantilever provides information about the elastic properties of the sample and a direct measure of the adhesion forces.

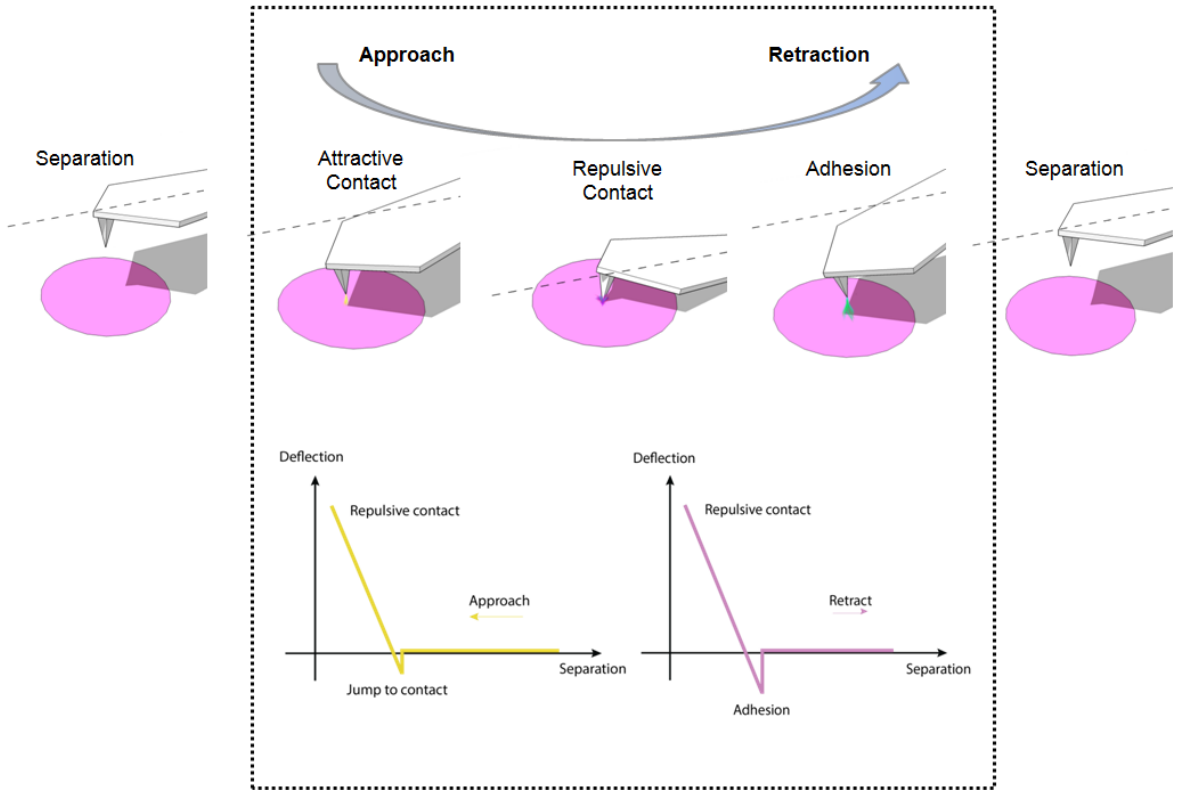

Figure 2.1 Schematic diagram of the vertical tip movement during the approach and retract process in force spectroscopy for the measurement of F-d curves. As the probe approaches within a few tens of nanometers, it comes into a regime of an attractive van der Waals forces. The probe is weakly attracted toward the sample surface and as it approaches closer to the sample, it enters in the repulsive realm of

Lennard-Jones potential, where the probe is strongly repelled from the surface. As the cantilever is retracted from the sample, the tip remains in contact with the surface due to interaction forces, and the cantilever is deflected downwards. At some point of retraction, the force required to disrupt the adhesion is reached. The attractive or repulsive forces can be measured by spring stiffness (Ikai, 2008).

However, unlike homogeneous hard samples, force spectroscopy of soft biological cells includes more complex interactions between the tip and the sample. Figure 2.2 shows a typical *F*-d indentation curve when indenting a single soft biological cell. The force curve includes compression of several cell's components, such as the membrane and CSK, hysteresis due to the viscous nature of the material and more complex adhesion between the tip and the sample. Due to the heterogeneity of a sample material, the gradient of a force curve changes as the sample is probed deeper and various structures of the cell are compressed. The depth of indentation has to conform to the specifications of the mechanical model, otherwise substrate effects may contribute to the determination of the mechanical properties. As the cantilever is retracted, a hysteresis phenomena is observed, which is common for viscoelastic materials such as cells. In addition, adhesion of the tip with long surface molecules requires an extended displacement range to avoid the issue of extendable contacts. Latest advancements of AFM-FS provide with an effective displacement range (100μm) that is sufficient to disrupt adhesion forces and facilitate the investigation of cell-to-cell contact. Another important consideration in AFM-FS experiments is the maintenance of biological cells in a physiological environment, which can be achieved by performing measurements in a fluid chamber. However, since force spectroscopy experiments have to be conducted in a liquid rather than air, the 'jump

to contact' phenomena is not observed, even in the case of hard samples. Instead, the force curve shows a gradual increase, which lacks the obvious sharp onset into contact. In fact, the contact point between the tip and the soft plasma membrane is difficult to define and requires the use of cantilevers with low spring constant (0.01-10 N/m) (Ikai, 2008). In addition, performing *F*-d curves in liquid results in adding external forces to the cantilever, due to the hydrodynamic drag and speeds less than 5μm/sec are recommended (Vinckier & Semenza, 1998).

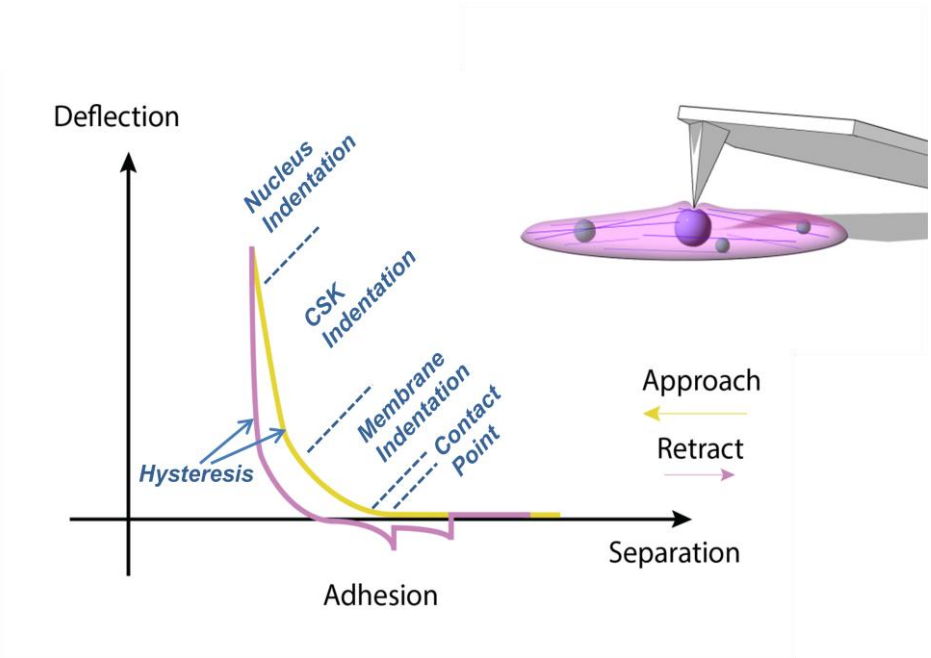

Figure 2.2 A schematic illustration of a single cell indentation and a representation of a F-d curve obtained from a single cell. Various elements of the cell are contributing to the overall determination of the E modulus. Special considerations regarding the depth of indentation and the fitting of the curve to a mechanical model needs to be taken into account according to the purpose of investigation i.e. whole cell elasticity, membrane or CSK elasticity etc.

Although AFM based nanoindentation is generally conducted by using a pyramidal tip, in several cases measurements of soft cells are conducted using spherical probes in order to avoid damage of the cell's membrane. Spherical probes commonly used for AFM-FS are typically in the μm range (1-11μm). Since, the purpose of this study is to use *E* modulus as a relative indicator between healthy and diseased treatments, the geometrical characteristics of the probe have been kept constant throughout the experiments. During cell-to-cell adhesion experiments tipless cantilevers were chemically modified so that a living cells can be attached at the free end of the lever. In this case, the attached cell was probing an adherent cell on the substrate in order to investigate the disruption forces between two cells. However, the adhesion process between two cells that are brought into contact is far more complex than the tip-cell contact, including several unbinding events, due to surface adhesion proteins involved in tethering as well as membrane tethers due to deformation during the cell separation process by pulling forces (Puech et al., 2006).

2.2 Hardware Overview

2.2.1 AFM-FS Instrumental Set-up

The primary aim of this project is to characterise single cell elasticity and cell-to-cell adhesion and to investigate the complex interplay between them. AFM-FS with an extended effective displacement range provides the core instrumentation to perform the long distance force spectroscopy experiments, required for this research, with certain modifications of the AFM cantilever. Figure 2.3 shows a schematic of the head of the AFM, designed to be used in combination with optical microscopy. Prior the experiments the cantilever is mounted on specially designed cantilever holder, an optical glass block. The glass block is chemically inert but very susceptible to

scratches, since it was polished on its top and bottom surfaces to allow the transmission of light to the objectives. Therefore, the polished surfaces should not be touched with tweezers and can only be used in buffer solutions as well as in low concentration bases and acids. The glass cantilever holder should only be cleaned while floating in an ultrasonic bath using mild detergents (2% Hellmanex solution, 5-10 min). The glass block is locked into the AFM head during force spectroscopy measurements, with the cantilever in a downwards direction. Therefore, the cantilever spring holder is also immersed during experiments. However, the glass holder can be immersed only until the upper edging of the opening in which the spring is inserted (4-5mm).

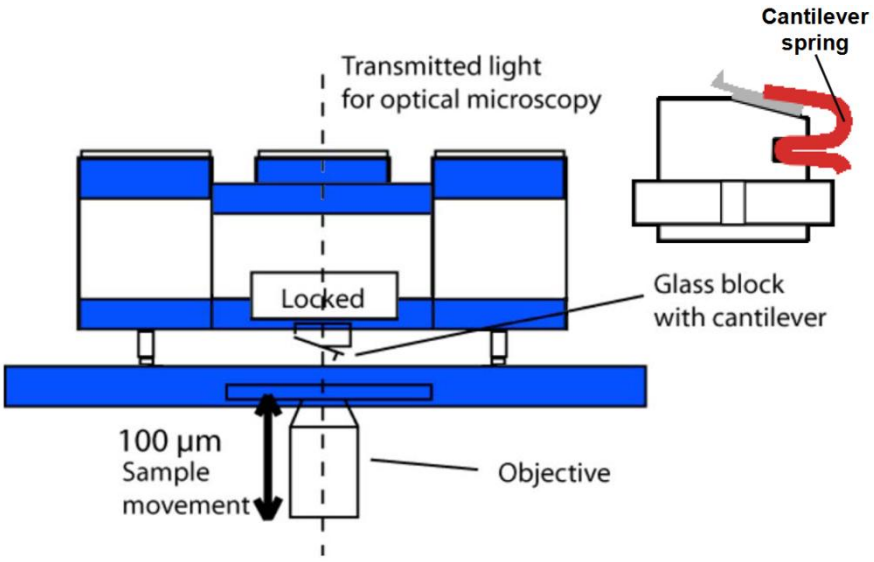

Figure 2.3 Schematic of an AFM head capable of long range displacement pulling (100µm) to facilitate long distance force spectroscopy i.e. complete separation of adherent cells during cell-to-cell adhesion experiments. The cantilever is mounted on the inclined part of the glass block holder using a spring. The incline of 10 degrees ensures that any contact between the sample and the holder will be prevented. The glass block remains locked on the AFM head during experiments. Image adapted from JPK instruments with permission.

The AFM head was integrated optically with a microscope. Figure 2.4 shows a photo of the complete system configuration. Experiments were performed using the Cell-Hesion®200 module (JPK Instruments, Berlin, Germany) that was installed on an Eclipse TE 300 inverted microscope (Nikon, USA). During each experiment, cells were maintained at a physiological temperature (37°C) by incorporating the Bio-Cell™ temperature controller (JPK, Berlin, Germany) into the AFM stage. Phase microscopy images were acquired using a CCD camera (DFK 31AF01 Firewire, The Imaging Source, Germany) connected on the side port of the microscope. The whole AFM-FS set-up with the CCD camera was driven by JPK's CellHesion200 software. Images were captured using a 20x magnification lens. Since such force measurements are extremely sensitive and susceptible to noise, vibrations and environmental conditions were well controlled. The entire optical microscope and AFM headset-up was supported on an anti-vibration table (TMC 63-530, USA). Changes in the temperature of the room were less than 0.5-1.0 ºC during experimental measurements. In addition, cables connecting the AFM head with the control station were firmly attached to the antivibrational table.

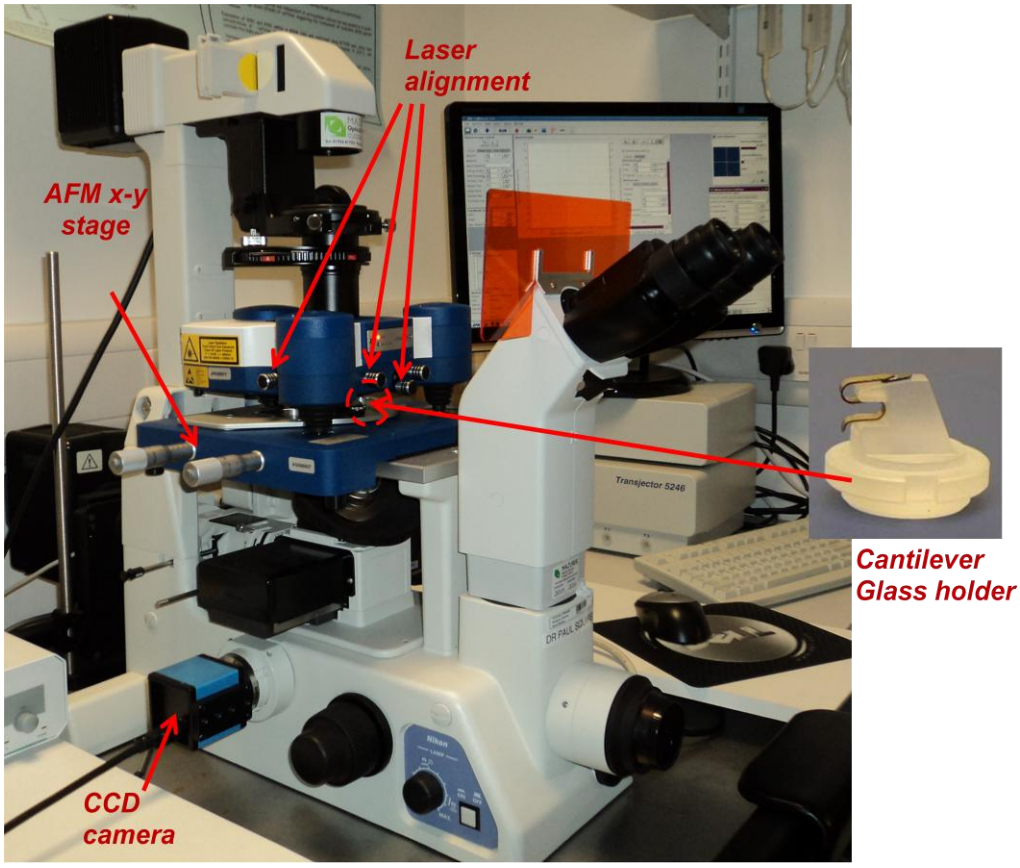

Figure 2.4 A photo of the instrument set-up showing the AFM head and stage mounted on a inverted microscope. A CCD camera was mounted on the left-side port on the microscope for monitoring the experiments. The cantilever glass holder is positioned on place by lifting up the AFM head prior the experiments. Once the cantilever is mourned on the head the alignment of laser can take place. After calibration of the cantilever the head must not be lifted nor the alignment of laser should be changed.

2.2.3 Set-up of the Optical Detection System - Laser Path Alignment

Force-extension curves can be compiled by measuring cantilever deflection as a function of the piezo-actuator position. Detection of the cantilever beam bending (deflection) is most important because the sensitivity of this operation is directly proportional to the value of the interaction force between the probe and the sample. To

date, various methods are available to detect beam deflection (Ikai, 2008), although the most popular method is by the use of an optical lever. In this set-up the magnitude of deflection itself is not recorded but the slope of the cantilever at the position where the laser beam is irradiated (Figure 2.5). This method utilizes a focused laser beam irradiated on the back of the cantilever into a quadric-sected photodiode. When the slope of the cantilever changes, the incident angle of the laser beam to the back of the cantilever is changed and consequently the direction of the reflected beam is also changed. The difference between the intensity of light going into the upper or lower parts of the photodiode gives the cantilever deflection.

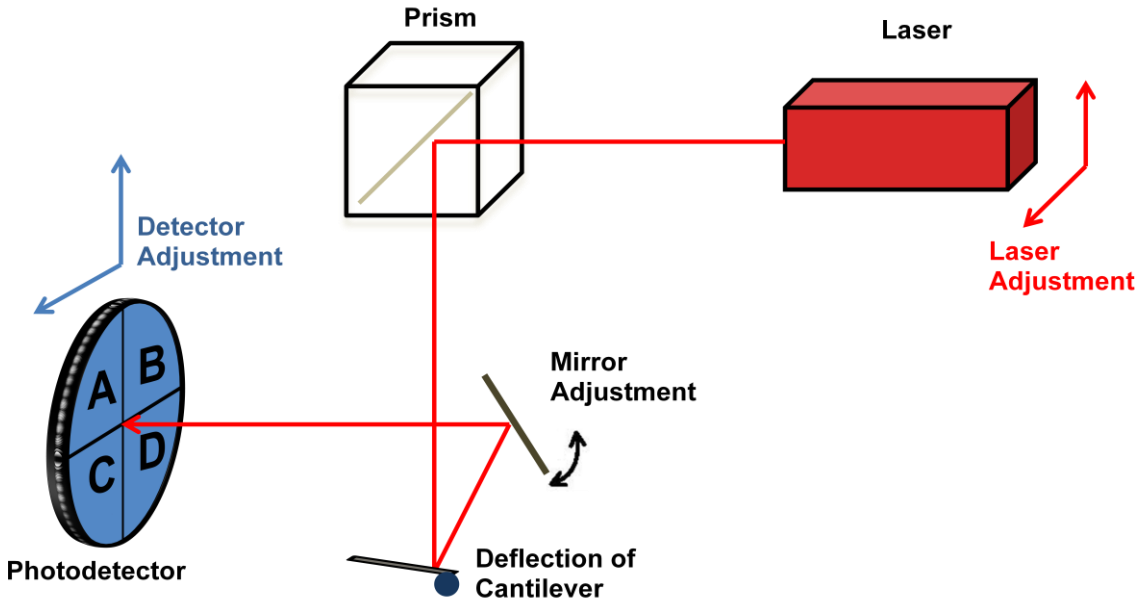

Figure 2.5 A schematic diagram showing the optical path of the laser. Initially the laser must be adjusted to get reflected from the end of the cantilever with the aid of the optical microscope. Then by adjusting both the mirror and the photodetector the laser spot must be adjusted to reach the centre of the photodetector to achieve maximum sensitivity.

Each time a new cantilever is mounted on the glass holder and the laser path has to be calibrated, since manual attachment of the cantilever onto the holder results in slightly different positioning. The first step for a proper alignment of the laser is to adjust the spot towards the end of the cantilever as shown in Figure 2.6. The illumination of the microscope can be decreased in order to ease the view of the laser onto the cantilever.

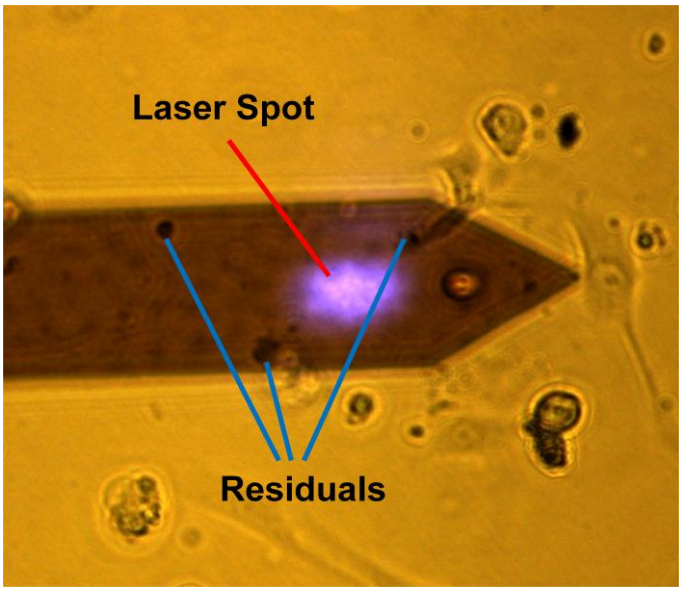

Figure 2.6 An optical image showing proper alignment of the infrared laser spot on a tipless functionalised cantilever. Any residuals left from the chemical modification will affect the sum value of the detector. As it can be seen from the photo soft cantilevers used for contact mode are relatively transparent.

When the optical image confirms that the laser spot is properly positioned onto the cantilever, the mirror should be adjusted in order for the laser beam to fall into the region of the photodetector. As soon as the beam is sent by the mirror to the detector a relatively stable sum value in volts will be generated by the vertical and lateral deflection of the cantilever. However, since the whole procedure is conducted in culturing media a small drift in sum value may appear. The mirror should be adjusted

until the maximum sum value is reached. Next, the detector should be adjusted until the spot hits the centre of the quadratic photodiode, meaning that equal light intensity is reached to each diode. This will result in the maximum sum value (>1V for silicon cantilevers) and will ensure sufficient sensitivity for the feedback control of the piezo actuator. The vertical and lateral deflection of the cantilever at this point should be close to zero with a small drift due to fluidic movements of the media. If, after proper alignment of the laser, the sum value is below 1V or in case there is a high drift in the deflection of the cantilever then a new cantilever or fresh media should be used. During cell-to-cell adhesion measurements where chemically modified cantilevers have to be used, it is important to choose a clean region for deflection. In some cases it may be necessary to wash the cantilever due to the potential risk of compromising functionalisation.

2.2.4 Selection of the Cantilever Sensor

The selection of the cantilevers is crucial for obtaining meaningful AFM-FS measurements. Several requirements need to be considered before selection, mainly arising from the nature of the testing sample and the experimental specifications. One special consideration is that during cell-to-cell adhesion experiments the probe that is attached to the cantilever is in fact a soft biological cell. While the cantilever-attached cell is probing the substrate cell, it is the deflection of the cantilever during extension or retraction that is being measured. Since the sample cells are from soft tissues/organs, the cantilever to which they will be attached must be soft enough for detecting changes i.e. it should have a low spring constant. Generally in cellular adhesion experiments of soft tissues, it is a rule-of-thumb that fragile biological samples require soft cantilevers. Moreover, the geometry of the cantilever must facilitate the

capture of a single cell. An arrow like geometry is designed to ease manipulation of a single cell among other cells in close proximity. Tipless cantilevers are more suitable for adhesion experiments since any contact of the tip with the surface of the cell or the substrate will disrupt the measurements. However, pyramidal cantilevers have been used for adhesion experiments in cases that AFM imaging was used as a complementary tool to force spectroscopy. This heavily depends on the size of the sample and the height of the pyramidal tip as any contact of the tip with the substrate/cell will interfere with the adhesion forces. Another major consideration for selecting the force constant of a cantilever is that during AFM indentation experiments the probe is initially in contact with a soft element, such as the plasma membrane, which may result in the disorientation of the contact point and difficulties in *E* modulus determination (A-Hassan et al., 1998). Determination of cell elasticity requires cantilevers with similar sample stiffness, i.e. very flexible, hence suitable cantilevers are those of contact mode with a low spring constant (0.01-0.06N/m) (Franz & Puech, 2008).

Arrow sensors (TL1, Nanoworld AG, Switzerland) are tipless cantilevers with force constant of 0.03N/m, which are suitable for special biological applications, such as attaching spheres or cells to the free end of the sensor. They are made from monolithic silicon that is highly doped to dissipate static charges. An arrow TL1 cantilever is shown in Figure 2.7. The chip of the cantilever serves as support for handling the sensor with tweezers when placed on the glass holder, during cleaning the cantilever's surface etc. The triangular free end of the cantilever serves as a tip or probe when a suspended cell or a microbead is attached at the very end.

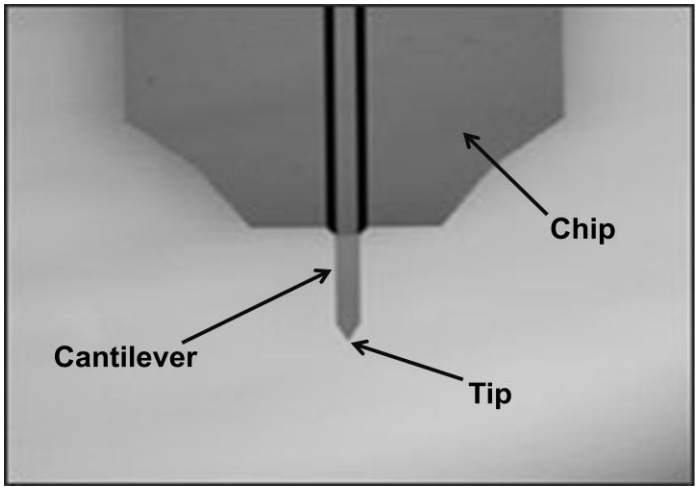

Cantilever Data	Value
Thickness	1.0μm
Width (rectangular part)	100μm
Length	500μm
Force Constant	0.03N/m
Pitch	250μm
Resonance Frequency	6kHz

Figure 2.7 An Arrow series rectangular tipless cantilever with a triangular free end, made from monolithic silicon for special applications, i.e. they can be used for attaching cells or spheres to the free end of the cantilever. The wide part of silicon is usually referred as 'chip', while the main of the cantilever has thickness: 1.0μm, width: 100μm and length: 500μm. At the end of the cantilever the tip can be seen where a cell or a microbead can be attached (Nanoworld Arrow™ TL1). Image adapted from NanoWorld Innovative Technologies, Neuchatel, Switzerland.

Cantilevers are expendable items and they are very susceptible to damage. The force constant should be calibrated each time before measurements and if there are discrepancies between the values provided by the manufacturer, the cantilever

should not be used. In addition, a cantilever that has been used for chemical modification for more than 2-3 times is likely to give low sum values at the photodetector, even if the laser path was aligned correctly. Residue on the cantilever can be removed by immersing the cantilever into a dish of sterilised water with alcohol or other mild detergent and then sonicated an ultrasonic bath for 5-10sec while inside the dish. However, the functionalisation of the cantilever will be compromised during this procedure and it is recommended to be performed only after the experimental measurements, prior storage of the cantilever. However, washing for more than 10secs can be detrimental for the force constant of the cantilever, and hence mechanical testing of the sensor in a hard surface in air after ultrasound cleaning is always recommended. After experiments, each cantilever should be irradiated with UV for 5-10 min to ensure that the surface is sterilised. For used cantilevers, optical inspection is necessary to certify that the surface of the cantilever is clean, apart from mechanical testing. Cantilevers with colloidal probes may suffer from sterilization issues since the ultraviolet (UV) treatment will dislocate the glued microbead. Therefore, it is critical to inspect the testing sample before measurements for bacteria, as well as minimise experimental times to avoid dilution of the plasma membrane. In general, any treatment on the cantilever is likely to cause changes in the spring constant values and therefore the cleaning procedure must be kept at a minimum level. Besides, cantilevers for mechanical testing of soft cells, such as the Arrow TL1, are very delicate and may be damaged by too high set-point values of force chosen for calibration or experimental measurements.

2.3 AFM Calibration

For small deflections the cantilever approximately constitutes a Hookean spring, therefore the deflection is linearly related to the acting force. If the cantilever spring constant is known, the deflection can be converted into the corresponding force causing the deflection (Ikai, 2008; Franz & Puech, 2008). Initially the deflection of the cantilever is displayed as the output of the photodetector in Volts. Before each experiment AFM cantilever must be calibrated, so that vertical deflection is converted from Volts in units of force (N). According to Hooke's law, the deflection (x) of the cantilever, considered as a spring with a defined spring constant *k*, is proportional to the force (*F*) between the cantilever and the testing sample.

$$F = kx \qquad \text{equation 2.1}$$

Initially the cantilever's vertical deflection, being the voltage difference between the different sections of the photodiode, is displayed in volts. Thus, the first step of cantilever's calibration is to determine sensitivity, or the distance of cantilever deflection for a given voltage difference measured by the photodiode. When this factor is known, cantilever deflection can be converted to distance (nm). Subsequently, by determining the spring constant of the cantilever, the deflection can be converted to force (N) (Franz et al., 2007).

2.3.1 Measuring the Sensitivity

Sensitivity depends on many parameters, such as the type of the cantilever and the mounting position of the cantilever on the AFM head. Therefore, it should be determined every time the cantilever is mounted or remounted. To determine sensitivity, it is necessary to perform a *F*–d curve on a stiff surface, such as clean glass, in order to achieve a robust approach. It is crucial that this measurement is performed in the same medium (buffer solution) and temperature as in the actual experiments. Therefore, a clean petri dish with fresh PBS solution at 37ºC was used for performing a force curve. The deflection signal is then analyzed in the repulsive contact region, which rises steeply upwards, and is linear for a hard surface and a tip. This measurement is the deflection of the tip in nanometers for a given movement of the detection laser on the photodetector. As a consequence, sensitivity strongly depends on the reflective characteristics of the cantilever as well as on the AFM laser system used to detect the cantilever deflection (Franz et al., 2007; Friedrichs et al., 2010). Figure 2.8 illustrates a *F*-d curve from a contact mode Arrow TL-1 cantilever on a clean petri dish surface under aqueous buffer solution (PBS) at 37ºC. This curve represents raw data and the cantilever deflection is displayed in volts. By calculating the sensitivity deflection can be converted into distance (nm). Typical sensitivity values, as given by the manufacturer, are in the range 30 - 100nm/V.

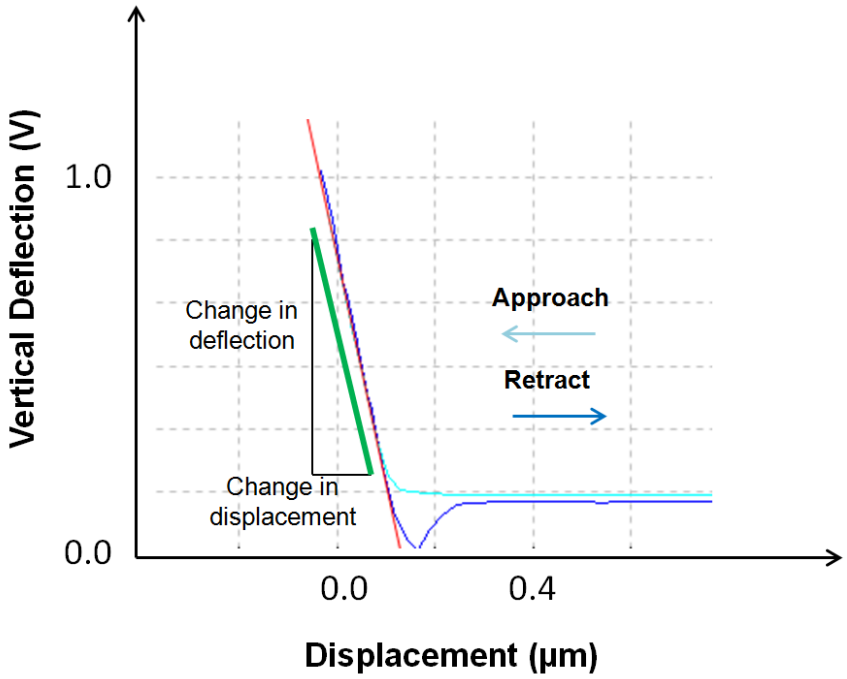

Figure 2.8 Measurement of force curve on a hard substrate (clean petri dish) in PBS solution for calibration. The linear part of the curve is chosen for the calculation of the gradient of the line. Here, the sensitivity is 55.3nm/V.

2.3.2 Spring Constant Calibration in Fluid using the Thermal Noise

Most manufacturers deliver data sheets to specify a nominal spring constant for a given cantilever. In general the value is given as a range, and usually it is calculated by the average cantilever geometry (length, width, thickness). Particularly, spring constant values are most affected by the thickness of the cantilever, which is difficult to control during the fabrication process. Hence, spring constants deviate from their nominal value and each cantilever has to be measured individually before experiments. In general, the true spring constants of cantilevers frequently differ from the nominal values by a factor of up to 3, and in most cases the range of spring constants supplied by the manufacturer gives some idea of the variability (Franz et al., 2007; Friedrichs et al., 2010).

Most AFM systems provide a software option to measure the spring constant of cantilevers based on the thermal noise method. This method measures the thermal fluctuations of the cantilever deflection and uses the equipartition theorem to calculate the cantilever spring constant. Essentially, the theorem equates the thermal energy at a given temperature with the energy within the oscillation of the cantilever. The assumptions and conditions of these calculations are described by Hutter & Bechhoefer (1993), and it can be argued that other calibration methods are more accurate. However, the thermal noise method still remains the most versatile and implementable method of cantilever calibration, as it can be performed *in-situ* using software analysis with no extra costs or equipment (Franz et al., 2007; Friedrichs et al., 2010). A study by Burnham et al. (2003) suggested that for silicon cantilevers with well defined geometry, 17% of the calculated calibration values agree with the nominal value of the manufacturer, regardless the calibration method. By calibrating all the cantilevers with a particular method, results are kept consisted and comparable within the studies where the effects of chemical agents on mechanics are examined.

Measuring of spring constant using the thermal noise is most suited to soft cantilevers where the free fluctuations due to thermal energy are more significant. The sensitivity measurement is the first stage in the thermal noise measurement of the cantilever spring constant. An example of a thermal noise measurement is shown in Figure 2.9. For a given temperature, the amplitudes of the fluctuations depend only on the spring constant of the cantilever; hence the thermal resonance curve can be fitted to a Lorenz function to allow spring constant calculation (Hutter & Bechhoefer, 1993). However, the resonance of soft cantilevers in fluid is much lower and very

susceptible to noise due to drifting of the cantilever. Nevertheless, the nature of living cells usually dictates that the experiments should be conducted in an aqueous buffer solution (PBS, DMEM etc). In this case the procedure of measuring a spring constant is slightly different and a correction factor should be used to calculate the true value of the spring constant (Butt & Jaschke, 1995). There are various sources of error when using the thermal noise spectrum for the determination of the spring constant. The sensitivity is obtained by the measurement of a static and relatively large deflection of the cantilever in comparison with the bending of the cantilever during dynamic oscillations. Also, when using cantilevers for soft biological material in liquid the first resonant peak is largely affected by low frequency noise. In that case, the second peak should be used as long as a different correction factor is considered. Table 2.1 shows the correction factors for rectangular cantilevers as described by Butt and Jaschke (1995). These factors compensate for the difference of the bending shape between the sensitivity determination and thermal noise fluctuations. For that reason calibration is largely affected by the position of the laser spot on the cantilever and the procedure of laser path alignment should be consistent between experiments. Differences in geometry between the cantilevers also affect the analysis of thermal noise. A more accurate calibration requires further minor corrections for hydrodynamic drag differences that arise from geometrical discrepancies between the cantilevers. In general, different batches of cantilevers may result in different calculations of the spring constant. Therefore, the results from the same type and batch of the cantilever must be compared, so that consistency between measurements can be maintained. In special cases where comparison of *E* modulus between physiological versus pathological conditions is required, the same cantilever can be used across all measurements. However, for cell-to-cell adhesion measurements, where

the cantilever is subjected to chemical modification, this is not possible since a cantilever can be functionalised for not more than three times.

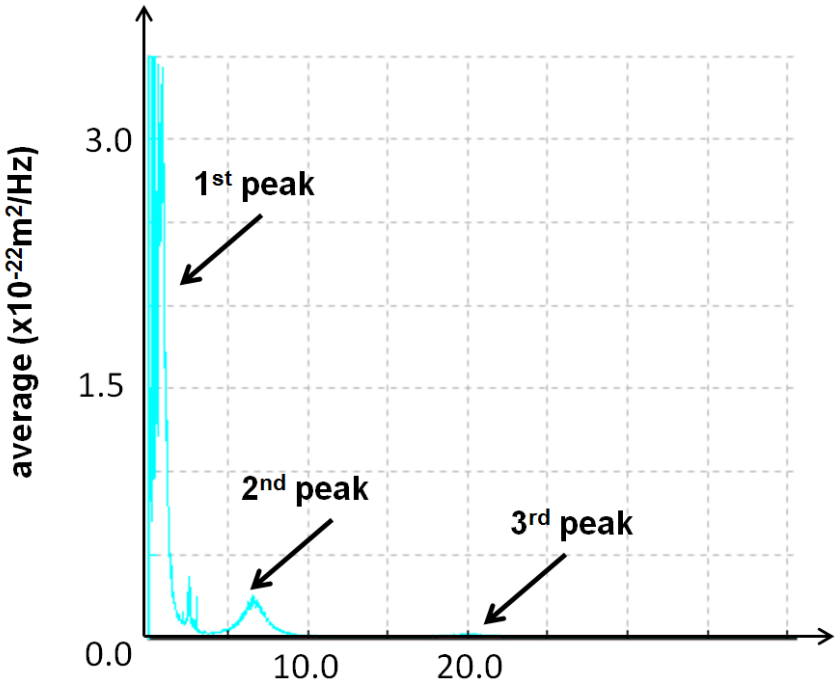

Figure 2.9 Free fluctuations are plotted against frequency for the thermal noise measurement of an Arrow TL-1 contact mode cantilever in fluid. Three resonant peaks, corresponding to the resonance at around 1kHz, are shown. Both phase and amplitude are reduced with comparison to the spectrum in air. The second peak was used to determine the spring constant by the use of a correction factor. The calculated value was 0.0206N/m, whilst the nominal value provided by the manufacturer is 0.03N/m.

Table 2.1 Correction factors for rectangular cantilevers as suggested by Butt and Jaschke (1995).

Peak	Correction Factor	Comments
1	0.817	Generally used
2	0.251	Used when first resonance frequency is noisy or too low
3	0.0863	Not generally used

2.4 Tissue Culture

Treatment of cells was focused upon two research questions; could an enhanced functional tethering via E-cadherin improves secretion responsiveness of pancreatic β-cells, and could TGF-β1 induced EMT instigates a loss of cell-to-cell adhesion via E-cadherin in the proximal nephron during diabetic nephropathy? Two established cell lines (MIN6 and HK2) were used as models to represent the primary functions of tissues under physiological and pathological conditions. Tissue culture was performed by Dr. Claire Hills at the School of Life Sciences in the framework of my collaboration.

2.4.1 Culture of HK2 Cells

HK2 cells were purchased from the American Type Culture Collection (ATCC; Gaithersburg, MD 20878 USA). Recombinant human TGF-β1 was obtained from Sigma (Poole, UK). Fibronectin was obtained from Sigma. Tissue culture media and plastic ware were from Invitrogen Life Technologies (Paisley, UK). Immobilon P

membranes (Millipore, Watford, UK), ECL detection reagents (Amersham Biosciences, Buckinghamshire, UK) and anti-fade Citifluor (glycerol/PBS solution: Agar Scientific, Essex, UK) were also obtained. For preparation of compartmental protein a Qproteome kit was obtained from Qiagen (Sussex, UK).

HK2 cells (passages 18-30) were maintained in DMEM/Hams F12 (DMEM/F12) medium, supplemented with 10% fetal calf serum (FCS), glutamine (2mM), and EGF (5ng/ml). Cells were seeded onto 40mm petri-dishes and cultured at 37^{o}C in a humidified atmosphere of 5% CO_2 in air**.** Prior to treatment, cells were cultured in DMEM/F12 low glucose (5mM) for 48hr. Basal (5mM) glucose culture media was generated as described previously (Hills et al., 2009). For all experiments, cells were cultured in low glucose containing un-supplemented DMEM/F12 medium for 48hr. Cells then treated with TGF-β1 (2-10ng/ml) for 48hr. In all experiments, cells were serum starved overnight before agonist stimulation.

2.4.2 Culture of MIN6 Cells

MIN6 cells were obtained from Dr. Y. Oka and J.-I. Miyazaki (Univ. of Tokyo, Tokyo, Japan). DMEM, glutamine, penicillin-streptomycin, gelatin (from bovine skin), PBS, foetal bovine serum and trypsin-EDTA were from Sigma-Aldrich (Poole, Dorset, UK). Tissue culture media and plasticware were from Invitrogen Life Technologies (Paisley, UK). Immobilon P membranes (Millipore, Watford, UK), ECL detection reagents (Amersham Biosciences, Buckinghamshire, UK). The calcimimetic R568 was granted from Amgen Inc (Thousand Oaks, CA, USA). BrdU, Alexa secondaries and Alexa Fluor 594 conjugated anti-BrdU were from Invitrogen (Molecular Probes, Eugene, Oregon, USA).

MIN6 cells (passage 35-40) were maintained at 37°C in a humidified atmosphere of 5% CO_2 in air, in DMEM supplemented with 15% FCS, glutamine (2mM) and penicillin/streptomycin (100U/ml/0.1mg/ml). Cells were split when 80% confluent, about every 3-4 days using Trypsin-EDTA. Prior to treatment, cells were seeded onto 40mm petri-dishes and serum starved overnight. Cells were then placed for 48hrs in DMEM containing both low glucose (5mM) and low calcium (0.5mM) +/- the calcium mimetic R568 (1μM) (Hills et al., 2012b).

2.5 Single Cell Force Spectroscopy for Cell-to-Cell Adhesion

In Single Cell Force Spectroscopy (SCFS) adhesion experiments a suspended cell is attached on chemically functionalised cantilever in order to be used as a probe to an adherent cell on the substrate or to any other sample substrate. Several experimental parameters, such as contact force and time, have to be considered and adjusted experimentally. Once those parameters were identified they were kept constant throughout the measurements for each type of cells. The contact force determines the force that is applied by the cantilever-cell probe to an adherent substrate cell. Higher contact forces result in a larger contact area and number of surface ligations. However, compression of the cells is larger with higher contact forces that results in flattening of the cell attached to the cantilever after a few measurements. Once the two cells are in contact, surface bonding is formed. The contact time is critical to this process since the cells tend to interact more with each other by increasing the number and strength of their adhesion molecules. Extended contact times may lead to insufficient pulling range for complete separation, inadequate detection area due to extreme beam bending and detachment of the cell from the cantilever due to higher

cell-to-cell adhesion forces than the cantilever-cell. Inevitably adhesion between cells strongly depends on contact force and time, hence several preliminary measurements were necessary. In addition, the determination of pause time between successive measurements is mainly based on contact force and time. Strong interactions between cells may require recovery times of several minutes, resulting fewer measurements. Visual inspection of the cantilever-cell is required between consecutive measurements.

2.5.1 Functionalisation of Cantilevers with Fibronectin

Tip-less cantilevers were chemically functionalised so that a single suspended cell could be attached. There are different methods of cantilevers functionalisation for different experimental set-ups. Weder et al. (2009) incubated TL-1 cantilevers in biotin-labeled concavalin A solution to achieve strong cell-cantilever bonding for Saos-2 cells. Since the method of functionalisation depends on the type of cells, preliminary experiments had to be done to investigate which protein binding suits HK2 and MIN6 cells. Poly-L-lysine (PLL) and fibronectin (Fn) are adhesion molecules that are widely used for promoting attachment of cells to culturing plastics. PLL is a polyvalent cation that alters the electrostatic charge of the surface and provides a coating that enhances the attachment of Fn. The Fn protein, independent of the culture conditions of the sample cells (unpublished data), binds to integrins and ECM. Various coatings, incubation times and temperatures were investigated. For both HK2 and MIN6 the attachment of cell to the cantilever was more stable when a layer of PLL was applied to the surface of the cantilever. Figure 2.10 shows a schematic of the elements of functionalisation on a tipless cantilever in contact with the plasma membrane. Initially the cantilevers were sterilised by UV treatment (10mins). Next, they

were incubated in poly-L-lysine (25μg/ml in PBS) for 30mins in room temperature (RT). Subsequently, the cantilevers were transferred in fibronectin solution (20μg/ml in PBS) and they were incubated for 2h at 37°C. After functionalisation cantilevers were stored in PBS solution at 4°C and used within 3 days.

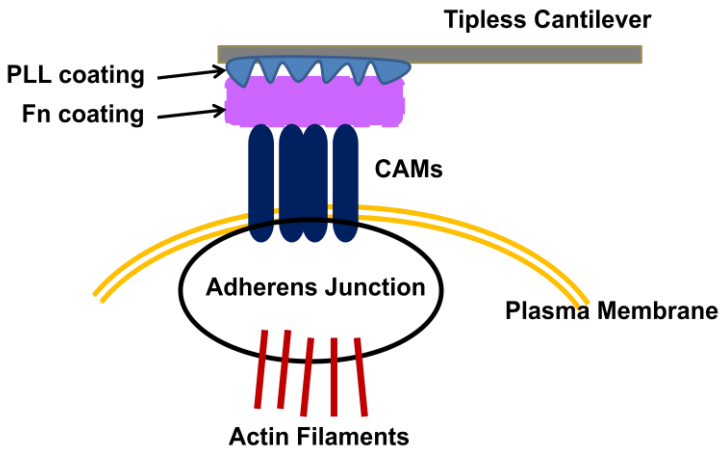

Figure 2.10 Schematic design of the elements functionalising a tipless cantilever. The surface of the cantilever is first coated with PLL (25μg/ml in PBS, 30min in RT), which promotes the attachment of Fn molecules. The cantilever was next incubated in Fn solution (20μg/ml in PBS, 2h at 37°C), and finally brought in contact with the membrane of a suspended cell. Molecules in the surface of the cell that are involved in adhesion readily attach to Fn in the extracellular domain, while in the intracellular domain they are connected with actin filaments through adherens junction.

When the cantilever is in touch with a suspended cell, Fn forms an attachment with the adhesion molecules at the surface of the cell. The method of functionalisation can be tested by the coarse moving of the cantilever-cell. This will indicate whether or not the cell is firmly attached to the cantilever. In general, if the method of functionalisation is not appropriate for a specific cell type, the surface of the cantilever for attachment will be rejected by the suspended living cell. In addition, a suspended

cell may be forced, by using high force and contact time settings, to attach to the cantilever, but remain unstable i.e. moving on the cantilever. In this case the functionalisation method needs to be revised since the cell-cantilever attachment is weak and a serious error in cell-to-cell adhesion measurements will be introduced.

2.5.2 Preparation of Suspended Cells - Scrape Delivery Procedure

The suspended (free) cells must be prepared in an identical chemical treatment as the substrate cells, however they must be released from the plastic culture surface prior the experiments. There are a number of points to be considered when preparing cells that will be attached to the cantilever. A key point is how the cells will be released from the substrate in which they are cultured. The cells can be detached by incubation with trypsin or other gentle cell detaching enzyme mixtures in the absence of any divalent metal ions. However, enzymatic digestion leads to the cleavage of proteins of the cell surface. Some of these membrane proteins may be involved in the adhesion process, therefore this method will seriously affect the experimental measurements when a specific adhesion protein is to be investigated. Incubation of cells in the absence of Ca^{2+} and Mg^{2+} will also release the cells from the substrate, although this might not be possible due to special experimental specifications i.e. treatment with Ca^{2+}. If this is not possible, cells can be gently scrapped off the substrate. Both HK2 and MIN6 monolayer cells were seeded onto T25 flasks for 80% confluence. They were sub-cultured overnight in serum-free media in T25 flasks.

In this project, the cells were gently scrapped off from the flask using a sterile cell scrapper with a rubber blade and a low-force sweeping motion (manufactured for minimum damage of the cells). The use of a flask instead of a petri dish has a con-

venient size for scrapping off the cells. Cells in petri dishes could not be effectively scrapped. Then the scrapped cells were transferred using the pipette on a sterile flask for centrifugation. After harvesting by centrifugation the medium was removed and replaced with sterile DMEM CO_2 free media. The use of CO_2 independent media was necessary since SCFS experiments were performed in an instrument that is not equipped with a CO_2 chamber. The cells were re-suspended by gently agitating up and down five times using the pipette. Gentle pipeting breaks up sheets of cells to give a uniform distribution of the non-adherent cells in the flask. Cells were allowed to recover for 5 mins and were introduced to the testing chamber. This procedure was kept consisted for all experiments in a set.

2.5.3 Single Cell Attachment

Suspended cells were introduced into the petri dish using a pipette. Since free cells tend to stick on the substrate quickly, it was important that the cell-cantilever attachment procedure was performed rapidly (within 2-5min). To reduce the likelihood of suspended cells re-attaching to the base of the dish rather than the cantilever, an anti adhesive coating (trypsin) had been applied to an area of the dish prior to culturing the cells on the petri-dish. With the aid of optical microscope the cantilever was pressed against a single free cell by performing a force curve. The set-point force and contact time was 1-1.5nN and 8-10secs for HK2 cells while for MIN6 cells it was 0.5nN and 5secs. During the contact time, it was preferred to set the instrument in a constant force mode, in which the applied force was kept constant by adjustments of the piezo-actuator height. Once a single cell was attached to the cantilever, it was left to recover for at least 5 mins (Friedrichs et al., 2010). Figure 2.11 (a) shows a single HK2 and (b) MIN6 cell attached to a fibronectin coated cantilever. Calibration

of functionalised cantilevers was performed before attaching a cell. To record a force curve for calibration, the cantilever was approached to a hard surface only once to minimize the loss of coating (set-point 2V).

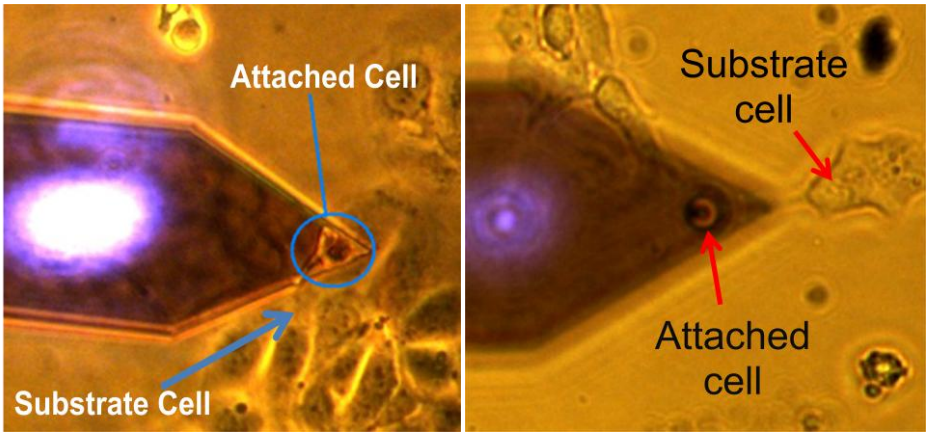

(a) (b)

Figure 2.11 Phase contrast images of(a) a single HK2 and (b) MIN6 cell attached to a TL1 arrow tipless cantilever. The cantilever-cell was brought in contact with a substrate cell and a predefined contact time it was retracted to investigate functional tethering between two cells. Width of the cantilever (rectangular part): 100μm. Note the laser spot (purple) used for measuring the deflection of the cantilever.

2.5.4 Cell-to-cell Adhesion Measurements

The cantilever-attached cell was brought in contact with another cell attached on the substrate, until a preset contact force was reached (1nN for HK2 and 0.5nN for MIN6 cells). The two cells remained in contact for a set period of time (10secs for HK2 and 5sces for MIN6). During this time bonding between cells was formed. The cantilever was then retracted at a constant speed (5μm/sec) and force versus displacement was measured until the two cells were completely detached (pulling length 60-80μm). The procedure was repeated three times for each tested cell, with 30s inter-

vals to allow the cells to recover. Based on the experimental specifications as well as the type of cell, a single cantilever-attached cell was used to perform measurements on maximum 10 cells, before getting flattened on the cantilever.

A force displacement curve from the retraction movement of the cantilever during a cell-to-cell measurement is shown in Figure 2.12. In the flat region of the curve (phase 1), there is no deflection of the cantilever to the photodiode since there is no contact between the cantilever-cell and the substrate-cell. As the cantilever is moving downwards towards the substrate cell, phase 2 is reached where the two cells are in contact and the cantilever deflects according to the predetermined force value. The piezo-actuator will remain static in that position for the set contact time. Then the cantilever is retracted (phase 3) and multiple unbinding events cause bending of the cantilever. As the cantilever is retracted further away from the sample bonding is disrupted, until phase 4 is reached in which the cells are completely detached. Retraction *F*-d curves provide important information regarding the adhesion between two cells, such as the energy or work of complete detachment, the maximum unbinding force, the distance of complete separation and the number of unbinding events. Maximum unbinding force, F_{max} is the maximum force required for the complete detachment between two cells. F_{max} can be determined by the minimum force value in phase 3 of the retraction curve. It corresponds to the difference between the highest negative deflection of the cantilever and the point of complete separation (baseline value). The total energy that is consumed until the two cells are completely detached, during phase 3 until phase 4, can be determined by the integration of the retraction curve, and is generally known as energy or work of detachment W_D. The pulling length from the highest negative deflection of the cantilever (phase 3) and the

point of complete separation (phase 4) represents the distance of complete separation d_s between two cells. Unbinding of ligations during the pulling phase mainly falls in two areas, those events in which a ramp in the deflection of the cantilevers is preceded ('*j*' events) and those which a deformation of membrane tethering is preceded ('*t*' events). Retraction *F-d* curves acquired during cell-to-cell adhesion experiments typically exhibit a step-like pattern that is resulted from the rupture of surface ligations. In the early part of the retraction curve complex unbinding events occur, while as the pulling distance increases a plateau in the displacement indicates that membrane tethering extrudes rupture of ligation (Friedrichs et al., 2010).

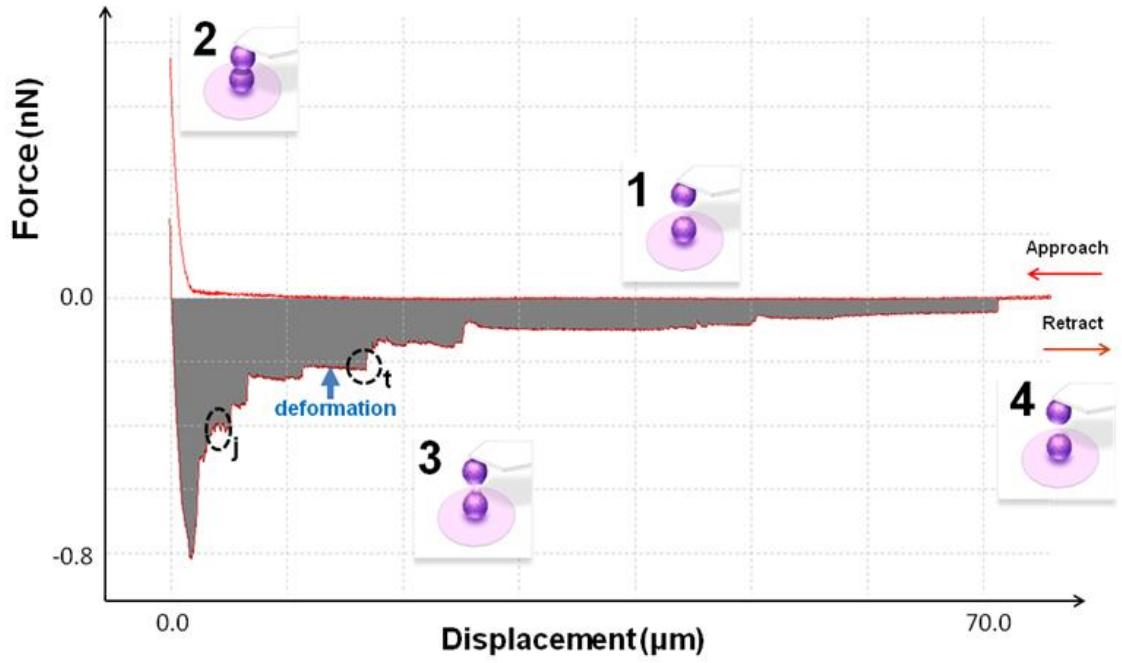

Figure 2.12 A force distance curve of two MIN6 cells that are brought in contact.Initially the cells are bounded into a cantilever and the substrate (phase 1). Then they are approached to each other, and after a short period of contact the two cells are attached. During this time bonding is formed (phase 2). Next, the cantilever is retracted and force versus displacement is measured (phase 3) until they are completely detached (phase 4). Based on the *F-d* retraction curve adhesion parameters

can be determined including maximum force of detachment from the highest negative deflection of the cantilever, work of removal from the area under the curve and distance of complete separation from maximum pulling range before separation. In addition unbinding steps that correspond to ligation rupture can be determined. Steps in the initial part of the curve, such as in 'j' area, are followed after a bond rupture while 't' steps are followed after a deformation of membrane tethering.

2.6 Single Cell Force Spectroscopy for Single Cell Elasticity

In AFM indentation the vertical deflection of a cantilever is measured as a function of the piezo-actuator height, in order to produce force-displacement curves and calculate the *E* modulus of the sample. The position of the piezo-actuator, after the contact point, corresponds to the indentation depth of the testing sample. Therefore, it is assumed that a force-displacement curve represents a force-indentation depth curve. However, the piezo-actuator movement during indentation does not represent the actual depth of indentation, due to the bending of the cantilever against a sample in the opposite direction of the indentation. As a consequence, an error is induced in the displacement axis *z* of the experimental measurements, since the indentation depth δ is deeper than it actually is. The experimental indentation depth δ measured using AFM is,

$$\delta=\delta_{\text{deflection}}+\delta_{\text{indentation}}$$

$$z=\delta+x \text{ (Figure 2.13a)}$$

In fact, this is a source of a error in the determination of elasticity when a mechanical model, such a Hertz theory, is applied to the experimental *F*-d curves. It is therefore

important to correct the experimental data before fitting the curves to a model (Figure 2.13(b)).

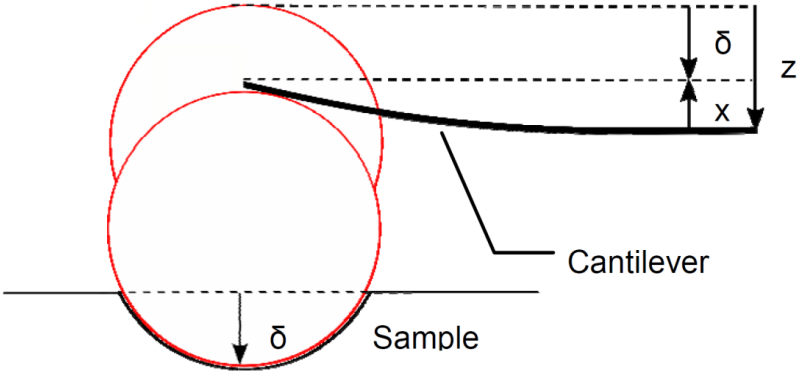

(a)

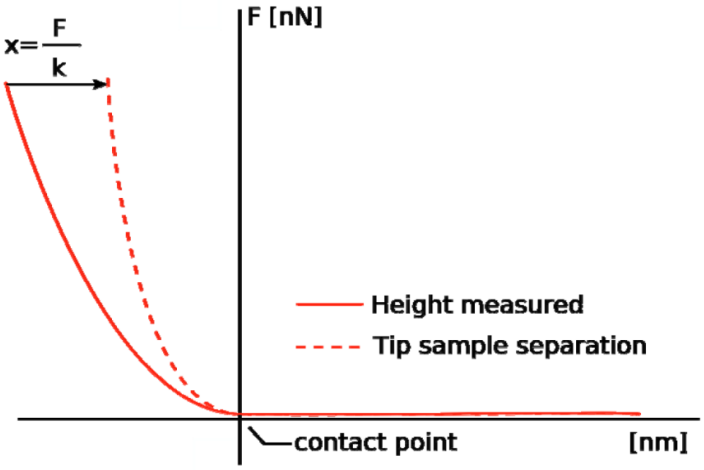

(b)

Figure 2.13 Schematic diagram of a single cell indentation experiment. (a) The displacement z of the piezo-actuator includes both the indentation height δ and the deflection of the cantilever x. (b) The deflection of the cantilever x, must be subtracted from the z height measured during AFM indentation. The corrected tip-sample-separation curve represents the actual F-d curve that can be used for calculation of elasticity. Image adopted by JPK instruments with permission.

2.6.1 Colloidal Probe Preparation

Spherical probes for measuring mechanical properties of soft biological samples are commercially available in precise monodisperse particle size distributions. Polystyrene microbeads are chemically inert and commonly used for biological studies. Tipless cantilevers can be modified with spherical indenters of 1-10μm in diameter. Colloidal probes were prepared by gluing an 10μm polystyrene microsphere (Polybeads ®, Polysciences, Eppelheim, Germany) on a tipless TL-1 cantilever. Microspheres are packaged as an aqueous suspension with a minimum amount of surfactant. Part of the stock was diluted in distilled water and vortexed using a pipette to eliminate aggregation. Besides, bead aggregation can be minimised by increasing the temperature of the dilution using the temperature controller of the AFM stage. Initially the microspheres were placed on a glass coverslip, which was positioned on the fine stage of the AFM. The coverslip was cleaned with ethanol and dried by air, and a drop of the bead stick was transferred on the surface of the glass using a fine pipette. A mixture of clusters and single beads is shown in (Figure 2.14).

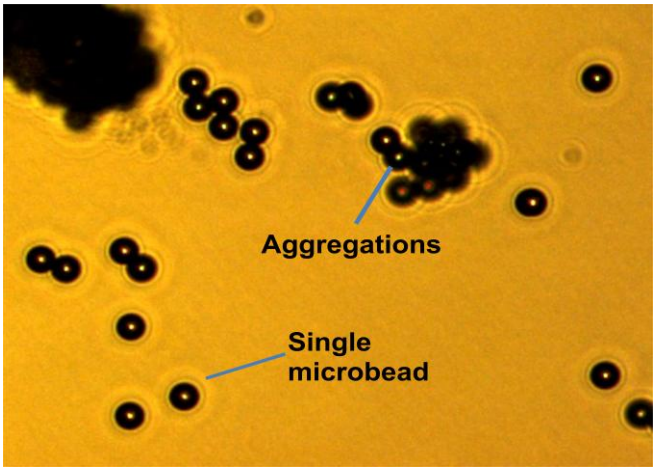

Figure 2.14 Single and clusters of Polystyrene microbeads on a glass coverslip. The mean diameter of the bead is 10μm with coefficient of variance ≤10%.

The procedure for mounting the microbead into the tipless cantilever is similar to that described by Carl & Schillers, (2008). In brief, after mounting the cantilever into the AFM head and perform alignment of the laser, the attachment procedure was as follows; a small amount of two-part fast setting (5mins) epoxy glue was poured using a syringe next to the microspheres. In a short time period, an approach curve was performed to slightly immerse the end of the cantilever into the glue with a relatively low setpoint (<0.5V). The cantilever was then swept along a clean area of the coverslip to remove excessive glue. Finally, using the stage positioning screws the tip of the cantilever was positioned directly above a microsphere and an approach curve was performed until contact was made. A setpoint of 1-1.5V and a contact time of 3-5secs was necessary for the bead to be attached. It is very important not to creep the cantilever, when in contact with the sphere, to avoid slipping of the glue over the probing surface. The whole procedure was facilitated with the use of the inverted optical microscope. Figure 2.15 (a)-(b) show optical images of a 10μm polymeric bead attached to a tipless cantilever.

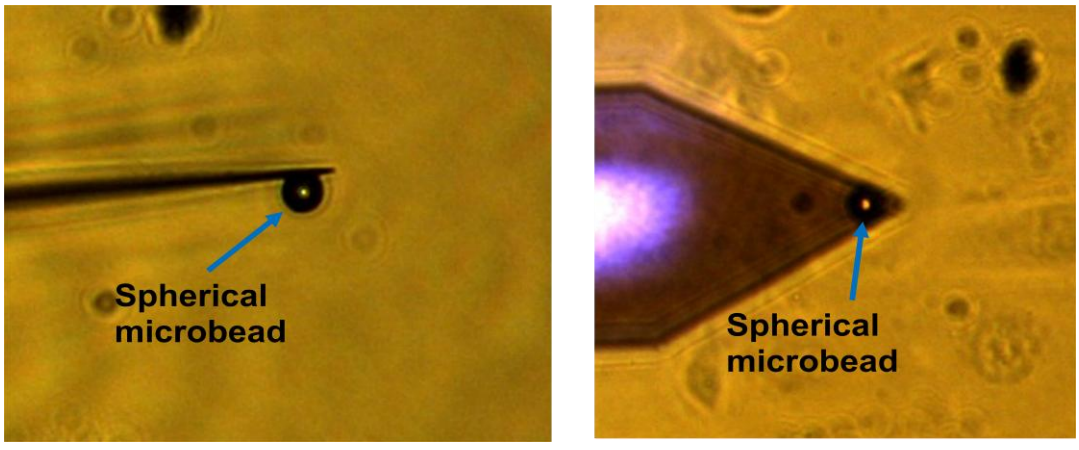

(a) (b)

Figure 2.15 A spherical polystyrene microbead of 10μm in diameter attached on the very end of an Arrow TL-1 tipless cantilever. (a) An optical image showing the side

view of the microsphere attached to the tip of the sensor. (b) An optical image showing the top view of the cantilever-bead and KH2 cells on the substrate.

2.6.2 Calculation of Elasticity using the Hertzian Mechanics Model

The Hertz model is commonly used to extract the elastic or Young's modulus from a force-displacement curve acquired by indentation measurements. Although this model is widely used for biological samples, there are several assumptions that need to be considered in order to match certain experimental conditions. Different indenter geometries lead to different radius of contact area α, therefore different extensions of the original model must be used. As shown schematically in Figure 2.16, for spherical probes, loading force *F* is related to indentation depth δ as follows,

$$F = \frac{E}{1-v^2}\left[\frac{a^2 + {R_S}^2}{2}\ln\frac{R_S + a}{R_S - a} - aR_S\right] \qquad \text{Equation 3.2}$$

$$\delta = \frac{a}{2}\ln\frac{R_S + a}{R_S - a} \qquad \text{Equation 3.3}$$

where *E* and *v* are the Young's Modulus and Poisson's ratio of the cell respectively, α is the radius of probe-cell contact circle, and R_S is the radius of the spherical probe.

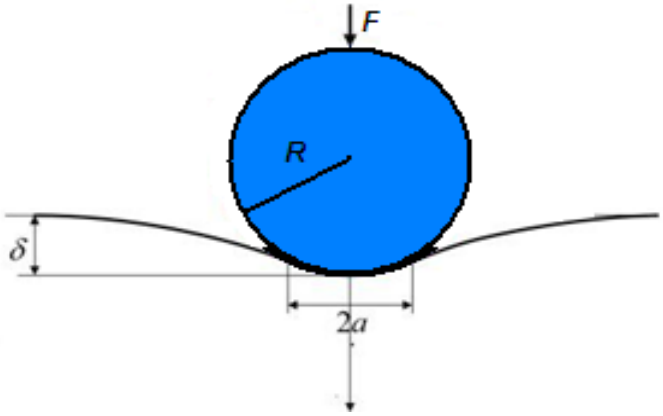

Figure 2.16 Indentation of a single cell using spherical indenter, where δ is the indentation depth, α is the radius of the contact area between the probe and the plasma membrane, R is the radius of the probe and F the loading force.

In addition, the Hertz model approximates the sample as a smooth, isotropic and linearly elastic homogeneous material and assumes that there is no interaction nor adhesion between the probe and the sample. If a biological cell is treated with trypsin then smoothness of the surface can be improved. However, in experiments where elastic and adhesive properties are studied simultaneously, the surface of a biological cell has to remain intact. As shown schematically in Figure 2.17 the surface of the cell is rough and includes various long chain molecules. In fact, inhomogeneity of the surface can induce a serious in the calculation of elasticity, since it is very difficult to determine the exact contact point between the probe and a living cell. Also, the contact area between the plasma membrane and a penetrating probe is hard to define. Hertz theory approximates the sample as a linear, homogeneous sphere. However, soft biological materials are characterized by non-linearity and inhomogeneity. Therefore, the Poisson parameter does not describe such complex material response and has to be approximated. Consequently, the Poisson's ratio of incompressible materials like rubber was assumed as 0.5 (Mahaffy et al., 2004).

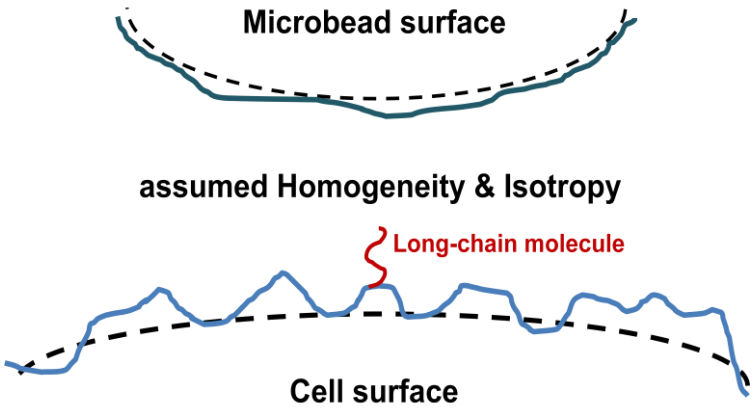

Figure 2.17 Schematic design of the surface of a probe and the sample. Dotted line represent the theoretical assumption, while continuous line is a representation of the actual micro-environment. Roughness at molecular level contributes to the uncertainty of the determination of initial contact point and contact area during indentation. Various membrane extensions such as long chain molecules on the surface of the cell can cause a force jump indicating a false contact point.

Hertz theory assumes indentation on an infinitely extending space. This means that the depth of indentation is negligible compared to the height of the sample and that the deformation of the sample induced by the indentation is very small in contrast to the extremely thick sample. However, since cells have a very limited thickness and Hertz theory assumes that the sample occupies an infinite half-space, it is very important to define the indentation depth before experiments. As the substrate effects are not considered in the model, this may lead to significant errors in the determination of elasticity of soft cells. The significantly higher Young's modulus of a hard substrate will induce a serious error in the calculation of cell elasticity, resulting in high values of the cell *E* modulus. The Hertz model is only valid for indentations up to 10% of the samples height, where substrate effects are considered insignificant (Dimitriadis et al., 2002). For that reason, all curves were fitted rigorously with the

restriction that the maximum depth of indentation is equal to or less than 10% of the height of each cell. To achieve that the thickness of the cell was measured with respect to the substrate for each tested cell. However, as cells tend to form clusters with each other, determination of the height with respect to a reference substrate was not always possible. Nevertheless, the experimental specifications require testing adherent cells that are in communication with neighbour cells. Therefore, determination of elasticity of cells inside a cluster was important to be valued. For that reason several preliminary measurements were taken to establish the general cell height for each cell line. In addition, cells that are situated in the side of a cluster are in contact with other cells and a clean substrate space is available for the measuring the height difference (Figure 2.18(a)). Figure 2.18 shows the procedure for determining the height of the cell prior conducting indentation measurements. A force setpoint of 0.2nN was used for the tip of the cantilever to touch the area adjacent to the cell, that is to used as a reference. Since cells in a small cluster (Figure 2.18(b)) or individual cells (Figure 2.18(c)) have more free space in their surrounding area, more reference points were measured. Next, the cantilever was positioned above the testing cell and was set to approach the surface of the cell. The height of each testing cell was subsequently determined by their displacement difference. The indentation measurements were performed immediately without moving the tip from the testing position in which the cell height was measured. However, even a small contact force (200pN) can induce deformation to the membrane, hence the cantilever was retracted and a new *F-d* curve with a pre-set indentation depth was performed.

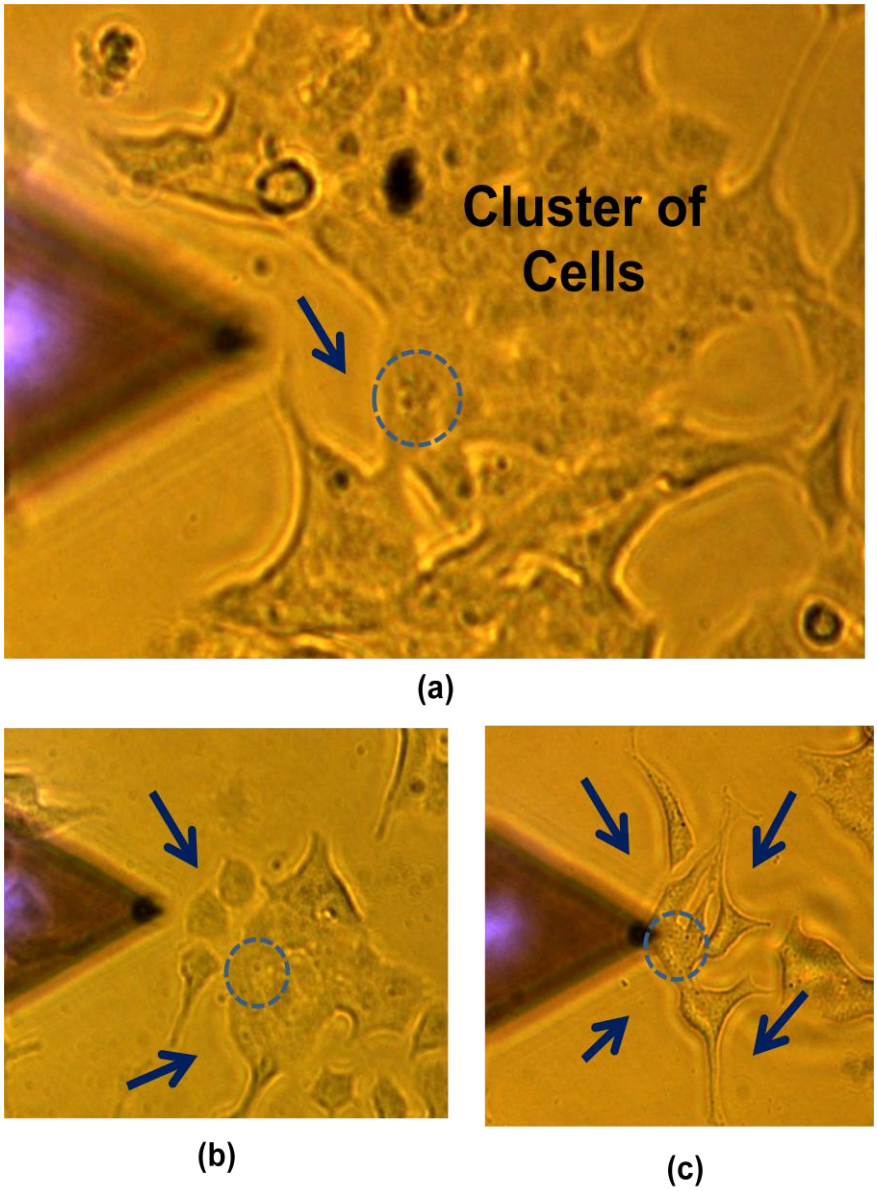

Figure 2.18 Optical image demonstrating the determination of cell height prior indentation experiments. The target cell is marked with a circle while arrows show the points of clean substrate area that can be used as a reference point. A low set-point force of 0.2nN was used for the cantilever to touch a point in a clean area next to a measuring cell and the surface of the cell. Their displacement difference was used to determine the height of the cell and subsequently the indentation depth. (a) When a single test within a cluster was tested one reference point was used for measuring the height of the cell. (b) &(c) For cells in smaller cluster or individuals the reference

values were obtained by measuring the area surrounding the cell. Obviously, individual cells had more reference points.

Cells are complex with several elements in their compartment, such as the plasma membrane, the nucleus, the cytoskeleton and various organelles, which all contribute to the overall stiffness of the cell. As the indentation depth increases the effects of the various parts of the cell will add to the slope of the *F-d* curve. Each part of a curve will correspond to a structure under investigation. By fitting discrete parts of the curve to the model, the elasticity of different structures can be is represented (Figure 2.19).

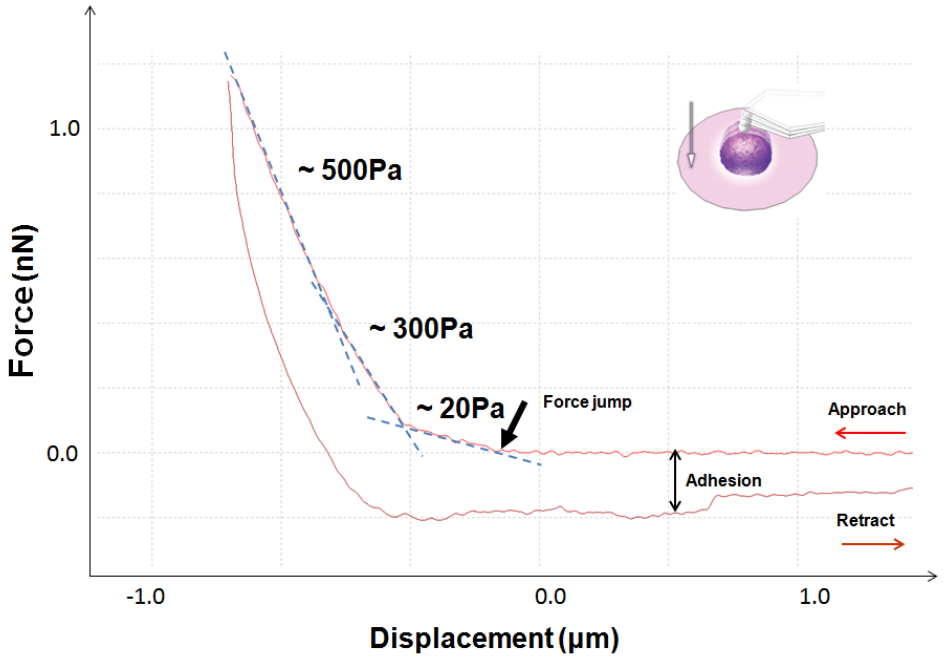

Figure 2.19 Elasticity can be determined by fitting the model to the *F-d* curves in the range of 5-10% of indentation. The spherical probe has large area of contact and it is important to take under consideration the effects of the substrate.

2.6.3 Force & Displacement Mode for AFM-FS Indentation

AFM indentation can be conducted either by force-controlled indentation or by displacement-controlled indentation. During force-controlled indentation the restriction for the indentation depth is not considered experimentally but while fitting the data to the model. The cell is indented according to a preset force value, without considering the height of the cell. As a result, the (corrected) displacement of the recorded curve corresponds to relatively high depths and may suffer from substrate effects when fitting the Hertz model. By this means, the indentation depth is determined from the fitting range of a *F-d* curve. The curve is fitted in various incremental indentation depths in order to observe any large differences in *E* modulus. At some point of the displacement fitting range, *E* modulus reaches a plateau that corresponds to the whole cell elasticity, up to the fitted depth. Any obvious difference above that value indicates that the fitted indentation depth is too high and substrate effects are contributing to the calculation. In this method the height of each tested cell does not have to be predetermined, and the height of a few cells would be enough to provide a general insight about the thickness of the sample (Figure 2.20(a)). This method has the advantage of a faster experimental procedure and as long as consistency is maintained during analysis the calculated elasticity values can be compared between different cell states. However, since cells are highly heterogeneous there might be no obvious plateau in the *F-d* curve. Especially when small indenters i.e. pyramidal, are used any movement of the cell or the cantilever will result in indenting a different area, thus resulting in different *E* modulus.

In height-controlled indentation, the depth of indentation is determined based on the height measurements of each tested cell. The indentation is then performed directly

above the point where the height of the cell is measured, with maximum indentation depth up to 10% of the thickness of the sample (Figure 2.20(b)). By this method it is guaranteed that the substrate effects on the calculation of *E* modulus are minimised. One issue of consideration using this method is related to the accuracy of the determination of cell height. For cells inside a cluster only one reference point is available on the clean substrate. In addition, the contact force between the tip and the membrane induces a deformation on the thin surface and it is absolutely necessary to use a low set point (<0.2nN). Higher set-points result in a significant deformation of the membrane, in a smaller value of cell height and consequently in shallow indentations.

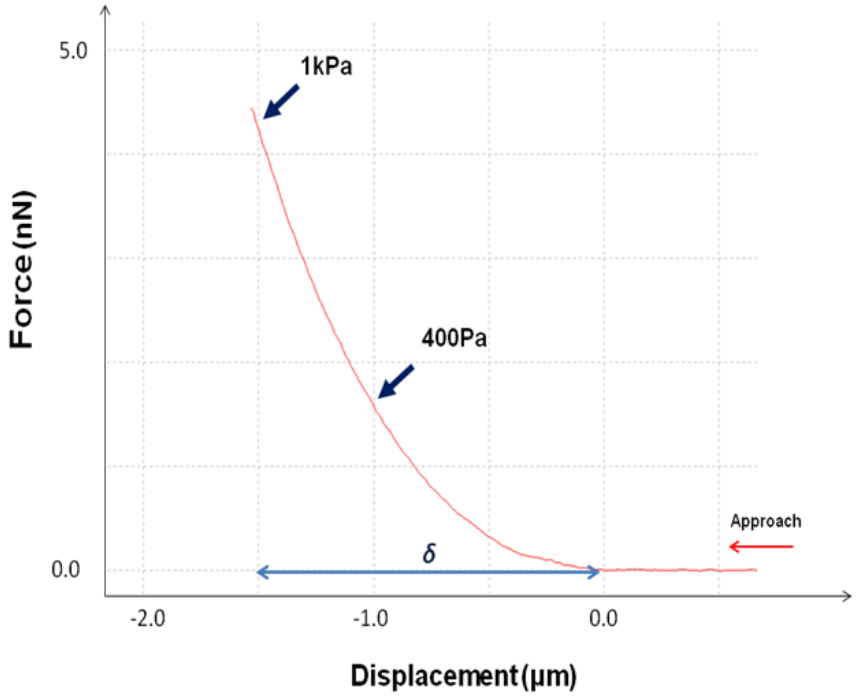

(a)

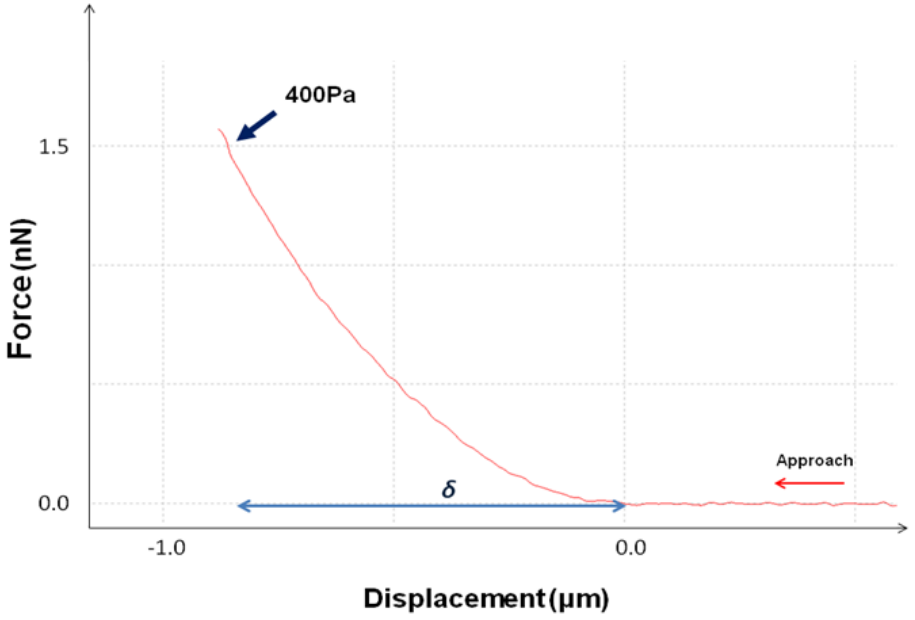

(b)

Figure 2.20 AFM indentation using force-controlled and height-controlled displacement of a cell with thickness 3.5μm. Hertz theory assumptions require that the depth of indentation depth δ is maximum 10% of the cell height. As shown in the *F-d* curves, the contact point can be determined by identifying a positive ramp of the force sensor. In (a), a set-point force of 4.5nN was used to indent the sample resulting in a displacement of approximately 1500nm. As δ was increased the value of E modulus was increased significantly, suggesting that stiffer elements (e.g. nucleus or substrate) are contributing to the calculation of elasticity. In (b) a set-point force of 100pN was used to determine sample thickness with regards to the reference substrate and indentation depth δ is fixed for the specific position on the cell. The procedure is then repeated for each testing cell.

2.6.4 Single Cell Indentation Measurements

The cantilever-bead was brought in contact with another cell on the substrate, until a preset contact force was reached (<0.2nN for both HK2 and MIN6 cells). A low set-point force is necessary in order for the probe to just touch the extracellular domain of the membrane. This is followed by a corresponding ramp on the output force. If the peak on the output force is higher than the set-point, then the deformation of the membrane is too high and the proportional-integral gains of the controller have to be adjusted. Then the piezo-actuator was retracted by a known value *d* and the thickness of the sample was determined. Next, the cantilever was extended exactly on the same point after adding in *d*, the calculated displacement, that corresponds to the depth of indentation based on cell thickness.

Each cell was indented 5 times with an interval pause of 60secs, while force versus displacement was recorded simultaneously. All cells were indented on the area directly above the nucleus. Since, the indentation depth was pre-determined for each cell, displacement-controlled or simply height indentation experiments were performed. The approach and retraction speeds were kept constant for all experiments at 5μm/sec to avoid hydrodynamic forces acting on the cantilever. Approximately 10 cells per petri dish were tested, while only the extended part of the *F*-d curve was used for analysis due to the adhesion between the tip and the living cell.

2.7 Data Processing & Analysis

Data of force spectroscopy measurements were recorded in a compressed binary format and they cannot be processed using a spreadsheet software. However, *F*-d curves can be converted one by one as a .txt file or into ASCII format, containing all the curve data, using the user interface or they can be converted as batches of force files using the Linux terminal. To process all force distance curves the JPK Data analysis software was used as described by Friedrichs et al. (2010).

To signify statistical differences data was evaluated using one-way ANOVA test or a paired t-test. Data are expressed as mean±SEM and 'n' shows number of experiments. $P<0.05$ was taken to indicate statistical significance.

2.7.1 Adhesion Data Processing

A raw *F-d* cell-to-cell adhesion curve as recorded from a force spectroscopy experiment is shown in Figure 2.21(a). All processing functions were applied to the retracted *F-d* curve. Initially the low frequency component caused by environmental noise was removed by smoothing the data (function 1). Next, the reference point that will be used for the determination of the adhesion parameters, such as F_{max}, W_D and d_s, had to be determined. Essentially this is the point of complete separation between the two cells and it is specified by setting the baseline of the complete separation of the retraction curve to match the zero x-axis (function 2). The exact point where the two cells are in contact does not affect the calculation of the adhesion parameters. Besides, the processing of *F-d* adhesion curves was performed on the retraction part of the curve. Therefore, detection of contact point (function 3) was only used for convenience of display, since hundreds of curves were analysed. The next

operation that performed was the detection of minimum value of force (function 4), which represents the maximum force required for the complete separation of the two cells. F_{max} is calculated by detecting the minimum negative value of force with respect to the x-axis baseline. In addition, by determining the area under the retracted part of the curve (function 5), work or energy of complete detachment was calculated. Unbinding of ligations can be detected by identifying sharp steps of force that occur after a plateau in x-axis that corresponds to membrane tethering (function 6). This automated step-fitting method for detecting small force ramps that correspond to bond rupture was developed by Kerssemakers et al. (2006). During the retraction phase of cell-to-cell adhesion curves, only upward steps are anticipated. However, small drifts of the cantilever can be caused due to fluidic nature of the experiments. As a result errors may be introduced to the analysis and hence only positive steps were selected. After applying the operations from (1) to (6), the curve of Figure 2.12(b) is obtained from which F_{max}, W_D and number of tether rupture events (TREs) can be determined. The determination of the point at which the cells are completely separated is the most important step, since the x-axis baseline will be derived upon that. Besides, the distance of complete separation d_s can be determined by the difference between F_{max} and point of complete detachment of the two cells.

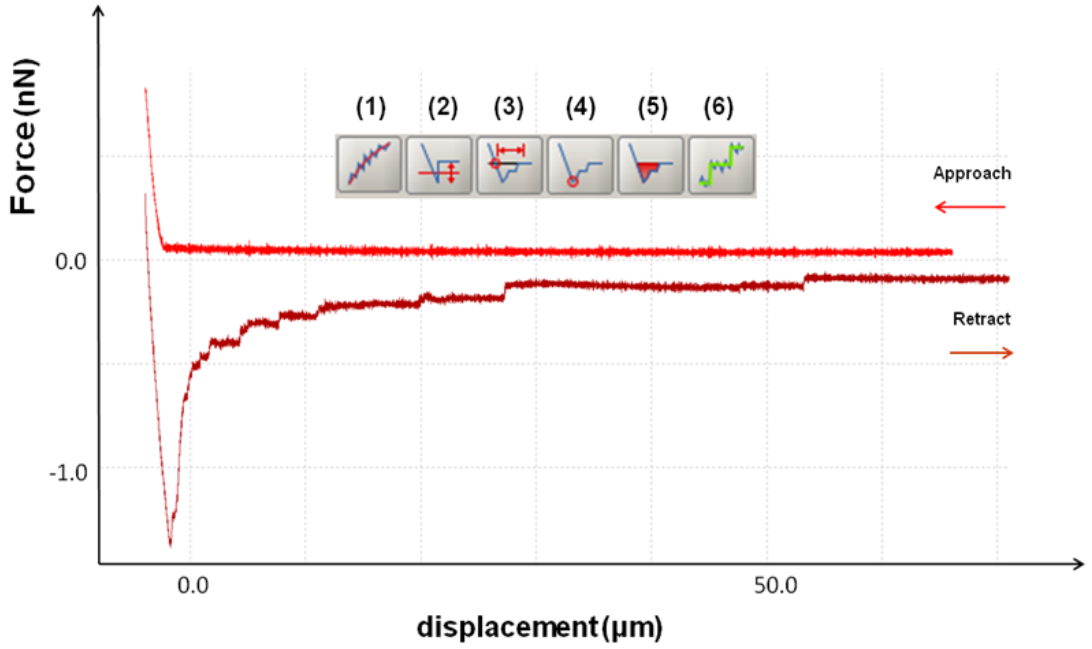

(a)

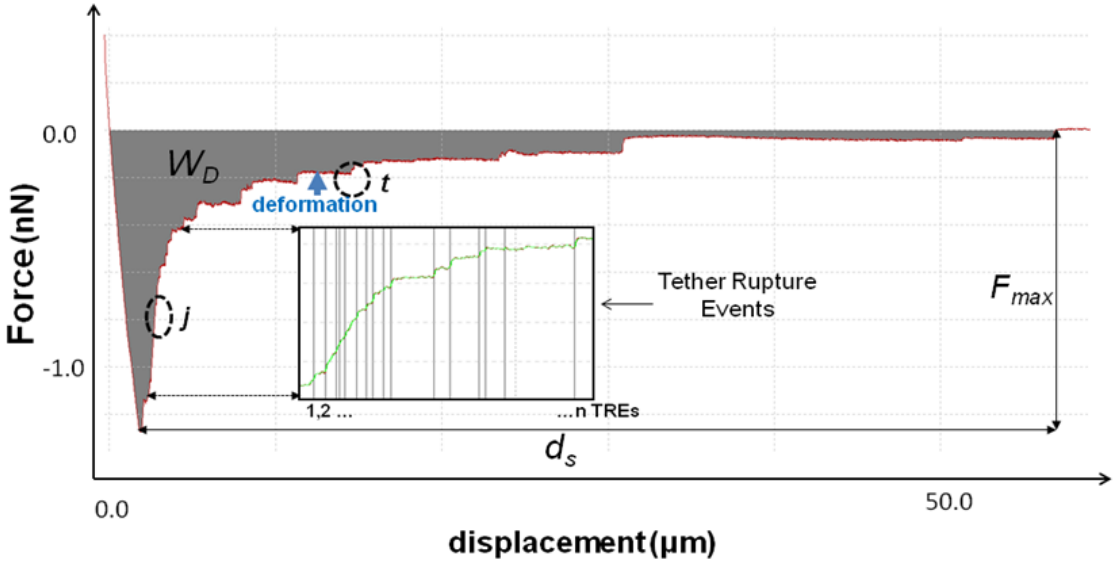

(b)

Figure 2.21 Processing of cell-to-cell adhesion force curves. In (a) a raw F-d curve, as measured by AFM-SCFS, is shown. After applying the following functions: (1) smoothing, (2) set the x-axis Baseline, (3) detect the Contact point, (4) detect the

Minimum Force value, (5) determine the area under the curve and (6) step fitting, the *F-d* retraction curve of (b) is resulted. As illustrated the determination of the point at which the cells are completely separated is the most important step, since the x-axis baseline acts as a reference for further analysis. F_{max} is the difference between the minimum force value and the baseline, while W_D (grey region) is the integral of the continuous area under the baseline. In addition, d_s can be determined by the difference between F_{max} and the point of complete separation. Zooming in the x-axis displays detection of early unbinding events.

2.7.2 Indentation Data Processing

A raw *F-d* indentation curve as recorded from a force spectroscopy experiment is shown in Figure 2.22(a). All processing functions were applied to the extended *F-d* curve. In order to detect the point in which the force ramps to a positive value, low frequency noise has to be removed from the baseline. Therefore, smoothing of data (1) was the first operation that needed to be applied. Then, any offset of the baseline in the vertical deflection had to be corrected (2), since movement of the aqueous buffer solution is likely to cause deflection of the cantilever. In general, the part of the curve on the right of the slope should be smooth and flat. However, environmental noises or particles on the media can cause a large deflection of the cantilever, which will be detected as notch peaks in the output or a drift on the baseline. After smoothing and correcting the baseline of the curve, the contact point (3) was calculated by detecting the point where the curve is crossing the zero force axis. However, as discussed earlier this point does not represent the absolute contact point where the probe touched the membrane and hence served only as an indication point for fitting a mechanical model. The next operation (4) corrected the displacement values for

the bending of the cantilever as described earlier. This function is important to be performed before the determination of Young's modulus using Hertz theory. To calculate elasticity function (5) was applied for a spherical indenter with radius of 5.0μm. The assumption for fitting the Hertz model were discussed earlier. After applying the operations from (1) to (5) various fitting ranges can be investigated to determine elasticity of a single cell (Figure 2.22(b)).

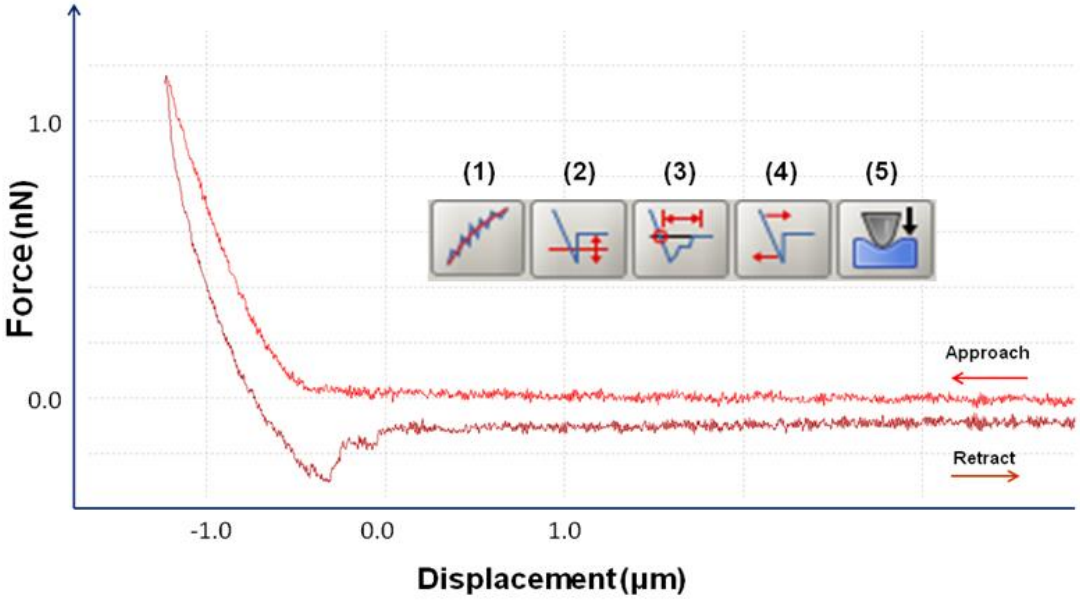

(a)

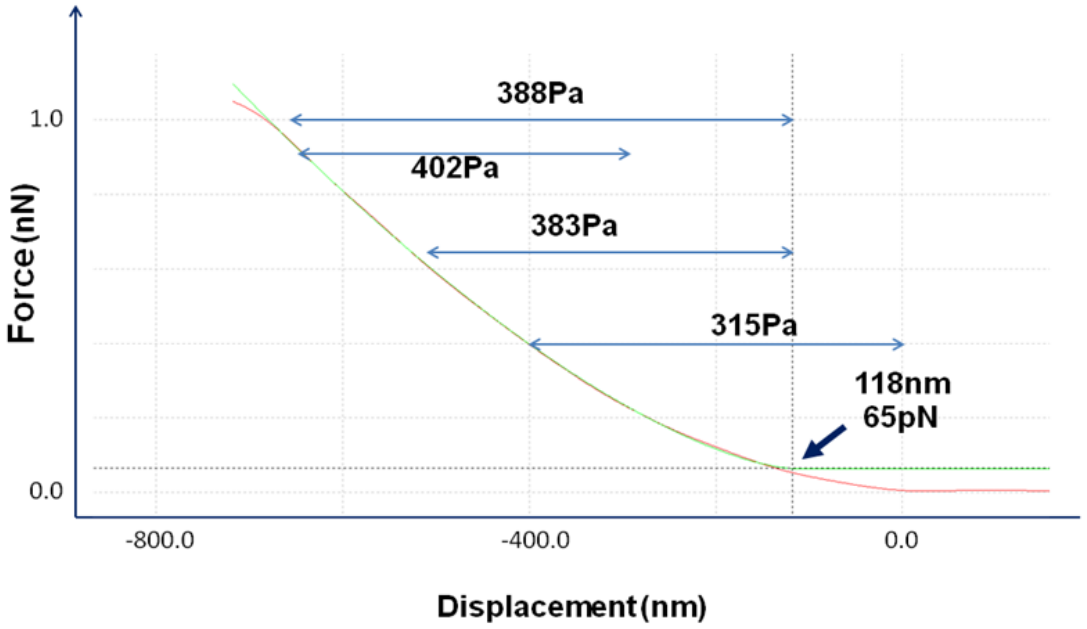

(b)

Figure 2.22 Processing of indentation force curves. In (a) a raw *F-d* curve, as measured by AFM-FS, is shown. After applying the following functions on the approach curve: (1) smoothing, (2) substract the baseline to set the zero force level, (3) detect the contact point, (4) correct the height of the cantilever bending and (5) apply the Hertz model, the *F-d* extension curve of (b) is resulted. In order to calculate the elasticity of a cell, an *F-d* curve was analysed as shown. Fitting in incremental and various parts of displacement confirmed that the experimental procedure was robust. A contact point of 118nm resulted in better fit of the data.

Chapter 3

Nanomechanical Characterisation of Pancreatic MIN6 Cell-to-Cell Adhesion

3. Nanomechanical Characterisation of Pancreatic MIN6 cell-to-cell adhesion

3.1 Introduction

In this chapter, a force spectroscopy study of monolayer MIN6 cells treated with the calcimimetic R568 (1μM) is presented. The calcimimetic activates the receptor at a physiologically appropriate extracellular calcium concentration (Hills et al., 2012b). Activation of the extracellular calcium-sensing receptor (CaSR) on β-cells increases expression of the adhesion protein epithelial (E)-cadherin. Glucose-responsiveness of the pancreatic islet relies on the interactions and coupling between neighbour cells. In this study the changes in E-cadherin mediated cell-to-cell adhesion and single cell elasticity in response to the calcimimetic R568 were quantified.

Figure 3.1 shows the morphological shape of healthy MIN6 cells. The cells were cultured in monolayers in low extracellular calcium (0.5mM Ca^{2+}) in order to enable activation of the CaSR by the R568 (Figure 3.1(a)). In physiological conditions clusters of cells are formed, since they maintain their adhesiveness with neighbouring cells. The morphology of a single cell adhered on a petri dish substrate is shown at Figure 3.1(b), illustrating a shape that resembles a cobblestone. However, the cobblestone shape may vary when cells are organised within clusters. For consistency all force measurements were performed on cells that resemble this morphology. Testing was performed above the central region of the cell, which normally corresponds to the area where the largest element of the cell, the nucleus (purple colour), is residing. The cytoskeleton (Figure 3.1(b); red colour) is the element of the cell that is principally responsible for maintaining its shape.

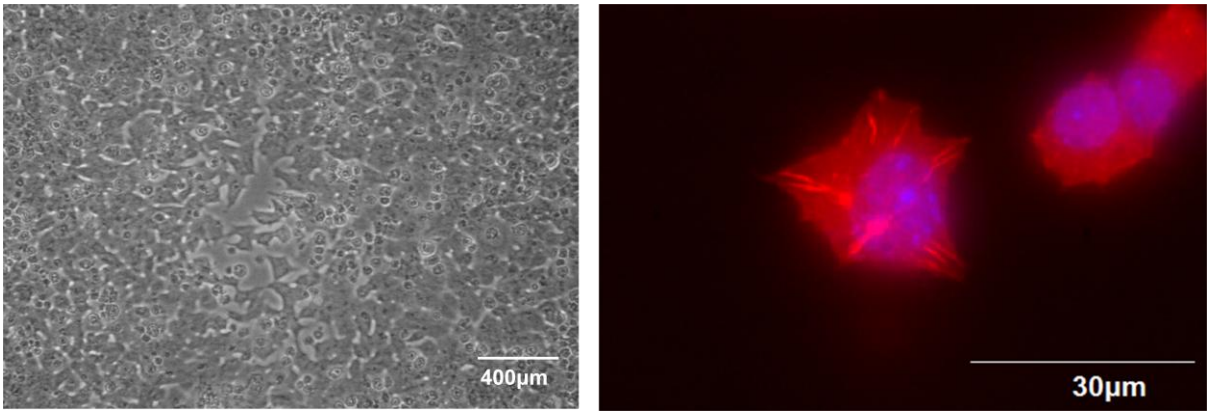

(a) (b)

Figure 3.1 The morphology of MIN6 cells cultured in low extracellular calcium (0.5mM). In (a), an optical image of MIN6 cells in monolayers demonstrates that cells are organised in low proximity between each others, forming clusters that enable cell-to-cell coupling and communication. In (b), a fluorescence microscopy image of a single cell illustrates the cobblestone morphology that is maintained by the CSK (stained in red colour). The nucleus of the cell, occupying a large area of the cyto-plasm, is clearly shown (purple colour).

3.2 Effects of CaSR Activation on Functional β-cell-to-β-cell Adhesion

MIN6 cells were treated for 48h in low extracellular calcium (0.5mM) +/- the receptor specific calcimimetic R568 (1μM). Chronic activation of CaSR using the R568, ele-vates E-cadherin expression while this is accompanied with relocalisation of the pro-tein into the membrane and the CSK (Hills et al., 2012b; Younis, 2012). In order to relate the changes in expression/localisation of E-cadherin to functional tethering, SCFS was used to quantify cell-to-cell adhesion parameters, such as the forces re-quired for the complete detachment of coupled cells. A single MIN6 cell was at-

tached into the end of a functionalised arrow cantilever and subsequently brought in contact with a single substrate cell within a cluster. In Figure 3.2 an optical image taken from the force spectroscopy experimental measurements is presented. In (a), the control group (0.5mM Ca^{2+}) is shown, while in (b) the treated sample (0.5mM Ca^{2+} +R568) is shown. The treatment did not cause any morphological or phenotypical changes of the cells.

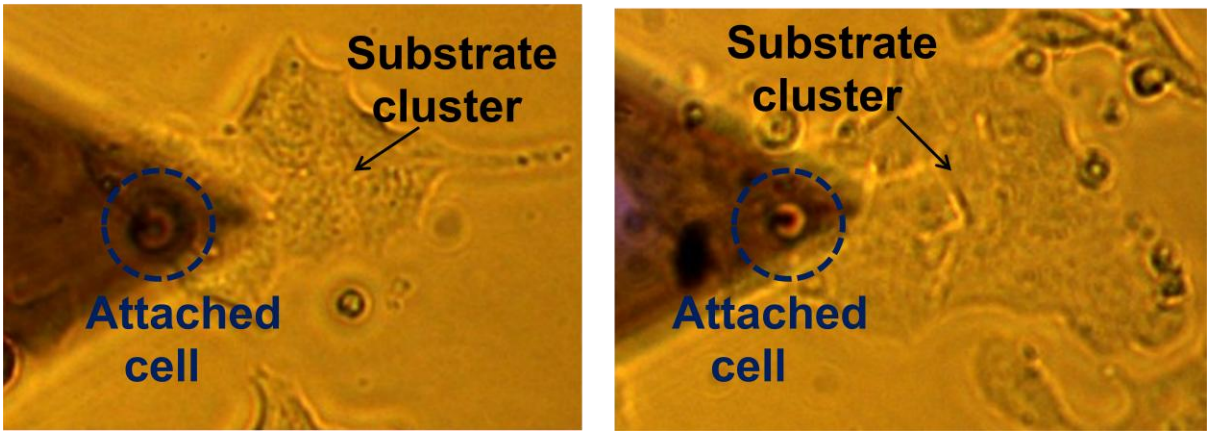

(a) (b)

Figure 3.2 Phase microscopy image showing a β-cell-to-β-cell SCFS adhesion experiment. No morphological changes between the samples were observed by optical images. The suspended cell was attached on the functionalised cantilever and then was brought in contact with a single substrate cell (within a cluster of cells) for 5secs, while force versus displacement were measured simultaneously. In (a), an optical image showing MIN6 cells incubated for 48h in 0.5mM Ca^{2+} (Control) while in (b) cells were incubated in 0.5mM Ca^{2+} +R568.

A few set of measurements were performed to select the parameters prior adhesion measurements. The main criterion that determined the choice of the parameters was the displacement range of complete separation. As discussed in the adhesion data

processing section, the point of complete detachment between two cells acts as the baseline for the determination of adhesion characteristics. Therefore it is important that the experimental specifications allow complete detachment of the cells under the specified speed. A fixed set-point force of 0.8nN was used for the probe cell to touch the surface of the substrate cell. The contact period between the two cells was set at 5 sec. During contact time E-cadherin surface ligation occurred. The cantilever was retracted at a constant speed of 5μm/sec and retraction *F-d* curves were recorded until the two cells were completely detached from each other. The procedure was repeated three times for each cell under investigation, with 30 sec intervals between each successive measurement. The attached cell was used to perform measurements on approximately 5-10 cells for each cultured petri dish.

Retraction curves acquired from adhesion measurements between two single β cells were analysed from multiple experiments in order to investigate the β cell function after chemical modification with the calcimimetic. Using identical experimental specifications more than 30 cells in separate experiments (n=4) were examined, resulting in the processing of more than 100 *F-d* retraction curves. The number of cells that were used for analysis for each treatment is shown in Table 3.1. As shown in the table, there is a noticeable number of retraction curves that have been discarded from further processing. There are many reasons that can cause a disturbance while recording a *F-d* curve. Since the attachment procedure between the suspended cell and the cantilever is performed in the cultured dish under testing, a large number of free floating particles into the media, such as cell debris, cause drifting in the measurements of the sensor. Moreover, movement of free cells causes a serious drift of the cantilever, which may lead in the incorrect determination of unbinding forces.

Therefore large numbers of data sets are necessary in order to obtain a valid outcome when comparing cells under chemical treatment.

Table 3.1 A table showing the number of tested MIN6 cells and retraction curves obtained using SCFS that were either processed or rejected. A total of 102 retraction measurements of 41 Ca^{2+} cells were analysed, while a total of 108 retraction curves of 41 Ca^{2+}+R568 cells were analysed. Approximately 1/3 of the curves were rejected due to disturbances when recording a retraction *F-d* curve.

MIN6 cells SCFS retraction measurements		
n=4	**Ca^{2+}**	**Ca^{2+} +R568**
Total No of Cells	48	45
No of accepted cells	41	36
Processed curves	102	108
Discarded curves	42	27

Retraction *F-d* curves provide important information regarding the adhesion parameters between two cells. The most common indicator of adhesion is the negative force value of the curve, due to the downwards deflection of the cantilever when being retracted from the sample signifies binding between the adherent cells. Functional changes in the expression of a protein under investigation in the surface of the cell can be shown by the detection of the maximum unbinding force. In fact, force of detachment is the most common relative parameter for comparing control and treated cells in an adhesion assay (Friedrichs et al., 2010). However, extraction of parameters such as work or distance to complete detachment from a retraction *F-d* curve, provide information regarding the contribution of cellular deformation into the sur-

face mediated cell-to-cell ligation. The retraction curves of Figure 3.3 illustrate the effects on adhesion parameters as resulted by CaSR activation, upon the treatment of MIN6 cells with the calcimimetic. As shown in the figure, cells treated with the calcimimetic (Figure3.3(b)) exhibit increased adhesion characteristics in comparison to the control group (figure 3.3(a)). Detection of the changes between the control and the +R568 treated group provided quantitative information regarding the functional adhesiveness of cells and confirmed that the function of a system is indeed altered after the changes in surface protein expression. Complete separation between the probe and the substrate cell, under the 5μm/sec speed, was ensured by using an effective retraction range of at least 80μm.

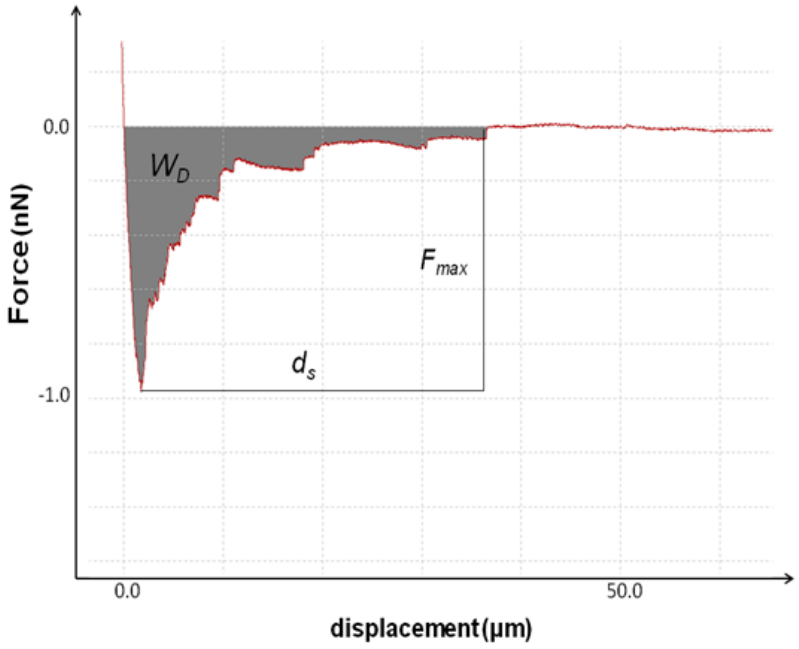

(a)

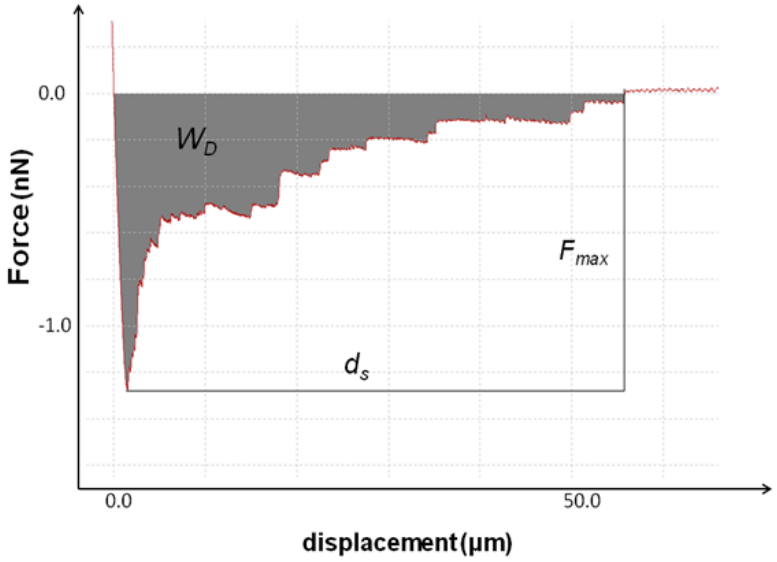

(b)

Figure 3.3 The effects of CaSR activation, followed by treatment with the calcimimetic R568, on E-cadherin mediated cell-to-cell adhesion were examined using AFM-SCFS. F_{max} is the difference between the minimum force value and the point of complete detachment, W_D (grey region) is the integral of the continuous area under the baseline of complete separation and d_s is the difference between F_{max} and the point of complete separation. Set-point force of 0.8nN, contact time of 5sec and pulling speed of 5μm/sec were remained constant throughout the experiments. Alterations of adhesion parameters such as F_{max}, W_D and d_s provide an important insight about functional cell-to-cell adhesion. In (a) F_{max} is 0.9nN, W_D is 6.7*f*Joule and d_s is 34.6μm while in (b) F_{max} is 1.3nN, W_D is 16.9*f*Joule and d_s is 54.2µm.

In addition, changes in the expression/localisation of E-cadherin also affected the number of unbinding events that occurred during the retraction process of the two cells. The retraction *F-d* curves of figure 3.4 illustrate the number of rupture tethers as detected by the step fitting function. CaSR activation increased the density of E-

cadherin ligands, corresponding to an increase of rupture bindings in the retraction curve of cells treated with the calcimimetic R568 (Figure 3.4(b)). Sharp steps of force that are not preceded by a displacement plateau (*'j'* events) occurred in the first 10-15μm of pulling range for the control cells, whereas in cells treated with calcimimetic '*j*' events occurred during the first 5μm of pulling range. As the pulling range increased an area was reached in which unbinding of surface ligations was also preceded by a displacement plateau ('*t*' events), indicating small cellular deformations. During the retraction process the displacement plateau increased with higher pulling range, as illustrated in Figure 3.4. For control cells (Figure 3.4(a)), '*j*' type unbinding events dominated the separation process between two cells. However, for cells treated with calcimimetic the number of '*t*' events that preceded a considerable displacement range was higher, indicating that cellular deformation occurred at many instances before the complete detachment of the cells. Therefore, cells treated with the R568 became more deformable, which clearly had a significant impact on work and distance of complete detachment.

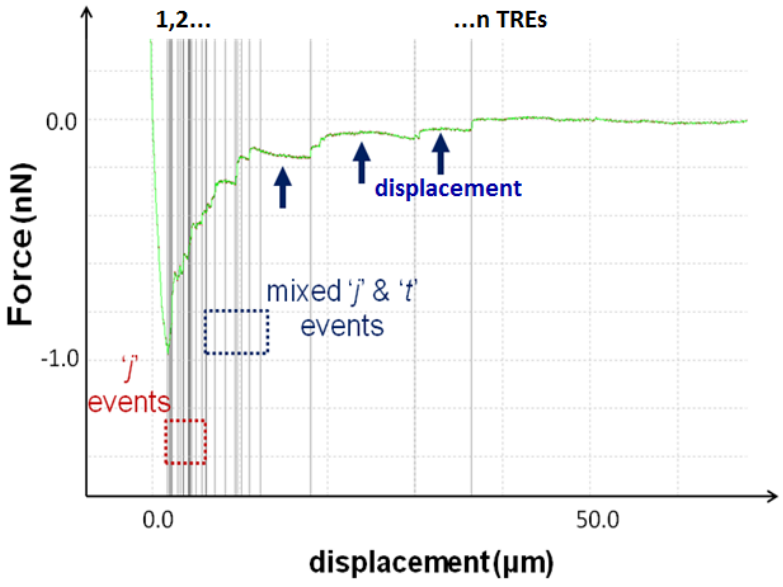

(a)

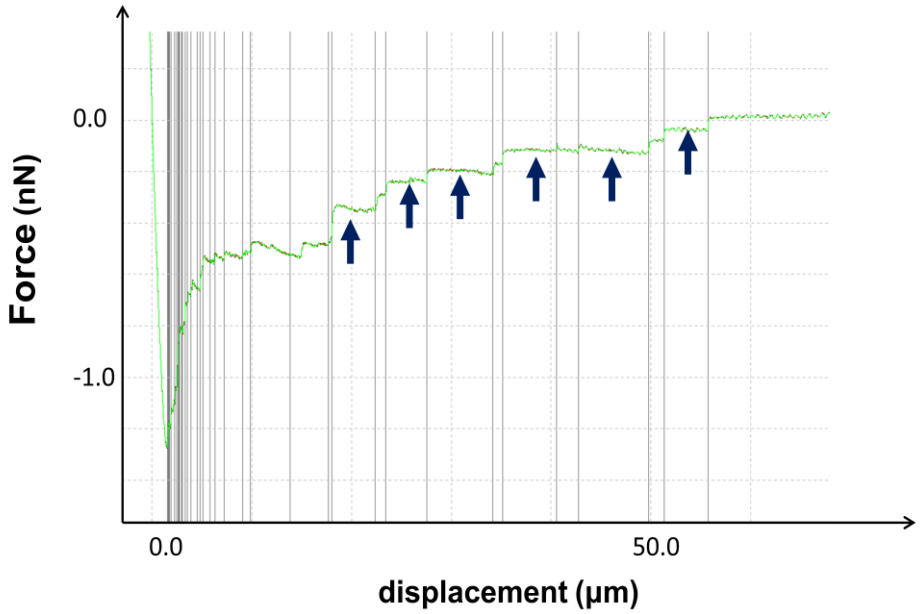

(b)

Figure 3.4 Retraction force-distance curves obtained by MIN6 cell-to-cell adhesion measurements, showing the effects of CaSR activation on the tether rupture events. Unbinding of ligations that occur during the early pulling phase (10*μ*m after the minimum force value) are preceded by a force ramp ('*j*' events). As the pulling distance increases an area is reached where the rupture events are preceded by a displacement plateau as well ('*t*' events) due to the deformation of the cell. In (a) the number of TREs is 39, whilst most of the unbinding events occurred in the first 11μm of pulling range, corresponding to the area of '*j*' and mixed '*j*' and '*t*' events. In (b) the number of TREs is 61, whilst most of the '*j*' events occurred in the first 3.2*μ*m. The arrows illustrating the displacement plateau combined with the fact that the initiation of '*t*' events occurred much earlier as shown in (b) indicates that MIN6 cells became more deformable after treatment with the calcimimetic.

The histograms of maximum unbinding force and work of detachment obtained from the *F-d* curve measurements of control cells are shown in Figure 3.5. Overall the data acquired from MIN6 cell-to-cell adhesion experiments were normally distributed, suggesting that the assumption for performing t-test has been satisfied. Table 3.2 shows the descriptive statistics for the various adhesion parameters that were extracted from the β-cell-to-β-cell retraction *F-d* curves; (a) For the control cells, the maximum unbinding force had a mean of 0.84nN and standard error of 0.02. For the calcimimetic cells, the maximum unbinding force had a mean of 1.09nN and a standard error of 0.03. (b) For the control cells, the work detachment had a mean of 11.10fJoule and a standard error of 0.46. For the calcimimetic cells, the work of detachment had a mean of 16.36fJoule and a standard error of 0.78. (c) For the control cells, the number of tether rupture events had a mean of 48.54 and standard error of 1.36. For the calcimimetic cells the tether rupture events had a mean of 70.38 and standard error of 1.53. (d) For the control cells, the distance of complete separation had a mean of 51.39μm and standard error of 1.55. For the calcimimetic cells, the distance of separation had a mean of 70.41*μ*m and standard error of 2.20.

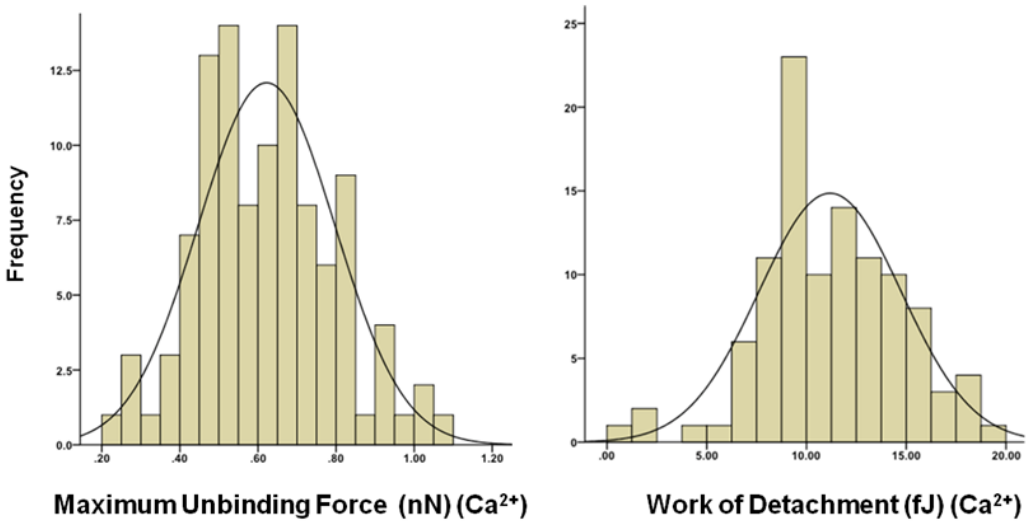

(a) (b)

Figure 3.5 (a) Distribution of frequencies of maximum unbinding forces and (b) distribution of frequencies of work of detachment.

Table 3.2 Table presenting descriptive statistics for the adhesion parameters, (a) of maximum unbinding force for the control and for the +R568 cells, (b) of work detachment for the control and for the +R568 cells, (c) of tether rupture events for the control and for the +R568 cells and (d) of distance separation for the control and for the +R568 cells.

F_{max} (nN)	Mean	N	Std. Deviation	Std. Error Mean
Ca^{2+}	0.8437	102	0.17546	0.02176
Ca^{2+}+R568	1.0891	108	0.25205	0.03126

(a)

W_d (fJoule)	Mean	N	Std. Deviation	Std. Error Mean
Ca^{2+}	11.1019	102	3.70880	0.46002
Ca^{2+}+R568	16.3635	108	6.25498	0.77583

(b)

No of TREs	Mean	N	Std. Deviation	Std. Error Mean
Ca^{2+}	48.5385	102	8.49720	1.36064
Ca^{2+}+R568	70.3846	108	9.54660	1.52868

(c)

d_s (µm)	Mean	N	Std. Deviation	Std. Error Mean
Ca^{2+}	51.3886	102	9.14159	1.54521
Ca^{2+}+R568	70.4143	108	13.03010	2.20249

(d)

The differences between control and +R568 treated cells for the various adhesion parameters obtained from retraction curves as analysed using paired samples t-test are shown in table 3.3. On average, Ca^{2+}+R568 cells showed to have higher maximum binding force (M=1.0891, SE=0.3126) than Ca^{2+} (M=0.8437, SE=0.02176) and this difference was statistical significant ($t(105)=12.23$, $p<0.001$). Also, Ca^{2+}+R568 showed to have higher work detachment (M=16.3635, SE=0.7758) than Ca^{2+} (M=11.1019, SE=0.46), showing statistically significant differences ($t(105)=5.98$,

p<0.001). In addition, Ca^{2+}+R568 showed to have higher distance of separation (M=70.4143, SE=2.2025) than Ca^{2+} (M=51.3886, SE=1.5452). This difference was statistical significant (t(105)=9.5, p<0.001). Furthermore, Ca^{2+}+R568 showed to have higher numbers of tether rupture events (M=70.3846, SE=1.5287) than Ca^{2+} (M=48.5385, SE=1.3606) that was statistically significant (t(105)=12.54, p<0.001).

Table 3.3 Table presenting the differences between control and +R568 treated cells using paired wise t-test, (a) of the maximum unbinding force between control and +R568 cells, (b) of work detachment between the control and +R568 cells, (c) of the number of tether rupture events between the control and +R568 cells and (d) of the distance of separation between control and +R568 cells.

Mean	SD	SE	95%CI		t	df	Sig
0.23	0.291	0.036	lower	Upper	12.23	105	0.000
			0.514	0.370			

(a)

Mean	SD	SE	95%CI		t	df	Sig
5.26	7.08	0.879	lower	Upper	5.98	105	0.000
			7.01	3.50			

(b)

Mean	SD	SE	95%CI		t	df	Sig
21.84	10.87	1.74	lower	Upper	12.544	105	0.000
			25.37	18.32			

(c)

Mean	SD	SE	95%CI		t	df	Sig
19.03	14.9	2.52	lower	Upper	9.50	105	0.000
			29.16	18.8			

(d)

More than 100 curves from 4 separate experiments were analysed and the data are expressed as mean ± SEM in Figure 3.6. The results indicate that the calcimimetic R568 (1μM) increased the number of tether rupture events by 48%, resulting in an increase of the maximum unbinding force by 30%. However, the detachment energy was increased more significantly by 39%, consistent with the distance of separation increasing by 37% (>30 cells, n=4, $p<0.001$) (Figure 3.6(a)-(d)).

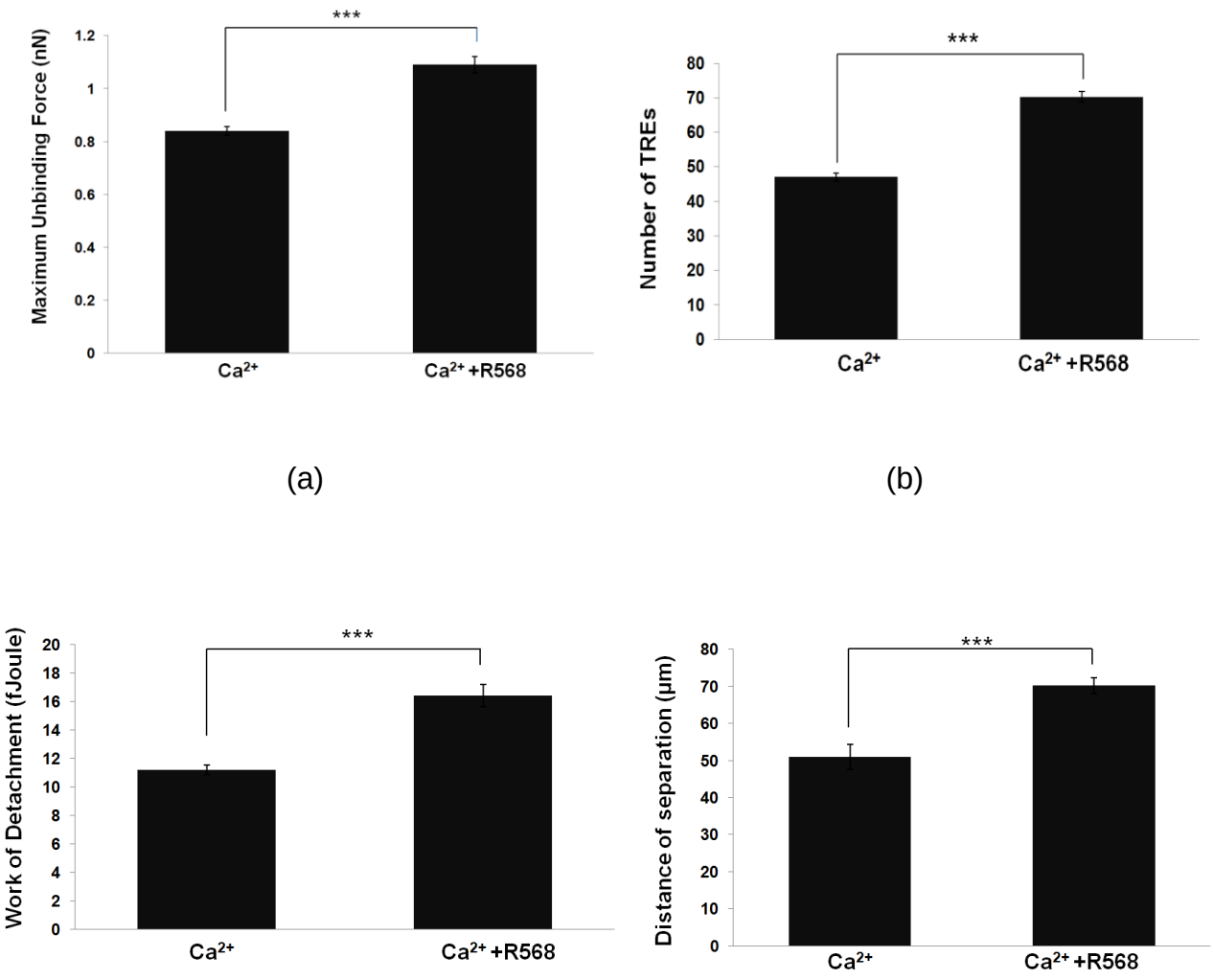

Figure 3.6 The effects of the calcimimetic R568 (1μM) on (a) the maximum unbinding force (increased by 30%), (b) the number of tethering rupture events (increased by 48%), (c) the work of detachment (increased by 39%) and (d) the distance to complete separation (increased by 37%) are shown. Data are expressed as mean ±SEM of more than 30 cells from 4 separate experiments, where key significances are shown, ***p<0.001.

Studying the cellular interactions is important for the understanding of improved islet function and insulin secretion (Hauge-Evans et al., 1999; Brereton et al., 2006). The

most characterised adhesion protein that mediates cell-to-cell adhesion and modulates the adherens junction is the E-cadherin molecule (Perez-Moreno et al., 2003). The CaSR is expressed in primary pancreatic islets (Rasschaert & Malaisse, 1999; Squires et al., 2000) and its expression and localisation on the periphery of MIN6 cells that are configured in monolayers was confirmed by Hills et al. (2012b) using whole-cell Western blot analysis. In addition it was shown that activation of the receptor increases the expression of E-cadherin at the surface of the cell. E-cadherin is a connective partner inside the AJ that facilitates cell-to-cell coupling and communication via signal transduction within the cell. One main concern when studying cell-to-cell adhesion is the difficulty to control the expressions of the adhesion proteins, due to the inhomogeneous nature of the sample resulting in complex molecular interaction between the cells (Zhang et al., 2002). For that reason, expression of E-cadherin on MIN6 cells had to be confirmed prior conduction of the experiments. The distribution and localisation of the adhesion molecule to the membrane and cytosol was confirmed using immunocytochemistry (Hills et al., 2012b). Detection of CaSR and E-cadherin confirms that the cell line is an appropriate model for investigating CaSR-evoked changes in β-cell-to-β-cell adhesion. In addition E-cadherins along with a-catenins and β- catenins are forming the adherens junction that connects the extracellular domain with the intracellular and acts as a 'hub' for downstream biological signalling. Therefore, chemical modification of the E-cadherin should have an impact in the intracellular domain as well, resulting in cytoskeletal reorganisation. In this study we have used AFM-SCFS to detect changes in functional tethering between two individual β cells. The results suggest that the activation of the receptor improves β-cell function by increasing cell adhesiveness through enhanced expression of E- cadherin. Ligation of E-cadherin to a partner protein on an

adjacent cell, stimulates other down-stream cytoskeletal-binding proteins including the phosphoinositide 3-kinase PI3K (Vaezi et al., 2002). Hence, CaSR activation could affect the intracellular domain via PI3K-dependent cytoskeletal reorganisation (Hills et al., 2012b). In this study, the changes in the elastic modulus upon activation of CaSR that reflect changes in the cytoplasmic domain have been detected. Moreover, for indentation depths at approximately 10% of the cell height it is suggested that the cytoskeleton is the main element of the cell that contributes to elasticity (Vinckier & Semenza, 1998; Leporatti et al., 2006). The average calculated value of *E* for the control cells is 503 Pa while for the treated cells is 331 Pa, indicating that the calcimimetic R568 (1μM) decreased the elastic modulus by 34%, hence resulting in higher elastic deformations during the separation process in cell-to-cell adhesion.

Although that the CaSR is a receptor involved in the control of Ca^{2+} levels in the blood stream, it has been suggested that there is an interplay between in CaSR and insulin release in the human pancreatic β-cells (Squires et al., 2000). Combined with the fact that the calcimimetic R568 stimulates release of insulin from MIN6 pseudoislets (Gray et al., 2006) and that R568 activate CaSR by increasing the affinity of the receptor for Ca^{2+}, then the role of the receptor as a mediator for an improved islet function was confirmed by the adhesion measurements between β cells. This is in agreement with Tu et al. (2008) who suggested that inactivation of the CaSR inhibits E-cadherin mediated cell-to-cell adhesion. The cell-to-cell adhesion results reported in this study provided quantitative data of the functional adhesion between β cells, by confirming that activation of the receptor in MIN6 cells increased E-cadherin mediated adhesion, thus suggesting a mechanism that underlies improved β-cell function via increased adhesion and coupling. In conclusion, the β-cell-to-β-cell adhesion

data along with the study of Rogers et al. (2007) suggest that enhanced adhesion results in improved secretion response.

3.3 Effects of CaSR Activation on Single Cell Elasticity

MIN6 cells were treated for 48h in low extracellular calcium (0.5mM) +/- the receptor specific calcimimetic R568 (1μM). The calcimimetic activates the CaSR, which increases the E-cadherin expression on the extracellular domain whist in the intracellular domain the trans-membrane protein binds to the actin cytoskeleton via the catenins (Hills et al., 2012b). In order to relate the changes of cell deformation to E-cadherin mediated functional adhesion measurements, single cell indentation was used to characterise cell elasticity. A spherical microbead of 10µm in diameter was attached into the end of a modified arrow cantilever and subsequently indented a single cell, according to a predetermined indentation depth based on cell height. In Figure 3.7 optical images showing a single cell force spectroscopy experiment for single cell elasticity are presented. In (a), the control group (0.5mM Ca^{2+}) is shown, while in (b) the treated sample (0.5mM Ca^{2+} +R568) is shown. As mentioned earlier cells that resemble a cobblestone morphology residing within a cluster of cells were tested.

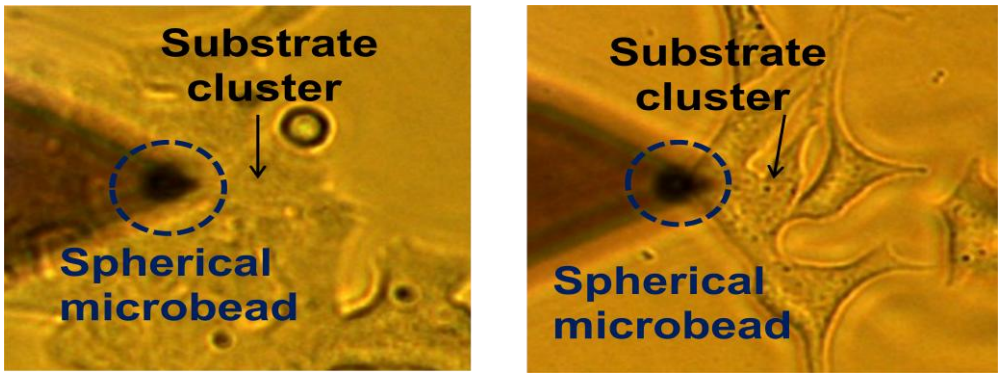

(a) (b)

Figure 3.7 Phase microscopy image showing a β cell indentation experiment. The cantilever was modified using a 10*μ*m polystyrene microbead probe to enable indentation of a single substrate cell (within a cluster of cells), while force versus displacement were measured simultaneously. In (a), an optical image showing MIN6 cells incubated for 48h in 0.5mM Ca^{2+} (Control) while in (b) cells were incubated in 0.5mM Ca^{2+} +R568.

Prior indentation of each cell, the height of the sample was determined as described earlier. Therefore the indentation depth was customised for individual cells according to their height. Although this methodology was found to be more time consuming in comparison with the force indentation method, the fact that sample height was known aided in the robust determination of *E* modulus, since substrate effects were minimised. Five *F-d* curves were performed on each cell under examination with 60 sec intervals between successive measurements. The speed was maintained constant at 5μm/sec throughout the experiments. Approximately 8-10 cells were tested for each cultured petri dish and extension curves from multiple experiments were analysed for the calculation of elasticity. The total number of cells that were used for analysis for each treatment is shown in Table 3.4.

Table 3.4 A table showing the number of tested MIN6 cells and extension curves obtained in AFM-FS indentation that were either processed or rejected. A total of 157 extension F-d curves from 31 Ca^{2+} cells were analysed, while a total of 162 extension curves of 32 cells treated with +R568 cells were analysed.

MIN6 cells indentation measurements		
n=3	**Ca^{2+}**	**Ca^{2+} +R568**
Total No of Cells	32	33
No of accepted cells	31	32
Processed curves	157	162
Discarded curves	3	3

Extension *F-d* curves provide important information regarding the elastic properties of a sample. *E* modulus is most commonly extracted by fitting the Hertz model for spherical beads (Vinckier & Semenza, 1998). As the cantilever is moving downwards, it reaches a point where the microbead is in contact with the plasma membrane and the cantilever is deflected upwards, resulting in the positive force values. Since the displacement positions of the substrate and the plasma membrane were predetermined, the depth of indentation was fixed before testing and was readjusted every time before testing each cell. Figure 3.8 shows the extension *F-d* curve of a cell with height of 4.5μm acquired from an AFM indentation measurement. Figure 3.8(a) shows the *F-d* extension curve of a Ca^{2+} cell and the elasticity values as determined using the Hertz model. The contact point for fitting the data to the specific curve was approximately at 0.1nN, which is almost 450nm after the initial upwards deflection of the cantilever as determined by the software of the AFM system. However, by fitting the model into parts of the curve with displacement ranges less than 10% of the cell height, the contact point was thoroughly investigated during the processing of the data and decided with correspondence to increases in *E* modulus. Figure 3.8(b) shows the *F-d* extension curve of a Ca^{2+} +R568 cell and the elasticity values as determined using the Hertz model and with the aid of incremental displace-

ment fitting. The height of the tested cell was 4.5μm, the contact point was at 0.1nN, which is approximately 400nm after the initial deflection of the cantilever. The changes in *E* modulus value was obvious by the differences of the slope of the curve. Since at this moderate degree of indentation depth the effects of the various organelles of the cell are not introduced to the calculation of elasticity (Leporatti, 2006), it is safe to assume that the differences in *E* modulus between control and +R568 treated cells are mainly contributed by changes in the cytoskeleton.

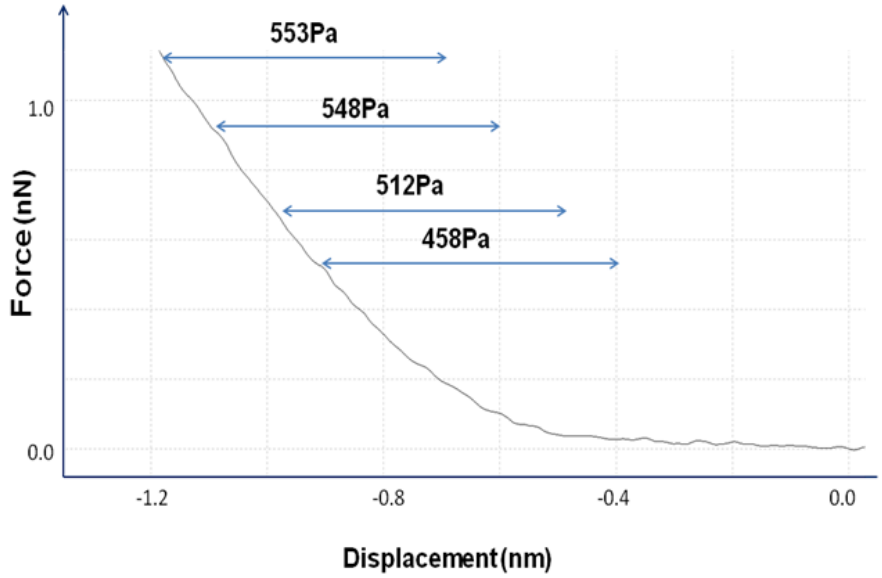

(a)

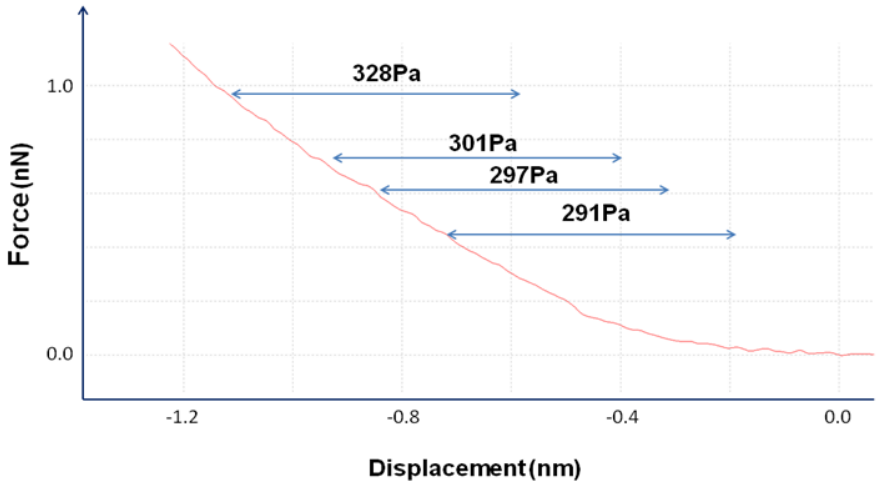

(b)

Figure 3.8 The effects of CaSR activation, followed by treatment with the calcimimetic R568, on *E* modulus as determined using AFM-FS indentation. For a cell of 4.5*μ*m in height the depth of indentation was 450nm. The contact point for each cell was identified by fitting various parts of the extension *F-d* curve with Hertz model. A contact point at approximately 0.1nN was used for the calculation of *E* modulus. The extension speed of 5*μ*m/sec was remained constant throughout the experiments. (a) For control cells the E modulus was 512Pa, (b) following treatment with R568 *E* modulus was 297Pa.

The histograms of *E* modulus obtained from the *F-d* curve measurements of control and +R568 treated cells are shown in Figure 3.9 (a) and (b) respectively. Since the data acquired from MIN6 AFM indentation experiments were normally distributed, t-testing analysis was performed. Table 3.5 shows the descriptive statistics for the *E* modulus that was calculated from retraction *F-d* curves of MIN6 cells indentation. For the control cells, the *E* modulus had a mean of 503Pa and a standard error of 10.5. For the cells treated with R568, the *E* modulus had a mean of 327Pa and standard error of 9.29. The differences in *E* modulus between control and +R568 treated cells calculated from extension curves as analysed using paired samples t-test are shown in table 3.6. On average, Ca^{2+}+R568 cells showed to have lower *E* modulus (M=327.9924, SE=9.29) than Ca^{2+} cells (M=503.0382, SE=10.5). This difference was statistically significant ($t(317)=12.53$, $p<0.001$). Figure 3.10 shows the changes in elasticity between the two groups of cells, resulted from the processing and analysis of than 150 curves for each treatment obtained from 3 separate AFM-FS indentation experiments. The results were analysed using paired samples t-test and the data are expressed as mean ± SEM. The data indicate that the calcimimetic R568

(1μM) decreased the elastic modulus by 34% (>30 cells, n=3, p<0.001) (Figure 3.10), suggesting that cells treated with the R568 became considerably softer.

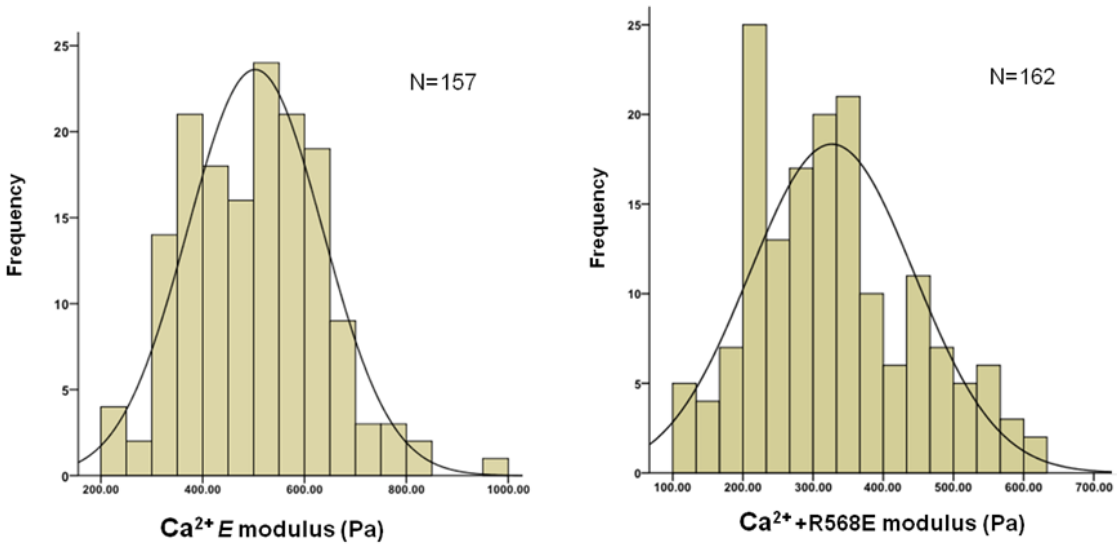

(a) (b)

Figure 3.9 Distribution of frequencies of *E* modulus (a) in Ca^{2+} cells and (b) in Ca^{2+}+R568.

Table 3.5 Table presenting the descriptive statistics of the E modulus for the control cells and for the cells treated with R568.

***E* modulus (Pa)**	Mean	N	Std. Deviation	Std. Error Mean
Ca^{2+}	503.0382	157	132.63424	10.58536
Ca^{2+}+R568	326.9924	162	116.44312	9.29317

Table 3.6 Table presenting the differences in E modulus between control and +R568 treated cells using paired wise t-test.

Mean	SD	SE	95%CI		t	df	Sig
172.04	172.03	13.72	lower	Upper	12.53	317	.000
			144.92	199.16			

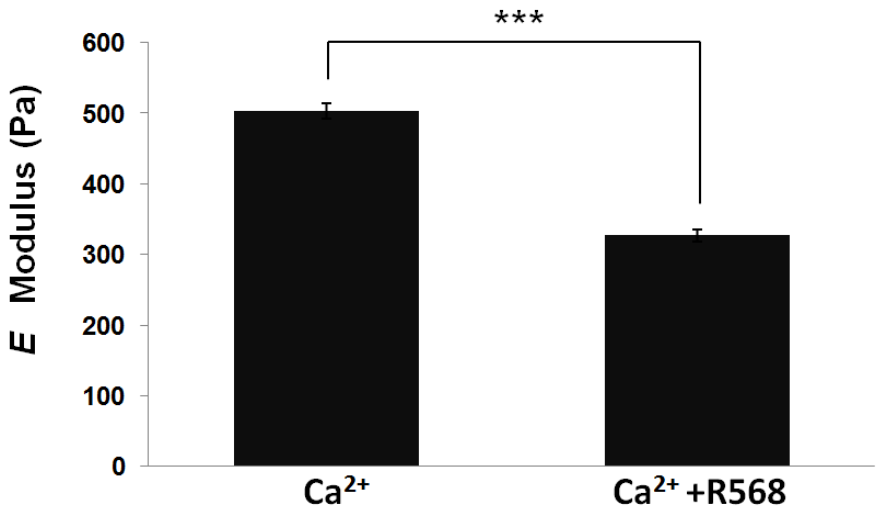

Figure 3.10 The effects of the calcimimetic R568 (1μM) on the *E* modulus (decreased by 34%) of MIN6 cells. Data are expressed as mean ±SEM of more than 30 cells from 3 separate experiments, where key significances are shown, ***p<0.001.

3.4 Effects of Pulling Speed on β-cell-to-β-cell Adhesion

In order to assess the effects of cellular viscoelastic deformation on cell-to-cell adhesion, SCFS retraction *F-d* curves were performed with incremental speed. The parameters of adhesion, such as contact force and time, were kept constant at 0.8nN and 5sec respectively. The cantilever was extended at constant speed of 5μm/sec and retracted at higher speeds, while retraction *F-d* curves were recorded for displacements up to 100*μ*m. Since the contact time was constant, no changes in the density of E-cadherin mediated ligation between incremental pulling speed measurements were expected. The procedure was repeated three times for each cell under examination at various speeds between 5-15*μ*m/sec. A 30sec interval was preceded before each successive *F-d* measurement and a 60sec was preceded before measurements with different pulling speed. Considering that experiments were performed using four different speeds, at least twelve *F-d* measurements were performed in each cell. A single cell, attached on the end of the cantilever, was used for testing up to 3 different substrate cells.

The number of cells tested in SCFS adhesion experiment and the number of processed or rejected *F-d* curves for velocities higher than 5*μ*m/sec is shown in table 3.7. Experiments with increased retraction pulling speed was performed to a number of 30 cells. The adhesion characteristics with pulling speed 5*μ*m/sec is presented in the first section of this chapter. As the speed was increased many cells had to be rejected from further processing. In fact, more than half of the acquired curves were rejected, since the displacement range was insufficient to completely detach the two cells from each other as the speed was increased. Accurate determination of the point of complete separation is important for the processing of the retraction curves

and the calculation of adhesion characteristics. As a consequence, measurements with speed 15*μ*m/sec had to be rejected and maximal pulling speed in which analysis was performed was 12.5*μ*m/sec.

Table 3.7 A table showing the number of tested MIN6 cells and number of processed or rejected retraction *F-d* curves obtained by SCFS adhesion experiment with incremental retraction velocities. As shown, more than 1/2 of the curves of 10 and 12.5*μ*m/sec were rejected, while no cells at 15*μ*m/sec were accepted for processing.

MIN6 cells SCFS incremental speed retraction measurements						
n=3	**Ca^{2+}**			**Ca^{2+} +R568**		
Pulling Speed (μm/sec)	**5**	**10**	**12.5**	**5**	**10**	**12.5**
Total No of Cells	48	30	30	45	30	30
No of accepted cells	41	14	14	36	10	11
Processed curves	102	41	40	108	29	32
Discarded curves	42	49	50	57	61	58

The effects of increasing pulling velocities to the retraction *F-d* curves of cells treated with +R568 are illustrated in Figure 3.11. Due to the soft nature of the cells, data were processed and analysed up to speed of 12.5*μ*m/sec. As shown, the retraction curve of speed 15*μ*m/sec of a Ca^{2+} +R568 cell exhibited large displacement plateaus, corresponding to high cellular deformation, while less than 10 unbinding events occurred after the first 2.3*μ*m of retraction, over the full range of displacement. A significantly higher displacement range than 100*μ*m was required for the complete separation of the cells in velocities higher than 12.5*μ*m/sec. In fact, even at

pulling speed of 10*μ*m/sec partial separation was observed, causing difficulties in the determination of the baseline for the calculation of adhesive parameters. In order to obtain correct values for maximum force work of detachment, in the instances of incomplete separation the x-axis reference was determined using the baseline of the extension curve. Any drift of the extension curve would result in misleading values, ultimately leading to the rejection of a large number of data. Moreover, since more displacement range was required to completely detach the two cells, measurements of work of adhesion are actually higher than presented. However, even at the range of 100*μ*m the changes in work of detachment are dramatic.

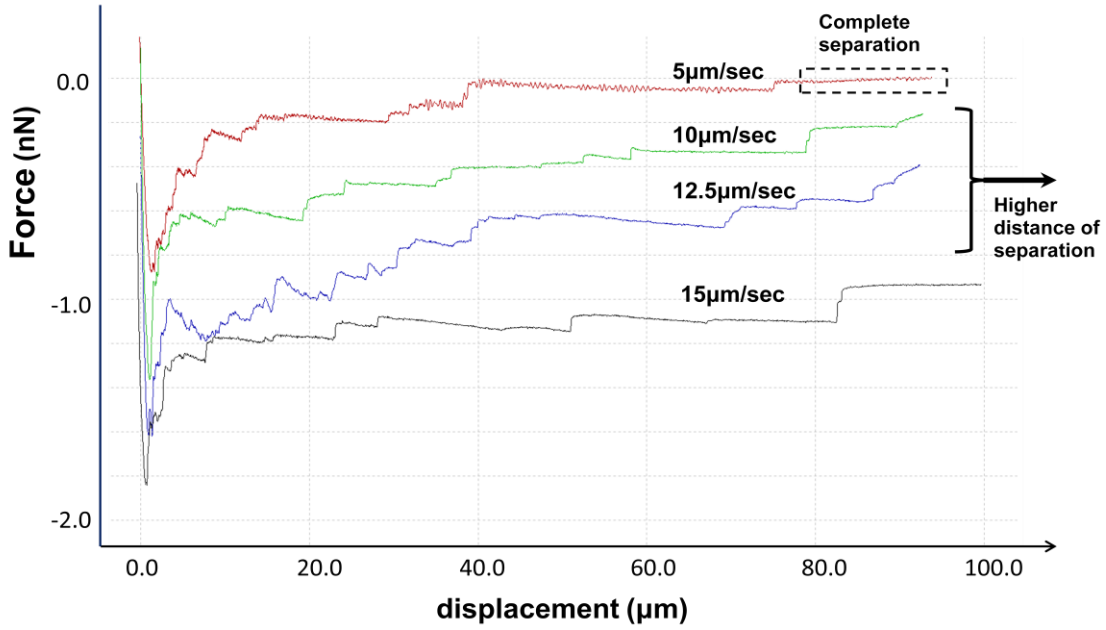

Figure 3.11 Retraction *F-d* curves acquired by adhesion measurements of MIN6 cells treated with +R568 with incremental pulling speed are shown. The effects of increasing pulling speed on adhesion characteristics are clearly shown. For speeds higher than 5*μ*m/sec partial separation was observed. The levels of incomplete separation were increasing with the increase of pulling speed resulting in the total rejection of measurements with pulling speed of 15*μ*m/sec due to the limitation of 100*μ*m in displacement range.

Approximately 10 cells from 3 different experiments with increasing pulling speed were analysed and the data are expressed as mean ± SD. The results demonstrate a tenfold increase of the W_D in comparison to the F_{max} as the pulling speed increases, up to the pulling distance of 100μm (Figure 3.12(a) & (b)). The decrease of number of TREs for a displacement range of 30μm after F_{max} was two times higher for the cells treated with the calcimimetic in comparison to the untreated (Figure 3.12(c)). This decrease on TREs does not reflect changes in the expression of E-cadherin on the surface of the cell, since no chemical modification was applied in between measurements with increasing velocities. The decrease in the number of TREs in higher speeds than 5μm/sec, shows that the softer cell showed less unbinding events, over the range of the first 30μm of pulling distance, due to its ability to deform further than the control cells.

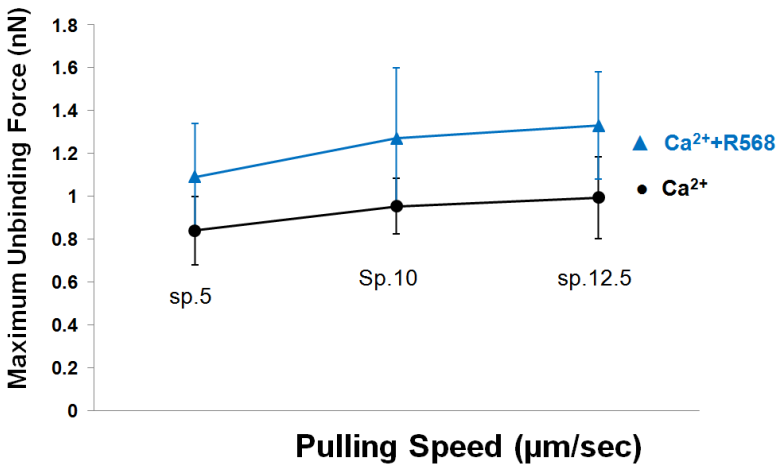

(a)

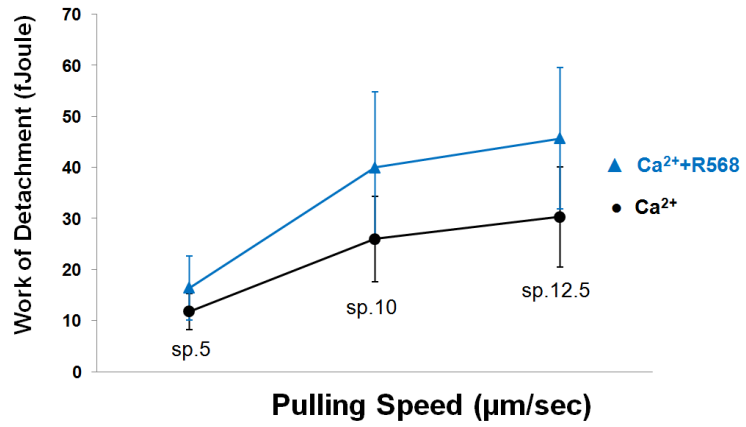

(b)

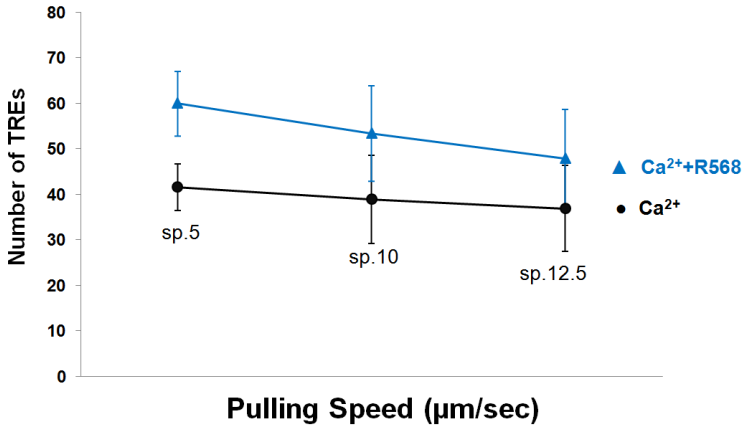

(c)

Figure 3.12 The effects of increasing pulling speed on the cell-to-cell adhesion parameters of MIN6 cells obtained by SCFS retraction F-d curves. Data are expressed as mean ± SD and the effects of increasing pulling speed on (a) maximum unbinding force, (b) work of detachment and (c) number of tethering rupture events are illustrated.

The changes in elasticity of single cells upon CaSR activation together with the adhesion results with incremental velocities suggest that elastic/viscoelastic deformation plays a key role in adhesion between β cells. Altering the pulling speed of the

coupled cells, affected dramatically the characteristics of the retraction *F-d* curves acquired by adhesion measurements. Work of detachment was mostly affected, resulting in a tenfold increase when pulling speed was increased by a factor of 2, in comparison to the maximum unbinding force. Surface protein binding affinity was responsible for the increase in maximum unbinding force, however the results suggested that this was only partially responsible for the increase in work of detachment, which was dominated by the changes of the mechanical properties of the cell. An increase in work of detachment could mirror changes in the compliance of cells, since it is partly contributed from the elastic deformation of an elastic sphere apart from the adhesion due to surface contact (Johnson & Greenwood, 1997). This is clearly demonstrated in this study by the increase in *E* as well as by the dramatic increase of work of detachment when pulling speed was increased. The comparison between increasing pulling speeds also suggests that although the surface properties were significant for changes in maximum unbinding force, changes in the mechanical properties in response to cytoskeleton reorganisation rather than ligation binding affinity or surface density of E-cadherin, contribute to the dramatic changes of the work of detachment. Besides, the increase in F_{max} with an increased pulling speed could be contributed to the viscoelastic deformation of the surface proteins themselves and membrane tethers. Diz-Munoz et al. (2010) measured the dynamics of tethering force between the AFM tip and cell membrane, also concluding that the unbinding force increased as the pulling velocity increased. Both the adhesion and indentation measurements clearly suggest that the viscoelastic deformation has a significant influence on the adhesion energy between two adherent cells and that cytomechanics contribute to the E-cadherin mediated adhesion in system under investigation.

3.6 Conclusion

The endocrine pancreatic islet is mainly constituting by β-cells that represent almost 60-70% of the islet. The aim of this study was to make use of an *in vitro* cell model that resembles the β-cell structure and function. MIN6 cells preserve physiological glucose-responsiveness and have been used in studies aiming to investigate the maintenance of insulin secretion (Hauge-Evans et al., 1999; Kelly et al., 2010; Skelin et al., 2010). In addition, the use of a simplified cell line, such as the MIN6, had the advantage that homotypic interactions between the cells were ensured (Miyazaki et al., 1990, Persaud, 1999). Hence, the study of β-cell-to-β-cell coupling by quantitatively determining their functional adhesiveness using AFM was facilitated.

In the current study the effects of whole cell elasticity under the influence of the calcimimetic R568 in the MIN6 clonal β-cell line were investigated. In addition, quantitative evidence that the mechanical properties of single cells have an effect on cell-to-cell interaction has been provided. Activation of CaSR increased the expression of the surface adhesion protein E-cadherin (Hills et al., 2012b), whilst affected on the intracellular domain of the protein by increasing the elasticity of the cell. The changes in the inner mechanical properties of the cells had a strong effect on cell-to-cell adhesion energy, mainly due to viscoelastic deformation of the cells during the pulling process. As a consequence, adhesion parameters were altered not only due to biomolecular changes in cell surface expression of E-cadherin, as previously reported, but also due to changes in the biomechanical properties of the cells. Therefore, in improving beta cell function, activation of CaSR not only increases E-cadherin expression and cell-to-cell adhesiveness but it also initiates and/or modu-

lates intracellular signalling of the F-actin cytoskeleton via the catenins. The net result is a change in the mechanistic behaviour of whole cell.

Chapter 4

Nanomechanical Characterisation of Renal Proximal Tubule HK2 Cell-to-Cell Adhesion

4. Nanomechanical Characterisation of Renal Proximal Tubule HK2 Cell-to-Cell Adhesion

4.1 Introduction

In this chapter, a force spectroscopy study of HK2 cells cultured in monolayers upon treatment with TGF-β1(10ng/ml) is presented. TGF-β1 mediates early epithelial-to-mesenchymal (EMT) transitions resulting in the excessive concentration of fibrotic material in the renal proximal tubule in diabetic nephropathy (Hills et al., 2012a). The aim of this study is to investigate the impact of TGF-β1-mediated EMT in cellular communication through functional cell-to-cell coupling. Figure 4.1(a) shows healthy (control) HK2 cells grown in a low glucose media (5mM). Under control non-stimulated conditions, control HK2 cells exhibited typical cobblestone morphology consistent with tubular epithelia. For consistency all *F-d* measurements were performed on cells that resemble this morphology. Testing was performed above the central region of the cell, which corresponds to the area where the nucleus resides. Figure 4.1(b) shows that the pro-fibrotic cytokine TGF-β1 (48h, 10ng/ml) altered the architecture of the cells and produced an elongated, fibroblast-like phenotype, which is a characteristic of TGF-β1 induced tubular damage and EMT. The elongated shape of the treated cells was used as a sign during the AFM experiments that the transformation occurred. As the β-cell experiments, all *F-d* measurements were performed directly above the nucleus.

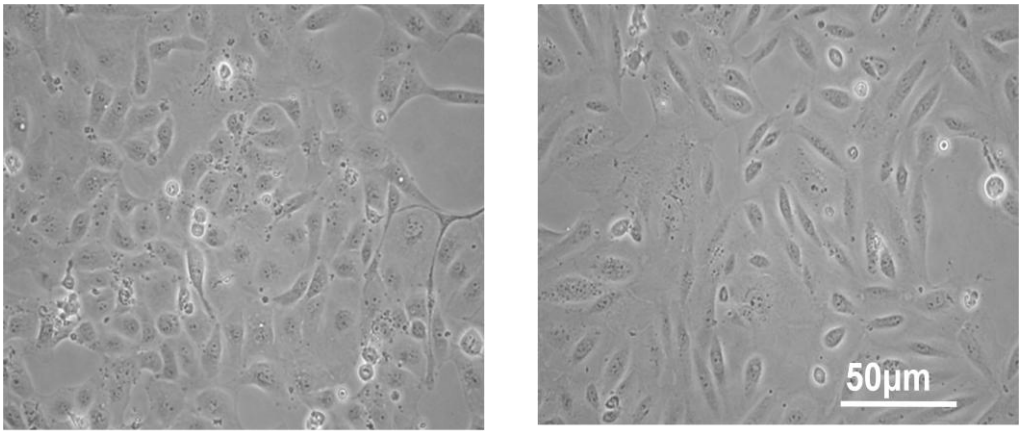

(a) (b)

Figure 4.1 Phase microscopy showing cell morphology of (a) healthy (control) cells and (b) cells treated with TGF-β1 (48h, 10ng/ml). It is clear that TGF-β1 evoked changes in cell morphology, resulting in translucent elongated cells that exhibited clear demarcation between neighbouring cells.

4.2 Effects of TGF-β1 on Functional Cell-to-Cell Adhesion

HK2 cells were treated for 48h in low glucose media (5mM) ± the TGF-β1 (10ng/ml). Treatment of control cells with the cytokine decreases expression of E-cadherin (Hills et al., 2012a). In order to relate the changes in the surface expression of E-cadherin to functional cell-to-cell tethering, SCFS was used to quantify cell-to-cell adhesion parameters, such as the forces required for the complete detachment of coupled cells. A single HK2 cell was attached at the end of a functionalised arrow cantilever and subsequently brought in contact with a single substrate cell within a cluster of coupled cells. Figure 4.2 shows optical images of the cantilever-cell system prior conducting adhesion measurements on single cells on the substrate. In (a), the control cells are shown, while in (b), the cells treated with TGF-β1 are shown. The morphological differences in favour of a fibroblast phenotype were clear during experiments.

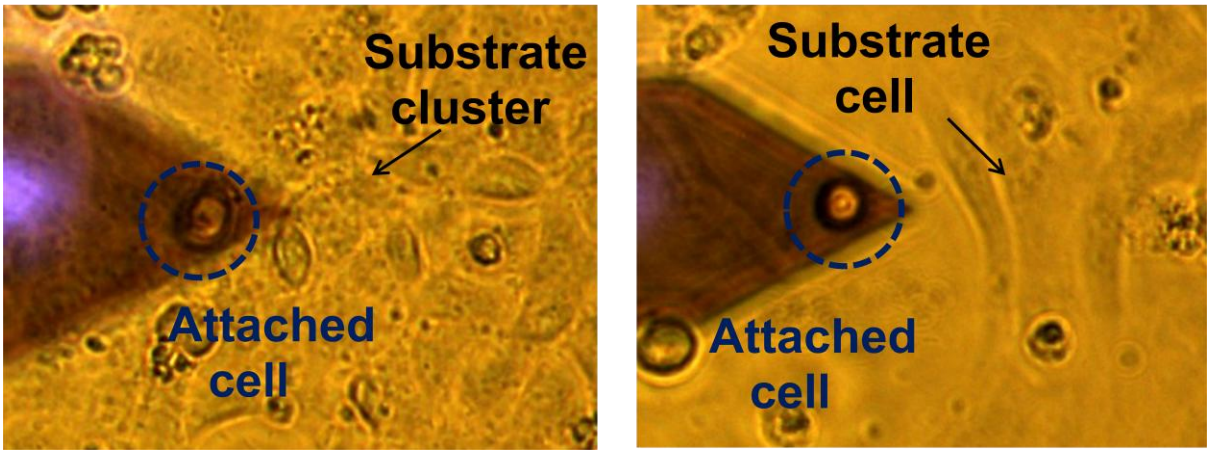

(a) (b)

Figure 4.2 Phase microscopy images showing a HK2 cell-to-cell experiment. In (a), HK2 cells incubated for 48h in low glucose media (control). The suspended cell was attached on the functionalised cantilever and then was brought in contact with a single substrate cell (within a cluster of cells) for 10 secs, while force versus displacement was measured simultaneously. In (b), HK2 cells incubated with TGF-β1 for 48 hours in low glucose media. Note that the substrate cells were elongated and were not organised in clusters.

A few set of measurements were performed to select the parameters prior adhesion measurements. As with the β-cells, the main criterion for determining the parameters was the displacement range of complete separation. The point of complete separation acts as a reference for the calculation of adhesion parameters. The experimental specifications had to allow complete detachment of the cells within the displacement range of the piezo actuator of the AFM. A fixed set-point force of 1.0nN was used for the probe cell to touch the substrate cell, while the contact time for ligation binding was 10sec. The cantilever was retracted at a constant speed of 5μm/sec and retraction *F-d* curves were recorded until the two cells were completely detached from each other. The procedure was repeated three times for each cell under investiga-

tion, with 30 sec intervals between each successive measurement. The attached cell was used to perform measurements on approximately 10 cells per cultured petri dish.

Retraction curves acquired from multiple HK2 cell-to-cell adhesion measurements were analysed in order to assess changes in functional tethering after chemical treatment with the cytokine. Altering the E-cadherin protein expression does not inevitably leads to changes in the functional adhesiveness of the cells. Therefore, by using identical SCFS experimental conditions in more than 40 cells from separate experiments (n=5), the function of the adhesion molecule was investigated. The number of cells that were used for analysis for each treatment is shown in Table 4.1. There is a noticeable number of retraction curves that have been discarded from further processing, mainly due to moving particles in the cultured media or environmental noise. As mentioned in section 3.2, the introduction of suspended cells into the dish under examination results in disturbances in the recording of *F-d* curves.

Table 4.1 A table showing the number of tested HK2 cells and retraction curves obtained from SCFS that were either processed or rejected. A total of 102 retraction measurements from 43 control cells were analysed, while a total of 130 retraction curves from 44 TGF-β1 treated cells were analysed. Approximately 1/3 of the curves were rejected due to disturbances when recording a retraction *F-d* curve.

HK2 cells SCFS retraction measurements		
n=5	**Ca^{2+}**	**Ca^{2+} +R568**
Total No of Cells	47	53

No of accepted cells	43	44
Processed curves	102	130
Discarded curves	39	29

Retraction *F-d* curves provided important information regarding the adhesion parameters between two cells. Functional changes in the expression of a protein under investigation in the surface of the cell were uncovered by the detection of the maximum unbinding force and the number of tether rupture events. Moreover, adhesion parameters such as work or distance to complete detachment, provided information regarding the contribution of cellular deformation on cell-to-cell adhesion that is mediated by surface ligation. Complete separation between the probe and the substrate cell, under the 5*μ*m/sec speed, was achieved by using an effective retraction range of at least 80*μ*m. The retraction curves of Figure 4.3 illustrate the effects of TGF-β1 treatment on adhesion parameters of HK2 cells.

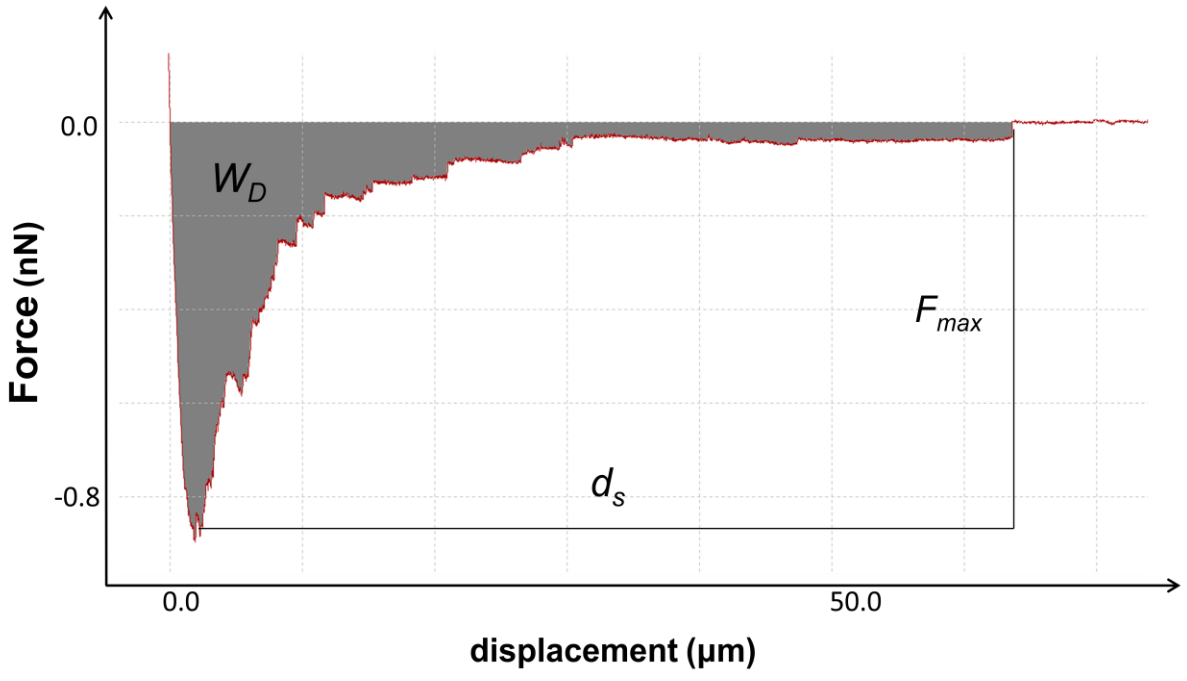

(a)

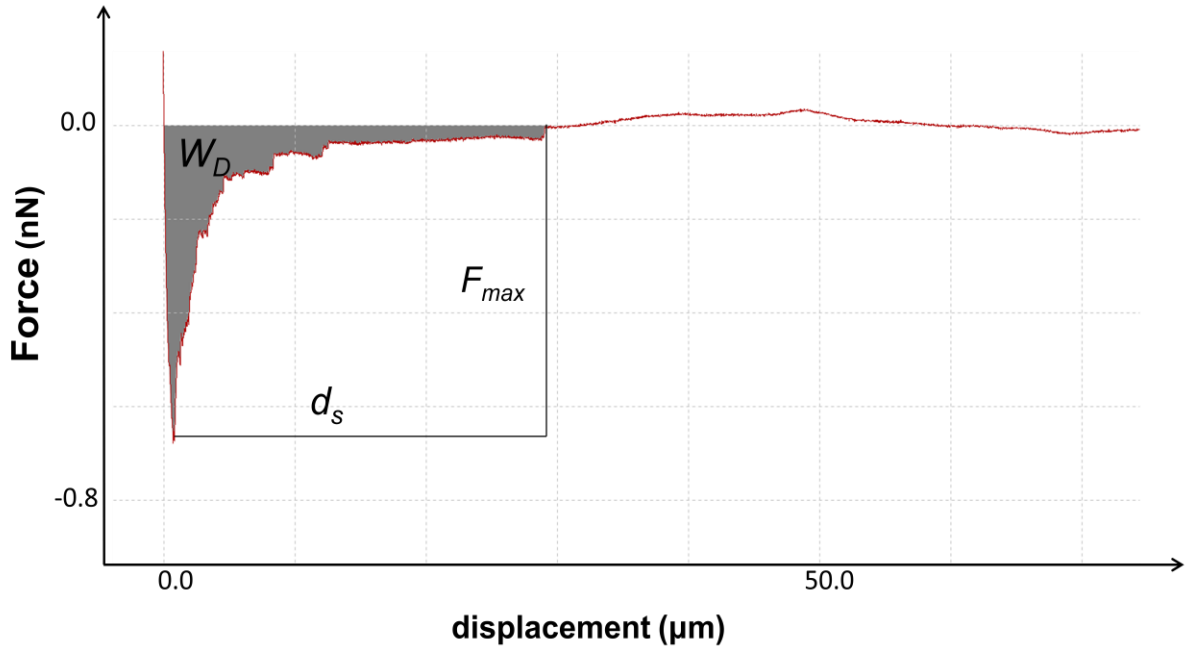

(b)

Figure 4.3 The effects of the cytokine TGF-β1 on E-cadherin mediated cell-to-cell adhesion of HK2 cells were examined using AFM-SCFS. F_{max} is the difference between the minimum force value and the point of complete detachment, W_D (grey region) is the integral of the continuous area under the baseline of complete separation and d_s is the difference between F_{max} and the point of complete separation. A set-point force of 1.0nN,a contact time of 10sec and a pulling speed of 5μm/sec were remained constant throughout the experiments. Alterations of adhesion parameters such as F_{max}, W_D and d_s provide an important insight about functional cell-to-cell adhesion. In (a) F_{max} is 0.9nN, W_D is 8.6fJoule and d_s is 61.7μm while in (b) F_{max} is 0.68nN, W_D is 2.7fJoule and d_s is 28.2μm.

Changes in the expression of E-cadherin upon treatment of HK2 cells with TGF-β1 were detected by calculating the number of unbinding events during the retraction process. The retraction *F-d* curves of figure 4.4 illustrate the number of rupture tethers as detected by the step fitting function of the software used for data processing.

Treatment with TGF-β1 decreased the TREs, corresponding to a decrease in the expression of the E-cadherin protein at the surface of the cell, which is in agreement with Hills et al. (2012a). In Figure 4.4(a) a retraction *F-d* curve of a healthy HK2 cell is shown. Sharp steps of force that are not preceded by a displacement plateau (*'j'* events) occurred in the first 4.15*μ*m of the pulling range. As the distance of separation increased, a point was reached where both *'j'* and *'t'* events occurred, indicating the initiation of cellular deformations. As the distance of separation was increased further, extended displacement plateaus were observed (noted with the arrows), as a result of the deformation of the cell. In Figure 4.4(b) a retraction *F-d* curve of a HK2 treated with TGF-β1 is shown. Type *'j'* events occurred in the first 3.85*μ*m of the pulling range, while the number of events that were preceded by a displacement plateau, due to cell deformation, was decreased. Therefore, cells treated with the cytokine became more rigid, as also indicated by the decrease in distance of complete detachment.

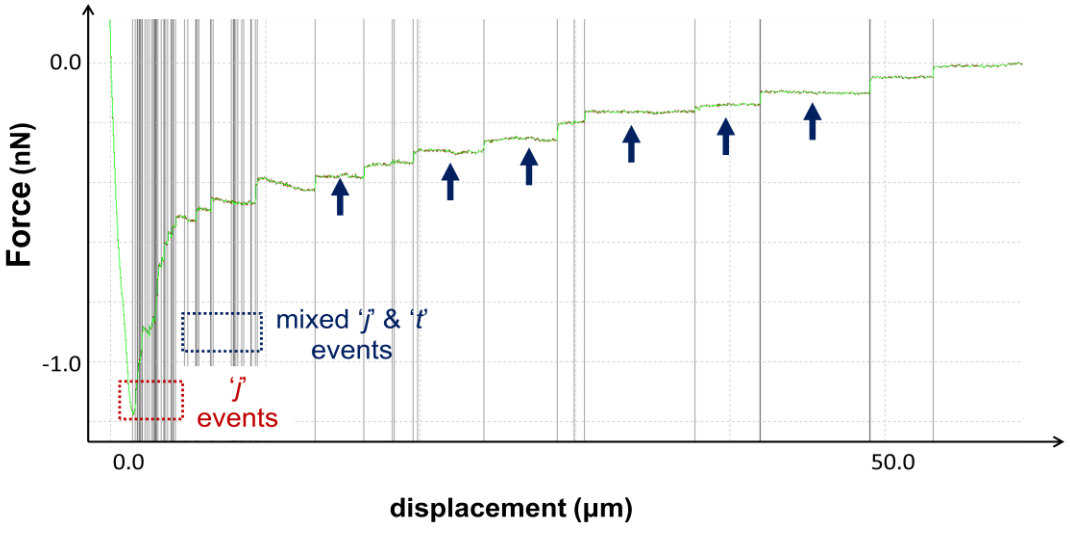

(a)

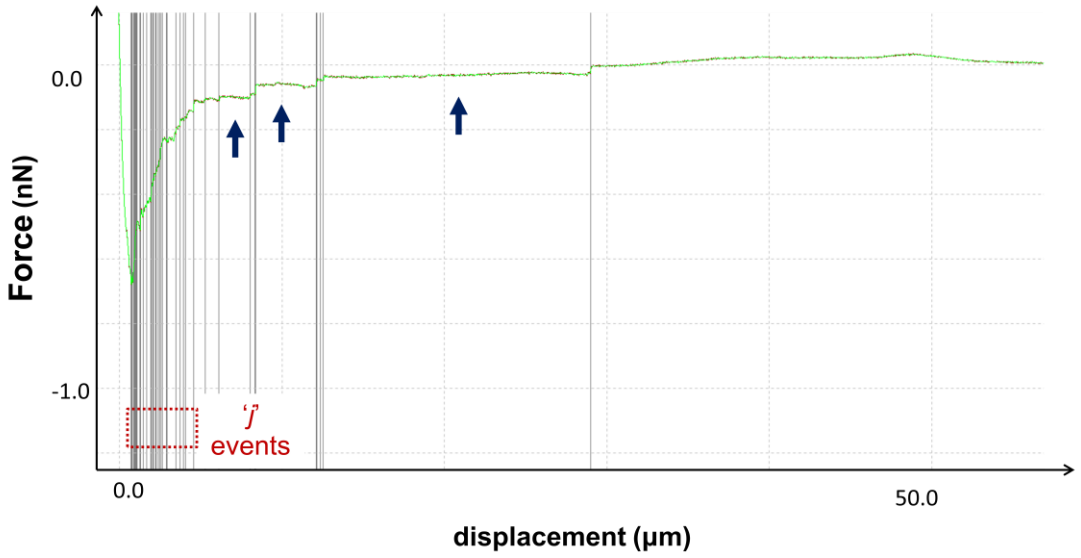

(b)

Figure 4.4 Retraction force-distance curves obtained by HK2 cell-to-cell adhesion measurements, showing the effects of TGF-β1 on the tether rupture events. Unbinding of ligations that occur during the early pulling phase (approximately 5µm after the minimum force value) are preceded by a force ramp (*'j'* events). As the pulling distance increases an area is reached where the rupture events are preceded by a displacement plateau as well (*'t'* events) due to the deformation of the cell. In (a) the number of TREs is 73, whilst most of the unbinding events occurred in the first 8.2*µ*m of pulling range, corresponding to the area of *'j'* and mixed *'j'* and *'t'* events. After that point and until the complete detachment of the cells extended separation displacements occurred (*'t'* events), owing to the deformation of the cell. In (b) the number of TREs is 51, whilst most of the unbinding events occurred in the first 3.85*µ*m, and were not preceded by a displacement plateau.

The histograms of maximum unbinding force and work of detachment obtained from the *F-d* curve measurements of control HK2 cells are shown in Figure 4.5. Overall the data acquired from HK2 cell-to-cell adhesion experiments were normally distributed, suggesting that the assumption for performing t-test has been satisfied. Table 4.2 shows the descriptive statistics for the various adhesion parameters that were extracted from the retraction *F-d* curves. The maximum unbinding force (nN) of HK2 control cells had a mean of 0.74 and a standard error of 0.026, whereas the TGF-β1 had a mean of 0.60 and a standard error of 0.029 (Table 4.2(a)). The work of detachment (fJoule) for the control cell had a mean value of 7.82 and standards error of 0.40, while for the cells treated with the cytokine had a mean of 3.68 and a standard error of 0.29 (Table 4.2(b)). The number of tether rupture events for the control cells had a mean value of 64.2 and a standard error of 0.77, whereas for the treated cells had a mean of 41.71 and a standard error of 0.95 (Table 4.2(c)). Finally, the distance of separation (μm) for the control cells had a mean of 62.15 and standard error of 0.89, while for the TGF-β1 had a mean value of 33.1 and standard error of 0.59 (Table 4.2(d)).

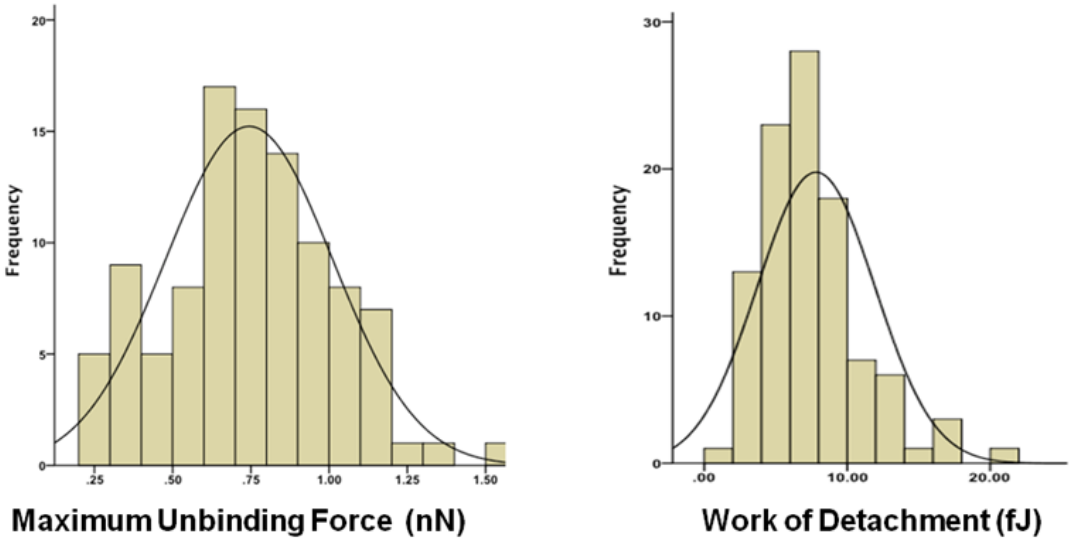

(a) (b)

Figure 4.5 (a) Distribution of frequencies of maximum unbinding forces and (b) distribution of frequencies of work of detachment.

Table 4.2 Table presenting descriptive statistics for the adhesion parameters, (a) of maximum unbinding force for the control and for the TGF-β1 treated cells, (b) of work detachment for the control and for the TGF-β1 treated cells, (c) of tether rupture events for the control and for the TGF-β1 treated cells and (d) of distance separation for the control and for the TGF-β1 treated cells.

F_{max}(nN)	Mean	N	Std. Deviation	Std. Error Mean
Control	0.7443	102	0.26728	0.02646
TGF-β1 (10ng/ml)	0.6022	130	0.29292	0.02900

(a)

W_d (fJoule)	Mean	N	Std. Deviation	Std. Error Mean
Control	7.8168	102	4.11457	0.40740
TGF-β1 (10ng/ml)	3.6764	130	3.00391	0.29743

(b)

No of TREs	Mean	N	Std. Deviation	Std. Error Mean
Control	64.2029	102	6.36530	0.76629
TGF-β1 (10ng/ml)	41.7101	130	7.94485	0.95645

(c)

d_s (μm)	Mean	N	Std. Deviation	Std. Error Mean
Control	62.1532	102	7.89409	0.88815
TGF-β1 (10ng/ml)	33.0949	130	5.28020	0.59407

(d)

The differences between control and TGF-β1 treated cells for the various adhesion parameters obtained from retraction curves were analysed using paired samples t-test and are presented shown in table 4.3. The t-test results showed that for all the measured adhesion parameters, the probability was very low, indicating that the there is only 0% probability that the null hypothesis of equal means was true. Thus, it is concluded that the control cells had higher unbinding force (nN) (M=0.74,

SE=0.026) than the TGF-β1 cells (M=0.60, SE=0.029) and that difference was statistical significant t(230)=5.722, p<0.001 (Table 4.3(a)). Similarly, the control cells had higher work of detachment (*f*Joule) (M=7.82, SE=0.407) than the TGF-β1 cells (M=3.67, SE=.029), and that difference was statistical significant t(230)=7.709, p<0.001 (Table 4.3(b)). Furthermore, the results showed that the control cells had higher number of unbinding events (M=64.2, SE=0.766) than the TGF-β1 (M=41.71, SE=0.95), and that difference was statistical significant t(230)=19.28, p<0.001 (Table 4.3(c)). Finally, the control cells had higher separation distance (μm) (M=62.15, SE=0.88) than the TGF-β1 cells (M=33.1, SE=0.59) and that difference was statistical significant t(230)=28.5, p<0.001 (Table 4.3(d)).

Table 4.3 Table presenting the differences between control and TGF-β1 treated cells using paired wise t-test, (a) of the maximum unbinding force between control and TGF-β1 cells, (b) of work detachment between the control and TGF-β1 cells, (c) of the number of tether rupture events between the control and TGF-β1 cells and (d) of the distance of separation between control and TGF-β1 cells.

Mean	**SD**	**SE**	**95%CI**		**t**	**df**	**Sig**
0.142	0.405	0.040	lower	Upper	5.722	230	0.000
			0.1499	0.3090			

(a)

Mean	SD	SE	95%CI		t	df	Sig
4.1404	5.55	0.55009	lower	Upper	7.709	230	0.000
			3.14	5.33			

(b)

Mean	SD	SE	95%CI		t	df	Sig
22.49	9.62	1.16	lower	Upper	19.28	230	0.000
			20.16	24.82			

(c)

Mean	SD	SE	95%CI		t	df	Sig
29.05	9.05	1.019	lower	Upper	28.514	230	0.000
			27.02	31.08			

(d)

More than 100 curves from 5 separate experiments were analysed and the data are expressed as mean ± SEM in Figure 4.6. The results indicate that TGF-β1 induced changes decreased the number of tether rupture events by 35%, resulting in an decrease of the maximum unbinding force by 19%. However, the work or energy of de-

tachment was decreased more significantly by 53%, consistent with a reduction of 46% in distance of separation (>30 cells, n=5, p<0.001) (Figure 4.6(a)-(d)).

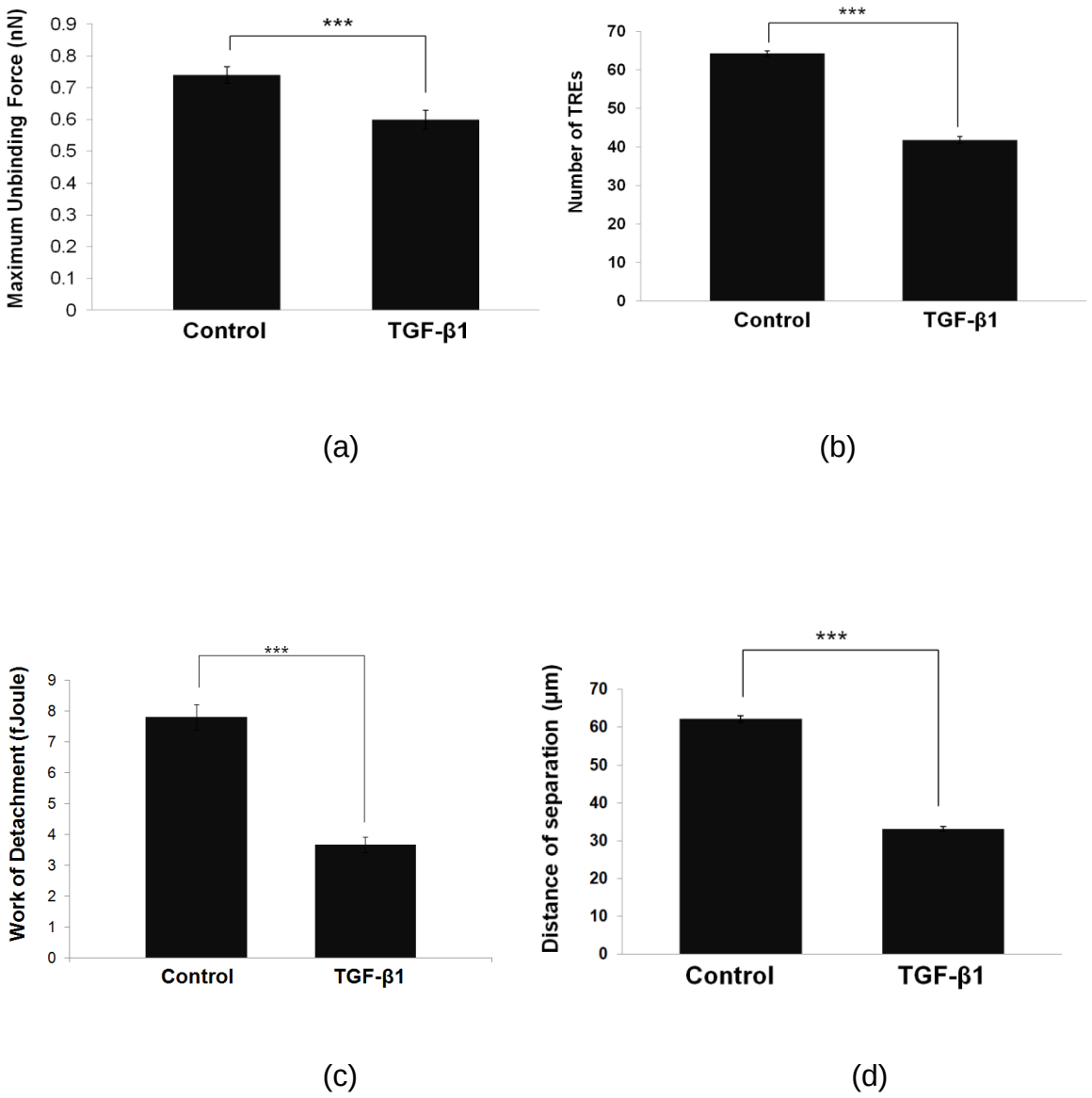

Figure 4.6 The effects of the cytokine TGF-β1(48h/10ng/ml) on (a) the maximum unbinding force (decreased by 19%), (b) the number of tethering rupture events (decreased by35%), (c) the work of detachment (decreased by 53%) and (d) the distance to complete separation (decreased by 46%) are shown. Data are expressed as mean ±SEM of more than 40 cells from 5 separate experiments, where key significances are shown, ***p<0.001.

The role of the TGF-β1 is significant in proximal tubule diseases where the changes in the epithelial characteristics are associated with disassembly of the adherens junction. E-cadherin together with the catenins aids in maintaining the epithelial characteristics in normal conditions by forming gap junctions to facilitate communication between cells. In addition, E-cadherin is the most well characterised adhesion protein that mediates epithelial cell-to-cell adhesion (Perez-Moreno et al., 2003; Hills et al., 2012a). In this study the effects of TGF-β1 on E-cadherin mediated cell-to-cell adhesion in renal proximal tubule HK2 cells were quantified using AFM-SCFS. Since HK2 cells maintain the functional characteristics of the proximal tubular epithelium, this cell line was ideal for studying the loss of epithelial characteristics that occur in the early EMT in diabetic nephropathy. In this study the effects of TGF-β1 induced EMT in the communication between cells through cell-to-cell adhesion have been investigated. The results showed that the cytokine decreased E-cadherin mediated functional tethering between two adherent HK2 cells. A main concern when studying cell-to-cell adhesion is the difficulty to control the expressions of the adhesion proteins at the surface of the cell. This is due to the heterogeneous nature of the sample resulting in some complex molecular interaction between the cells. One method to overcome this by examining the frequency of adhesion events from the *F-d* retraction curves of each group under chemical treatment was suggested by Zhang et al. (2002). In this research project the localisation of specific protein binding as well as the distribution of the candidate protein was assessed prior conducting SCFS by immunoblotting and immunocytochemistry respectively (Hills et al., 2012a). Nevertheless, by altering the expression of a candidate protein does not absolutely indicate that the function of the cell will respond. Changes in the functional cell-to-cell adhesion were signified by SCFS, showing that TGF-β1 evoked reduction of E-

cadherin decreased functional tethering between treated cells. The frequency of specific binding events was confirmed by the retraction *F-d* curves showing a reduction in the number of TREs at the surface of the cells after TGF-β1 treatment.

4.3 Effects of TGF-β on Single Cell Elasticity

HK2 cells were treated for 48h in low glucose media (5mM) ± the TGF-β1 (10ng/ml). Treatment of control cells with the cytokine decreases expression of E-cadherin (Hills et al. 2012a), which in the extracellular domain mediates ligation with adherent cells and in the intracellular domain is linked with actin cytoskeleton via the catenins. In order to investigate the role of the CSK in the E-cadherin mediated functional adhesion measurements, single cell indentation was used to characterise cell elasticity. A spherical microbead of 10μm in diameter was attached at the end of a modified arrow cantilever and subsequently indented a single cell, according to a predetermined indentation depth based on cell height. Figure 4.7 presents optical microscopy images of a single cell force spectroscopy experiment for determining cell elasticity. In (a), normal HK2 cells are shown (control group), while in (b) cells treated with the cytokine TGF-β1 are shown. The morphological differences in favour of a fibroblast phenotype were clear during experiments. For the control group, cells that resemble a cobblestone morphology that reside within a cluster of cells were selected for testing. For the treated group cells that exhibit an elongated morphology were selected for testing. All measurements were performed in the area directly above the nucleus.

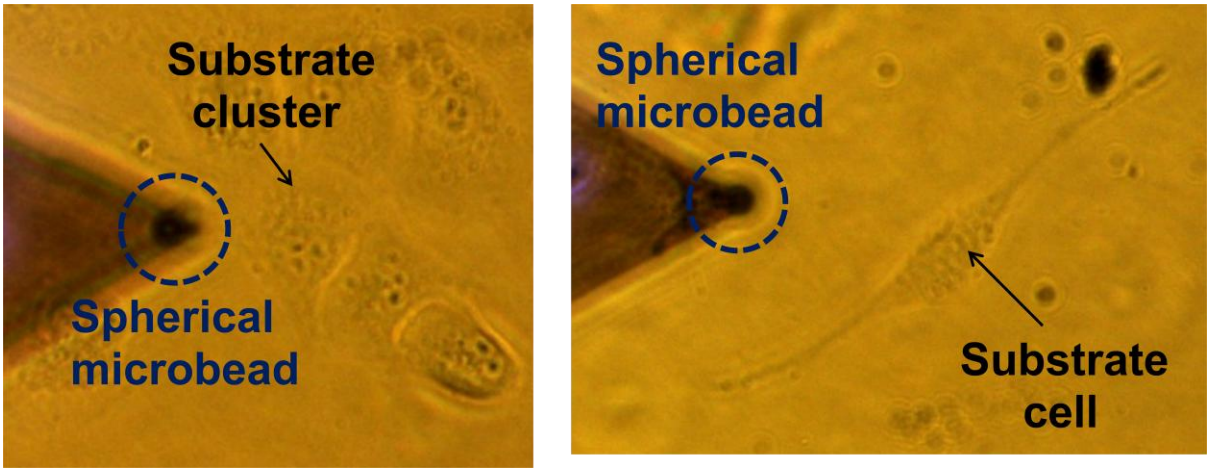

(a) (b)

Figure 4.7 Phase microscopy images showing HK2 cells indentation experiment. The cantilever was modified using a 10μm polystyrene microbead probe to enable indentation of a single substrate cell (within a cluster of cells for control group). In (a), an optical image showing normal HK2 cells (control) while in (b) cells that were treated for 48h with TGF-β1 are shown.

Prior indentation of each cell, the height of the sample was determined as described earlier. Therefore the indentation depth was customised for individual cells according to their height. Although this methodology was found to be more time consuming in comparison with the force indentation method, the fact that sample height was known aided in minimising the effects of the hard substrate in the calculation of *E* modulus. Five *F-d* curves were performed on each cell under examination with 60 sec intervals between successive measurements. The speed was maintained constant at 5μm/sec throughout the experiments. Approximately 8-10 cells were tested for each cultured petri dish and extension curves from multiple experiments were analysed for calculating single cell elasticity. The total number of cells that were used for analysis for each treatment is shown in Table 4.4.

Table 4.4 The number of HK2 cells used for the calculation of *E* modulus and extension curves obtained in AFM-FS indentation that were either processed or rejected. A total number of 264 extension *F-d* curves acquired from 53 control cells were analysed, while a total of 181 extension *F-d* curves out of 37 cells treated with the cytokine cells were analysed.

HK2 cells indentation measurements		
n=5	**Control**	**TGF-β1**
Total No of Cells	53	37
No of accepted cells	53	37
Processed curves	264	181
Discarded curves	1	4

Extension *F-d* curves provide important information regarding the elastic properties of a sample. *E* modulus is most commonly extracted by fitting the Hertz model for spherical beads (Vinckier & Semenza, 1998). As the cantilever is moving downwards, it reaches a point where the microbead is in contact with the plasma membrane and the cantilever is deflected upwards, resulting in the positive force values. Since the displacement positions of the substrate and the plasma membrane were determined for each single cell prior testing, the depth of indentation was tailored for each cell under investigation.

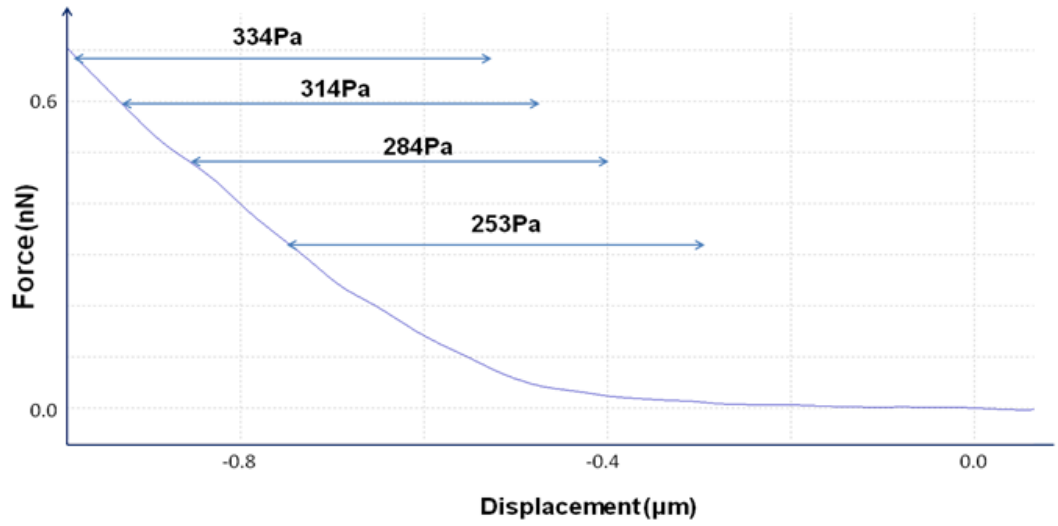

(a)

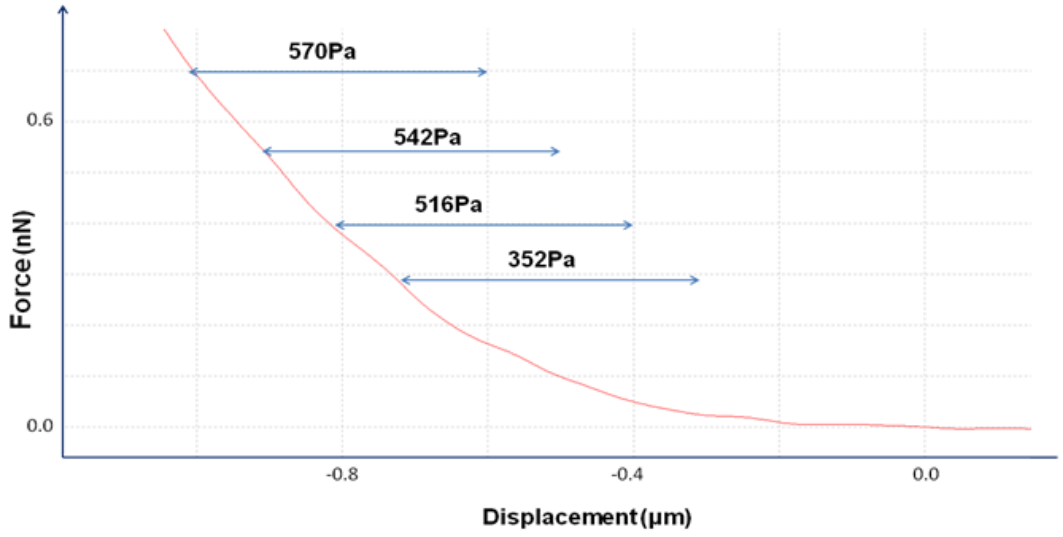

(b)

Figure 4.8 The effects of TGF-β1 treatment on *E* modulus as determined by the extension *F-d* curves acquired using AFM-FS indentation.

The histograms of *E* modulus derived from the processing of the extension part of the *F-d* indentation curves for control and TGF-β1 treated cells are shown in Figure 4.9 (a) and (b) respectively. Table 4.5 shows the descriptive statistics for the *E* modulus that was calculated from the retraction *F-d* curves of HK2 cells indentation. For the control cells, the *E* modulus (Pa) had a mean of 320 and a standard error of 16.58. For the cells treated with R568, the *E* modulus (Pa) had a mean of 549 and standard error of 20.61. The differences in *E* modulus between control and TGF-β1 treated cells calculated from extension curves as analysed using paired samples t-test are shown in table 4.6. Although that the histogram for the control cells is not totally bell-shaped, the mean values of *E* modulus for each treatment were considerably different. The student's t-test results showed that the probability value in the column Sig. was very low indicating that the there is only 0% probability that the null hypothesis of equal means was true. Treated cells had higher elasticity (M=549Pa, SE=20.61) than the control cells (M=320Pa, SE=16.58) and that difference was statistically significant ($t(443)=9.55$, $p<0.001$)

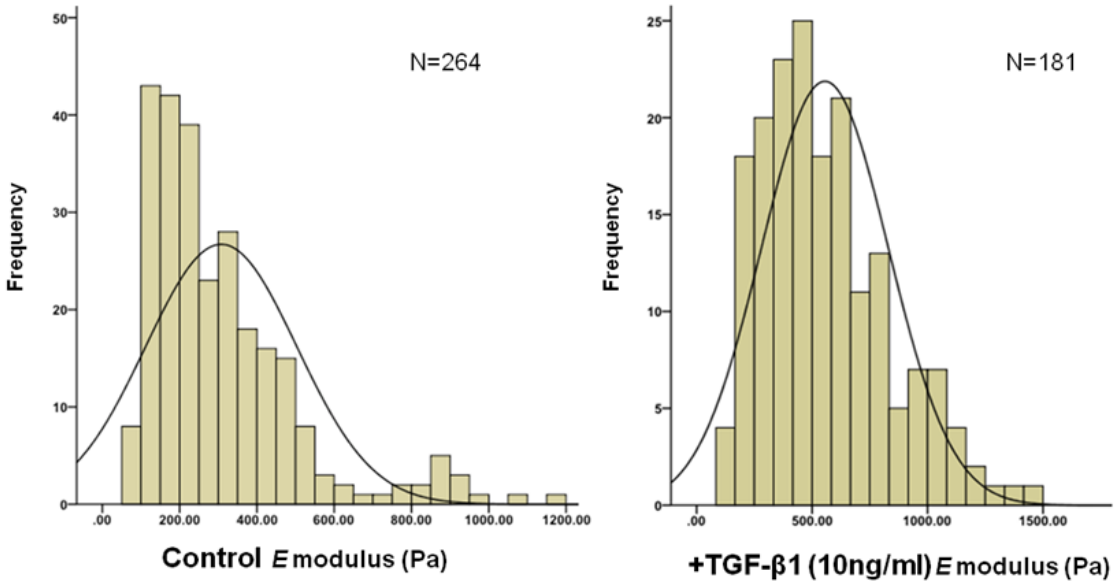

(a) (b)

Figure 4.9 Histograms of control cells showing distribution of frequencies of *E* modulus (a) in control cells and (b) in TGF-β1 treated cells.

Table 4.5 Table presenting the descriptive statistics of the *E* modulus for the control cells and for the cells treated with TGF-β1.

E modulus (Pa)	Mean	N	Std. Deviation	Std. Error Mean
Control	319.5519	264	221.79356	16.57763
TGF-β1 (10ng/ml)	549.1932	181	275.71449	20.60787

Table 4.6 Table presenting the differences in *E* modulus between control and TGF-β1 treated cells using paired wise t-test.

Paired Differences							
Mean	**SD**	**SE**	**95% CI**		**t**	**df**	**Sig.**
			Lower	**Upper**			
229.64	336.94	25.18	290.33	190.93	9.555	443	.000

Figure 4.10 shows the changes in elasticity between the two groups of cells, resulted from the processing and analysis of than 150 curves for each treatment obtained from 5 separate AFM-FS indentation experiments. The results were analysed using paired samples t-test and the data are expressed as mean ± SEM. The data indicate that the TGF-β1 (10ng/ml) increased the elastic modulus by 71% (>30 cells, n=5, $p<0.001$) (Figure 4.10), suggesting that cells treated with the cytokine became considerably more rigid.

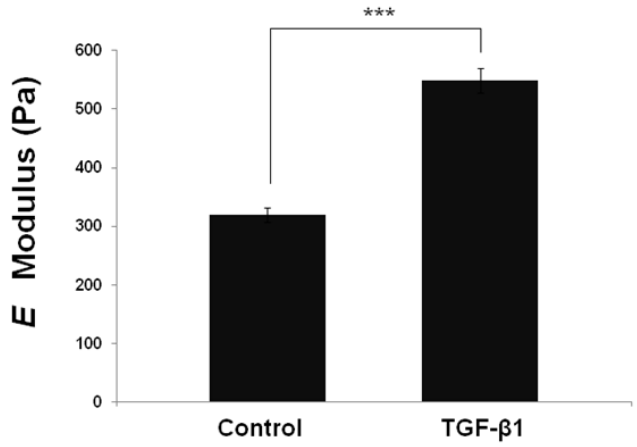

Figure 4.10 The effects of the cytokine TGF-β1 (10ng/ml) on the *E* modulus of HK2 cells. Treated cells showed an increase of 71% compared to the untreated group.

Data are expressed as mean ±SEM of more than 30 cells from 3 separate experiments, where key significances are shown, ***p<0.001.

As illustrated at Figure 4.1 the pro-fibrotic cytokine TGF-β1 (48h; 10ng/ml) altered the architecture of normal HK2 cells and produced an elongated, fibroblast-like phenotype, characteristic of TGF-β1 induced tubular damage and epithelial-to-mesenchymal transition (Figure 4.1(a)). Using tetramethylrhodamine (TRITC)-conjugated phalloidin to detect filamentous actin, these morphological changes were found to be associated with reorganization of the cytoskeleton into peripheral stress fibres. Since, changes of *E* modulus are considered to be associated with changes of the cytoskeleton, the changes in elastic response of the treated cells due to the distribution of the cytoskeleton into the periphery of the cell as illustrated in figure 4.11(b), seemed reasonably secure (Radmacher et al., 1996).

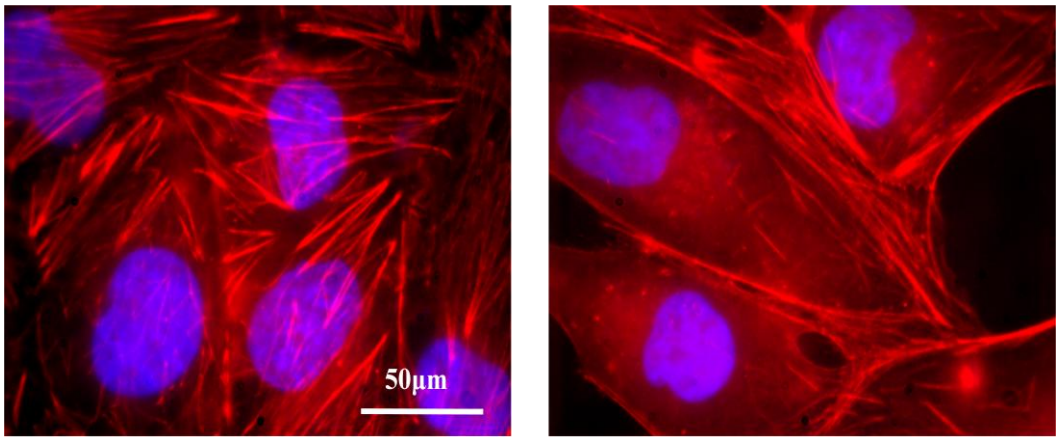

(a) (b)

Figure 4.11 Fluorescence microscopy images showing the effects of TGF-β1 on both cell morphology and cytoskeletal reorganisation. The changes in the arrangement of the cytoskeleton (red) mainly affected the cell architecture. The nucleus of

each cell is shown in purple. In (a), normal cells are shown that were grown in low glucose (5mM) alone, while in (b) cell treated with TGF-β1 (10ng/ml) are shown.

Cell adhesion is a complex process that is regulated by the involvement of the cytoskeleton and a number of surface receptors. In order to assess the effects of CSK reorganisation to cell adhesion, single cell indentation was performed for indentation depths up to 10% of the cell height. At this moderate degree of indentation changes in elasticity are considered to be manifested by the changes in CSK rearrangement (Radmacher et al., 1996; Leporatti et al., 2006). In addition E-cadherins along with a-catenins and β- catenins are forming the adherens junction, by which the extracellular domain connects with the intracellular, and is mainly responsible for the downstream of biological signals. As a consequence, chemical modification of the E-cadherin protein had an impact in the intracellular domain as well, resulting in cytoskeletal reorganisation through catenins (D'Souza-Schorey, 2005). The morphological changes in the TGF-β1 cells were associated with the remodelling of the cytoskeleton at the periphery of the cell forming a thick layer of actin filament. This phenomena was also observed in other epithelial systems (Ivanov et al., 2005). In our study the changes of the cytoskeletal structure were manifested by alterations in gross cell morphology. Changes in cell architecture in diseased states of cells, by CSK reorganisation, compared with single cell mechanics were also reported by Li e al. (2008). In their study, changes in *E* modulus of breast cancer cells were investigated through AFM indentation, suggesting that changes in cell morphology were caused by the rearrangement of the CSK structure. This is in agreement with the current study regarding the effects of TGF-β1 on single cell elasticity. The average calculated value of *E* for the control cells was 320 Pa while for the treated cells was

549 Pa, indicating an raise of 71% that signifies a dramatic increase in cell rigidity upon treatment. This result combined with phase and fluorescence imaging of the cells demonstrates that changes in *E* modulus could be compared with changes in cell architecture, resulting from CSK rearrangement. Therefore, a potential structure-mechanics-disease correlation is suggested during TGF-β1 induced EMT in diabetic nephropathy.

Further, it is suggested that, apart from the surface molecular properties, deformation of the CSK influenced in cell-to-cell adhesion characterisation of HK2 cells. Retraction *F-d* curves confirmed that treatment of HK2 cells with TGF-β1 reduced the number of tethering rupture events by 35% resulting in the reduction of maximum unbinding force by 19% and in a notable decrease of work of detachment by 53%. The greater reduction in the work of detachment has been accompanied by a decrease in distance of separation by 46% and could be partly explained by the increase in cell rigidity as manifested by the remarkable increase in *E* modulus potentially due to CSK rearrangement into peripheral stress fibers upon treament with TGF-β1 (Hubchak et al., 2003). This may imply that the rise in the rigidity of the treated cells was due to localisation of the CSK in the outer region of the cytoplasm, since the increase of *E* modulus when filamentous actin is re-distributed on the periphery of the cell is observed in other epithelial systems (Li et al., 2008). In addition, Weder et al. (2009) reported that the increased *E* modulus of mitotic cells is related to a reorganisation of the CSK into peripheral stress fibers and suggested that in SCFS adhesion measurements, cytoskeletal components are inevitable deformed during the separation process. The measured work of detachment of the cells is therefore contributed partly from the work consumed due to cell deformation, apart

from the energy required to unbind the ligation bonding at the contact surface between the two cells. The coupling effects of E-cadherin mediated cell-to-cell adhesion and CSK rearrangement in malignant states have been studied in various systems, for example, in epithelial and colorectal cancer metastasis (Cress et al., 2006; Buda et al., 2011). However, these studies are limited to qualitative data without considering the influences of the CSK deformation on the various adhesion parameters. Recently, an AFM-SCFS approach was applied to study the molecular controlling cell migration linked to the cytomechanics underlying this process (Diz-Munoz et al., 2010). Their study showed that cytomechanics had profound influence on tether forming during the pulling or separation process of an AFM-tip binding with cell membrane. In addition, the viscoelasticity of membrane tether and its importance of cell adhesion was studied via using SCFS to measure their point of cell-to-surface bond breakage when retracting adherent cells from adhesive surface (Schmitz et al., 2008). Studies on the changes in cell-to-cell adhesion during mitosis using SCFS concluded that changes in the stiffness/deformation of cells, caused by CSK reorganisation, during the pulling phase influenced the distance of separation between the cells and the displacement ranges at which unbinding events occurred (Weder et al., 2009).

4.4 Effects of Pulling Speed on β-Cell-to-β-Cell Adhesion

In order to assess the effects of cellular viscoelastic deformation on cell-to-cell adhesion, SCFS retraction *F-d* curves were performed with incremental speed. The parameters of adhesion, such as contact force and time, were kept constant at 1nN and 10sec respectively. The cantilever was extended at constant speed of 5μm/sec and retracted at higher speeds, while retraction *F-d* curves were recorded for dis-

placements up to 100μm. Since the contact time was constant, no changes in the density of E-cadherin mediated ligation between incremental pulling speed measurements were expected. The procedure was repeated three times for each cell under examination at various speeds between up to 12.5*μ*m/sec. A 30sec interval was preceded before each successive *F-d* measurement and a 60sec was preceded before measurements with different pulling speed. Considering that experiments were performed using at least three different speeds, more than nine *F-d* measurements were performed in each cell. For that reason, a single cell, attached on the end of the cantilever, was used for testing up to 3-4 different substrate cells. The number of the cells tested with speed higher than 5*μ*m/sec is presented in Table 4.7.

Table 4.7 A table showing the number of tested HK2 cells and number of processed or rejected retraction *F-d* curves obtained by SCFS adhesion experiment with incremental retraction velocities. As shown, for pulling velocities higher than 7.5*μ*m/sec more than 2/3 of the curves were rejected, while for control cells no curves were accepted for processing after 10*μ*m/sec.

HK2 cells SCFS incremental speed retraction measurements						
n=3	**Control**			**TGF-β1**		
Pulling Speed (μm/sec)	**7.5**	**10**	**12.5**	**7.5**	**10**	**12.5**
Total No of Cells	30	30	15	24	24	15
No of accepted cells	14	9	0	18	11	5
Processed curves	42	27	0	54	32	14
Discarded curves	48	63	0	18	58	31

The effects of increasing pulling velocities on the retraction *F-d* curves of control cells are illustrated in Figure 4.12, clearly demonstrating the viscoelastic nature of soft biological materials. This was also manifested by the incomplete separation of the cells at velocities higher than 5μm/sec, resulting to the complete rejection of the 12.5μm/sec data from further processing. As shown in the figure, the retraction curve for speeds higher than 5μm/sec exhibited large displacement plateaus, corresponding to high cellular deformation. As a consequence a higher displacement range than 100μm was required for the complete separation of the cells in velocities higher than 5μm/sec. In fact, even at pulling speed of 7.5μm/sec partial separation was observed in a large number of data, causing difficulties in the determination of the baseline for the calculation of adhesive parameters. In order to obtain correct values for maximum unbinding force and work of detachment, in the instances of incomplete separation the x-axis reference was determined using the baseline of the extension curve. However, even small drifts of the extension curve, due to environmental noise or kinesis in the media, resulted in misleading values, ultimately leading to the rejection of a large number of data. Moreover, since a larger displacement range was required to completely detach the two cells, measurements of work of adhesion are actually higher than presented. However, even at the range of 100μm the changes in work of detachment were dramatic.

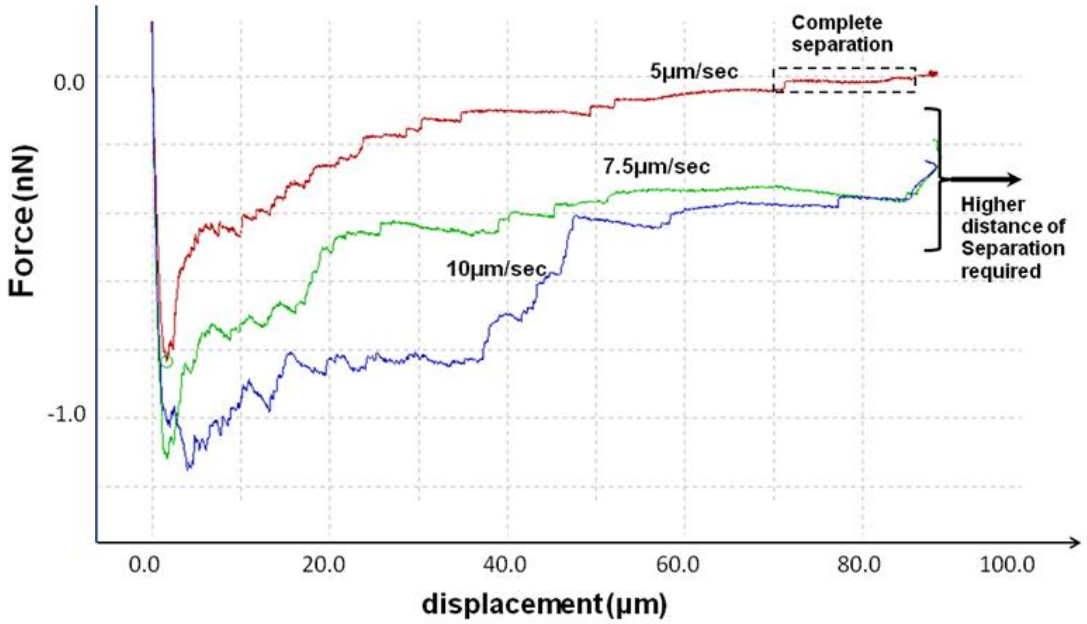

Figure 4.12 Retraction *F-d* curves acquired by adhesion measurements of control HK2 cells with incremental pulling speed are shown. The effects of increasing pulling speed on adhesion characteristics are clearly represented by the changes in the work of detachment. Further, for speeds higher than 5*µ*m/sec partial separation was observed. The levels of incomplete separation were increasing with the increase of pulling speed resulting in the complete rejection of measurements with pulling speed higher than 10*µ*m/sec due to the limitation of 100*µ*m in displacement range.

Approximately 10 cells from 3 different experiments were analysed and the data are expressed as mean ± SD. The results demonstrate a 6-fold increase of the W_D in comparison to the F_{max} as the pulling speed increases, up to the pulling distance of 100µm (9-11 cells, n=3) (Figure 4.13 (a)-(b)). Figure 4.13 (c) shows the number of TREs for a displacement range of 5µm after the minimum value of force. The decreased number of TREs with increasing velocities, does not reflect changes in the expression of E-cadherin on the surface of the cell, since no chemical modification was applied in between measurements with altering speed. It rather demonstrated

the ability of the control cells to extend further than the treated, since a larger displacement range was required for the softer cells to cause an equal number of bond rupturing, for the same displacement, as the velocities increased.

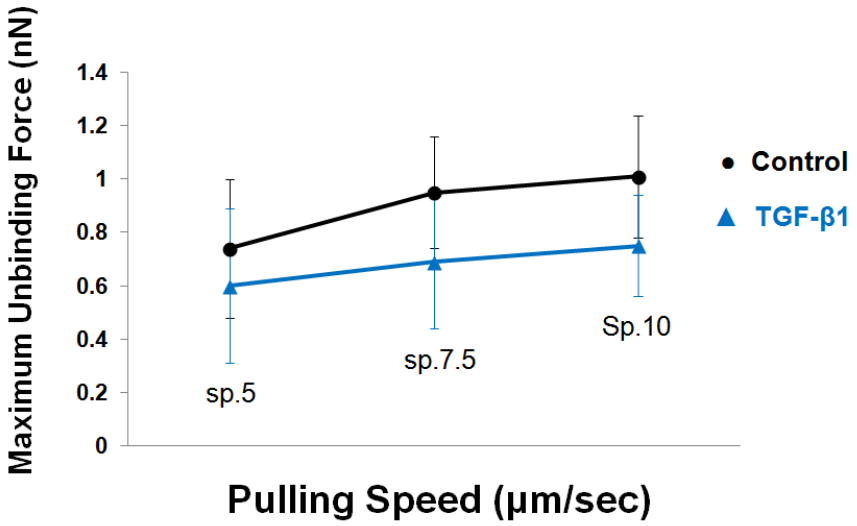

(a)

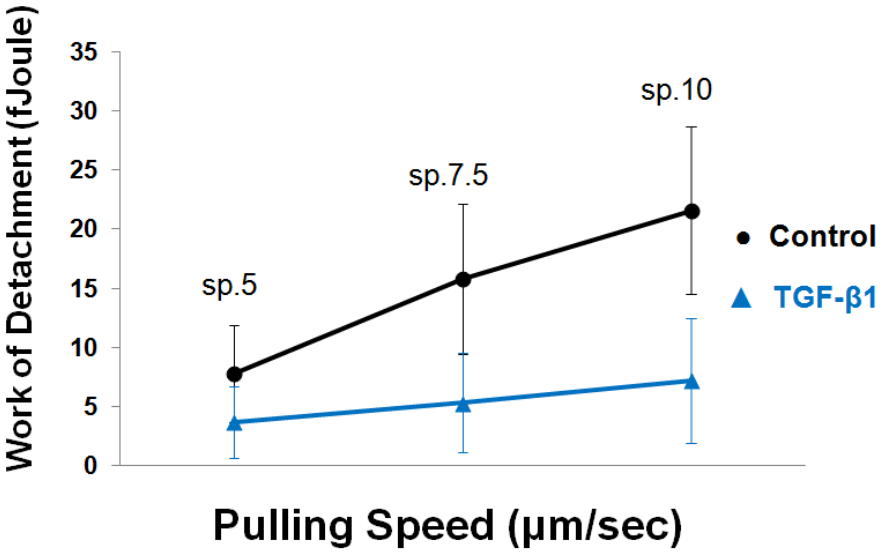

(b)

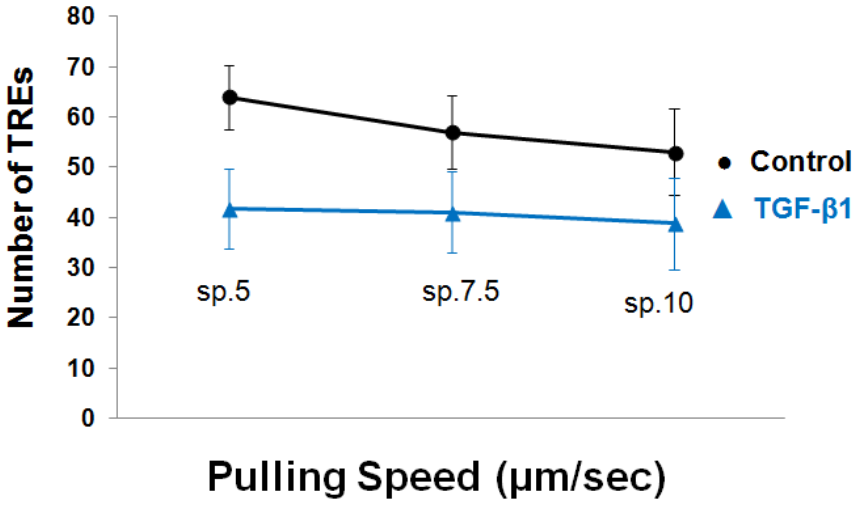

(c)

Figure 4.13 Effects of increased pulling speed on cell-to-cell adhesion parameters as acquired by SCFS retraction F-d curves of HK2 cells. Data are expressed as mean ± SD and the effects of increasing pulling speed on (a) maximum unbinding force, (b) work of detachment and (c) number of tethering rupture events are illustrated.

In order to assess the cytomechanical influences on E-cadherin mediated cell-to-cell adhesion of HK2 cells, *F-d* retraction curves at incremental pulling or separation velocities were performed. Due to the viscoelastic nature of the cells, data were analysed up to a speed of 10μm/sec, since a displacement range higher than 100μm was required for measurements with increasing velocities. The results demonstrated a fivefold increase in the W_D in comparison to F_{max} for the control cells, whilst a threefold increase for the TGF-β1 treated cells. Our results suggest a higher dependence of the W_D on the compliance of the cells since the higher increase in work

of complete detachment is contributed by the higher elastic deformation of the control HK2 cells (Johnson & Greenwood, 1997).

These findings combined with the indentation results and fluorescence microscopy suggest considerable influences of CSK deformation on cell-to-cell adhesion. Therefore, it is resonable that biochemical changes induced biophysical changes , which in turn affected the adhesion between HK2 cells. Overall, the cohesive results between cell elasticity, cell adhesion and image of cytoskeleton have facilitated better revelation about the intricate interplay between cytomechanics and cell adhesion. Therefore, it is reasonable to suggest that biochemical changes induced biophysical changes, which in turn affected the adhesion between HK2 cells. The net effect of these changes is illustrated in Figure 4.14 (a)-(d).

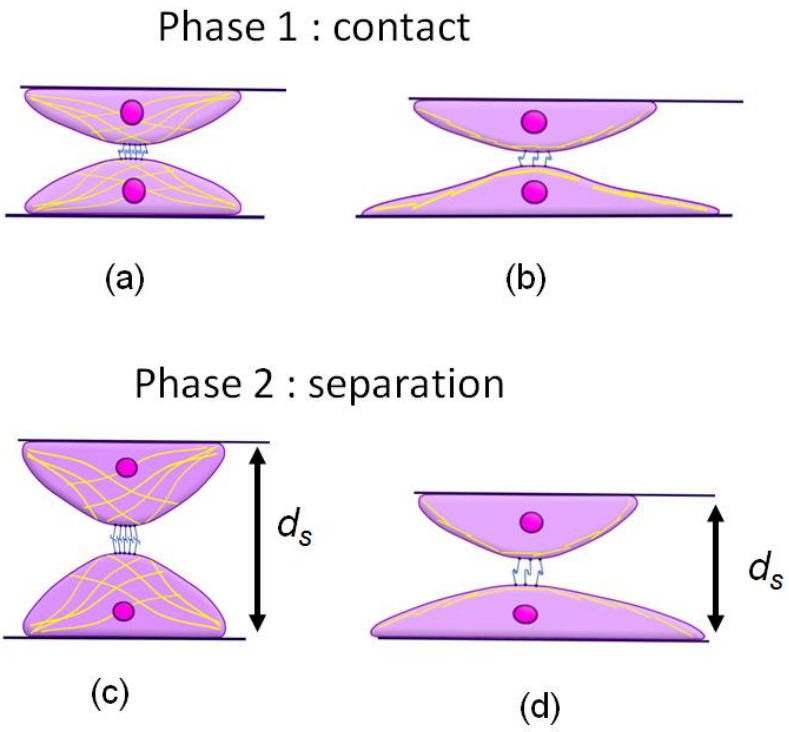

Figure 4.14 Cell-to-cell adhesion process of HK2 cells showing the changes in surface molecular binding and re-arrangement of the cytoskeleton into the periphery upon treatment with TGF-β1. During phase 1 the cells are in contact with each other and E-cadherin ligation is formed. In (a), a schematic of control cells is shown while in (b), a schematic of cells after treatment with TGF-β1 is shown. In phase 2 the separation process between the two cells is illustrated. In (c), increased distance of separation due to cell deformation, corresponded to higher work of detachment for normal cells while in (d) cells became more rigid due to cytoskeletal reorganisation into the periphery after TGF-β1 resulting in decreased distance of separation inevitably leading to a dramatic reduction of work of detachment. Overall, surface binding affinity was partially responsible for the changes in work of detachment that was mainly influenced by changes in the elastic properties of each cell.

4.6 Conclusion

In the current study the changes of E-cadherin mediated cell-to-cell adhesion upon treatment with the pro-fibrotic cytokine TGF-β1 (48h, 10ng/ml) in the renal proximal tubule HK2 cell line have been investigated. In addition, quantitative evidence that the elastic properties of individual cells influenced the separation process between two adherent cells has been provided. TGF-β1 affected the extracellular domain by decreasing the expression of E-cadherin at the surface of the cell (Hills et al., 2012a) causing a reduction in the number of tether rupturing events, whilst in the intracellular domain initiated cytoskeletal reorganisation into peripheral stress fibers, resulting in the increase of *E* modulus of individuals cells. The changes in the mechanical properties of single cells had a strong effect on work of detachment owing to

changes of the viscoelastic deformation of cells as manifested by the increase of the distance of complete separation. As a consequence, TGF-β1 induced EMT in diabetic nephropathy instigates a loss of E-cadherin that resulted in the reduction of the adhesive properties between cells by decreasing the number of ligation tethering and rigidity of the cells. Therefore, in addition to surface molecular tethering, the effects of the cytomechanic alterations during E-cadherin detachment process in EMT were pivotal.

Chapter 5

Synopsis & Future Work

5. Synopsis & Future Work

5.1 Research Highlights

In this research project the adhesive and mechanical properties of soft biological cells (MIN6 & HK2) under the influence of specific chemical agents were investigated quantitatively using AFM-SCFS. The significance of the technique to investigate cell-to-cell adhesion and single cell mechanics at various biological states was also clearly demonstrated. The obtained results contributed to the understanding of cellular adhesion in a variety of physiological and pathological states primarily concerning diabetes and its implications, such as diabetic nephropathy. By using AFM-SCFS cell-to-cell adhesion parameters and *E* moduli of MIN6 and HK2 cells were measured after treatment of R568 and TGF-β1 respectively. Chemical modification of cells led to significant changes of the surface molecular binding and the mechanistic behaviour of each individual cell that can be partially explained by cytoskeletal reorganisation. More importantly the results demonstrated that changes in the biological states initiated complex interactions between E-cadherin and F-actin cytoskeleton at the adherens junction as signified by the intricate interplay between adhesive and mechanical characteristics of cells. As a consequence it can be deduced that E-cadherin, apart from an adhesion molecule, constitutes a signalling diavlos with a significant role in cell-to-cell communication.

It has been suggested that E-cadherin mediated cell-to-cell adhesion contributed to an enhanced insulin secretion of β cells (Rogers et al., 2007). The first goal was to develop an experimental protocol for characterising quantitatively β-cell-to-β-cell adhesion and elucidate if an increase in the expression of E-cadherin has functional

consequences on enhanced β cell coupling. SCFS measurements showed that E-cadherin mediated cell-to-cell adhesion was increased upon CaSR activation using the R568 (1μM). More specifically activation of the receptor affected the extracellular domain by increasing the number of TREs by 48%, whilst affected the intracellular domain of the trans-membrane protein by decreasing the *E* modulus by 34%. As a consequence β-cell-to-β-cell adhesion parameters were altered not only due to bio-molecular changes of the protein in the cell surface, but also due to changes in the biomechanical properties of individual cells. F_{max} was increased by 30%, whilst W_D was increased more significantly by 39% consistent with an increase in d_s by 37%. To further assess the effects of viscoelastic deformation on cell-to-cell adhesion, *F-d* retraction curves with incremental velocities were performed, resulting in the tenfold increase of W_D in relation with F_{max} for both treatments when pulling speed was increased by a factor of 2.

It has been reported that the pro-fibrotic cytokine TGF-β1 mediates early EMT resulting in the fibrosis of renal proximal tubule in DN (Hills et al., 2012a). Therefore, the next goal was to investigate TGF-β1 induced changes in epithelial characteristics, which are maintained via E-cadherin. SCFS measurements showed that E-cadherin mediated cell-to-cell adhesion was decreased after treatment with TGF-β1(10ng/ml). Treatment with the cytokine affected the extracellular domain by decreasing the number of TREs by 35%, whilst affected the intracellular domain of the trans-membrane protein by increasing the *E* modulus by 71% due to CSK rearrangement into peripheral stress fibers. As a result, changes in the mechanical properties of single cells had a significant effect on cell adhesion characterisation, in addition to effects arising from surface ligation binding. After treatment F_{max} was decreased by

19%, whilst W_D was decreased more significantly by 53% corresponding to a decrease in d_s by 46%. In order to assess the effects of viscoelastic deformation on E-cadherin mediated cell-to-cell adhesion, *F-d* retraction curves with incremental velocities were performed, resulting in a fivefold increase in the W_D in comparison to F_{max} for the control cells, whilst a threefold increase for the TGF-β1 treated cells when pulling speed was increases by a factor of 1/2.

In conclusion, biophysical changes induced by biochemical modification of both cell types, resulted in the alteration of the mechanistic behaviour of the cell during the separation process between the two cells that were brought in contact. This is clearly shown by the higher alterations of the work of detachment in comparison to the maximum unbinding forces. Furthermore, the results demonstrate that changes in *E* modulus could be compared with changes in cell architecture, resulting from CSK rearrangement. This signifies the diagnostic content that is included in the measurements of *E* modulus and could inspire the development of novel biosensing techniques that could potentially provide useful indicators about the development of the diseases in the early stages.

5.2 Limitations

Although that the AFM-SCFS instrument was incorporated with an improved piezo-actuator (100μm) that enables long range force spectroscopy, adhesion parameters such as contact force, contact period and pulling speed should be carefully chosen prior experiments. Extended contact times or high contact forces will ultimately lead to incomplete separation of the attached cells. In this study the z-displacement range was insufficient for the complete separation of soft biological cells when the pulling

speeds was increased from 5 to 15μm/sec, which led to the rejection of a large number of data. In addition, although that the instrumental set-up compensated for the preservation of cells at a physiological temperature, it did not compensate for the CO_2 requirements of living cells. The media for both the cells treated in the petri dish and the free cells during experiment was replaced by CO_2 free media, resulting in limited experimental time (<2h).

One drawback of the SCFS technique is that experiments are time consuming, since the cantilever-single cell attached system can characterise one cell each time and has to be replaced every time the AFM head is lifted i.e. for removimg unwanted adherent particles or replacing the petri dish under testing with a new one. This procedure requires re-calibration of the cantilever that additionally results in an loss of functionalisation. Once the cantilever is chemically modified then it can be used only up to 3 times since the cleaning process significantly alters the spring constant value. Cantilevers are disposable items with a considerable cost. In this project cantilevers were used up to three times while the cleaning procedure involved washing with ultrasound.

5.3 Future Work

Altering the expression of a protein of a cell, for testing a specific hypotheses such as improved or malignant function of a system, does not guarantee that its function will be altered accordingly. AFM-SCFS is a valuable tool to elucidate the corresponding function of a cell after chemical modification, when cell's behaviour is dependent upon cell-to-cell coupling. In this study the role of the cytokine TGF-β1 in altering cell-to-cell adhesion in early EMT of the proximal tubule has been investigated and

the results suggested that the cytokine has a significant role in this malignant transformation during fibrosis of the tubule. Furthermore, a potential method for the reversion of this catastrophic process in DN should be investigated. There is evidence in the literature suggesting that C-peptide can alleviate this damage and act as a therapeutic agent, through specific binding to receptors at the surface of the cell that could potentially lead to enhanced cell coupling (Johansson et al., 2000; Wahren et al., 2001; Nordquist et al., 2009; Hills et al., 2010). It is therefore an urgency to design a SCFS experiment that will functionally investigate the changes of cell-to-cell adhesion after chemical treatment with C-peptide. The experiment should include adhesion measurements of healthy (control) HK2 versus TGF-β1 treated versus C-peptide treated and versus TGF-β1/C-peptide treated cells. The use of the HK2 cell line is advised for consistency with the results reported in this study. This interdisciplinary work could provide promising data regarding the role of C-peptide in diabetes and DN and/or elucidate the mechanism underlying the interactions between TGF-β1 and C-peptide. In addition, since it was shown that mechanical properties of cells, such as elasticity, not only changed by the chemical modification in the diseased state, but also affected cell-to-cell adhesion through the ability of cells to deform at extended ranges, a set of indentation experiments should be performed along with the adhesion experiments. In addition to calculation of elasticity, it is suggested that stress relaxation experiments should be performed using the AFM-SCFS system (Okajima et al., 2007; Moreno-Flores et al., 2010), to further assess the changes in viscoelasticity of the cells after each treatment.

In this project the *E* modulus of treated cells for indentation depths up to 10% of the cell height have been characterised using the Hertz model. Apart from the fact that

these data showed that the mechanical properties can serve as an indicator for diseased states, the study mainly involved mechanics of soft cell, an area that has a great impact in the advances of regenerative medicine and tissue engineering for the development of biomaterials that will resemble the mechanical behaviour of soft membranes and tissues. It is well known that soft biological materials exhibit large deformations (Scott et al., 2004; Lulevich et al., 2006; Ikai, 2008). However, the study for the determination of E modulus was limited to indentation depths up to 10% of the height of the cell. Therefore, AFM indentation measurements of single cells using higher indentation depths than 10% of cell height is desirable. The data should be processed by an appropriate mechanical model that compensates for the heterogeneity of the cells, such as finite element analysis. It is suggested that measurements will be performed at various depths of indentation to assess the mechanical properties of the cytoskeleton and the nucleus separately and in combination. In addition, confocal microscopy should be performed in order to assess the position of the nucleus in the cytoplasm. The generated results could potentially contribute to a novel study concerning the multi-scale mechanical characterisation of engineered tissue.

References

A-Hassan, E., Heinz, W. F., Antonik, M. D., D'Costa, N. P., Nageswaran, S., Schoenenberger, C. a, & Hoh, J. H. (1998). Relative microelastic mapping of living cells by atomic force microscopy. *Biophysical Journal*, 74(3), 1564–78.

Alonso, J. L., & Goldmann, W. H. (2003). Feeling the forces: atomic force microscopy in cell biology. *Life Sciences*, 72(23), 2553–2560.

Bai, S., Sun, J., Wu, H., Zhang, N., Li, H., Li, G., … Xu, C. (2012). Decrease in calcium-sensing receptor in the progress of diabetic cardiomyopathy. *Diabetes Research And Clinical Practice*, 95(3), 378–385.

Ban, C. R., & Twigg, S. M. (2008). Fibrosis in diabetes complications: pathogenic mechanisms and circulating and urinary markers. *Vascular Health and Risk Management*, 4(3), 575–596.

Bao, G. and Suresh, S. (2003). Cell and molecular mechanics of biological materials. *Nature Mater*, 2(11): 715-725.

Bao, G., Vaziri, A. and Espinosa, H. (2009). Modelling and experiments in cell and biomolecular mechanics. *Experimental Mechanics*, 49 (1): 1-2.

Bao, G., Kamm, R. D., Thomas, W., Hwang, W., Fletcher, D. A, Grodzinsky, A. J., Mofrad, M. R. K. (2010). Molecular biomechanics: The molecular basis of how forces regulate cellular function. *Molecular & Cellular Biomechanics: MCB*, *3*(2), 91–105.

Benninger, R. K. P., Head, W. S., Zhang, M., Satin, L. S., & Piston, D. W. (2011). Gap junctions and other mechanisms of cell-cell communication regulate basal insulin secretion in the pancreatic islet. *The Journal of Physiology*, *589*(22), 5453–5466.

Bershadsky, A. D., Balaban, N. Q., & Geiger, B. (2003). Adhesion-dependent cell mechanosensitivity. *Annual review of cell and developmental biology*, *19*, 677–695.

Bilous, R., & Donnelly, R. (2010). *Handbook of diabetes*. Wiley-Blackwell, Chichester, West Sussex, UK.

Brereton, H. C., Carvell, M. J., Asare-Anane, H., Roberts, G., Christie, M. R., Persaud, S. J., & Jones, P. M. (2006). Homotypic cell contact enhances insulin but not glucagon secretion. *Biochemical and biophysical research communications*, 344(3), 995–1000.

Brown, E. M, Gamba, G., Riccardi, D., Lombardi, M., Butters, R., Kifor, O., Hebert, S. C. (1993). Cloning and characterization of an extracellular Ca2+-sensing receptor from bovine parathyroid. *Nature*, 366(6455), 575–580.

Brown, E. M, & MacLeod, R. J. (2001). Extracellular calcium sensing and extracellular calcium signaling. *Physiological Reviews*, 81(1), 239–297.

Brown, E. M. (2007). Clinical lessons from the calcium-sensing receptor. *Nature Clinical Practice. Endocrinology & Metabolism*, 3(2), 122–133.

Bruce, J. I., Yang, X., Ferguson, C. J., Elliott, A. C., Steward, M. C., Case, R. M., & Riccardi, D. (1999). Molecular and functional identification of a Ca2+ (polyvalent cation)-sensing receptor in rat pancreas. *The Journal of Biological Chemistry*, 274(29), 20561–20568.

Buda, A., & Pignatelli, M. (2011). E-cadherin and the cytoskeletal network in colorectal cancer development and metastasis. *Cell Communication & Adhesion*, 18(6), 133–143.

Burnham, N. a, Chen, X., Hodges, C. S., Matei, G. a, Thoreson, E. J., Roberts, C. J., Tendler, S. J. B. (2003). Comparison of calibration methods for atomic-force microscopy cantilevers. *Nanotechnology*, 14(1), 1–6.

Butt, H.-J., & Jaschke, M. (1995). Calculation of thermal noise in atomic force microscopy. *Nanotechnology*, 6(1), 1.

Calabrese, A., Zhang, M., Serre-Beinier, V., Caton, D., Mas, C., Satin, L. S., & Meda, P. (2003). Connexin 36 controls synchronization of Ca2+ oscillations and insulin secretion in MIN6 cells. *Diabetes*, 52(2), 417–424.

Carl, P., & Schillers, H. (2008). Elasticity measurement of living cells with an atomic force microscope: data acquisition and processing. *European Journal of Physiology*, 457(2), 551–9.

Castano, L., & Eisenbarth, G. S. (1990). TYPE-I DIABETES: A chronic autoimmune disease of human, mouse and rat. *Annual Review Immunology,* 8, 647-79

Chaudhuri, O., Parekh, S. H., Lam, W. A. & Fletcher, D. A. (2009). Combined atomic force microscopy and side-view optical imaging for mechanical studies of cells. *Nature Meth*, 6 (5): 383-387.

Cheng, S. X., Geibel, J. P., & Hebert, S. C. (2004). Extracellular polyamines regulate fluid secretion in rat colonic crypts via the extracellular calcium-sensing receptor. *Gastroenterology*, 126(1), 148–158.

Cohen, B. J., & Wood, D. L. (2000). *Memmler's the human body in health and disease*. Lippincott Williams and Wilkins, Philadepphia, USA.

Cooper, G. M., & Hausman, R. E. (2009). *The cell. A molecular approach.* ASM press, Washighton, USA.

Cigliola, V., Chellakudam, V., Arabieter, W., & Meda, P. (2013). Connexins and β-cell functions. *Diabetes Research and Clinical Practice*, *99*(3), 250–259.

Cross, S. E., Jin, Y.-S., Rao, J., & Gimzewski, J. K. (2007). Nanomechanical analysis of cells from cancer patients. *Nature Nanotechnology*, 2(12), 780–783.

D'Souza-Schorey, C. (2005). Disassembling adherens junctions: breaking up is hard to do. *Trends in Cell Biology*, 15(1), 19–26.

Dahl, U., Sjødin, a, & Semb, H. (1996). Cadherins regulate aggregation of pancreatic beta-cells in vivo. *Development*, 122(9), 2895–902.

Dimitriadis, E. K., Horkay, F., Maresca, J., Kachar, B., & Chadwick, R. S. (2002). Determination of elastic moduli of thin layers of soft material using the atomic force microscope. *Biophysical Journal*, 82(5), 2798–810.

Diz-Muñoz, A., Krieg, M., Bergert, M., Ibarlucea-Benitez, I., Muller, D. J., Paluch, E., & Heisenberg, C.-P. (2010). Control of directed cell migration in vivo by membrane-to-cortex attachment. *PLoS Biology*, *8*(11), e1000544–e1000544.

Elter, P., Weihe, T., Lange, R., Gimsa, J., & Beck, U. (2011). The influence of topographic microstructures on the initial adhesion of L929 fibroblasts studied by single-cell force spectroscopy. *European Biophysics Journal,* 40(3), 317–27.

Franz, C M, & Puech, P.-H. (2008). Atomic Force Microscopy: A versatile tool for studying cell morphology, adhesion and mechanics. *Cellular and Molecular Bioengineering*, 1(4), 289–300.

Franz, Clemens M, Taubenberger, A., Puech, P.-H., & Muller, D. J. (2007). Studying integrin-mediated cell adhesion at the single-molecule level using AFM force spectroscopy. *Science's STKE: Signal Transduction Knowledge Environment*, 406, pl5.

Friedrichs, J., Helenius, J., & Muller, D. J. (2010). Quantifying cellular adhesion to extracellular matrix components by single-cell force spectroscopy. *Nature protocols*, 5(7), 1353–61.

Friedrichs, J., Legate, K. R., Schubert, R., Bharadwaj, M., Werner, C., Müller, D. J., & Benoit, M. (2013). A practical guide to quantify cell adhesion using single-cell force spectroscopy. *Methods*, 60(2), 169–178.

Gerbino, A., Maiellaro, I., Carmone, C., Caroppo, R., Debellis, L., Barile, M., Colella, M. (2012). Glucose increases extracellular [Ca2+] in rat insulinoma (INS-1E) pseudoislets as measured with Ca2+-sensitive microelectrodes. *Cell Calcium*, 51(5), 393–401.

Grandbois, M., Dettmann, W., Benoit, M., & Gaub, H. E. (2000). Affinity imaging of red blood cells using an Atomic Force Microscope. *Journal of Histochemistry & Cytochemistry*, 48(5), 719–724.

Gray, E., Muller, D., Squires, P. E., Asare-Anane, H., Huang, G.-C., Amiel, S., Jones, P. M. (2006). Activation of the extracellular calcium-sensing receptor initiates insulin secretion from human islets of Langerhans: involvement of protein kinases. *The Journal of Endocrinology*, 190(3), 703–10.

Halban, P. A., Powers, S. L., George, K. L., & Bonner-Weir, S. (1988). Altered differentiated cell surface properties of transformed (RINm5F) compared with native adult rat pancreatic B cells. *Endocrinology*, *123*(1), 113–119.

Han, S. Y., Jee, Y. H., Han, K. H., Kang, Y. S., Kim, H. K., Han, J. Y. Cha, D. R. (2006). An imbalance between matrix metalloproteinase-2 and tissue inhibitor of matrix metalloproteinase-2 contributes to the development of early diabetic nephropathy. *Nephrology, Dialysis, Transplantation: Official Publication of The European Dialysis and Transplant Association - European Renal Association*, 21(9), 2406–2416.

Haque, M., & Saif, M. (2002). In-situ tensile testing of nano-scale specimens in SEM and TEM. *Experimental Mechanics*, 42(1), 123-128.

Harris, A. R., & Charras, G. T. (2011). Experimental validation of atomic force microscopy-based cell elasticity measurements. *Nanotechnology*, *22*(34), 345102.

Hauge-Evans, A. C., Squires, P. E., Persaud, S. J., & Jones, P. M. (1999). Pancreatic beta-cell-to-beta-cell interactions are required for integrated responses to nutrient stimuli: enhanced Ca2+ and insulin secretory responses of MIN6 pseudoislets. *Diabetes*, 48(7), 1402–1408.

Hills, C. E, Siamantouras, E., Smith, S. W., Cockwell, P., Liu, K.-K., & Squires, P. E. (2012a). TGFβ modulates cell-to-cell communication in early epithelial-to-mesenchymal transition. *Diabetologia*, 55(3), 812–24.

Hills, C. E, Al-rasheed, N., Al-rasheed, N., Willars, G. B., & Brunskill, N. J. (2009). C-peptide reverses TGF-beta1-induced changes in renal proximal tubular cells:

implications for treatment of diabetic nephropathy. American Journal of Psysiology Renal Psysiology, 296(3),F614–F621.

Hills, C. E, Jin, T., Siamantouras, E., Liu, I. K.-K., Jefferson, K. P., & Squires, P. E. (2013). “Special k” and a loss of cell-to-cell adhesion in proximal tubule-derived epithelial cells: modulation of the adherens junction complex by ketamine. *PLoS One*, 8(8), e71819.

Hills, Claire E, Younis, M. Y. G., Bennett, J., Siamantouras, E., Liu, K.-K., & Squires, P. E. (2012b). Calcium-sensing receptor activation increases cell-cell adhesion and β-cell function. *Cellular Physiology and Biochemistry*, *30*(3), 575–586.

Hochmuth, R. (2000). Micropipette aspiration of living cells. *Journal of Biomechanics*, 33(1): 15-22

Hoffmann, S. C., Wabnitz, G. H., Samstag, Y., Moldenhauer, G., & Ludwig, T. (2011). Functional analysis of bispecific antibody (EpCAMxCD3)-mediated T-lymphocyte and cancer cell interaction by single-cell force spectroscopy. *International journal of cancer. Journal International du Cancer*, 128(9), 2096–104.

Hoh, J. H., & Schoenenberger, C. A. (1994). Surface morphology and mechanical properties of MDCK monolayers by atomic force microscopy. *Journal of Cell Science*, 107,*5*, 1105–14.

Hubchak, S. C., Runyan, C. E, Kreisberg, J. I., Schnaper, H. W. (2003). Cytoskeletal rearrangement and signal transduction in TGF-β1 stimulated mesangial cell collagen accumulation. *Journal of the American Society of Nephrology*, 8(14), 1969-1980.

Hutter, J. L., & Bechhoefer, J. (1993). Calibration of atomic-force microscope tips. *Review of Scientific Instruments*, 64(7), 1868.

Ikai, A. (2008). *The world of nano-biomechanics : mechanical imaging and measurement by atomic force microscopy*. Amsterdam, .Oxford: Elsevier.

Ingber, D. (2006). Cellular mechanotransduction: putting all the pieces together again. *The FASEB Journal*, 20, 811–827.

Ingber, D. E. (2002). Mechanical Signaling and the cellular response to extracellular matrix in angiogenesis and cardiovascular physiology. *Circulation Research*, 91(10), 877–887.

Ishihara, H., Asano, T., Tsukuda, K., Katagiri, H., Inukai, K., Anai, M., Oka, Y. (1993). Pancreatic beta cell line MIN6 exhibits characteristics of glucose metabolism and glucose-stimulated insulin secretion similar to those of normal islets. *Diabetologia*, 36(11), 1139–1145.

Ivanov, A. I., Hunt, D., Utech, M., Nusrat, A., & Parkos, C. A. (2005). Differential roles for actin polymerization and a myosin II motor in assembly of the epithelial apical junctional complex. *Molecular Biology of The Cell*, 16(6), 2636–2650.

Jaitovich, A., & Jaim Etcheverry, G. (2004). Adhesion molecules. Their role in cardiovascular physiopathology. *Medicina*, 64(5), 455–462.

Johansson, B., & Wahren, J. (2000). Beneficial effects of C-peptide on incipient nephropathy and neuropathy in patients with Type 1 diabetes mellitus. *Diabetic Medicine*, 17, 181-189

Johnson, K.L., Greenwood, J.A. (1997). An adhesion map for the contact of elastic spheres. *Journal of Colloid and Interface Science*, 192, 326-333.

Jones, P. M., Kitsou-Mylona, I., Gray, E., Squires, P. E., & Persaud, S. J. (2007). Expression and function of the extracellular calcium-sensing receptor in pancreatic beta-cells. *Archives of Physiology and Biochemistry*, 113(3), 98–103.

Justinich, C. J., Mak, N., Pacheco, I., Mulder, D., Wells, R. W., Blennerhassett, M. G., & MacLeod, R. J. (2008). The extracellular calcium-sensing receptor (CaSR) on human esophagus and evidence of expression of the CaSR on the esophageal epithelial cell line (HET-1A). *American Journal of Physiology. Gastrointestinal and Liver Physiology*, 294(1), G120–G129.

Kam, L. C., & Roy, P. (2010). Special Issue: Cell mechanics and signaling: from micro to nano. *Cellular and Molecular Bioengineering*, 3(1), 1–2.

Kanwar, Y. S., Wada, J., Sun, L., Xie, P., Wallner, E. I., Chen, S., Danesh, F. R. (2008). Diabetic nephropathy: mechanisms of renal disease progression. *Experimental Biology and Medicine*, 233(1), 4–11.

Kasas, S., & Dietler, G. (2008). Probing nanomechanical properties from biomolecules to living cells. *European Journal of Physiology*, 456(1), 13–27.

Kato, M., Doi, R., Imamura, M., Furutani, M., Hosotani, R., & Shimada, Y. (1997). Calcium-evoked insulin release from insulinoma cells is mediated via calcium-sensing receptor. *Surgery*, 122(6), 1203–1211.

Kelly, C., Guo, H., McCluskey, J. T., Flatt, P. R., & McClenaghan, N. H. (2010). Comparison of insulin release from MIN6 pseudoislets and pancreatic islets of Langerhans reveals importance of homotypic cell interactions. *Pancreas*, 39(7), 1016–1023.

Kerssemakers, J. W. J., Munteanu, E. L., Laan, L., Noetzel, T. L., Janson, M. E., & Dogterom, M. (2006). Assembly dynamics of microtubules at molecular resolution. *Nature*, 442(7103), 709–12.

Kiss, R., Bock, H., Pells, S., Canetta, E., Adya, A. K., Moore, A. J. Willoughby, N. a. (2011). Elasticity of human embryonic stem cells as determined by atomic force microscopy. *Journal of Biomechanical Engineering*, 133(10), 101009.

Kitsou-Mylona, I., Burns, C. J., Squires, P. E., Persaud, S. J., & Jones, P. M. (2008). A role for the extracellular calcium-sensing receptor in cell-cell communication in pancreatic islets of langerhans. *Cellular Physiology And Biochemistry: International Journal of Experimental Cellular Physiology, Biochemistry, and Pharmacology*, 22(5-6), 557–566.

Kuznetsova, T. G., Starodubtseva, M. N., Yegorenkov, N. I., Chizhik, S. A. & Zhdanov, R. I. (2007). Atomic Force Microscopy probing of cell elasticity. *Micron*, 38(8), 824-833.

Leporatti, S., Gerth, A., Köhler, G., Kohlstrunk, B., Hauschildt, S., & Donath, E. (2006). Elasticity and adhesion of resting and lipopolysaccharide-stimulated macrophages. *FEBS letters*, *580*(2), 450–4.

Li, Q. S., Lee, G. Y. H., Ong, C. N., & Lim, C. T. (2008). AFM indentation study of breast cancer cells. *Biochemical and biophysical research communications*, *374*(4), 609–13.

Li, Q. S., Lee, G. Y. H., Ong, C. N., & Lim, C. T. (2009). Probing the Elasticity of Breast Cancer Cells Using AFM. *International Federation for Medical and Biological Engineering Proceedings*, 23, 2122–2125.

Lim, C. T., Zhou, E. H. & Quek, S. T. (2006). Mechanical models for living cells: a review. *Journal of Biomechanics*, 39(2), 195-216.

Liu, K.-K. (2006). Deformation behaviour of soft particles: a review. *Journal of Physics D: Applied Physics*, 39(11), R189–R199.

Luft, R. (1989). Oskar Minkowski: discovery of the pancreatic origin of diabetes, 1889. *Diabetologia*, *32*(7), 399–401.

Lulevich, V., Zink, T., Chen, H.-Y., Liu, F.-T., & Liu, G.-Y. (2006). Cell mechanics using atomic force microscopy-based single-cell compression. *Langmuir,* 22(19), 8151–5.

MacDonald, P. E., Joseph, J. W., & Rorsman, P. (2005). Glucose-sensing mechanisms in pancreatic beta-cells. *Philosophical Transactions of The Royal Society of London. Series B, Biological Sciences*, 360(1464), 2211–2225.

Mahaffy, R. E., Park, S., Gerde, E., Käs, J., & Shih, C. K. (2004). Quantitative analysis of the viscoelastic properties of thin regions of fibroblasts using atomic force microscopy. *Biophysical Journal*, 86(3), 1777–1793.

Meda, P. (2003). Cx36 involvement in insulin secretion: characteristics and mechanism. *Cell Communication & Adhesion*, 10(4-6), 431–435.

Miyazaki, J., Araki, K., Yamato, E., Ikegami, H., Asano, T., Shibasaki, Y., Yamamura, K. (1990). Establishment of a pancreatic beta cell line that retains glucose-inducible insulin secretion: special reference to expression of glucose transporter isoforms. *Endocrinology*, 127(1), 126–132.

Moreno, A. P., Berthoud, V. M., Pérez-Palacios, G., & Pérez-Armendariz, E. M. (2005). Biophysical evidence that connexin-36 forms functional gap junction channels between pancreatic mouse beta-cells. *American Journal of Physiology. Endocrinology and Metabolism*, 288(5), E948–E956.

Moreno-Flores, S., Benitez, R., Vivanco, M. dM, & Toca-Herrera, J. L. (2010). Stress relaxation and creep on living cells with the atomic force microscope: a means to calculate elastic moduli and viscosities of cell components. *Nanotechnology*, 21(44), 445101.

Nielsen, H. M., & Cam, I. (2012). Cell adhesion molecules in Alzheimer's disease. *Degenerative Neurological and Neuromuscular Disease*, 2, 65–77.

Nordquist, L., & Wahren, J. (2009). C-Peptide: the missing link in diabetic nephropathy? *The review of Diabetic Studies*, 6(3), 203–10.

Norhammar, A., Tenerz, A., Nilsson, G., Hamsten, A., Efendíc, S., Rydén, L., & Malmberg, K. (2002). Glucose metabolism in patients with acute myocardial infarction and no previous diagnosis of diabetes mellitus: a prospective study. *Lancet*, 359(9324), 2140–2144.

Ohashi, T., Ishii, Y., Ishikawa, Y., Matsumoto, T., & Sato, M. (2002). Experimental and numerical analyses of local mechanical properties measured by atomic force microscopy for sheared endothelial cells. *Bio-Medical Materials and Engineering*, 12(3), 319–327.

Okajima, T., Tanaka, M., Tsukiyama, S., Kadowaki, T., Yamamoto, S., Shimomura, M., & Tokumoto, H. (2007). Stress relaxation of HepG2 cells measured by atomic force microscopy. *Nanotechnology*, 18(8), 084010.

Okamoto, K., Iwasaki, N., Doi, K., Noiri, E., Iwamoto, Y., Uchigata, Y. Tokunaga, K. (2012). Inhibition of glucose-stimulated insulin secretion by KCNJ15, a newly identified susceptibility gene for type 2 diabetes. *Diabetes*, 61(7), 1734–1741.

Oldfield, M. D., Bach, L. A., Forbes, J. M., Nikolic-Paterson, D., McRobert, A., Thallas, V., Cooper, M. E. (2001). Advanced glycation end products cause epithelial-

myofibroblast transdifferentiation via the receptor for advanced glycation end products (RAGE). *The Journal of Clinical Investigation*, 108(12), 1853–1863.

Panchapakesan, U. (2013). DPP4 Inhibition in Human Kidney Proximal Tubular Cells - Renoprotection in Diabetic Nephropathy. *Journal of Diabetes & Metabolism*, 1(S9), 1-8.

Pelling, A. E., & Horton, M. A. (2008). An historical perspective on cell mechanics. *Pflügers Archiv: European Journal of Physiology*, 456(1), 3–12.

Perez-Moreno, M., Jamora, C., & Fuchs, E. (2003). Sticky business: orchestrating cellular signals at adherens junctions. *Cell*, 112(4), 535–548.

Persaud, S. J. (1999). Pancreatic β-Cell Lines: Their roles in β-cell research and diabetes therapy. *The Biology of the Pancreatic β-Cell,* 29, 21–46.

Pocock, G., & Richards, C. (2009). *The human body: an interoduction for the biomedical and health*. Oxford Universtiy Press, Oxford, UK.

Puech, P.-H., Taubenberger, A., Ulrich, F., Krieg, M., Muller, D. J., & Heisenberg, C.-P. (2005). Measuring cell adhesion forces of primary gastrulating cells from zebrafish using atomic force microscopy. *Journal of Cell Science*, 118(18), 4199–206.

Puech, P.-H., Poole, K., Knebel, D., & Muller, D. J. (2006). A new technical approach to quantify cell-cell adhesion forces by AFM. *Ultramicroscopy*, 106(8-9), 637–644.

Qi, W., Chen, X., Zhang, Y., Holian, J., Mreich, E., Gilbert, R. E. Pollock, C. A. (2007). High glucose induces macrophage inflammatory protein-3 alpha in renal proximal tubule cells via a transforming growth factor-beta 1 dependent mechanism. *Nephrology, Dialysis, Transplantation*, 22(11), 3147–3153.

Racusen, L. C., Monteil, C., Sgrignoli, a, Lucskay, M., Marouillat, S., Rhim, J. G., & Morin, J. P. (1997). Cell lines with extended in vitro growth potential from human renal proximal tubule: characterization, response to inducers, and comparison with established cell lines. *The Journal of Laboratory and Clinical Medicine*, 129(3), 318–29.

Radmacher, M., Fritz, M., Kacher, C. M., Cleveland, J. P., & Hansma, P. K. (1996). Measuring the viscoelastic properties of human platelets with the atomic force microscope. *Biophysical Journal*, 70(1), 556–567.

Radmacher, Manfred. (2002). Measuring the elastic properties of living cells by the atomic force microscope. *Methods In Cell Biology*, *68*, 67–90.

Rasschaert, J., & Malaisse, W. J. (1999). Expression of the calcium-sensing receptor in pancreatic islet B-cells. *Biochemical and Biophysical Research Communications*, 264(3), 615–618.

Rogers, G. J., Hodgkin, M. N., & Squires, P. E. (2007). E-cadherin and cell adhesion: a role in architecture and function in the pancreatic islet. *Cellular Physiology And Biochemistry: International Journal of Experimental Cellular Physiology, Biochemistry, and Pharmacology*, 20(6), 987–994.

Rosenbluth, M. J., Lam, W. A, & Fletcher, D. A. (2006). Force microscopy of nonadherent cells: a comparison of leukemia cell deformability. *Biophysical Journal*, 90(8), 2994–3003.

Rotsch, C., & Radmacher, M. (2000). Drug-induced changes of cytoskeletal structure and mechanics in fibroblasts: an Atomic Force Microscopy study. *Biophysical Journal*, 78(1), 520–35.

Ryan, M. J., Johnson, G., Kirk, J., Fuerstenberg, S. M., Zager, R. A., & Torok-Storb, B. (1994). HK-2: an immortalized proximal tubule epithelial cell line from normal adult human kidney. *Kidney International*, *45*(1), 48–57.

Sakuraba, H., Mizukami, H., Yagihashi, N., Wada, R., Hanyu, C., & Yagihashi, S. (2002). Reduced beta-cell mass and expression of oxidative stress-related DNA damage in the islet of Japanese Type II diabetic patients. *Diabetologia*, 45(1), 85–96.

Scanon, V. C., & Sanders, T. (2002). Essentials of anatomy and physiology. F.A. Davis Plus. Philadelphia, USA.

Schmitz, J., Benoit, M., & Gottschalk, K.-E. (2008). The viscoelasticity of membrane tethers and its importance for cell adhesion. *Biophysical Journal*, 95(3), 1448–59.

Scott, O., Begley, M., Komaragiri, U., & Mackin, T. (2004). Indentation of freestanding circular elastomer films using spherical indenters. *Acta Materialia*, 52 (16), 4877-4885.

Sharma, K., & Ziyadeh, F. N. (1995). Hyperglycemia and diabetic kidney disease. The case for transforming growth factor-beta as a key mediator. *Diabetes*, 44(10), 1139–1146.

Sharp, G. W. (1996). Mechanisms of inhibition of insulin release. *The American Journal of Physiology*, 271(6), C1781–C1799.

Shaw, J. E., Sicree, R. A, & Zimmet, P. Z. (2010). Global estimates of hte prevalence of diabetes for 2010 and 2030. *Diabetes Research and Clinical Practice*, 87, 1-14.

Shih, D. Q., Heimesaat, M., Kuwajima, S., Stein, R., Wright, C. V. E., & Stoffel, M. (2002). Profound defects in pancreatic beta-cell function in mice with combined heterozygous mutations in Pdx-1, Hnf-1alpha, and Hnf-3beta. *Proceedings of the National Academy of Sciences of The United States of America*, 99(6), 3818–3823.

Sirghi, L., Ponti, J., Broggi, F., & Rossi, F. (2008). Probing elasticity and adhesion of live cells by atomic force microscopy indentation. *European Biophysics Journal*, 37(6), 935–45.

Skelin, M., Rupnik, M., & Cencic, A. (2010). Pancreatic beta cell lines and their applications in diabetes mellitus research. *Altex*, 27(2), 105–13.

Slattery, C., Campbell, E., McMorrow, T., & Ryan, M. P. (2005). Cyclosporine A-induced renal fibrosis: a role for epithelial-mesenchymal transition. *The American Journal of Pathology*, 167(2), 395–407.

Smajilovic, S., Yano, S., Jabbari, R., & Tfelt-Hansen, J. (2011). The calcium-sensing receptor and calcimimetics in blood pressure modulation. *British Journal of Pharmacology*, 164(3), 884–893.

Squires, P. E., Harris, T. E., Persaud, S. J., Curtis, S. B., Buchan, a M., & Jones, P. M. (2000). The extracellular calcium-sensing receptor on human beta-cells negatively modulates insulin secretion. *Diabetes*, 49(3), 409–17.

Straub, S. G., Kornreich, B., Oswald, R. E., Nemeth, E. F., & Sharp, G. W. (2000). The calcimimetic R-467 potentiates insulin secretion in pancreatic beta cells by activation of a nonspecific cation channel. *The Journal of Biological Chemistry*, 275(25), 18777–18784.

Tian, Y.-C., Chen, Y.-C., Chang, C.-T., Hung, C.-C., Wu, M.-S., Phillips, A., & Yang, C.-W. (2007). Epidermal growth factor and transforming growth factor-beta1 enhance HK-2 cell migration through a synergistic increase of matrix metalloproteinase and sustained activation of ERK signaling pathway. *Experimental Cell Research*, 313(11), 2367–77.

Trivedi, R., Mithal, A., & Chattopadhyay, N. (2008). Recent updates on the calcium-sensing receptor as a drug target. *Current Medicinal Chemistry*, 15(2), 178–186.

Tu, C.-L., Chang, W., Xie, Z., & Bikle, D. D. (2008). Inactivation of the calcium sensing receptor inhibits E-cadherin-mediated cell-cell adhesion and calcium-induced differentiation in human epidermal keratinocytes. *The Journal of Biological Chemistry*, 283(6), 3519–3528.

Vaezi, A., Bauer, C., Vasioukhin, V., & Fuchs, E. (2002). Actin cable dynamics and Rho/Rock orchestrate a polarized cytoskeletal architecture in the early steps of assembling a stratified epithelium. *Developmental Cell*, 3(3), 367–381.

Van Vliet, K. J., Bao, G. & Suresh, S. (2003). The biomechanics toolbox: experimental approaches for living cells and biomolecules. *Acta Materialia*, 51(19), 5881-5905.

Vinckier, A, & Semenza, G. (1998). Measuring elasticity of biological materials by atomic force microscopy. *FEBS Letters*, 430(1-2), 12–6.

Wahren, J., Ekberg, K., Samnegård, B., & Johansson, B.-L. (2001). C-peptide: A new potential in the treatment of diabetic nephropathy. *Current Diabetes Reports*, 1(3), 261–266.

Weder, G., Vörös, J., Giazzon, M., Matthey, N., Heinzelmann, H., & Liley, M. (2009). Measuring cell adhesion forces during the cell cycle by force spectroscopy. *Biointerphases*, 4(2), 27–34.

Wennstrom, M., & Nielsen, H. M., (2012). Cell adhesion molecules in Alzheimer's disease. Degenerative Neurological and Neuromuscular Disease, 2, 65–77

Wierup, N., Yang, S., McEvilly, R. J., Mulder, H., & Sundler, F. (2004). Ghrelin is expressed in a novel endocrine cell type in developing rat islets and inhibits insulin secretion from INS-1 (832/13) cells. *Journal of Histochemistry & Cytochemistry*, 52(3), 301–310.

Wojcikiewicz, E. P., Zhang, X., & Moy, V. T. (2004). Force and compliance measurements on living cells using Atomic Force Microscopy (AFM). *Biological Procedures Online*, 6(1), 1–9.

Yoon, J.-W., & Jun, H.-S. (2005). Autoimmune destruction of pancreatic beta cells. *American Journal of Therapeutics*, 12(6), 580–91.

Zeisberg, M., & Kalluri, R. (2004). The role of epithelial-to-mesenchymal transition in renal fibrosis. *Journal of Molecular Medicine*, 82(3), 175–181.

Zhang, X., Wojcikiewicz, E., & Moy, V. T. (2002). Force spectroscopy of the leukocyte function-associated antigen-1/intercellular adhesion molecule-1 interaction. *Biophysical Journal*, 83(4), 2270–2279.

Zhang, H., & Liu, K.-K. (2008). Optical tweezers for single cells. *Journal of the Royal Society*, 5(24), 671–90.

Zhang, P., Zhang, X., Brown, J., Vistisen, D., Sicree, R., Shaw, J., & Nichols, G. (2010). Global healthcare exprenditure on diabetes for 2010 and 2030. *Diabetes Research and Clinical Practice*, 87, 293-301.

Zheng, G., Lyons, J. G., Tan, T. K., Wang, Y., Hsu, T.-T., Min, D. Harris, D. C. H. (2009). Disruption of E-cadherin by matrix metalloproteinase directly mediates epithelial-mesenchymal transition downstream of transforming growth factor-beta1 in renal tubular epithelial cells. *The American Journal of Pathology*, 175(2), 580–591.

Zhu, C., Bao, G., & Wang, N. (2000). Cell mechanics: mechanical response, cell adhesion, and molecular deformation. *Annual Review of Biomedical Engineering*, *2*, 189–226.

Zimmet, P., Alberti, K. G., & Shaw, J. (2001). Global and societal implications of the diabetes epidemic. *Nature*, 414(6865), 782–787.

Bibliography

CellHesion200 User Manual (2012), Version 4.2, *JPK Instruments*. Berlin, Germany.

Data Processing Software Manual (2012), Version 4.2, *JPK Instruments*. Berlin, Germany.

Owen, R. (2009) A practical guide to AFM force spectroscopy and data analysis. *JPK Technical Report.* Berlin, Germany.

Poole, K. (2010) Using the CellHesion module-a practical guide. *JPK Technical Report.* Berlin, Germany.

Appendix

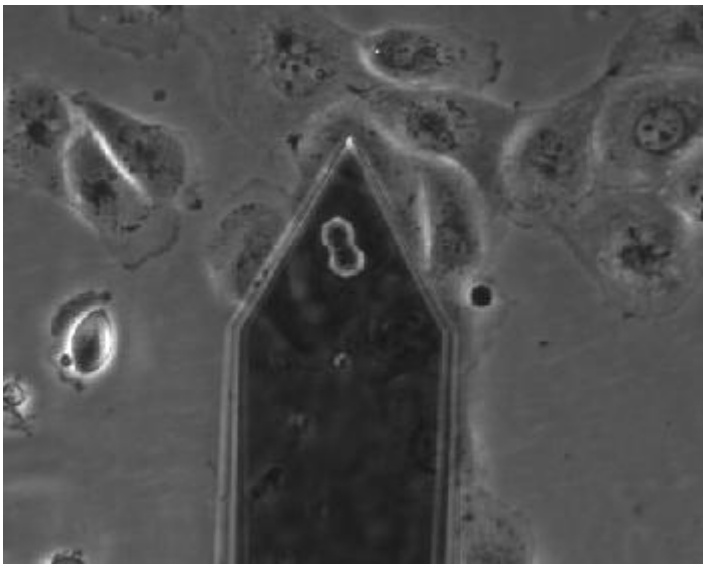

Figure A-1: The change in morphology of a cantilever-attached cell while performing AFM-SCFS. The cell is splitting and it cannot be used anymore for cell-to-cell adhesion measurements. In that case a new functionalised cantilever is required and the cantilever-cell attachment procedure must be repeated.

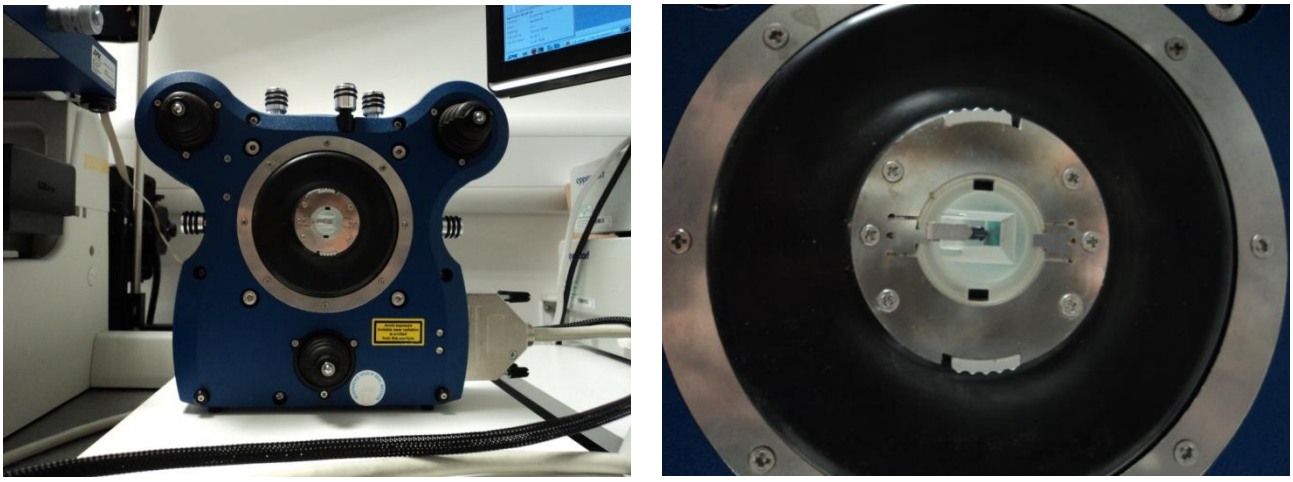

(a) **(b)**

Figure A-2: (a) The head of CellHesion200 with the glass block at its centre. (b) The cantilever is mounted on glass block with the aid of a spring.

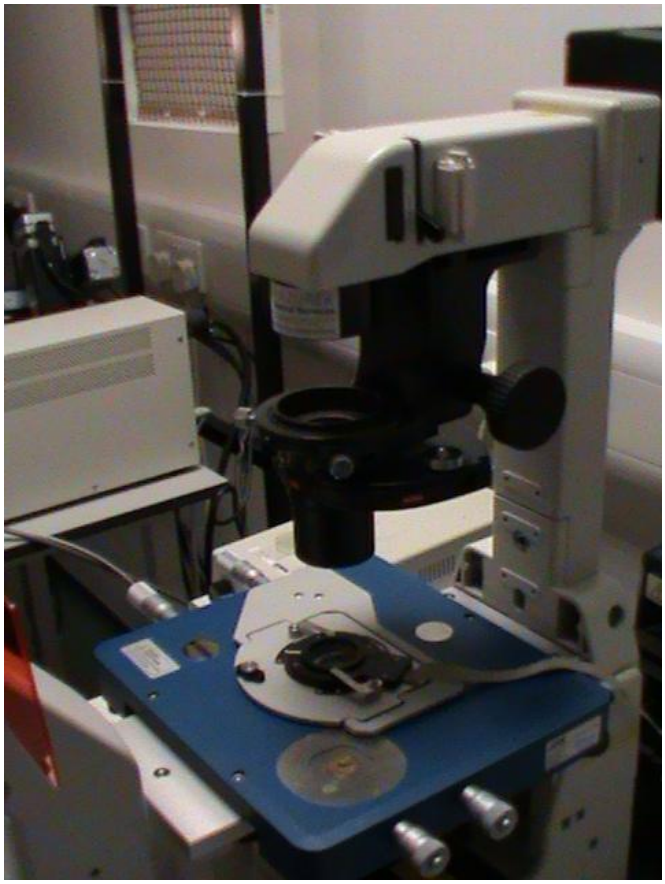

Figure A-2: The stage of the AFM mounted on an inverted microscope. The temperature controller was installed on the stage to maintain the sample at 37ºC. After injecting the suspended cells on the petri dish the head was mounted on the stage to perform AFM-SCFS measurements.

FEBS Letters 588 (2014) 1178–1183

journal homepage: www.FEBSLetters.org

Quantitative investigation of calcimimetic R568 on beta cell adhesion and mechanics using AFM single-cell force spectroscopy

Eleftherios Siamantouras [a], Claire E. Hills [b], Mustafa Y.G. Younis [b], Paul E. Squires [b], Kuo-Kang Liu [a,*]

[a] School of Engineering, University of Warwick, CV4 7AL, UK
[b] School of Life Sciences, University of Warwick, CV4 7AL, UK

ARTICLE INFO

Article history:
Received 20 December 2013
Revised 14 February 2014
Accepted 24 February 2014
Available online 5 March 2014

Edited by Lukas Huber

Keywords:
AFM-SCFS
Cell adhesion
Indentation
Elasticity
CaSR
Calcimimetic

ABSTRACT

In this study we use a novel approach to quantitatively investigate mechanical and interfacial properties of clonal β-cells using AFM-Single Cell Force Spectroscopy (SCFS). MIN6 cells were incubated for 48 h with 0.5 mM Ca^{2+} ± the calcimimetic R568 (1 μM). AFM-SCFS adhesion and indentation experiments were performed by using modified tipless cantilevers. Hertz contact model was applied to analyse force–displacement (*F–d*) curves for determining elastic or Young's modulus (*E*). Our results show CaSR-evoked increases in cell-to-cell adhesion parameters and *E* modulus of single cells, demonstrating that cytomechanics have profound effects on cell adhesion characterization.

1. Introduction

The role of the calcium-sensing receptor CaSR in the systemic circulation is to sense changes in extracellular Ca^{2+} and evoke appropriate counter-regulatory responses to regain normocalcaemia [4]. The functional link between the receptor and regulation of systemic calcium in normal physiology and disease has been extensively studied [4]. However, CaSR expression is not restricted to the cells involved in the control of systemic Ca^{2+} [5]. It has been well recognized that CaSR activation affects function in disparate tissue types, including pancreatic beta-cells [29,12,19,21].

Epithelial (E)-cadherin is a surface adhesion protein involved in tethering adjacent cells and ensuring close cell–cell interaction. E-cadherin ligation mediates beta-cell-to-beta-cell coupling and regulates intercellular communication within islets [3]. A study by Rogers et al. [27] suggested that E-cadherin mediated cell adhesion contributes to the enhanced secretory function of beta-cell clusters. Neutralization of E-cadherin reduced glucose-evoked synchronicity in calcium signals between adjacent cells and reduced insulin secretion [27]. These data imply that E-cadherin mediated cell adhesion has important repercussions for the islet function in terms of glucose responsiveness and insulin secretion.

We have previously demonstrated that the activation of CaSR using the calcimimetic R568, increased the expression of E-cadherin, which in turn increased functional tethering between beta-cells [15]. In the current study we quantitatively monitored changes in cell elasticity induced by activation of the CaSR by the calcimimetic R568. Atomic Force Microscopy based Single Cell Force Spectroscopy (AFM-SCFS) was used to perform cell-to-cell adhesion and single cell indentation experiments. The SCFS system incorporates an improved positioner to allow for longer displacement measurements up to 100 μm for separating two adherent cells, in a high force resolution (~pN) over a large dynamic range (~5 pN to ~100 nN). This system provides sufficient force and displacement ranges to ensure accurate detection of maximum unbinding force of ligand-receptor interactions in cell-to-cell adhesion measurement [2,26,9,14], while it has been used extensively for studying cadherin mediated adhesion [1,25,22]. In the current study the instrument was also fitted with a spherical bead-attached cantilever beam to indent single cells and thereby calculate cell elasticity, i.e. Young's modulus, from the measured force–displacement curves using Hertzian contact model [32]. The novel use of this improved AFM-SCFS system permits us to examine cellular adhesion, tethering of cells and cell elasticity and more importantly to elucidate the intricate interplay between these factors.

* Corresponding author. Address: School of Engineering, University of Warwick, Coventry CV4 7AL, UK.
E-mail address: I.K.Liu@warwick.ac.uk (K.-K. Liu).

http://dx.doi.org/10.1016/j.febslet.2014.02.058
0014-5793/

2. Materials and methods

2.1. Materials

MIN6 cells were obtained from Dr. Y. Oka and J.-I. Miyazaki (Univ. of Tokyo, Japan). Fibronectin, Dulbecco's Modified Eagles Medium (DMEM), Hams-F12, glutamine, penicillin-streptomycin and phosphate buffered saline (PBS) were from Sigma–Aldrich (Poole, Dorset, UK). The calcimimetic R568 was from Amgen Inc. (Thousand Oaks, CA, USA). Tissue culture plastic-ware was from Invitrogen Life Technologies (Paisley, UK).

2.2. Maintenance of MIN6 cells

MIN6 cells (passage 35–40) were maintained at 37 °C in a humidified atmosphere of 5% CO_2 in air in DMEM supplemented with 15% FCS, glutamine (2 mM) and penicillin/streptomycin (100 U/ml/0.1 mg/ml). Prior to treatment, cells were seeded onto 40 mm petri-dishes and serum starved overnight. Cells were then placed for 48 h in DMEM containing both low glucose (5 mM) and low calcium (0.5 mM) +/− the calcimimetic R568 (1 μM) [15]. Suspended (free) cells were prepared under identical conditions before being physically scrapped off the T25 flasks with gentle agitation and re-suspended in fresh DMEM.

2.3. Atomic Force Microscopy

Experiments were performed using the CellHesion®200 module (JPK Instruments, Germany) installed on an Eclipse TE 300 inverted microscope (Nikon, USA). During each experiment, cells were maintained at 37 °C using a BioCell™ temperature controller (JPK Instruments, Berlin, Germany). All experiments were performed in CO_2 – independent media. Phase microscopy images were acquired using a CCD camera connected on the side port of the microscope. The entire set-up was supported on an anti-vibration table (TMC 63-530, USA).

Tip-less silicon nitride cantilevers (Arrow TL-1, NanoWorld, Switzerland), with force constant 0.03 N/m, were used for conducting cell-to-cell adhesion and single cell indentation experiments. The actual spring constant of the cantilever was determined before experiments by using the manufacturer's software (JPK instruments, Germany) based on the thermal noise method [17]. Since the resonance of soft cantilevers in fluid is much lower and very susceptible to noise a correction factor of 0.251 was used [6].

2.4. Cell-to-cell adhesion experiments

The tip-less cantilevers were chemically functionalized for a single suspended cell to be attached. Initially the cantilevers were sterilised by UV treatment (15 min), before being incubated in poly-L-lysine (25 μg/ml in PBS, 30 min, RT) and then fibronectin (20 μg/ml in PBS, 2 h, 37 °C) [16]. After functionalization cantilevers were stored in PBS solution at 4 °C and used within 3 days. To record a force curve for calibration, the cantilever was configured to approach the base of a cell-free petri-dish once, to minimize the loss of coating (set-point 2 V). Suspended cells were dispensed into the petri dish using a pipette. Free cells stick on the substrate within 5 min, hence the cell-cantilever attachment procedure was performed rapidly (2 min). With the aid of optical microscope the cantilever was pressed against a single free cell by performing a force curve. The set-point force and contact time was 0.8 nN and 5 s, respectively. During the contact period, the instrument was set in a constant force mode, in which force is kept constant by adjustments of the piezo-actuator height. Once a single cell was attached to the cantilever, it was left to recover for at least 5 min to form strong binding with the functionalized surface [11].

The cantilever-attached cell was brought in contact with another cell adhering on the substrate, until a preset contact force of 0.8 nN was reached. The cells remained in contact for 5 s, in which surface bonding was formed. Next, the cantilever was retracted and force versus displacement measured until the two cells were completely separated. The procedure was repeated three times for each cell tested, with 30 s intervals between each measurement. The attached cell was used to perform measurements on approximately 3–5 cells for each dish, using multiple dishes from at least 3 separate samples of cells in each experiment ($n = 3$).

2.5. Cell indentation experiments

Using a small amount of two-part fast setting epoxy glue (5 min), colloidal probes were prepared by gluing an 11 μm polystyrene microsphere (Polybeads®, Polysciences, USA) on a tipless TL-1 cantilever. The attachment procedure was performed on the stage of AFM with the aid of the inverted optical microscope. The microsphere was attached immediately by performing an approach curve directly above the sphere. Fig. 1(a) shows optical images of polymeric bead attached to a tipless cantilever.

Each substrate cell was indented 5 times with an interval pause of 60 s, while force–displacement (F–d) curves were recorded simultaneously. For consistency, all cells were indented immediately

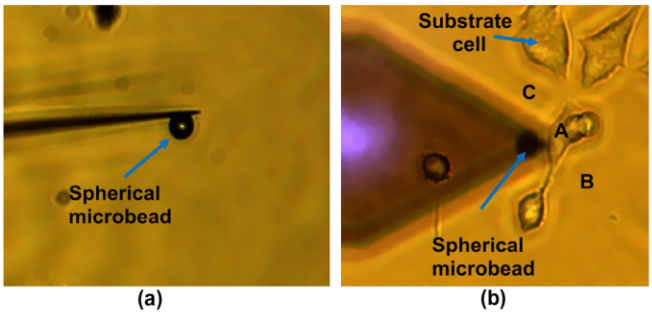

Fig. 1. (a) An optical image showing the side view of a 10 μm silica microsphere attached to the end of an arrow TL1 tipless cantilever. (b) An optical image showing the top view of the cantilever-bead and MIN6 cells on the substrate. The determination of cell height prior indentation experiments is also demonstrated; a low set-point force (0.2 nN) was used for the AFM cantilever to touch a point in a clean area, such as B and C, next to a measured cell (A area). The displacement difference between B (or C) and A was used to determine the height of the cell.

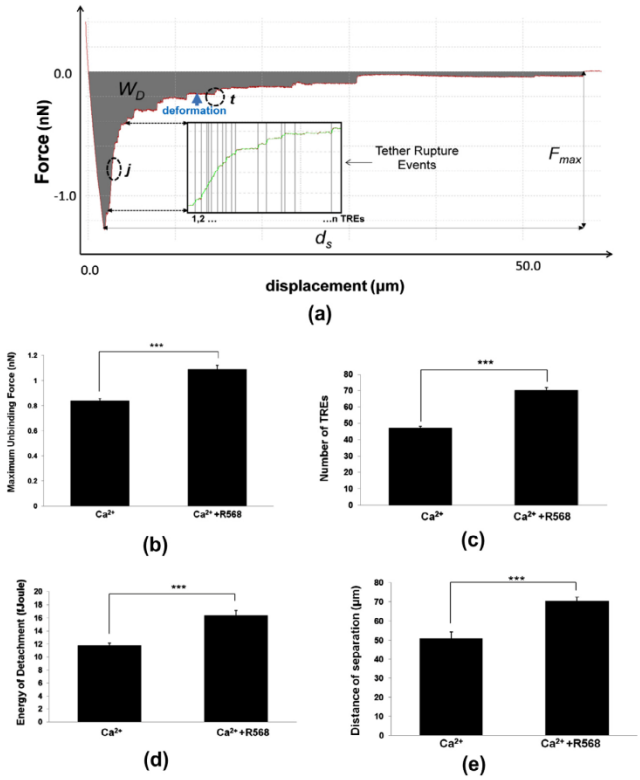

Fig. 2. (a) Example of a retraction force–distance curve obtained by cell-to-cell adhesion measurement. F_{max} is the difference between the minimum force value and the baseline, while W_D (grey region) is the integral of the continuous area under the baseline. Next, d_s can be determined by the difference of displacements between F_{max} and the point of complete separation. Unbinding of ligations during the pulling phase mainly falls in two areas, those events in which a ramp in the deflection of the cantilevers is preceded ('j' events) and those which a deformation of membrane tethering is preceded ('t' events). Zooming in the *x*-axis displays detection of the number of early TREs. The effects of the calcimimetic R568 (1 µM) on (b) the maximum unbinding force F_{max} (increased by 30%), (c) the number of tethering rupture events (TREs) increased by 48%, (d) the energy of detachment W_D (increased by 39%) and (e) the distance to complete separation (increased by 37%) are shown. Data are expressed as mean ± S.E.M. of 10–12 cells from 3 separate experiments, where key significances are shown, $^{***}P < 0.001$.

above the nucleus. To determine height of the cell, approach curves with low set-point (0.2 nN) were performed in the area surrounding the cell and on its surface. The height of each cell was calculated by their displacement difference, as illustrated in Fig. 1(b). Since, the indentation depth was pre-determined for each cell, indentation experiments were performed to measure the force–displacement curves up to the pre-set indentation depth, according to the height measurement of the cell. Approach and retraction speed was kept constant at 5 µm/s to minimize hydrodynamic forces acting on the cantilever [10].

2.6. Theoretical model

Force–displacement curves acquired by indentation experiments were analyzed using Hertz model. When a cell is indented by a spherical probe, the force *F* applied on the cell was determined as function of indentation depth δ as follows,

$$F = \frac{E}{1-\nu^2}\left[\frac{a^2+R_S^2}{2}\ln\frac{R_S+a}{R_S-a} - aR_S\right] \quad \text{(eq.1)}$$

$$\delta = \frac{a}{2}\ln\frac{R_S+a}{R_S-a} \quad \text{(eq.2)}$$

where E and ν are the Young's Modulus and Poisson's ratio of the cell respectively, α is the radius of probe-cell contact circle, and R_S is the radius of the spherical probe.

The Hertz model is only valid for indentations up to 10% of the samples height, where substrate effects are considered insignificant [7]. To meet such a criterion, all the force–displacement curves obtained from cell indentation experiments were fitted in the range of 5–10% of the height of each cell. The Poisson's ration was set to 0.5 in the study, since this value is generally accepted for soft biological cells [24].

2.7. Data analysis

To process all force–displacement curves the JPK Data analysis software was used. To signify statistical differences data were evaluated using a paired *t*-test. Data are expressed as mean ± SEM. and '*n*' shows number of experiments. $P < 0.05$ was taken to indicate statistical significance.

3. Results

A few sets of measurements were performed to confirm the selected parameters for adhesion measurements. Using identical experimental specifications 10–12 cells were examined and the results are shown in Fig. 3. Retraction force–displacement (F–d) curves provide important information regarding the adhesion between two cells, such as the energy of detachment W_D, the maximum unbinding force F_{max}, the distance of complete separation d_s, and the number of tethering rupture events (TREs) (Fig. 2(a)). The determination of the point at which the cells are completely separated represents the x-axis baseline, which acts as a reference for further analysis. The unbinding force is the force required to break the ligation bonding between E-cadherin on coupled cells, whilst the energy of detachment is the total energy that is consumed until the two cells are completely detached. The pulling length from the highest negative deflection of the cantilever and the point of complete separation represents the distance of complete separation d_s between two cells. Retraction F–d curves acquired during cell-to-cell adhesion experiments typically exhibit a step-like pattern resulting from the rupture of surface ligations. Number of TREs can be detected by identifying sharp steps of force that correspond to bond ruptures [20]. In the early part of the retraction curve complex unbinding events occur ('j' events) that are preceded by a force ramp, while as the pulling distance increases a plateau in the displacement indicates that membrane tethering extrudes rupture of ligation ('t' events) [11]. The results indicate that the calcimimetic R568 (1 μM) increased the number of tether rupture events by 48%, resulting in an increase of the maximum unbinding force by 30%. However, the detachment energy was increased more significantly by 39%, consistent with the detachment distance increasing by 37% (10–12 cells, $n = 3$, $P < 0.001$) (Fig. 2(b–e)).

A typical indentation F–d curve for investigating the elastic properties of single cells is shown in Fig. 3(a). By applying the Hertz model for elastic indentation to F–d curves recorded during indentation, information about the local elastic or Young's modulus (E) was extracted. The contact point is defined as the point where cantilever deflection starts to rise and in fact accurate determination of the contact point is crucial for a reliable calculation of the elastic modulus. By fitting discrete parts of the extension curve to the model, the point where the probe is in contact with the plasma membrane can be identified. Fig. 3(b) shows a histogram of elastic modulus E determined from the F–d curves measured on a central region above the nucleus of cells. More than 100 curves were analysed and the average calculated value of E for the control cells is 503 Pa while for the treated cells is 331 Pa. The results indicate that the calcimimetic R568 (1 μM) decreased the elastic modulus by 34% (30 cells, $n = 3$, $P < 0.001$) (Fig. 4).

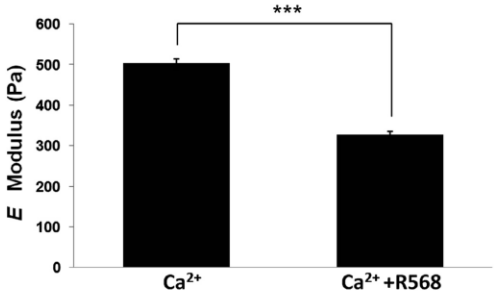

Fig. 4. The effects of calcimimetic R568 (1 μM) on the elastic modulus (decreased by 54%). Data are expressed as mean ± S.E.M. of at least 30 cells from 3 separate experiments, where key significances are shown, ***$P < 0.001$.

To further assess the effects of viscoelastic deformation on cell-to-cell adhesion, F–d curves were performed with incremental pulling or separation speed. Due to the soft nature of the cells, data were analysed up to a speed of 12.5 μm/s, since a significantly higher displacement range than 100 μm was required for higher velocities. The results demonstrate a tenfold increase of the W_D in comparison to the F_{max} as the pulling speed increases, up to the pulling distance of 100 μm (10–12 cells, $n = 3$) (Fig. 5(a and c)). The decrease in the number of TREs for a displacement range of 30 μm after F_{max} was two times higher for the cells treated with the calcimimetic in comparison to the untreated. Fig. 6 shows respectively that for both control and treated cells, F_{max} is dependent on velocity, based on Eq. (eq. 3), which is derived from the Bell–Evans model [28,23].

$$F_i \sim f_\beta \ \ln(\text{loading rate}) + \text{constant} \qquad \text{(eq.3)}$$

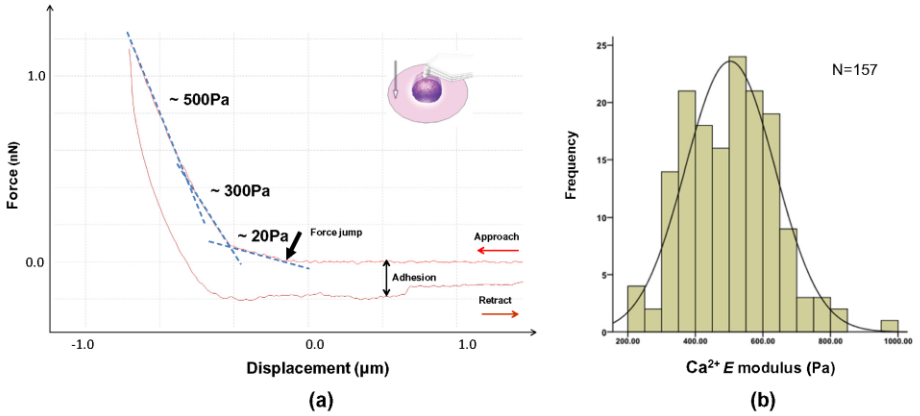

Fig. 3. (a) A typical force displacement curve obtained by a nanoindentation measurement. Elasticity can be calculated by fitting Hertz model into the extended part of the curve, in which adhesion is negligible. (b) A histogram of elastic modulus E obtained from the F–d curve measurements of MIN6 cells measured on a central region.

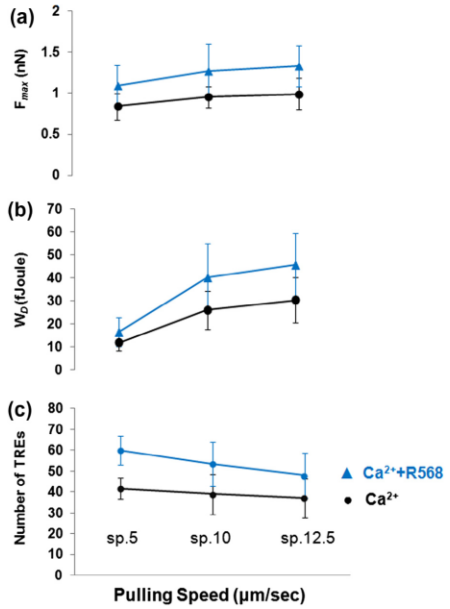

Fig. 5. Effects of increasing pulling speed on (a) maximum unbinding force F_{max}, (b) work of detachment W_D and (c) number of tethering rupture events TREs.

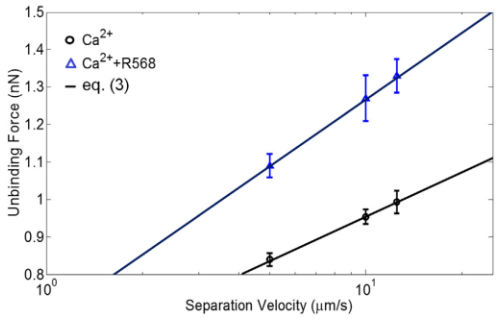

Fig. 6. Dependence of unbinding forces on separation velocities of Ca^{2+} and Ca^{2+}+R568 treated beta-cells.

where F_i is the unbinding force and f_β is the characteristic force scale over the single energy barrier until the complete separation of the surface ligation.

4. Discussion

Extracellular calcium promotes the interaction between the extracellular domains of E-cadherin on adjacent cells, whilst the intracellular domain of the trans-membrane protein binds to β-catenin, α-catenin and the actin cytoskeleton. Ligation of E-cadherin to a partner protein on an adjacent cell, stimulates other down-stream cytoskeletal-binding proteins including the phosphoinositide 3-kinase PI3K [31]. In keratinocytes it was suggested that the CaSR was involved in regulating calcium stimulated formation of the E-cadherin complex [30]. Our previous results suggest that the activation of the receptor improves β-cell function by increasing cell adhesiveness through enhanced expression of E-cadherin and via PI3K-dependent cytoskeletal reorganisation [15]. Under appropriate conditions MIN6 cells grow as 3-dimensional cell clusters known as pseudoislets [13]. Analysis of whole cell protein suggested that CaSR expression is higher in monolayers compared to pseudoislets [19]. As adhesion and indentation experiments are only possible on monolayers, and due to the fact that CaSR expression is greater in this type of cell configuration, all experiments were performed on monolayers.

Surface protein binding affinity was responsible for the increase in F_{max}, however our results suggest that this was only partially responsible for the increase in W_D, which was influenced by the changes in the elastic mechanical properties of the cell. An increase in W_D could mirror changes in the compliance of cells, since W_D is partly contributed from the elastic deformation of an elastic sphere apart from the adhesion due to surface contact [18]. This is clearly demonstrated by the increase in E as well as by the dramatic increase of W_D when pulling speed was increased. The comparison between increasing pulling speeds suggests that although the surface properties were significant for changes in F_{max}, changes in the mechanical properties in response to cytoskeletal reorganization, rather than ligation binding affinity or surface density of E-cadherin, contribute to the dramatic changes of the W_D. The larger decrease of the treated cells' TREs also implies that fewer bindings were ruptured over the same distance of separation, due to their higher compliance. Moreover, the increase in F_{max} with increased pulling speed could be contributed to the viscoelastic deformation of the surface proteins themselves and membrane tethers. Diz-Muñoz et al. [8] measured the dynamics of tethering force between the AFM tip and cell membrane, also concluding that the unbinding force increased as the separation speed increased. Both our adhesion and indentation measurements clearly suggest that the viscoelastic deformation has a significant influence on the adhesion energy between two adherent cells and that cytomechanics contribute to the E-cadherin mediated adhesion in our system.

5. Conclusion

In the current study we have investigated the effects of whole cell elasticity under the influence of the calcimimetic R568 in the MIN6 clonal β-cell line and we have provided quantitative evidence that the mechanical properties of cells have an effect on cell-to-cell interaction. Activation of CaSR increases the expression of the surface adhesion protein E-cadherin [15], whilst affecting the intracellular domain of the protein by increasing the elasticity of the cell. The changes in the inner mechanical properties of the cells had a strong effect on cell-to-cell adhesion energy, mainly due to viscoelastic deformation. As a consequence, adhesion parameters were altered not only due to biomolecular changes in cell surface expression of E-cadherin, as previously reported, but also due to changes in the biomechanical properties of the cells. Therefore, in improving beta cell function, activation of CaSR not only increases E-cadherin expression and cell-to-cell adhesiveness but it also initiates &/or modulates intracellular signalling of the F-actin cytoskeleton via the catenins. The net result is a change in the mechanistic behaviour of whole cell.

Acknowledgements

This work was supported by grants from Diabetes UK (BDA: 09/0003913, and 12/0004546) and Leverhulme Trust (PRG-2012-738).

The authors are grateful to Amgen Inc. for their supply of the calcimimetic R568 and JPK instrument for their technical support in the use of single-cell force spectroscopy.

References

[1] Baumgartner, W. (2000) Cadherin interaction probed by atomic force microscopy. Proc. Natl. Acad. Sci. USA 97 (8), 4005–4010.
[2] Benoit, M. et al. (2000) Discrete interactions in cell adhesion measured by single-molecule force spectroscopy. Nat. Cell Biol. 2 (6), 313–317.
[3] Brereton, H.C. et al. (2006) Homotypic cell contact enhances insulin but not glucagon secretion. Biochem. Biophys. Res. Commun. 344 (3), 995–1000.
[4] Brown, E.M. (2007) Clinical lessons from the calcium-sensing receptor. Nat. Clin. Pract. Endocrinol. Metab. 3 (2), 122–133.
[5] Brown, E.M. and MacLeod, R.J. (2001) Extracellular calcium sensing and extracellular calcium signaling. Physiol. Rev. 81 (1), 239–297.
[6] Butt, H.-J. and Jaschke, M. (1995) Calculation of thermal noise in atomic force microscopy. Nanotechnology 6 (1), 1–7.
[7] Dimitriadis, E.K. et al. (2002) Determination of elastic moduli of thin layers of soft material using the atomic force microscope. Biophys. J. 82 (5), 2798–2810.
[8] Diz-Muñoz, A. et al. (2010) Control of directed cell migration in vivo by membrane-to-cortex attachment. PLoS Biol. 8 (11), e1000544.
[9] Franz, C.M. et al. (2007) Studying integrin-mediated cell adhesion at the single-molecule level using AFM force spectroscopy. Sci. STKE 406, l5.
[10] Franz, C.M. and Puech, P.-H. (2008) Atomic force microscopy: a versatile tool for studying cell morphology, adhesion and mechanics. Cell. Mol. Bioeng. 1 (4), 289–300.
[11] Friedrichs, J. et al. (2010) Quantifying cellular adhesion to extracellular matrix components by single-cell force spectroscopy. Nat. Protoc. 5 (7), 1353–1361.
[12] Gray, E. et al. (2006) Activation of the extracellular calcium-sensing receptor initiates insulin secretion from human islets of Langerhans: involvement of protein kinases. J. Endocrinol. 190 (3), 703–710.
[13] Hauge-Evans, A.C. et al. (1999) Pancreatic beta-cell-to-beta-cell interactions are required for integrated responses to nutrient stimuli: enhanced Ca2+ and insulin secretory responses of MIN6 pseudoislets. Diabetes 48 (7), 1402–1408.
[14] Helenius, J. et al. (2008) Single-cell force spectroscopy. J. Cell Sci. 121 (Pt 11), 1785–1791.
[15] Hills, C.E. et al. (2012) Calcium-sensing receptor activation increases cell–cell adhesion and β-cell function. Cell. Physiol. Biochem. 30 (3), 575–586.
[16] Hills, C.E. et al. (2013) "Special K" and a loss of cell-to-cell adhesion in proximal tubule-derived epithelial cells: modulation of the adherens junction complex by ketamine. PLoS One 8 (8), e71819.
[17] Hutter, J.L. and Bechhoefer, J. (1993) Calibration of atomic-force microscope tips. Rev. Sci. Instrum. 64 (7), 1868–1873.
[18] Johnson, K.L. and Greenwood, J.A. (1997) An adhesion map for the contact of elastic spheres. J. Colloid Interface Sci. 192 (2), 326–333.
[19] Jones, P.M. et al. (2007) Expression and function of the extracellular calcium-sensing receptor in pancreatic beta-cells. Arch. Physiol. Biochem. 113 (3), 98–103.
[20] Kerssemakers, J.W.J. et al. (2006) Assembly dynamics of microtubules at molecular resolution. Nature 442 (7103), 709–712.
[21] Kitsou-Mylona, I. et al. (2008) A role for the extracellular calcium-sensing receptor in cell–cell communication in pancreatic islets of langerhans. Cell. Physiol. Biochem. 22 (5–6), 557–566.
[22] Leckband, D. and Sivasankar, S. (2012) Biophysics of cadherin adhesion. Curr. Opin. Cell Biol. 24 (5), 620–627.
[23] Lo, Y.S. et al. (2001) Loading-rate dependence of ligand-receptor bond-rupture forces studied by atomic force microscopy. Langmuir 17 (12), 3741–3748.
[24] Mahaffy, R.E. et al. (2004) Quantitative analysis of the viscoelastic properties of thin regions of fibroblasts using atomic force microscopy. Biophys. J. 86 (3), 1777–1793.
[25] Panorchan, P. et al. (2006) Single-molecule analysis of cadherin-mediated cell–cell adhesion. J. Cell Sci. 119 (Pt 1), 66–74.
[26] Puech, P.-H. et al. (2006) A new technical approach to quantify cell-cell adhesion forces by AFM. Ultramicroscopy 106 (8–9), 637–644.
[27] Rogers, G.J. et al. (2007) E-cadherin and cell adhesion: a role in architecture and function in the pancreatic islet. Cell. Physiol. Biochem. 20 (6), 987–994.
[28] Strunz, T. et al. (1999) Dynamic force spectroscopy of single DNA molecules. Proc. Natl. Acad. Sci. USA 96 (20), 11277–11282.
[29] Squires, P.E. et al. (2000) The extracellular calcium-sensing receptor on human beta-cells negatively modulates insulin secretion. Diabetes 49 (3), 409–417.
[30] Tu, C.-L. et al. (2008) Inactivation of the calcium sensing receptor inhibits E-cadherin-mediated cell–cell adhesion and calcium-induced differentiation in human epidermal keratinocytes. J. Biol. Chem. 283 (6), 3519–3528.
[31] Vaezi, A. et al. (2002) Actin cable dynamics and Rho/Rock orchestrate a polarized cytoskeletal architecture in the early steps of assembling a stratified epithelium. Dev. Cell 3 (3), 367–381.
[32] Vinckier, A. and Semenza, G. (1998) Measuring elasticity of biological materials by atomic force microscopy. FEBS Lett. 430 (1–2), 12–16.

Diabetologia
DOI 10.1007/s00125-011-2409-9

ARTICLE

TGFβ modulates cell-to-cell communication in early epithelial-to-mesenchymal transition

C. E. Hills · E. Siamantouras · S. W. Smith · P. Cockwell · K.-K. Liu · P. E. Squires

Received: 22 June 2011 / Accepted: 10 November 2011

Abstract
Aims/hypothesis A key pathology in diabetic nephropathy is tubulointerstitial fibrosis. The condition is characterised by increased deposition of the extracellular matrix, fibrotic scar formation and declining renal function, with the prosclerotic cytokine TGF-β1 mediating many of these catastrophic changes. Here we investigated whether TGF-β1-induced epithelial-to-mesenchymal transition (EMT) plays a role in alterations in cell adhesion, cell coupling and cell communication in the human renal proximal tubule.
Methods Whole-cell and cell compartment abundance of E-cadherin, N-cadherin, snail, vimentin, β-catenin and connexin-43 was determined in human kidney cell line (HK)2 and human proximal tubule cells with or without TGF-β1, using western blotting and immunocytochemistry, followed by quantification by densitometry. The contribution of connexin-43 in proximal tubule cell communication was quantified using small interfering RNA knockdown, while dye-transfer was used to assess gap junctional intercellular communication (GJIC). Functional tethering was assessed by single-cell force spectroscopy with or without TGF-β1, or by immunoneutralisation of cadherin ligation.
Results High glucose (25 mmol/l) increased the secretion of TGF-β1 from HK2 cells. Analysis confirmed early TGF-β1-induced morphological and phenotypical changes of EMT, with altered levels of adhesion and adherens junction proteins. These changes correlated with impaired cell adhesion and decreased tethering between coupled cells. Impaired E-cadherin-mediated adhesion reduced connexin-43 production and GJIC, these effects being mimicked by neutralisation of E-cadherin ligation. Upregulation of N-cadherin failed to restore adhesion or connexin-43-mediated GJIC.
Conclusions/interpretation We provide compelling evidence that TGF-β1-induced EMT instigates a loss of E-cadherin, cell adhesion and ultimately of connexin-mediated cell communication in the proximal tubule under diabetic conditions; these changes occur ahead of overt signs of renal damage.

Keywords Cell adhesion · Cell communication · Diabetic nephropathy · Epithelial-to-mesenchymal transition · Fibrosis · Gap junctions · Proximal tubule

Abbreviations

EMT	Epithelial-to-mesenchymal transition
GJ	Gap junction
GJIC	Gap junctional intercellular communication
HK	Human kidney cell line
hPTC	Human proximal tubule cells
siRNA	Small interfering RNA
SMAD	Small mothers against decapentaplegic

Electronic supplementary material The online version of this article (doi:10.1007/s00125-011-2409-9) contains peer-reviewed but unedited supplementary material, which is available to authorised users.

C. E. Hills (✉) · P. E. Squires
School of Life Sciences, University of Warwick,
Coventry CV4 7AL, UK
e-mail: C.hills@warwick.ac.uk

E. Siamantouras · K.-K. Liu
School of Engineering, University of Warwick,
Coventry, UK

S. W. Smith · P. Cockwell
Department of Renal Immunobiology,
Institute of Biomedical Research, University of Birmingham,
Birmingham, UK

Published online: 04 January 2012

TBM Tubular basement membrane
TBR Transforming growth factor beta receptor

Introduction

The crucial pathology underlying progressive chronic kidney disease in diabetes is tubulointerstitial fibrosis [1, 2]. Central to this process is epithelial-to-mesenchymal transition (EMT) or the trans-differentiation of tubular epithelial cells into myofibroblasts [3–5]. Overwhelming evidence implicates TGF-β1 as the predominant cytokine mediating these phenotypical fibrotic changes [6, 7]. In diabetes, production of TGF-β1 in the proximal tubule is stimulated by high glucose [8, 9]. TGF-β1 modulates the production of several epithelial cell recognition and organisational proteins, while contributing to the reciprocal loss of tubular epithelial cells and accumulation of interstitial fibroblasts, changes associated with declining excretory function [10–12]. In EMT, the loss of epithelial characteristics, e.g. epithelial (E)-cadherin and the zonula occludens protein-1, coincides with the acquisition of proteins associated with a mesenchymal phenotype, e.g. α-smooth muscle actin, fibroblast-specific protein and vimentin, a process that culminates in cytoskeletal remodelling and disruption of the tubular basement membrane [13, 14]. Loss of cell adhesion, associated with reduced E-cadherin levels, represents a pivotal step in those early phenotypical and morphological changes previously observed in response to TGF-β1-induced tubular injury [15]. Cadherins have a central role in forming the multi-protein adherens junction that links cell-to-cell contact to the actin cytoskeleton and various other signalling molecules [16]. The extracellular domain mediates ligation with E-cadherin on adjacent cells [17], while the cytoplasmic domain binds to β-catenin, linking cadherin to the actin cytoskeleton via α-catenin. Interaction, via the catenins, of cadherin with F-actin not only increases the adhesive strength of the junction, but also acts as a signalling 'node' for proteins that influence adhesiveness and/or initiate intracellular signalling. Co-localised with E-cadherin and β-catenin at the sites of cell-to-cell contact [18], connexins oligomerise into hexameric hemichannels (connexons) that connect the cytoplasm of adjoining cells and form gap junctions (GJs). Gap junctions allow transfer of solutes, metabolic precursors and electrical currents [19], and are essential for synchronising activity to ensure appropriate function. Inhibition of cadherin-based cell adhesion inhibits GJ assembly [20], while production of recombinant cadherins into cells lacking strong coupling increases connexin phosphorylation at the adherens junction [21] and increases cell-to-cell communication [22]. Since intercellular adhesion precedes GJ formation and inhibition of cadherin-based cell adhesion is known to inhibit GJ assembly, we hypothesised that glucose-evoked increases in TGF-β would compromise cell communication and function in the proximal tubule.

In retinal capillaries of diabetic mice, connexin-43 production is reduced and apoptosis increased, resulting in a loss of cell communication, and in a decline in the number of pericytes and acellular capillaries [23]. This suggests that a loss of connexin production may be crucial in the development of the vascular lesions observed in diabetic retinopathy. Similar findings from vascular endothelial cells confirm that high glucose decreases connexin production and function, and that this is an early trigger of apoptosis [24]. These data highlight the importance of GJ-mediated cell coupling and suggest that a loss of cell-to-cell communication may contribute to some microvascular complications of the disease. Glucose decreases GJ conductance and disrupts cellular homeostasis in various cell systems [25, 26], and glucose-dependent downregulation of connexin-43 and of GJ communication has been reported in bovine retinal pericytes [27], and in endothelial [28, 29] and epithelial cells [30]. While the presence of GJs in the kidney has long been known, details on their function in the proximal tubule are sparse. Studies on renal vasculature have confirmed a role for various connexins in renin secretion and the regulation of blood pressure [31], but minimal data exist on their role in tubular function, where levels are also high. The novel findings presented here demonstrate a link between high glucose, TGF-β1, impaired cell adhesion and reduced GJ abundance in the proximal tubule. These changes have profound effects on overall cellular integrity and function, and may be among the key events orchestrating loss of function in diabetic nephropathy.

Methods

Materials for tissue culture Tissue culture supplies were purchased from Invitrogen (Paisley, UK). Immobilon P membrane was from Millipore (Watford, UK) and electrochemoluminescence from Amersham Biosciences (Amersham, UK). A Qproteome kit was obtained from Qiagen (Crawley, UK). Antibodies and small interfering RNA (siRNA) were obtained from Santa Cruz (Santa Cruz, CA, USA), R&D Systems (Abingdon, UK) and Affinity Bioreagents (Cambridge, UK). Recombinant human TGF-β1, fibronectin, lipofectamine and Lucifer yellow were obtained from Sigma (Poole, UK), as were all other general chemicals. The anti-TGF-β1 ELISA was from R&D Systems.

Model cell line Human kidney cell line (HK)2 cells (passages 18–30) were maintained in DMEM/Hams F12 medium, which was supplemented with 10% FCS wt/vol, glutamine (2 mmol/l) and EGF (5 ng/ml), and were cultured

at 37°C in a humidified atmosphere with 5% CO_2. Prior to treatment, cells were transferred to DMEM/F12 low glucose (5 mmol/l) for 48 h as described previously [32]. Cells were serum-starved overnight before applying either TGF-β1 (2–10 ng/ml), anti-E-cadherin-neutralising antibody (20 μg/ml) or anti-N-cadherin-neutralising antibody (10 μg/ml) for 48 h. To assess the effect of high glucose, cells were treated with 5 mmol/l (control), 25 mmol/l (high) glucose or 25 mmol/l mannitol (osmotic control) for 48 h or 7 days.

Human proximal tubular cells Following patient consent and ethical approval from South Staffordshire Research Ethics Committee (application number 08/H1203), cells were obtained from anonymised nephrectomy procedures for renal carcinoma. Renal cortex was longitudinally sectioned, the fibrous capsule removed and 1 cm^3 portions cut from the outer region. Pieces were placed into DMEM and further cut into 1 mm^3 sections. Each piece was placed into a well of a 24-well plate that had been previously coated with gelatine for 20 min, followed by incubation in FCS overnight. Sections were cultured in DMEM/Nutrient Ham's F12 1:1, which was supplemented with 5 mg/ml insulin, 5 mg/ml transferrin, 5 ng/ml sodium selenite, 36 ng/ml hydrocortisone, 4 pg/ml triiodothyronine, 10 ng/ml EGF, 2 mmol/l glutamine, 10,000 U/ml penicillin and 10,000 mg/ml streptomycin. Culture was at 37°C in atmosphere with 5% CO_2. Immunohistochemical staining showed cells to be positive for cytokeratin, human epithelial antigen and alkaline phosphatase, but negative for factor VIII-related antigen and actin.

Quantification of TGF-β1 Total TGF-β1 was measured by specific ELISA of cell culture supernatant fractions collected from growth-arrested HK2 cells stimulated under serum-free conditions. Active TGF-β1 was measured directly, while latent TGF-β1 was measured indirectly following acid activation of samples. The assay used has <1% cross-reactivity for TGF-β2 and TGF-β3. The TGF-β1 concentration was normalised to mg/ml of protein. Quantities of TGF-β1 are expressed as pg ml^{-1}(mg protein)$^{-1}$.

Immunoblotting Cytosolic proteins were prepared and separated by gel electrophoresis and electro-blotting on to Immobilon P membranes as described previously [32]. For determination of protein localisation, proteins were collected using the Qproteome (Qiagen) cell compartment kit. Membranes were probed with specific polyclonal antibodies against anti-E-cadherin (R&D Systems), N-cadherin (Sigma), snail (R&D Systems), vimentin (Affinity Bioreagents), β-catenin (Santa Cruz) and connexin-43 (Santa Cruz) at dilutions of 1:1,000, 1:500, 1:500, 1:800, 1:1,000 and 1:400 respectively.

Connexin-43 knockdown Cells were grown to 40% confluence in six-well plates or on cover-slips treated with

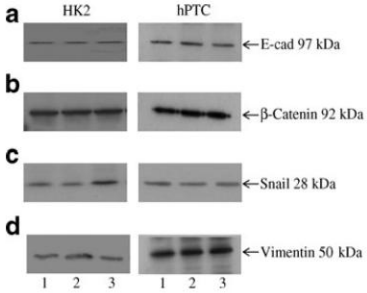

Fig. 1 HK2 and hPTC produce adherens junction proteins. Western blot analyses of HK2 and hPTC cell lysates (5 μg protein/lane) using antibodies against human (**a**) E-cadherin (E-cad), (**b**) β-catenin, (**c**) snail and (**d**) vimentin detected appropriate bands as labelled. Controls included antibody pre-absorbed with a tenfold excess of immunising peptide (data not shown)

3-aminopropyltriethoxy-silane. Knockdown of *CX43* (also known as *GJA1*) expression was achieved using siRNA. Transfection of siRNAs was carried out using lipofectamine as described previously [33]. Cells were collected and assayed at 48, 72 and 96 h after transfection. Negative controls included untransfected cells, lipid alone, and two scrambled siRNAs, one of which was fluorescein-conjugated. *CX43* knockdown was confirmed by Western blot analysis.

Immunocytochemistry Cells at 80% confluence were fixed with 4% paraformaldehyde. After blocking, the nuclear stain DAPI (1 mmol/l) was added for 3 min. Cells were then either incubated for 1 h at 25°C with tetramethyl rhodamine isothiocyanate (TRITC)-conjugated phalloidin (Sigma), diluted at 1:100, in PBS-Triton, or they were incubated overnight at 4°C with primary antibody (1:100) diluted in PBS-Triton. Candidate proteins were visualised using Alexa488-conjugated secondary antibody (1:400) in PBS-Triton for 1 h at 25°C. Fluorescence was visualised using a fluorescence

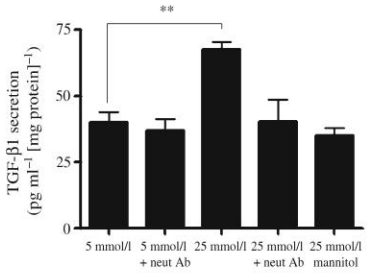

Fig. 2 High glucose stimulates TGF-β1 secretion in HK2 cells. HK2 cells were grown in either low glucose (5 mmol/l, control) or high glucose (25 mmol/l) with or without TGF-β1-neutralising antibody (neut Ab; 10 μg/ml) for 7 days under serum-free conditions. Mannitol (25 mmol/l) was used as an osmotic control. The supernatant fraction was removed and TGF-β1 secretion quantified by ELISA. Results are representative of three separate experiments; $^{**}p<0.01$

microscope (Axiovert 200; Carl Zeiss, Welwyn Garden City, UK).

Dye transfer Lucifer yellow was dissolved in 250 µl fresh LiCl (150 mmol/l) with HEPES (10 mmol/l; pH 7.2). Individual cells within a cell cluster were injected using a delivery system (Injectman/Femtojet 5247; Eppendorf, Hamburg, Germany). The duration of injection was set at 1 s, with an injection pressure of 14,000 Pa and a compensation pressure of 4,800 Pa. Dye transfer between coupled cells was recorded over 4 min using a software package (Metamorph; Molecular Devices, Sunnyvale, California, USA) and a Cool Snap HQ CCD camera (Roper Scientific, Gottingen, Germany).

Single cell force spectroscopy Atomic force microscope force spectroscopy (CellHesion module; JKP Instruments, Berlin, Germany) was used to measure cell-to-cell adhesion and the separation forces required to uncouple these cells. A single HK2 cell was bound to a cantilever using fibronectin (20 mg/ml) and poly-L-lysine (25 µg/ml), and subsequently brought into contact with an adherent cell (in a cluster of coupled cells) using a known force (1 nN). The two cells remained in contact for a defined period of time (10 s) while bonding formed. The cantilever was then retracted at a constant speed (5 µm/s), and force (in nanonewton) versus displacement (deflection of the cantilver) was measured using a laser until the cells were completely separated (pulling length 60 80 µm). Each cell cell recording was repeated in triplicate with a 30 s interval between successive measurements. Retraction recordings from multiple cells (approx. 50) in separate experiments ($n=5$) were made and the maximum unbinding force (in nanonewton) and detachment energy (in femtojoules) calculated.

Statistical analysis Autoradiographs were quantified by densitometry using a device (TotalLab 2003; NonLinear Dynamics, Durham, NC USA). Where data were quantified,

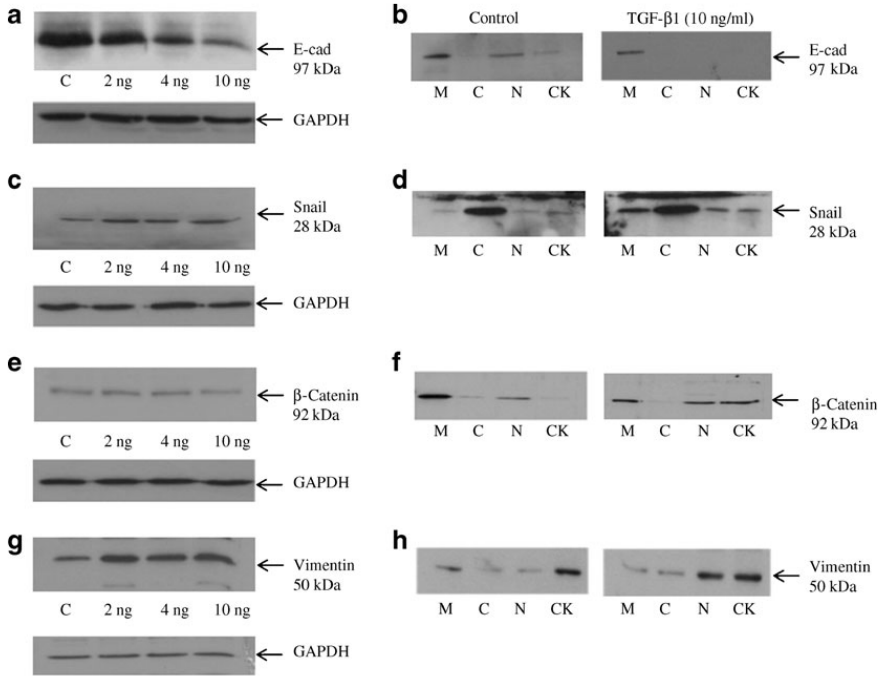

Fig. 3 TGF-β1 evoked changes in adherens junction protein abundance in HK2-cells. **a**, **c**, **e**, **g** To assess the effect of TGF-β1 on production of key adherens junction proteins, HK2 cells were grown in low glucose (5 mmol/l) alone (control [C]), or together with 2, 4 or 10 ng/ml TGF-β1. Whole-cell abundance of E-cadherin (E-cad) (**a**) and its transcriptional co-repressor snail (**c**) was determined by immunoblotting. TGF-β1 decreased E-cadherin levels (**a**) and reciprocally increased the abundance of snail (**c**). **b** Compartmental localisation of E-cadherin and (**d**) snail production was determined in membrane (M), cytosol (C), nuclear (N) and cytoskeletal (CK) fractions of HK2 cells with or without TGF-β1 (10 ng/ml). The cytokine altered the cellular localisation of both proteins compared with control. **e** The cytokine did not alter whole-cell production of β-catenin, but (**g**) did increase vimentin abundance in a concentration-dependent manner. **f** The distribution of β-catenin and (**h**) vimentin between the different cell compartments was altered in response to TGF-β1. Representative blots for each protein were re-probed for GAPDH as a loading control

the non-stimulated, low-glucose control condition was normalised to 100% and data from all other experimental conditions compared with this. Statistical analysis of data was performed using a one-way ANOVA test with Tukey's multiple comparison post-test. Data are expressed as mean± SEM, with '*n*' denoting the number of experiments. A value of $p<0.05$ was taken to signify statistical significance.

Results

HK2 and human proximal tubule cells produce adherens junction proteins Western blot analysis confirmed that E-cadherin, β-catenin, snail and vimentin are produced in HK2 and human proximal tubule cells (hPTC), giving rise to bands at 97, 92, 28 and 50 kDa respectively (Fig. 1).

High glucose increases secretion of TGF-β1 ELISA of supernatant fractions from HK2 cells showed a 68% increase in total TGF-β1 secretion (67±2.9 pg/ml [mean±SEM]) after exposure to high glucose (25 mmol/l) for 7 days under serum-free conditions (Fig. 2) compared with exposure to 5 mmol/l glucose (40±3.9 pg/ml; $n=3$; $p<0.01$). Differences in TGF-β1 were only detected following acidification of the samples, suggesting that TGF-β1 was produced in its latent form. Incubation with a TGF-β1-neutralising antibody (10 μg/ml) blocked the effects of high glucose, restoring TGF-β1 secretion to basal (40±8.2 pg/ml). Mannitol (25 mmol/l) failed to increase TGF-β1 secretion. There was no difference in TGF-β1 secretion in supernatant fractions taken from cells exposed to high glucose for 48 h (data not shown).

TGF-β1 alters adherens junction protein abundance in HK2-cells TGF-β1 (2 10 ng/ml for 48 h) altered cell morphology from an epithelial-like cobblestone appearance, to an elongated fibroblast-like phenotype (electronic supplementary material [ESM] Fig. 1a). These changes were accompanied by re-organisation of the actin cytoskeleton into peripheral stress fibres (ESM Fig. 1b). The cytokine (2 10 ng/ml for 48 h) induced a concentration-dependent decrease in whole-cell abundance of E-cadherin (Fig. 3a), attributable to reduced production from the membrane and nuclear cell compartments (Fig. 3b). In contrast, TGF-β1 increased levels of the transcriptional repressor snail throughout the cell (Fig. 3c, d). Integral to E-cadherin cell adhesion under basal conditions, β-catenin was primarily localised at the membrane (Fig. 3f). In the current study, TGF-β1 failed to alter whole-cell production of β-catenin (Fig. 3e), but did redistribute the catenin from the membrane to the nuclear and cytoskeletal fractions (Fig. 3f). TGF-β1 produced a concentration-dependent increase in whole-cell levels of the intermediate filament protein, vimentin (Fig. 3g), with the greatest change in the cytoskeleton and nucleus (Fig. 3h).

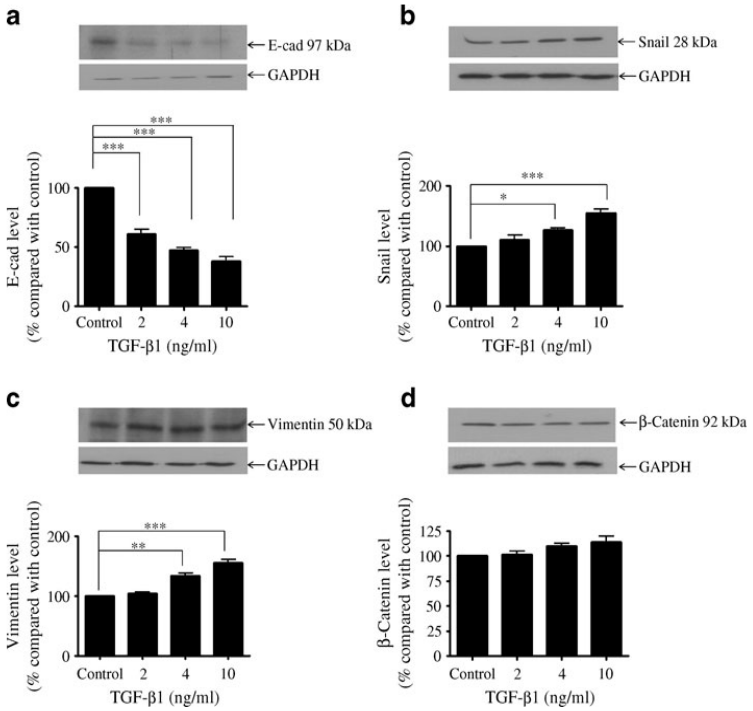

Fig. 4 TGF-β1 evoked changes in adherens junction protein abundance in hPTCs. hPTCs were grown in low glucose (5 mmol/l) with or without TGF-β1 (2–10 ng/ml) for 48 h and whole-cell abundance of (**a**) E-cadherin (E-cad), (**b**) snail, (**c**) vimentin and (**d**) β-catenin was determined by immunoblotting. Representative blots are shown for each protein with re-probing for GAPDH done as loading control. Quantification (mean± SEM) was by densitometry, normalised against the non-stimulated low glucose control (100%). Bars in the histograms correspond to the associated lanes in the respective blot. Results were from three or more separate experiments; *$p<0.05$, **$p<0.01$ and ***$p<0.001$

TGF-β1 alters adherens junction protein abundance in hPTC Human proximal tubule cells were incubated for 48 h in low glucose (5 mmol/l) with increasing concentrations of TGF-β1 (2 10 ng/ml). TGF-β1 reduced levels of E-cadherin by 68±3.7% (mean±SEM), 51±2.3% and 45±4.6% of control at 2, 4 and 10 ng/ml respectively (n=3; p<0.001) (Fig. 4a). It also upregulated snail production to 110±10.4%, 127±7.8% (n=3; p< 0.05) and 154±8.5% (n=3; p<0.01) of control (Fig. 4b), but failed to alter the production of β-catenin (Fig. 4d). Production of the intermediate filament protein, vimentin, increased to 104±7.5%, 133±9.4% and 155± 8.4% of control at 2, 4 and 10 ng/ml (n=3; p<0.01) (Fig. 4c).

TGF-β1 decreases connexin-43 production Following in vitro activation of latent TGF-β1 by repeated freeze thaw cycles in 7 day conditioned medium [34], a subsequent 48 h exposure of cells to the activated medium significantly decreased connexin-43 levels to 72±2.1% (mean±SEM) of that with conditioned 5 mmol/l control medium (n=3; p<0.05) (Fig. 5a). Mannitol (25 mmol/l) failed to alter connexin-43 production. In Fig. 5b, TGF-β1 (48 h) decreased connexin-43 abundance in HK2 cells to 40±6.1%, 37±7.9% and 30± 12.6% of control at 2, 4 and 10 ng/ml (n=3; p<0.001). These data were comparable to the cytokine-induced inhibition of connexin-43 in hPTC, where levels fell to 53±4.8%, 53± 3.7% and 51±3.5% of control at similar concentrations of TGF-β1 (n=3; p<0.001) (Fig. 5c). In the absence (Fig. 5d) or presence (Fig. 5e) of the cytokine (10 ng/ml), connexin-43 was predominantly localised to the cell membrane. The reduction of whole-cell abundance of the protein therefore reflects a decrease in production, rather than redistribution to other cell compartments.

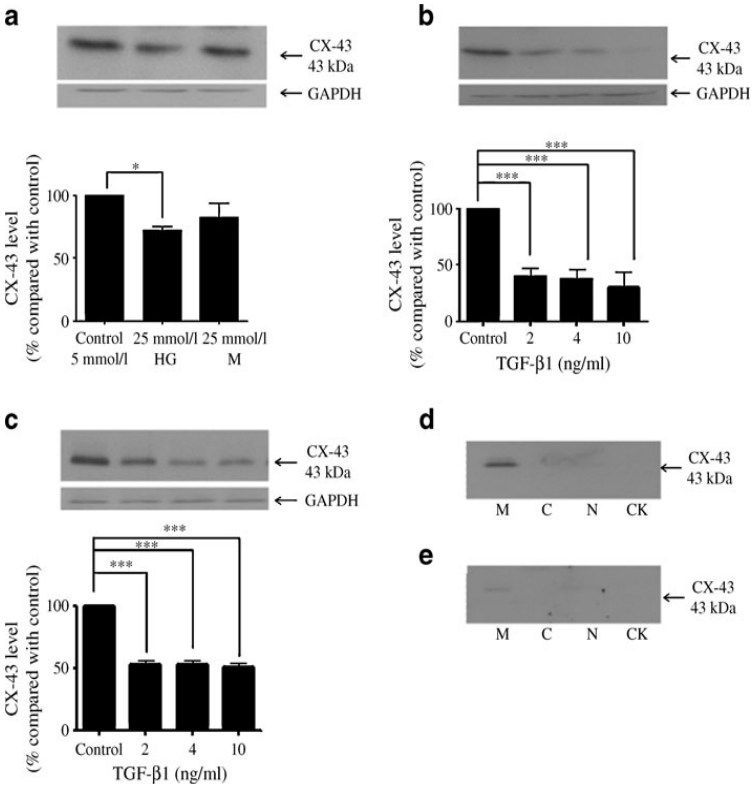

Fig. 5 TGF-β1 downregulates connexin-43 levels in proximal tubule cells. To assess the effects of glucose on connexin-43 (CX-43) abundance, HK2 cells were cultured (**a**) in either low glucose (5 mmol/l, control), high glucose (HG, 25 mmol/l) or mannitol (M, 25 mmol/l) for 7 days. Secreted TGF-β1 was activated by repeat freeze–thaw procedure and the conditioned medium applied for 48 h. **b** In a separate series of experiments, HK2 and (**c**) hPTC cells were grown in low glucose (5 mmol/l) with or without 2, 4 or 10 ng/ml TGF-β1. Whole-cell connexin-43 abundance was determined by immunoblotting. The representative immunoblots show changes in protein production versus the same blots stripped and re-probed for GAPDH as a loading control. Blots were quantified (mean±SEM) by densitometry data from three or more separate experiments and data normalised against the unstimulated low glucose control (100%). Bars in the histograms correspond to the associated lanes in the respective blot. *p<0.05 and ***p<0.001. **d** Compartmental localisation of connexin-43 production was determined in membrane (M), cytosol (C), nuclear (N) and cytoskeletal (CK) fractions of control and (**e**) TGF-β1-treated (10 ng/ml) HK2 cells

Loss of connexin-43 decreases gap junctional intercellular communication in proximal tubule cells HK2 cells and hPTC produce connexin-43 (Fig. 6a). siRNA was used to knockdown *CX43* expression to 30±3.4% (mean±SEM) of control (n=4, p<0.001), while scrambled siRNA and transfection reagent alone had no effect (Fig. 6b). In separate experiments, cells were transfected with fluorescein-tagged *CX43* siRNA to identify transfected cells expressing reduced *CX43* (Fig. 6). Injection of Lucifer yellow into the transfected cells failed to exhibit dye transfer (Fig. 6g j), while dye moved away from the site of injection in non-transfected cells within the same cell cluster, confirming connexin-43-mediated intercellular communication (Fig. 6m p).

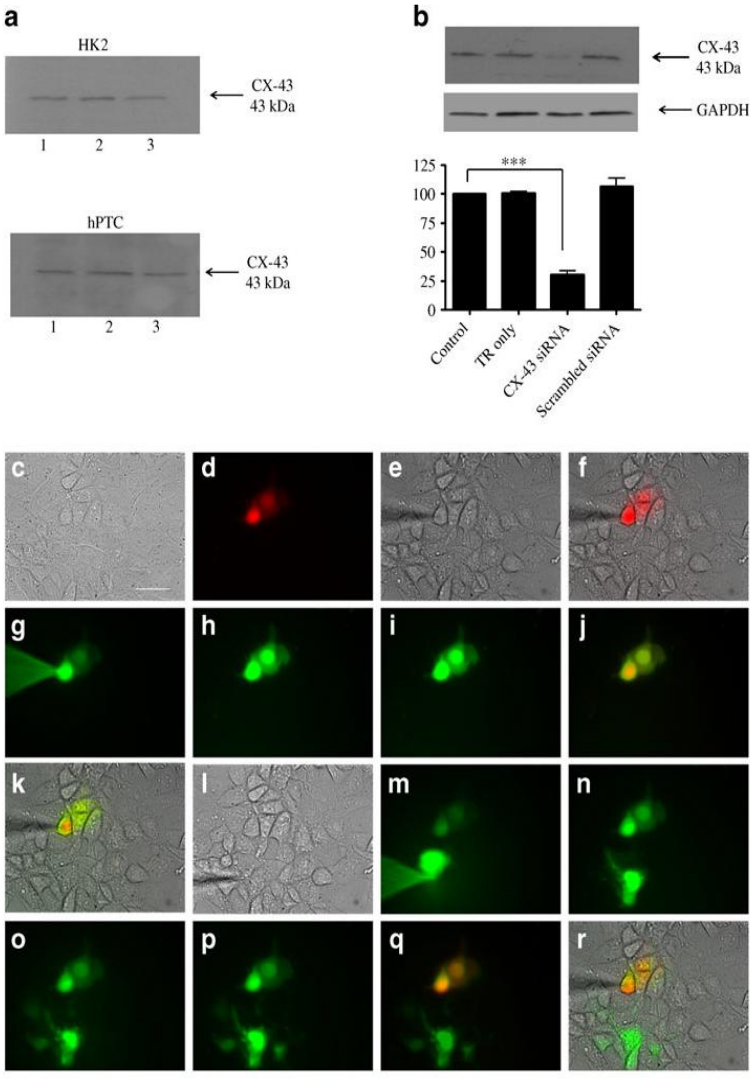

Fig. 6 Knockdown of *CX43* prevents GJIC in HK2 cells. **a** Confirmation of connexin-43 (CX-43) production in three separate preparations from HK2 cells and hPTC. **b** *CX43* siRNA significantly reduced connexin expression in HK2 cells. The representative immunoblot shows changes in protein abundance for the transfection reagent (TR) alone, for *CX43* siRNA and scrambled siRNA versus the same blot stripped and re-probed for GAPDH as a loading control. Blots were quantified by densitometry and data normalised against the non-stimulated low glucose (5 mmol/l; 100%). Bars in the histogram correspond to the associated lanes in the respective blot. Values are mean±SEM from three separate experiments; ***p<0.001. **c** Red fluorescent protein was used to identify cells exhibiting anti-connexin-43 transfection within a cluster of non-transfected cells. The red transfected cell (**d**) was injected (**e**, **f**) with Lucifer yellow (**g**) and dye spread (green) examined between 0 min (**h**) and 4 min (**i**). **j** An overlay (yellow) of red transfection and green dye spread, with phase (**k**) at 4 min after the initial injection of dye. The micro-injector (**l**) was repositioned over a non-transfected cell in the same cluster. **m**, **n** Injection of Lucifer yellow led to spreading of dye (green) between 0 min (**o**) and 4 min (**p**). An overlay (yellow) of red transfection and green dye spread (**q**), with (**r**) a triple overlay with a phase image. Scale bar (**c**) 50 μm

Loss of E-cadherin ligation replicates TGF-β1-induced changes in connexin-43 production To determine whether the reduction in gap junctional intercellular communication (GJIC) induced by TGF-β1 depended on a decrease in E-cadherin production or reflected reduced E-cadherin-mediated ligation between adjacent cells, HK2 cells were treated for 48 h with an immunoneutralising antibody for E-cadherin. The antibody (antiuvomorulin, 20 μg/ml; Sigma) prevents ligation, but has no effect on production of the protein. Neutralisation of E-cadherin ligation altered cell morphology in a manner consistent with those changes observed in response to TGF-β1 (Fig. 7a). The cytokine and anti-E-cadherin significantly downregulated whole-cell abundance of connexin-43 to 43±4.0% (mean±SEM) and 37±7.6% of control (n=3; p<0.001) (Fig. 7b), an effect mainly attributable to a decrease in production at the membrane (Fig. 7c, d). Co-application of TGF-β1 and anti-E-cadherin did not potentiate the changes in connexin-43 production compared with TGF-β1 alone (data not shown). Although, as expected, TGF-β1 significantly reduced E-cadherin levels to 32±6.1% of control (n=3; p<0.01), neutralisation of ligation failed to alter abundance (112.7±12.2% of control; n=3) (Fig. 7e) or localisation of E-cadherin (Fig. 7f, g). In agreement with data presented in Figs 3 and 4, TGF-β1 increased the abundance of snail to 125±13.8% of control (n=3; p<0.05), while neutralisation of E-cadherin ligation had little effect on whole-cell abundance (Fig. 7h) or localisation of the protein (Fig. 7i, j). Whole-cell levels of β-catenin were unchanged by TGF-β1 or loss of E-cadherin ligation; however, the latter re-localised to the cytoskeleton (Fig. 7k–m).

TGF-β1 reduces GJIC in proximal tubule cells HK2 cells were cultured for 48 h in low (5 mmol/l) or high (25 mmol/l)

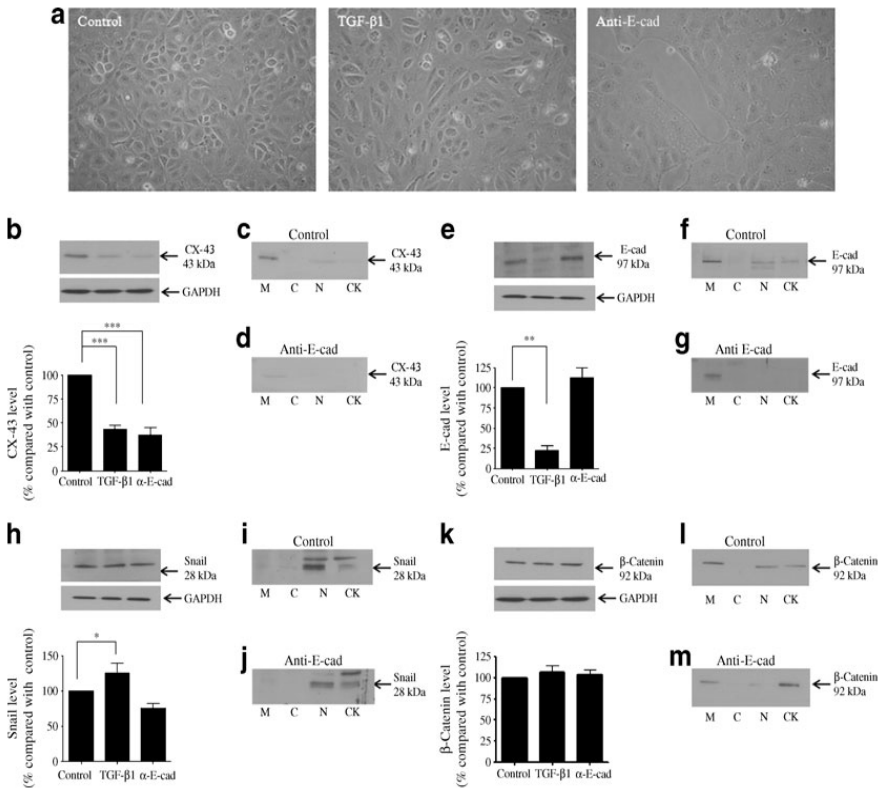

Fig. 7 Loss of E-cadherin (E-cad) ligation partially mimics the effects of TGF-β1 on cell morphology and connexin-43 (CX-43) production in HK2 cells. **a** Phase contrast microscopy demonstrated that TGF-β1 (10 ng/ml) and loss of E-cadherin ligation altered gross cell morphology in favour of a fibroblast phenotype. Magnification ×20. **b**–**d** The effects of the cytokine and anti-E-cadherin (E-cad) on the abundance of connexin-43, (**e**–**g**) E-cadherin, (**h**–**j**) snail and (**k**–**m**) β-catenin were examined in HK2 whole-cell lysates and cell fractions. Representative immunoblots (**b**, **e**, **h**, **k**) show changes in candidate protein production versus the same blots stripped and re-probed for GAPDH as a loading control. Blots were quantified by densitometry and data normalised against the unstimulated low glucose (5 mmol/l) control (100%). Bars in the histograms correspond to the associated lanes in the respective blots. Densitometry values are mean±SEM from three or more separate experiments; *p<0.05, **p<0.01 and *** p<0.001. **c**, **d**, **f**, **g**, **i**, **j**, **l**, **m** Compartmental localisation for each protein as labelled was determined in membrane (M), cytosol (C), nuclear (N) and cytoskeletal (CK) fractions of HK2 cells with or without anti-E-cadherin antibody (20 μg/ml) for 48 h

glucose, and in low glucose with or without TGF-β1 (2 10 ng/ml), or with or without anti-E-cadherin antibody (20 μg/ml). Individual cells within a cluster were injected with Lucifer yellow (green) and the degree of dye spread assessed 4 min after injection (Fig. 8). In control cells, dye permeated away from the injected cell into neighbouring cells (Fig. 8a). This cell cell coupling was reduced under high (25 mmol/l) glucose conditions (Fig. 8b). TGF-β1 (2 10 ng/ml) produced a concentration-dependent reduction in the extent of dye-transfer (Fig. 8c e). This loss of GJIC was mimicked in cells treated with anti-E-cadherin (Fig. 8f).

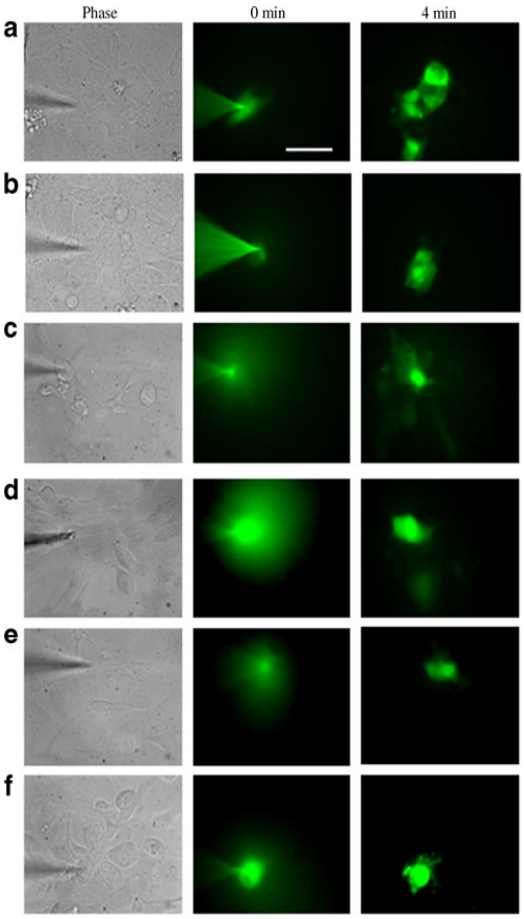

Fig. 8 TGF-β1 reduces GJIC in HK2 cells. GJIC was determined by the extent of dye (green) spread following micro-injection of Lucifer yellow into a single HK2 cell within a cell cluster. **a** Control cells exhibited a rapid (0 to 4 min) transfer of dye between neighbouring cells. **b** Exposure for 48 h to high glucose (25 mmol/) or (**c**) low glucose (5 mmol/l) plus incubation with 2 ng/ml, (**d**) 4 ng/ml and (**e**) 10 ng/ml TGF-β1 evoked a concentration-dependent decrease in dye spread. **f** Neutralisation of E-cadherin ligation using an immunoneutralising antibody (20 μg/ml) also restricted intercellular communication and prevented dye transfer. Scale bar 50 μm

Decreased E-cadherin increases N-cadherin production N-cadherin abundance (135 kDa) (Fig. 9a) was predominantly localised to the cell membrane (Fig. 9b) and was significantly upregulated by TGF-β1 (48 h) to 176±23% (mean± SEM), 280±17% and 325±62% of control at 2, 4 and 10 ng/ml TGF-β1 in HK2 cells (n=3; p<0.05) (Fig. 9c), and to 237±45%, 240±18% and 305±27.5% of control in hPTC (n=3; p<0.01) (Fig. 9d). In a separate series of experiments in HK2-cells, TGF-β1 (10 ng/ml) upregulated N-cadherin to 310±66% of control (n=3; p<0.05) (Fig. 9e), while neutralisation of E-cadherin ligation only increased production to 172±47% of control. The neutralising antibody had little effect on connexin-43 production (91±8.4% of control, n= 3) (Fig. 9f) compared with TGF-β1 or anti-E-cadherin, which significantly decreased connexin-43 abundance by 54±4.8% and 40±8.9% respectively (n=3; p<0.001).

TGF-β1 reduces adherence between coupled cells of the proximal tubule Atomic force microscope force spectroscopy was used to measure cell-to-cell adhesion and the separation forces required to uncouple cells. Prior to attachment, cells were cultured for 48 h under identical conditions with or without TGF-β1 (10 ng/ml). A single HK2 cell (cell-1) was bound to a cantilever and subsequently brought into contact with an adherent cell (cell-2) within a cluster, using a fixed force (Fig. 10). After 10 s, the cantilever was then retracted (5 μm/s) and force versus displacement measured until the cells were completely separated. Retraction force displacement curves provide important information on adhesion between two cells, such as the energy required to separate them (Fig. 10a c, grey area) and the maximum force of detachment (Fig. 10a c, red circle). The former is normally referred to as 'detachment energy' (Fig. 10e) and the latter as the 'maximum unbinding force' (Fig. 10d). The retraction measurements of control (47 cells in five separate experiments) and TGF-β1-treated HK-2 cells (53 cells in five separate experiments) are shown in Fig. 10a, b. The results indicate that TGF-β1 decreases the maximum unbinding force by 20±6% (mean±SEM) (n=5; p<0.001), while the detachment energy was decreased to 53±6% (n=5; p<0.001). Neutralisation of E-cadherin ligation had minimal effect on detachment energy (112% of control; 47 cells in five separate experiments), but actually increased the maximum unbinding force by 32±0.5% (Fig. 10c).

Discussion

TGF-β1 is important in many tubulointerstitial diseases where disassembly of the adherens junction represents the initial overt change in epithelial organisation, well before

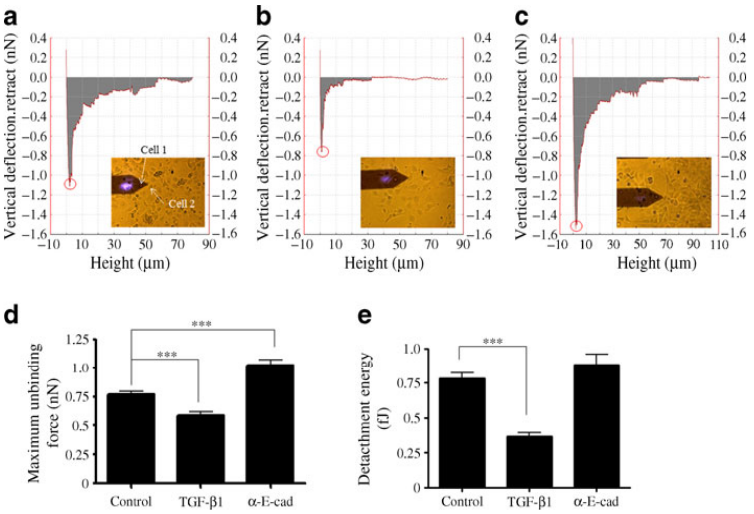

Fig. 10 TGF-β1 reduces cell adhesion. Atomic force microscopy force spectroscopy was used to measure the detachment energy (in femtojoules) and maximum unbinding force (in nanonewton) required to uncouple two HK2 cells. **a** A single HK2 control cell was bound to the cantilever (Cell 1, phase insert). This was brought into contact with an adherent cell (Cell 2) using a fixed force (1 nN) for 10 s, while bonding formed. The cantilever was then retracted (5 μm/s) and force versus displacement measured until the cells separated (approximate pulling length 60 to 80 μm). The energy required to separate the cells (grey area) and the maximum force of detachment (red circle) was measured. Values for height (in micrometres) were smoothed. **b** The same procedure was repeated after treatment with TGF-β1 and (**c**) anti-E-cadherin (E-cad). **d** Quantification of maximum unbinding force' and (**e**) 'detachment energy', showing that TGF-β1 (10 ng/ml) decreased the maximum unbinding force by 20% and the detachment energy decreased by 53% compared with control. Data are expressed as mean±SEM of multiple cells from five separate experiments; ***$p<0.001$

protein abundance as such that controls connexin production and GJIC. Retraction force displacement curves confirmed that TGF-β1 reduced the maximum unbinding force required to begin separation of two cells by 20%, while halving the detachment energy required to completely separate them. The greater decrease in the detachment energy could be partly explained by the increase in cell rigidity following TGF-β1 treatment, as demonstrated by the rearrangement of the cytoskeleton into peripheral stress fibres (ESM Fig. 1).

A switch in cadherin isoform from E-cadherin to neural (N)-cadherin is associated with EMT [37]. TGF-β1 dramatically increased N-cadherin production in our model. However, this switch was unable to reverse morphological changes or the reduction in cell-to-cell adhesion in response to the cytokine. Surprisingly, neutralisation of E-cadherin ligation actually increased the maximum unbinding force. Counter-intuitively, this observation suggests that the modest increase in N-cadherin evoked by blocking E-cadherin ligation (Fig. 9e) can maintain tethering between coupled cells when the cadherin catenin complex is intact, i.e. when only ligation is impaired. However, TGF-β1 dramatically reduced E-cadherin production and forced β-catenin to move away from the membrane. In this scenario, and in the absence of a catenin binding partner, upregulation of N-cadherin is redundant and the switch is unable to maintain tethering. These data suggest that it is decreased E-cadherin production and dissolution of the catenin cadherin complex that drive the detachment of cells in EMT.

Type 2 EMT is commonly defined as the ability of adult epithelial cells to undergo de-differentiation, traverse the tubular basement membrane (TBM) into the interstitium and transdifferentiate into a myofibroblast phenotype that is capable of synthesising and increasing the deposition of extracellular matrix. While these activated myofibroblasts are thought of as key effector cells in the pathogenesis of renal fibrosis, it is clear that they originate from multiple lineages. Accumulating evidence suggests that local interstitial fibroblasts [38], pericytes [39], local mesenchymal stem cells [40] or the injured epithelium itself [10] may contribute to this pool, and there is considerable debate for and against a role of EMT in renal fibrosis [41]. The established criteria supporting a role of EMT in fibrosis are based on the identification of morphological changes and altered levels of key epithelial/mesenchymal markers. Failure of fibroblasts to fully migrate and traverse the TBM is more commonly known as partial EMT, a phenomenon where cells produce epithelial and mesenchymal markers, yet lack migratory capacity. The argument against full phenotypic transformation has been fuelled by data from Humphreys et al., who suggest that not only is EMT unlikely to

occur in vivo, but that vascular pericytes are the source of fibrosis-generating myofibroblasts [39].

As summarised in a recent review, TGF-β1 binds to a trans-membrane TGF-β receptor II (TBRII) and initiates several intracellular signalling cascades, including small mothers against decapentaplegic (SMAD) and mitogen-activated protein kinases such as extracellular regulated kinase, p38 and Jun kinase [42]. SMADs are subdivided into three classes: (1) receptor regulated SMADs (SMAD1, -2, -3, -5 and −8); (2) the common SMADs (SMAD4); and (3) the inhibitory SMADs (SMAD6 and −7) [43]. Following TBRII activation, receptor-regulated SMADs form oligomeric complexes with the common SMAD prior to translocation into the nucleus and regulation of gene transcription. The majority of TGF-β1-targeted genes that are regulated in EMT rely on SMAD3-dependent transcriptional regulation. Recent studies in cells from the proximal tubule have demonstrated that angiotensin II-induced tubular EMT was SMAD3-dependent [44]. Similarly, (β)1-integrin gene expression, a potential therapeutic target for renal fibrosis, is also upregulated in unilateral obstruction and in chronic tubulointerstitial fibrosis via a SMAD3-dependent mechanism [45]. However, despite the predominant involvement of SMAD3, a role for SMAD2 should not be discounted [46].

The hyperactive SMAD-signalling observed in certain types of renal disease reflects aberrant levels of both SMAD co-repressors and their subsequent regulators [47]. The inhibitory SMADs (SMAD6 and SMAD7) inhibit receptor-regulated SMAD phosphorylation by blocking their access to TBRI, and/or by promoting degradation of the receptor complexes. SMAD7 represents a general antagonist of TGF-β1 and bone morphogenic protein signalling, with reports showing that induction of SMAD7 blocks tubular EMT and the development of fibrotic lesions [48]. The role and regulation of SMAD signalling in regulation of GJ expression and GJIC in the proximal tubule remain to be confirmed; however, it is highly likely that these effects are SMAD-dependent and subject to regulation via endogenous inhibitors. The potential of exogenous agonist application to reverse these disrupted changes in cell-to-cell communication represents an area of therapeutic interest and forms the basis of our continuing research.

Reduced cell adhesion, cell coupling and cell-to-cell communication have profound effects on overall integrity and function of the proximal tubule, and altered GJIC and renal haemodynamics have recently been reported in a Zucker fatty rat model of type2 diabetes [49]. In the current study, we concede that our in vitro data provide a minimalistic model of the early events in EMT and thus recommend caution in translating these novel findings to the in vivo situation, where the multifactorial molecular pathology of renal fibrosis may modify responses. However, despite this caveat, our current data provide a compelling foundation for the identification of future therapies aimed at maintaining or restoring renal function in diabetes, a supposition supported by recent data from mesangial cells, where glucose-induced hypertrophy was reversed by overproduction of connexin-43 [50].

Acknowledgements We would like to thank JPK Instruments for their professional support in the use of single-cell force spectroscopy.

Funding This work was supported wholly or in part by the generous support of Diabetes UK (11/0004215) and the Diabetes Research and Wellness Foundation. The work is also supported by an EFSD/Janssen grant and a University of Warwick Research Development Strategic Award. C.E. Hills was a Wellcome Trust 'Value in People' Research Fellow.

Duality of interest The authors declare that there is no duality of interest associated with this manuscript.

Contribution statement All authors contributed to the conception, design and analysis of the data, and to the drafting of the manuscript, and have approved the final version for publication.

References

1. Eddy AA (1996) Molecular insights into renal interstitial fibrosis. J Am Soc Nephrol 12:2495–2508
2. Remuzzi G, Ruggenenti P, Benigni A (1997) Understanding the nature of renal disease progression. Kidney Int 51:2–15
3. Iwano M, Plieth D, Danoff TM, Xue C, Okada H, Neilson EG (2002) Evidence that fibroblasts derive from epithelium during tissue fibrosis. J Clin Invest 110:341–350
4. Okada H, Danoff TM, Kalluri R, Neilson EG (1997) Early role of Fsp1 in epithelial–mesenchymal transformation. Am J Physiol 273:F563–F574
5. Hills CE, Squires PE (2010) TGF-beta1-induced epithelial-to-mesenchymal transition and therapeutic intervention in diabetic nephropathy. Am J Nephrol 31:68–74
6. Kanwar YS, Wada J, Sun L et al (2008) Diabetic nephropathy: mechanisms of renal disease progression. Exp Biol Med 233:4–11
7. Sharma K, Ziyadeh FN (1995) Hyperglycaemia and diabetic kidney disease. The case for transforming growth factor-beta as a key mediator. Diabetes 44:1139–1146
8. Oldfield MD, Bach LA, Forbes JM et al (2001) Advanced glycation end products cause epithelial-myofibroblast transdifferentiation via the receptor for advanced glycation end products (RAGE). J Clin Invest 108:1853–1863
9. Qi W, Chen X, Zhang Y et al (2007) High glucose induces macrophage inflammatory protein-3 alpha in renal proximal tubule cells via a transforming growth factor-beta 1 dependent mechanism. Nephrol Dial Transplant 11:3147–3153
10. Mauer SM, Steffes MW, Ellis EN, Sutherland DE, Brown DM, Goetz FC (1984) Structural functional relationships in DN. J Clin Invest 74:1143–1155
11. Steffes MW, Osterby R, Chavers B, Mauer SM (1989) Mesangial expansion as a central mechanism for loss of kidney function in diabetic patients. Diabetes 38:1077–1081
12. Hills CE, Al-Rasheed N, Al-Rasheed N, Willars GB, Brunskill NJ (2009) C-peptide reverses TGF-beta-1 induced changes in renal proximal tubular cells: implications for treatment of DN. Am J Physiol 296:F614–F621

13. Bakin AV, Tomlinson AK, Bhowmick NA, Moses HL, Arteaga CL (2000) Phosphatidylinositol 3-kinase function is required for transforming growth factor beta-mediated epithelial to mesenchymal transition and cell migration. J Biol Chem 275:36803–36810
14. Masszi A, Fan L, Rosivall L et al (2004) Integrity of cell–cell contacts is a critical regulator of TGF-beta 1-induced epithelial-to-myofibroblast transition: role for beta-catenin. Am J Pathol 165:1955–1967
15. Zheng G, Lyons JG, Tan TK et al (2009) Disruption of E-cadherin by matrix metalloproteinase directly mediates epithelial–mesenchymal transition downstream of transforming growth factor-beta1 in renal tubular epithelial cells. Am J Pathol 175:580–591
16. Moreno AP, Berthoud VM, Pérez-Palacios G, Pérez-Armendariz EM (2005) Biophysical evidence that connexin-36 forms functional gap junction channels between pancreatic mouse beta-cells. Am J Physiol Endocrinol Metab 288:E948–E956
17. Boggon TJ, Murray J, Chappuis-Flament S, Wong E, Gumbiner BM, Shapiro L (2002) C-cadherin ectodomain structure and implications for cell adhesion mechanisms. Science 17:1308–1313
18. Fujimoto K, Nagafuchi A, Tsukita S, Kuraoka A, Ohokuma A, Shibata Y (1997) Dynamics of connexins, E-cadherin and alpha-catenin on cell membranes during gap junction formation. J Cell Sci 110:311–322
19. Caton D, Calabrese A, Mas C, Serre-Beinier V, Wonkam A, Meda P (2002) Beta-cell crosstalk: a further dimension in the stimulus-secretion coupling of glucose-induced insulin release. Diabetes Metab 28:3S45–S53
20. Kanno Y, Sasaki Y, Shiba Y, Yoshida-Noro C, Takeichi M (1984) Monoclonal antibody ECCD-1 inhibits intercellular communication in teratocarcinoma PCC3 cells. Exp Cell Res 152:270–274
21. Musil LS, Cunningham BA, Edelman GM, Goodenough DA (1990) Differential phosphorylation of the gap junction protein connexin43 in junctional communication-competent and -deficient cell lines. J Cell Biol 111:2077–2088
22. Mege RM, Matsuzaki F, Gallin WJ, Goldberg JI, Cunningham BA, Edelman GM (1988) Construction of epithelioid sheets by transfection of mouse sarcoma cells with cDNAs for chicken cell adhesion molecules. Proc Natl Acad Sci U S A 85:7274–7278
23. Bobbie MW, Roy S, Trudeau K, Munger SJ, Simon AM, Roy S (2001) Reduced connexin 43 expression and its effect on the development of vascular lesions in retinas of diabetic mice. Invest Opthalmol Vis Sci 51:3758–3763
24. Li AF, Roy S (2009) High glucose induced downregulation of connexin 43 expression promotes apoptosis in microvascular endothelial cells. Invest Opthalmol Vis Sci 50:1400–1407
25. Zhang J, Hill CE (2005) Differential connexin expression in preglomerular and postglomerular vasculature: accentuation during diabetes. Kidney Int 68:1171–1185
26. Zhang JH, Kawashima S, Yokoyama M, Huang P, Hill CE (2006) Increased eNOS accounts for changes in connexin expression in renal arterioles during diabetes. Anat Rec A Discov Mol Cell Evol Biol 288:1000–1008
27. Li AF, Sato T, Haimovici R, Okamoto T, Roy S (2003) High glucose alters connexin 43 expression and gap junction intercellular communication activity in retinal pericytes. Invest Ophthalmol Vis Sci 44:5376–5382
28. Sato T, Haimovici R, Kao R, Li AF, Roy S (2002) Downregulation of connexin 43 expression by high glucose reduces gap junction activity in microvascular endothelial cells. Diabetes 51:1565–1571
29. Fernandes R, Girão H, Pereira P (2004) High glucose down-regulates intercellular communication in retinal endothelial cells by enhancing degradation of connexin 43 by a proteasome-dependent mechanism. J Biol Chem 279:27219–27224
30. Gomes P, Malfait M, Himpens B, Vereecke J (2003) Intercellular Ca (2+)-transient propagation in normal and high glucose solutions in rat retinal epithelial (RPE-J) cells during mechanical stimulation. Cell Calcium 34:185–192
31. Hanner F, Sorensen CM, Holstein-Rathlou NH, Peti-Peterdi J (2010) Connexins and the kidney. Am J Physiol Regul Integr Comp Physiol 298:R1143–R1155
32. Hills CE, Bland R, Bennett J, Ronco PM, Squires PE (2006) High glucose up-regulates ENaC and SGK1 expression in HCD-cells. Cell Physiol Biochem 18:337–346
33. Hills CE, Bland R, Wheelans DC, Bennett J, Ronco PM, Squires PE (2006) Glucose-evoked alterations in connexin43-mediated cell-to-cell communication in human collecting duct: a possible role in diabetic nephropathy. Am J Physiol Renal Physiol 291: F1045–F1051
34. Tian YC, Fraser D, Attisano L, Phillips AO (2003) TGF-beta1-mediated alterations of renal proximal tubular epithelial cell phenotype. Am J Physiol Renal Physiol 285:F130–F142
35. Hills CE, Willars GB, Brunskill NJ (2010) Proinsulin C-peptide antagonizes the profibrotic effects of TGF-beta1 via up-regulation of retinoic acid and HGF-related signaling pathways. Mol Endocrinol 24:822–831
36. Tian YC, Phillips AO (2002) Interaction between the transforming growth factor-β type II receptor/Smad pathway and β-catenin during transforming growth factor-β1-mediated adherens junction disassembly. Am J Pathol 160:1619–1628
37. Maeda M, Johnson K, Wheelock MJ (2005) Cadherin switching: essential for behavioural but not morphological changes during an epithelium-to-mesenchyme transition. J Cell Sci 118:873–887
38. Strutz F, Zeisberg M (2006) Renal fibroblasts and myofibroblasts in chronic kidney disease. J Am Soc Nephrol 17:2992–2998
39. Humphreys BD, Lin SL, Kobayashi A et al (2010) Fate tracing reveals the pericyte and not epithelial origin of myofibroblasts in kidney fibrosis. Am J Pathol 176:85–97
40. Keeley EC, Mehrad B, Strieter RM (2010) Fibrocytes: bringing new insights into mechanisms of inflammation and fibrosis. Int J Biochem Cell Biol 42:535–542
41. Zeisberg M, Duffield JS (2010) Resolved: EMT produces fibroblasts in the kidney. J Am Soc Nephrol 21:1247–1253
42. Hills CE, Squires PE (2011) The role of TGF-β and epithelial-to mesenchymal transition in diabetic nephropathy. Cytokine Growth Factor Rev 22:131–139
43. Dennler S, Itoh S, Vivien D, Dijke P, Huet S, Gauthier J (1998) Direct binding of smad3 and smad4 to critical TGF-β inducible elements in the promoter of the human plasminogen activator inhibitor-type 1 gene. EMBO 17:3091–3100
44. Yang F, Huang XR, Chung AC, Hou CC, Lai KN, Lan HY (2010) Essential role for Smad3 in angiotensin II-induced tubular epithelial-mesenchymal transition. J Pathol 221:390–401
45. Yeh YC, Wei WC, Wang YK, Lin SC, Sung JM, Tang MJ (2010) Transforming growth factor-β1 induces Smad3-dependent β1 integrin gene expression in epithelial-to-mesenchymal transition during chronic tubulointerstitial fibrosis. Am J Pathol 177:1743–1754
46. Brown KA, Pietenpol JA, Moses HL (2007) A tale of two proteins: differential roles and regulation of Smad2 and Smad3 in TGF-beta signaling. J Cell Biochem 101:9–33
47. Tan R, Zhang J, Tan X, Zhang X, Yang J, Liu Y (2006) Down-regulation of SnoN expression in obstructive nephropathy is mediated by an enhanced ubiquitin-dependent degradation. J Am Soc Nephrol 17:2781–2791
48. Li JH, Zhu HJ, Huang XR, Lai KN, Johnson RJ, Lan HY (2002) Smad7 inhibits fibrotic effect of TGF-Beta on renal tubular epithelial cells by blocking Smad2 activation. J Am Soc Nephrol 13:1464–1472
49. Takenaka T, Inoue T, Okada H et al (2011) Altered gap junctional communication and renal haemodynamics in Zucker fatty rat model of type 2 diabetes. Diabetologia 54:2192–2201
50. Liu L, Hu X, Cai GY et al (2011) High glucose-induced hypertrophy of mesangial cells is reversed by connexin43 over-expression via PTEN/Akt/mTOR signaling. Nephrol Dial Transplant. doi:10.1093/ndt/gfr265

Cellular Physiology and Biochemistry

Cell Physiol Biochem 2012;30:xx-xx
DOI:
Published online: July 26, 2012
Accepted: June 29, 2012

1015-8987/12/0302-0001$38.00/0

Original Paper

Calcium-sensing Receptor Activation Increases Cell-cell Adhesion and β-cell Function

Claire E. Hills[1]* Mustafa Y.G. Younis[1]* Jeanette Bennett[1] Eleftherios Siamantouras[2] Kuo-Kang Liu[2] Paul E. Squires[1]

[1]Schools of Life Sciences and [2]Engineering, University of Warwick, Coventry, *To be considered equally as first authors

Key Words
Calcium-sensing Receptor • E-cadherin • Calcimimetic • Cell-coupling • β-cell • Insulin Secretion

Abstract
***Background/Aims*:** The extracellular calcium-sensing receptor (CaR) is expressed in pancreatic β-cells where it is thought to facilitate cell-to-cell communication and augment insulin secretion. However, it is unknown how CaR activation improves β-cell function. ***Methods*:** Immunocytochemistry and western blotting confirmed the expression of CaR in MIN6 β-cell line. The calcimimetic R568 (1μM) was used to increase the affinity of the CaR and specifically activate the receptor at a physiologically appropriate extracellular calcium concentration. Incorporation of 5-bromo-2'-deoxyuridine (BrdU) was used to measure of cell proliferation, whilst changes in non-nutrient-evoked cytosolic calcium were assessed using fura-2-microfluorimetry. AFM-single-cell spectroscopy related CaR-evoked changes in epithelial (E)-cadherin expression to improved functional tethering between coupled cells. ***Results*:** Activation of the CaR over 48hr doubled the expression of E-cadherin (206±41%) and increased L-type voltage-dependent calcium channel expression by 70% compared to control. These changes produced a 30% increase in cell-cell tethering and elevated the basal-to-peak amplitude of ATP (10μM) and tolbutamide (100μM)-evoked changes in cytosolic calcium. Activation of the receptor also increased PD98059 (1-100iM) and SU1498 (1-100μM)-dependent β-cell proliferation. ***Conclusion*:** Our data suggest that activation of the CaR increases E-cadherin mediated functional tethering between β-cells and increases expression of L-type VDCC and secretagogue-evoked changes in $[Ca^{2+}]_i$. These findings could explain how local changes in calcium, co-released with insulin, activate the CaR on neighbouring cells to help ensure efficient and appropriate secretory function.

Paul Edward Squires, Ph.D.
School of Life Sciences,
The University of Warwick, Coventry, CV4 7AL (UK)
Tel. +44 (0) 24 7657-2976, Fax+44 (0) 24 7652-3701
E-Mail P.E.Squires@warwick.ac.uk

Introduction

The extracellular calcium sensing receptor (CaR) plays a central role in maintaining systemic Ca^{2+}-homeostasis by regulating the secretion of parathyroid hormone and urinary calcium concentration [1]. However, since the identification and characterisation of the receptor [2], it has become increasingly apparent that this cationic ion binding receptor is found on many tissues not associated with the control of plasma [Ca^{2+}] including; oesophageal [3] and colonic epithelia [4], the cardiovascular system (reviewed in [5]), hypothalamic neurons [6], pancreatic ducts [7] and pancreatic α- and β-cells [8-10]. The functional significance of the CaR in tissue not involved in the control of systemic Ca^{2+} is not fully understood [11, 12]. In exocrine pancreas it has been suggested that the CaR monitors extracellular Ca^{2+} in pancreatic juice to limit the risk of Ca^{2+} carbonate stone formation [13], whilst the receptor may detect changes in levels of dietary Ca^{2+} in gastrin secreting cells of the human antrum [14-16]. However, a more global explanation for the role of the CaR in these disparate tissues could be in its ability to detect local fluctuations in Ca^{2+}, mediating cell-cell coupling, communication and function.

The possibility that local changes in extracellular Ca^{2+} resulting from the efflux of mobilised Ca^{2+} in one cell are sufficient to activate the CaR on an adjacent cell was elegantly demonstrated in a model system of the kidney epithelium [17]. In this novel study, Ca^{2+}-extrusion from fibroblasts was to activate the CaR on co-cultured HEK cells to elicit a response [18]. In the pancreas, cell-to-cell communication improves the functional responsiveness of cells and augments insulin secretion [19, 20]. Specific activation of the CaR using calcimimetics [21] enhances insulin secretion from human islets [10]. Secretory granules contain high concentrations of Ca^{2+} which is released upon exocytosis [22]. Recently Ca^{2+}-sensitive microelectrodes have been used to demonstrate that the extracellular spaces surrounding β-cells constitute a restricted domain where Ca^{2+}, co-released during exocytosis reaches millimolar concentrations [23]. These direct measurements support the concept of local 'hot-spots' of extracellular Ca^{2+} which are able to activate the CaR on neighbouring β-cells.

The use of calcimimetics to specifically activate the CaR by increasing receptor affinity for its ligand avoids the many non-specific effects observed when using supra-physiological changes in calcium concentration. Activation of the CaR in β-cells is associated with rapid increases in cytoslic calcium and marked, but transient, increases in insulin secretion [24, 25]. Our earlier work suggests that the CaR can mediate cell-to-cell communication within islets; however, how this communication is facilitated has yet to be resolved. In the present study we confirm CaR expression in our model of homotypic β-cell-β-cell interaction and provide compelling evidence that activation of the receptor increases expression of the epithelial (E) adhesion protein E-cadherin and increases functional tethering between β-cells. These data could explain why the secretory efficiency of the intact islet is far greater than the sum of its composite β-cells when studied in isolation.

Materials and Methods

Materials

MIN6 cells were obtained from Dr. Y.Oka and J.-I. Miyazaki (Univ. of Tokyo, Tokyo, Japan). DMEM, glutamine, penicillin-streptomycin, gelatin (from bovine skin), PBS, foetal bovine serum and trypsin-EDTA were from Sigma-Aldrich (Poole, Dorset, UK). Tissue culture media and plasticware were from Invitrogen Life Technologies (Paisley, UK). Immobilon P membranes (Millipore, Watford,UK), ECL detection reagents (Amersham Biosciences, Buckinghamshire, UK). For preparation of compartmental protein a Qproteome kit was obtained from Qiagen (Sussex, UK). Anti-fade Citifluor (glycerol/PBS solution: Agar Scientific, Essex, UK). The MEK inhibitor PD98059 and the inhibitor of VEGF receptor 2, SU1498, that inhibits ERKs phosphorylated by growth factors,were from Calbiochem (Nottingham, UK). The calcimimetic R568 was from Amgen Inc (Thousand Oaks, CA, USA). BrdU, Alexa secondaries and Alexa Fluor 594 conjugated anti-

BrdU were from Invitrogen (Molecular Probes, Eugene, Oregon, USA). Antibodies were obtained from Santa Cruz (CA, USA) and Sigma-Aldrich (Poole, Dorset, UK).

Maintenance of MIN6 cells

MIN6 cells (passasge 35-40) were maintained at 37°C (95% air/5% CO_2) in DMEM supplemented with 15% foetal calf serum (FCS), 2mM glutamine and 100U/ml penicillin/0.1mg/ml streptomycin (all Sigma Chemical Co. Poole, Dorset). Cells were split when 80% confluent, about every 3-4 days using Trypsin-EDTA. Prior to treatment, cells were placed in fresh DMEM containing glucose (5mmol/l) and low calcium (0.5mM) overnight.

Immunoblotting

Whole-cell proteins were prepared and separated by SDS-PAGE and electroblotted onto Immobilon P membranes as described previously [26]. Membranes were probed with polyclonal antibodies against human β-catenin (Santa Cruz Biotechnology), raised against amino acids 680-781 mapping at the C-terminus of β-catenin, mouse E-cadherin (Sigma UK product code U3254-anti-uvomorulin), mouse CaR raised against a synthetic peptide corresponding to residues 18-29 of the mouse CaR (CSAYGPDQRAQKK; Genosphere Biotechnologies, Paris-France) and human L-Type voltage gated calcium channel (Santa Cruz Biotechnology) raised against amino acids 1661-1900 mapping within an internal region of L-type Ca^{2+} CP α1D at dilutions of 1:5000, 1:500, 1:1000, and 1:500 respectively in PBS, 0.05% Tween-20. After three 10-min washes (PBS, 0.1% Tween 20), membranes were incubated with the following secondary antibodies (horseradish peroxidase-conjugated), anti-rat (E-Cadherin diluted 1:20,000 in PBS, 0.05% Tween-20), and anti-rabbit secondary (L-Type Voltage gated calcium channel, β-catenin and CaR all diluted at 1:40,000 in PBS, 0.05% Tween-20) for 60 min at 25°C followed by three 10-min washes (PBS, 0.1% Tween 20). Proteins were visualized using enhanced chemiluminescence and exposure to film. Blots were stripped and re-probed with anti-rabbit glyceraldehyde-3-phosphate dehydrogenase (GAPDH) (1:20,000; R&D Systems) to control for protein loading in subsequent densitometry analysis.

Immunocytochemistry

Cells at 80% confluence were fixed with 4% paraformaldehyde (PFA). Following blocking, the nuclear stain 4', 6-diamidino-2-phenylindole, dihydrochloride (DAPI; 1mM) was added for 3mins. Cells were then incubated with antibodies against anti- E-cadherin (Sigma), CaR (Genosphere Biotechnologies, Paris-France), β-catenin (Santa Cruz), and L-Type voltage gated calcium channel (Santa Cruz) diluted at 1:100 in PBS-Triton overnight at 4°C. Candidate proteins were visualized using Alexa488 or 594-conjugated secondary antibodies (1:1,000) in PBS-Triton for 1hr at 25°C. Fluorescence was visualized using an Axiovert 200 fluorescence microscope (Carl Zeiss, Welwyn Garden City, UK).

Calcium Microfluorimetry

MIN6 cells were transferred to APES-coated coverslips and allowed to adhere overnight under standard tissue culture conditions. Cells were then either maintained in control media or cultured in with R568 (1iM) for 48hrs. To determine agonist-evoked changes in cytosolic calcium, cells were loaded for 30 minutes in 5mM glucose at 37°C with 5μM Fura-2/AM (Sigma, UK). Washed coverslips formed the base of a stainless steel bath placed into a heating platform on the microscope stage (Axiovert 200 Research Inverted microscope, Carl Zeiss Ltd., Welwyn Garden City, UK). All experiments were carried out at 37°C using a Na^+-rich balanced salt solution as the standard extracellular medium (137mM NaCl, 5.4mM KCl, 1.3mM $CaCl_2$, 0.8mM $MgSO_4$, 0.3mM Na_2HPO_4, 0.4mM KH_2PO_4, 4.2mM $NaHCO_3$, 10mM HEPES and 5mM glucose, pH 7.4). A low-pressure rapid-superfusion system (flow rate 1-2ml/min) was used to change the solutions in the bath to allow for the acute addition of the non-nutrient secretagogues ATP (50μM), tolbutamide (100iM) and KCl (20mM). Cells were illuminated alternatively at 340nm and 380nm using a Metaflour imaging workbench (Universal Imaging Corp Ltd., Marlow, Bucks, UK). Emitted light was filtered using a 510nm long-pass barrier filter and detected using a Cool Snap HQ CCD camera (Roper Scientific). Data was collected at 3-second intervals for multiple regions of interest in any one field of view. All records have been corrected for background fluorescence (determined from cell-free coverslip).

Cell Proliferation

DNA synthesis as a marker of cell proliferation was assessed by measuring the incorporation of 5-bromo-2'-deoxyuridine (BrdU) in individual cells using micro-fluorimetric localisation of BrdU-immunoreactivity as described previously [27]. Briefly, MIN6 cells were seeded onto 3-aminopropyl-triethoxysilane (APES) treated cover glass at a density of 30,000 cells/well and left to adhere overnight under standard tissue culture conditions (95% air/5% CO_2, 37°C) in DMEM supplemented with 15% FCS. Cells were then washed in sterile PBS and serum starved overnight in fresh DMEM containing glucose (5mM) and low calcium (0.5mM). As required, PD98059 [27] or SU1498 [28] were applied as a 1hr pre-treatment, before adding the incubation media containing, calcium (0-10mM), calcimimetic (+/-R568 (1μM)) and +/-PD98059 or SU1498 (1-100μM). All solutions contained BrdU (10μM) for the final 2hr incubation. Cells were fixed with 4% paraformaldehyde (PFA) and their DNA denatured using 1M HCl (30min at RT) before incubating in Alexa-594-conjugated anti-BrdU (Molecular Probes, Invitrogen) at 1:200 and storing overnight at 4°C. After repeated washing (PBS /triton (0.01%)) BrdU incorporation was determined using an Axiovert 200 inverted fluorescent microscope (Carl Zeiss, Welwyn Garden City, UK). Six different wells in three separate experiments were used for each treatment and the number of BrdU-positive cells compared to non-BrdU-immunoreactive cells, determined for several (4-6) arbitrary regions/well in 3-4 separate experiments.

Single cell force spectroscopy

Atomic force microscopy-single-cell force spectroscopy (AFM-SCFS) was carried out using the CellHesion®200 module (JPK Instruments, Berlin, Germany) installed on an Eclipse TE 300 inverted microscope (Nikon, USA). The BioCell™ temperature controller (JPK, Berlin, Germany) was incorporated into the stage of the microscope so that all force spectroscopy measurements were performed at a constant temperature of 37°C. The entire system was placed on top of an anti-vibration table (TMC 63-530, USA). As described previously [29], tipless Arrow TL-1 cantilevers (NanoWorld, Switzerland), with force constant 0.03N/m, were coated with poly-L-lysine (25μg/ml in PBS, 30min, RT) and then fibronectin (20μg/ml in PBS, 2hr, 37°C), in order to capture a single suspended cell. Prior to cell attachment, a single Force-Displacement (F-D) curve was conducted to calibrate the instrument, using the thermal fluctuation method for fluids (JPK Software Release 3.4, Berlin, Germany). Subsequently, SCFS was conducted by bringing the cantilever-bounded cell into contact with an adherent substrate cell until a determined force (0.8nN) is reached. The two cells remained in contact for a set period of time (5sec), while bonding formed. The cantilever was then retracted at a constant speed (5μm/sec) and force (nN) versus displacement (μm) was continuously measured until the cells were completely separated. For each cell, three successive measurements were performed with 30sec interval pause. F-D measurements from multiple cells (approx 40) in separate experiments (n=4) were completed and the maximum unbinding force (nN) and the detachment energy (fJoules) calculated.

Data Analysis

Autoradiographs were quantified by densitometry using TotalLab 2003 (NonLinear Dynamics, Durham, NC USA). In all experiments where data was quantified, the control condition was normalized to 100% and data from all other experimental conditions compared to this. Statistical analysis of data was performed using either a paired t-test or a one-way ANOVA test with a Tukey's multiple comparison post-test. Data are expressed as mean + SEM, and 'n' denotes the number of experiments. $P<0.05$ was taken to signify statistical significance. All statistical analyses were performed using the Prism GraphPad software version 4.0 (San Diego, CA, USA).

Results

MIN6 cells express the CaR and adherens junction proteins

Western blot analysis confirmed expression of (A) E-cadherin, (B) β-catenin, (C) CaR and (D) L-type VDCC in 3 separate preparations of MIN6 cells, giving rise to bands at 120kDa, 97kDa, 130kDa and 200kDa respectively (Fig. 1). The distribution of each protein was examined by immunocytochemistry. E-cadherin, β-catenin and the CaR exhibited membrane and cytosolic localisation, whilst the L-type VDCC appeared more diffusely spread throughout

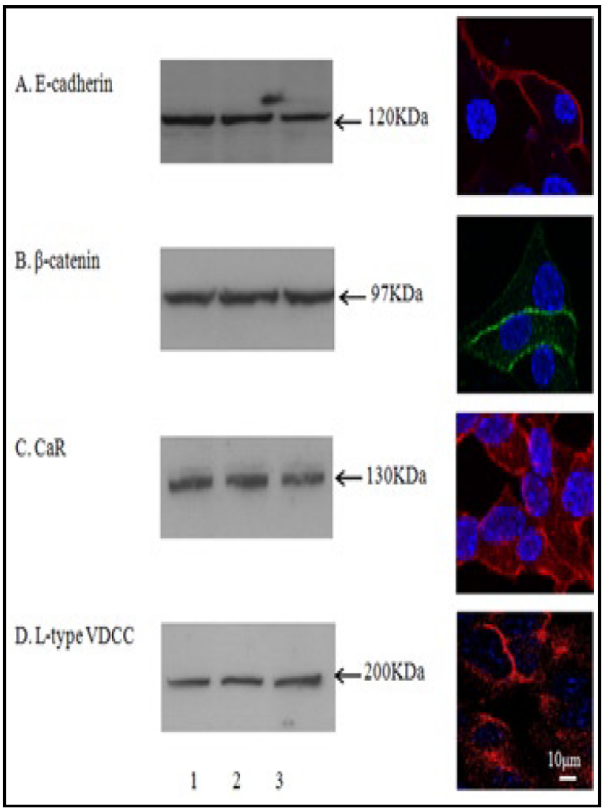

Fig. 1. MIN6 cells express the CaR and adherens junction proteins. Western blot analyses of MIN6 cell lysates (5μg protein/lane) using antibodies against mouse (A) E-cadherin, (B) β-catenin, (C) CaR, and (D) L-type VDCC detected appropriate bands of approximately 120kDa, 97kDa, 130kDa and 200kDa respectively. Controls included antibody pre-absorbed with a 10-fold excess of immunizing peptide (data not shown). Immunocytochemistry confirmed that each of the proteins studied exhibited membrane and cytosolic localization.

all cell compartments.

Activation of the CaR increases the expression of E-cadherin and L-type VDCCs

MIN6 cells were incubated for 48hrs in low glucose (5mmol/l) with increasing concentrations of extracellular calcium (nominal-no added calcium, 0.5, 5 and 10mM) or 0.5mM calcium ± the active (R) or inactive (S) stereo-isomers of 568 (1μM). Over 48hrs, supra-physiological increases in $[Ca^{2+}]_e$, or addition of the less active S568 isomer of the calcimimetic, failed to alter the expression of any the candidate proteins. Conversely, specific targeting of the CaR by R568 increased whole–cell expression of E-cadherin by 206±41% of control (n=4; $P<0.05$, Fig. 2A) and up-regulated expression of the L-type VDCC to 174±10% (n=4; $P<0.05$) of control (Fig. 2D), but failed to alter the expression of β-catenin (Fig. 2B) or the CaR itself (Fig. 2C). The changes in E-cadherin and L-type VDCC were not observed at earlier time points (e.g. 12 and 24hrs; data not shown).

Activation of the CaR increases adherence between coupled β-cells

In order to relate the change in expression/localisation of E-cadherin to functional tethering, atomic force microscopy-single-cell-force spectroscopy (AFM-SCFS) was used to measure cell-cell adhesion and the separation forces required to uncouple cells. Prior to attachment, cells were cultured for 48hrs under identical conditions +/-R568 (1μM). A single MIN6 cell (cell-1) was bound to a cantilever and subsequently brought into contact with an adherent cell (cell-2) within a cluster, using a fixed force (Fig. 3A phase inserts). After 5sec, the cantilever was then retracted (5μm/sec) and force versus displacement measured until the cells were completely separated. Retraction force-displacement curves provide important information regarding the adhesion between two cells, such as the energy required to separate them (the grey area in panel A), and maximum force of detachment (red

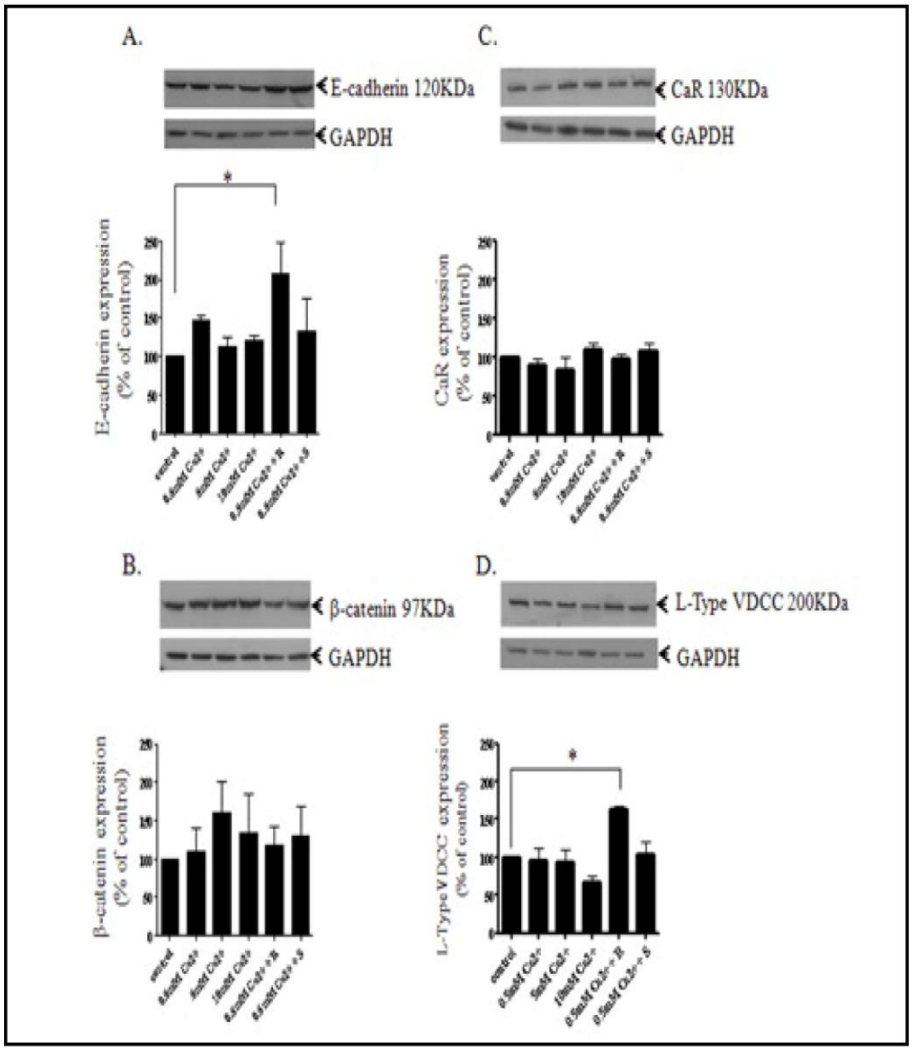

Fig. 2. Activation of the CaR increases expression of E-cadherin and L-type VDCC. MIN6 were grown in low glucose (5mmol/l) +/- calcium (5 or 10mM) or calcium (0.5mM) +/- R568 or S568 (1μM) for 48hrs and whole cell expression of (A) E-cadherin, (B) β-catenin, (C) CaR and (D) L-type VDCC was determined by immunoblotting. Upper panels show representative blots for each protein and re-probed for GAPDH as a loading control. Lower panels show mean (±SEM) densitometry data, normalised against the non-stimulated low glucose, nominal calcium control (100%), from 3 or more separate experiments. Each bar in the histogram corresponds to the associated lane in the representative blot. Key significances are shown, **P*<0.05.

circle). The former is normally referred to as "detachment energy" (panel C) and the latter the "maximum unbinding force" (panel B). The retraction measurements of control (38cells in 4 separate experiments) and R568-treated MIN6 cells (43cells in 4 separate experiments) are shown in the figure 3B & C. The results indicate that the calcimimetic R568 (1μM) increases the maximum unbinding force by 29±3.1% (n=4; *P*<0.001), whilst the detachment energy, or the total energy (fJoules) required to uncouple cells following R568 treatment, was increased 31±3.9% (n=4; *P*<0.001).

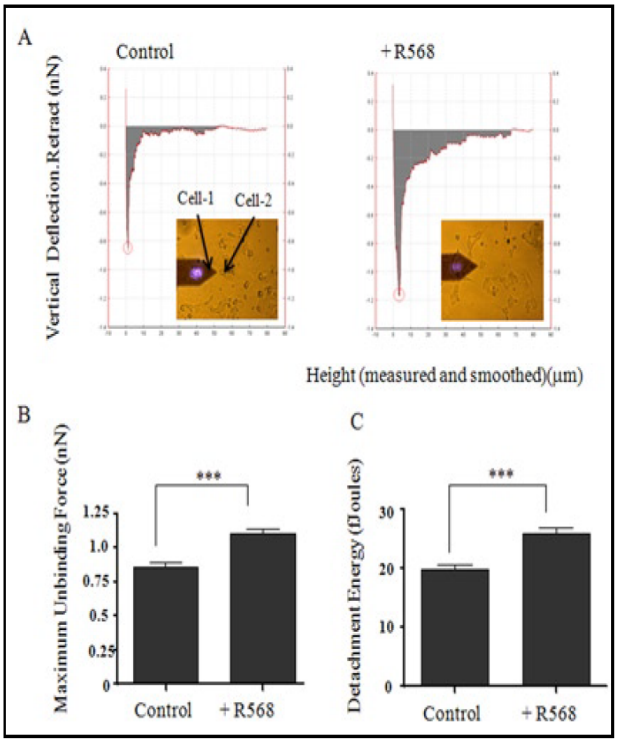

Fig. 3. Activation of the CaR reduces functional tethering. AFM-force spectroscopy was used to measure the detachment energy (fJoules) and maximum unbinding force (nN) required to uncouple two MIN6 cells. In panel A, a single MIN6 cell can be seen bound to the cantilever (cell-1, phase insert). This was bought into contact with an adherent cell-2 using a fixed force (1nN) for 10sec, whilst bonding formed. The cantilever was then retracted (5μm/sec) and force versus displacement measured until the cells separated (approximate pulling length 10-30im). The energy required to separate the cells (grey area in panel A), and maximum force of detachment (red circle) was measured. The former is known as the "detachment energy" (panel C) and the later is "maximum unbinding force" (panel B). The calcimimetic R568 (1μM) increased the maximum unbinding force by 29%, and the work of adhesion increased by 31% compared to control. Data is expressed as mean ± SEM. of multiple cells from 4 separate experiments, where key significances are shown, *** $P<0.001$.

Activation of the CaR alters the amplitude of non-nutrient-evoked $[Ca^{2+}]_i$ oscillations in β-cells

G-protein coupled receptors, such as the P_2-purinoreceptors, are important modulators of β-cell function, whilst sulphonylureas (such as tolbutamide) stimulate insulin secretion by closing the ATP-sensitive K^+-channels (K^+_{ATP}) leading to membrane depolarization and Ca^{2+}-entry. To relate the CaR-evoked change in protein expression of E-cadherin and L-type VDCC, the effects of chronic activation of the CaR on these non-nutrient evoked changes in $[Ca^{2+}]_i$ were examined. In figure 4, the effects of ATP (50μM), Tolbutamide (100μM) and KCl (20mM) on changes in $[Ca^{2+}]_i$ from MIN6 cells cultured in R568 (48hrs, 1iM) in low glucose (5mmol/l) is determined. Figure 4A is a representative trace from 3 regions (cells) in a single experiment (R1-3) showing that ATP, tolbutamide and KCl evoked increases in intracellular calcium in both control and R568-treated cells (in a total of five separate experiments). The basal-to-peak change in $[Ca^{2+}]_i$ induced by ATP and tolbutamide were respectively increased to 164±19% and 161±12% of control (n=3; $P<0.05$). The calcimimetic failed to significantly alter the basal-to-peak KCl response.

Activation of the CaR increases MAPK-dependent proliferation

MIN6 cells were incubated in 0.5mM $[Ca^{2+}]_e$ ± R568 (48hrs, 1iM) and BrdU-incorporation was used to determine cell proliferation (Fig. 5A). Low extracellular calcium (0.5mM) increased proliferation compared to nominal calcium conditions (154%±12%). This increase in proliferation was enhanced in the presence of R568 (218±37% compared to nominal calcium control, n=3 $P<0.05$, Fig. 5B). It has been previously reported that p42/44 MAPK are active in non-stimulated MIN6 cells. In a separate series of experiments, the R568 (1μM) significantly increased proliferation by 171±18% as compared to 0.5mM Ca^{2+}-alone (n=3

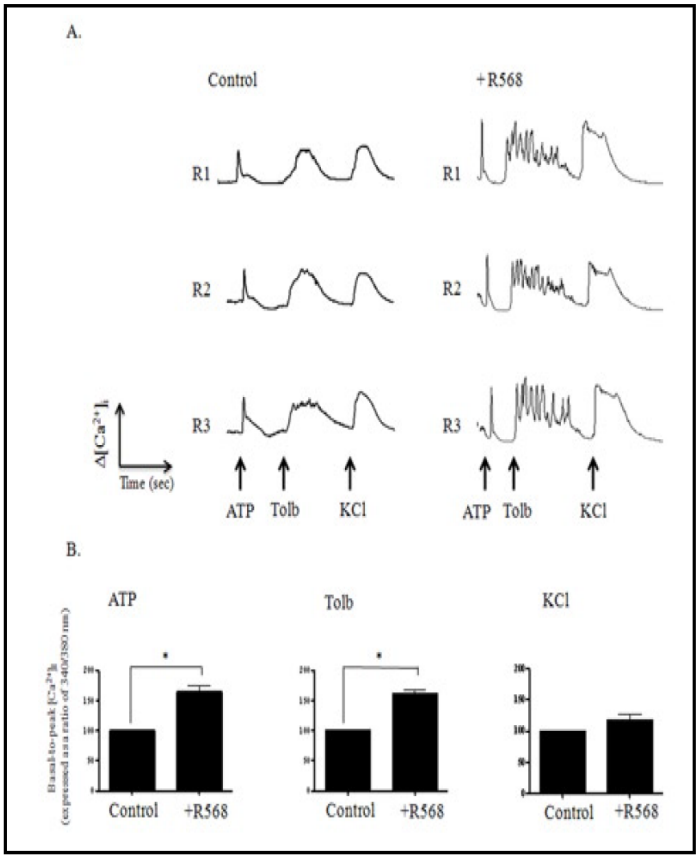

Fig. 4. Activation of the CaR increases ATP and Tolbutamide-evoked changes in $[Ca^{2+}]_i$. In panel A, ATP (50μM), tolbutamide (100μM) and KCl (20mM)-evoked changes in $[Ca^{2+}]_i$ in MIN6 cells +/- R568 (1μM). The calcimimetic altered the profile of the response to the non-nutrient secretagogues and increased the basal-to-peak amplitude to ATP and the sulphonylurea (panel B). There was no significant change in the amplitude to KCl in response to R568. Key significances are shown, **P*<0.05.

P<0.01). This CaR-evoked increase in cell turnover was dramatically reduced to 29±5.1% and 7±2% of the low calcium control by both PD98059 (100iM) and SU1498 (100μM) respectively (n=3 *P*<0.001, see Fig. 5C). In a further series of experiments (n=4), inhibition was found to be concentration-dependent with 1μM, 10μM and 100μM PD98059 reducing proliferation to 86±10%, 52±1% (*P*<0.01), and 11±11% (*P*<0.001) of 0.5mM calcium alone, whilst 1μM, 10μM and 100iM SU1498 inhibited basal β-cell turnover by 52±12% (*P*<0.01), 43±6% (*P*<0.01), and 3±3% (*P*<0.001) respectively, data not shown.

Discussion

Cadherins are important in forming the multi-protein adherens junction (AJ) that links cell-cell contact to the actin cytoskeleton and various signalling molecules [30]. The extracellular domain mediates ligation with E-cadherin on adjacent cells [31], whilst the cytoplasmic domain binds to β-catenin linking cadherin to the actin cytoskeleton via α-catenin. Interaction of cadherin with F-actin, via the catenins, not only serves to increase adhesive strength of the junction but also acts as a signalling 'node' for proteins that influence adhesiveness &/or initiate intracellular signalling. Co-localised with ECAD and βCAT at the sites of cell-cell contact, connexins (Cx) oligomerise into hexameric hemichannels (connexons) connecting the cytoplasm of adjoining cells and forming gap junctions (GJ). These GJs allow transfer of solutes, metabolic precursors and electrical currents [32], and are essential for synchronising activity across the bulk mass of the islet to ensure effective and appropriate secretion [33]. Inhibiting cadherin-based cell adhesion inhibits GJ-assembly [34], whilst expression of recombinant cadherins into cells lacking strong coupling, increases

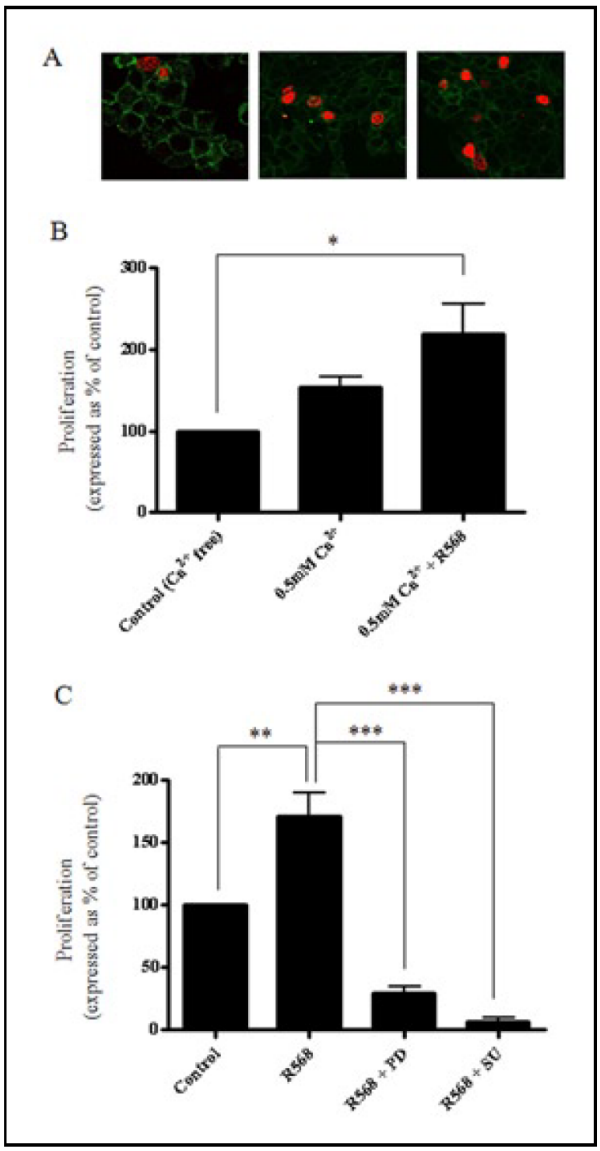

Fig. 5. Activation of the CaR increases MAPK-dependent cell proliferation. Cell proliferation was determined by the incorporation of 5-bromo-2'-deoxyuridine (BrdU) into MIN6 DNA and visualized by ALEXA 594-tagged anti-BrdU (red cells, representative panel A). Data represent cell counts from 4-6 arbitrary regions (10-50cells/region) from 3-4 repeat slides in 3 separate experiments. All data were recorded in the absence of FCS and expressed as a % of a nominal Ca^{2+} control (panel B). Small increases in proliferation induced by low $[Ca^{2+}]_e$ (0.5mM) were significantly increased by R568 (1μM). Inhibition of the p42/44 MAPK pathway using the MEK inhibitor PD098059 (100iM) or SU1498 (100μM) reduced proliferation by 71% and 93% respectively (C). Key significances are shown where ** $P<0.01$, *** $P<0.001$ for 3 separate experiments.

Cx-phosphorylation at the AJ [35] and increases cell-to-cell communication [36]. Since intercellular adhesion precedes GJ-formation and inhibiting cadherin-based cell adhesion inhibits GJ-assembly, we hypothesize that a gain in cell-cell adhesion will have beneficial effects on β-cell function.

There is considerable evidence suggesting that the extracellular calcium-sensing receptor (CaR) can mediate cell-to-cell communication within the pancreatic islet [8, 10, 24, 25]; however, how this communication is facilitated has yet to be resolved. In the present study we confirm CaR expression in our model of homotypic β-cell-β-cell interaction and report that chronic activation of the receptor increases expression of the epithelial (E) adhesion protein E-cadherin. Furthermore, using single-cell force-spectroscopy we present novel data confirming that the CaR-evoked increase in E-cadherin produces a 30% increase in functional tethering between coupled β-cells. The relationship between the CaR and E-cadherin is consistent with data from other cell types. In colonic cells, regulation of E-cadherin and β-catenin was found dependent on CaR expression and function [37], whilst

inactivation of the CaR inhibited E-cadherin-mediated cell-cell adhesion in human epidermal keratinocytes [38], further supporting our hypothesis that the link between CaR function and AJ proteins can sustain/improve function.

In addition to promoting cell-cell adhesion, chronic activation of the CaR also increased the expression of the L-type voltage-dependent calcium channel (VDCC). Essential for insulin secretion, these channels permit Ca^{2+}-entry ahead of nutrient-evoked exocytosis in the β-cell. Spatial interactions between voltage dependent calcium channels and the CaR have recently been suggested to be important in the first phase of insulin secretion from β-cells [39], and the increased CaR-evoked expression seen in our study could explain the increase in the basal-to-peak amplitude of secretogue-evoked changes in $[Ca^{2+}]_i$ in response to both the purinergic agonist ATP, or sulphonylurea activation of the K^+_{ATP} channel by tolbutamide.

There are a number of studies from diverse cell types that suggest a role for the CaR in regulating cell proliferation, including work in fibroblasts [40], astrocytoma [41], and osteoblasts [42]. The low mitotic index of primary β-cells leads to considerable technical difficulties in measuring β-cell proliferation in islets. Previous studies demonstrate that although MIN6 cells are transformed, their proliferative capacity is regulated by extracellular signals, validating these clonal β-cells as a representative experimental model of β-cell proliferation [43-46]. Elevated $[Ca^{2+}]_e$ can activate p38 and p42/44 MAP kinases [27, 47] and increase cell proliferation [48]. In addition to the effect of chronic activation of the CaR on cell-cell-adhesion we have also shown that specific activation of the CaR by the calcimiemtic R568, enhances MEK-dependent proliferation of β-cells at physiologically appropriate concentrations of extracellular calcium.

Conclusion

In the current study we have provided compelling evidence that activation of the calcium-sensing receptor increases expression of the epithelial (E) adhesion protein E-cadherin and increases functional tethering between β-cells. The increase in cell-cell interaction is mirrored by an increase in the expression of the L-type VDCC and augmented secretagogue-evoked changes in $[Ca^{2+}]_i$. Together, these findings could help explain how local changes in co-released calcium activate the CaR on neighbouring cells to help propagate and synchronise activity within the intact islet to help ensure efficient and appropriate insulin secretion.

Acknowledgements

This work was supported by the generous grant support of Diabetes UK (BDA: 09/0003913). The authors are grateful to Amgen Inc. for the supply of R568 and S568. We would like to thank JPK Instruments for their professional support in the use of single-cell force spectroscopy and we are grateful to Dr MN Hodgkin and Dr GJ Rogers who contributed to some of our early ideas on CaR-activity in the β-cell. The authors have nothing to disclose.

References

1 Brown EM: The calcium-sensing receptor: physiology, pathophysiology and CaR-based therapeutics. Subcell Biochem 2007;45:139-167.

2 Brown EM, Gamba G, Riccardi D, Lombardi M, Butters R, Kifor O, Sun A, Hediger MA, Lytton J, Herber SC: Cloning and characterization of an extracellular Ca^{2+}-sensing receptor from bovine parathyroid. Nature 1993;366:575-580.

3 Justinich CJ, Mak N, Pacheco I, Mulder D, Wells RW, Blennerhassett MG, MacLeod RJ: The extracellular calcium-sensing receptor (CaSR) on human esophagus and evidence of expression of the CaSR on the esophageal epithelial cell line (HET-1A). Am J Physiol 2008;294:G120-G129.

4 Cheng SX, Geibel JP, Herbert SC : Extracellular polyamines regulate fluid secretion in rat colonic crypts via the extracellular calcium-sensing receptor. Gastroenterology 2004;126:148-158.
5 Smajilovic S, Tfelt-Hansen J: Calcium acts as a first messenger through the calcium-sensing receptor in the cardiovascular system. Cardiovas Res 2007;75:457-467.
6 Vizard TN, O'Keefle GW, Guiterrez H, Kos CH, Riccardi D, Davies AM: Regulation of axonal and dendritic growth by the extracellular calcium-sensing receptor. Nature Neurosci 2008;11:285-291.
7 Racz GZ, Kittel A, Riccardi D, Case RM, Elliott AC, Varga G: Extracellular calcium sensing receptor in human pancreatic cells. Gut 2002;51:705-711.
8 Squires PE, Harris TE, Persaud SJ, Curtis SB, Buchan AMJ, Jones PM: The extracellular calcium-sensing receptor on human β-cells negatively modulates insulin secretion. Diabetes 2000;49:409-417.
9 Rasschaert J, Malaisse WJ : Expression of the calcium-sensing receptor in pancreatic islet B-cells. Biochem Biophys Res Comm 1999;264:615-618.
10 Gray E, Squires PE, Muller D, Asare-Anane H, Cai Huang G, Amiel S, Persaud SJ, Jones PM: Activation of the extracellular calcium sensing receptor initiates insulin secretion from human islets of Langerhans: involvement of protein kinases. J Endocrinol 2006;190:711-718.
11 Squires PE: Non Ca^{2+}-homeostatic functions of the extracellular Ca^{2+}-sensing receptor (CaR) in endocrine tissues. J Endocrinology 2000;165:173-177.
12 Hodgkin MN, Hills CE, Squires PE: The calcium-sensing receptor and insulin secretion: a role outside systemic control 15years on. J Endocrinol 2008;199:1-4.
13 Bruce JI, Yang X, Ferguson CJ, Elliott AC, Steward MC, Case RM, Riccari D: Molecular and functional identification of a Ca^{2+} (polyvalent cation)-sensing receptor in rat pancreas. J Biol Chem 1999;274:20561-20568.
14 Ray JM, Squires PE, Curtis SB, Meloche RM, Buchan AMJ: Expression of the calcium-sensing receptor on human antral gastrin cells in culture. J Clin Invest 1997;99:2328-2333.
15 Buchan AMJ, Squires PE, Ring M, Meloche RM: Mechanism of action of the calcium-sensing receptor in human antral gastrin cells. Gastroenterology 2001;120:1128-1139.
16 Squires PE, Meloche RM, Buchan AMJ: Bombesin-evoked gastrin release and calcium signaling in human antral G-cells in culture. Am J Physiol 1999;276:G227-G237.
17 Hofer AM, Curci S, Doble MA, Brown EM, Soybel DI: Intercellular communication mediated by the extracellular calcium-sensing receptor. Nature Cell Biol 2000;2:392-398.
18 Hofer AM, Gerbino A, Caroppo R, Curci S: The extracellular calcium-sensing receptor and cell-cell signalling in epithelia. Cell Calcium 2004;35:297-306.
19 Rogers GJ, Hodgkin MN, Squires PE: E-cadherin and cell adhesion: a role in architecture and function in the pancreatic islet. Cell Physiol Biochem 2007;20:987-994.
20 Hauge-Evans AC, Squires PE, Persaud, Jones PM: Pancreatic beta-cell-to-beta-cell interactions are required for integrated responses to nutrient stimuli: enhanced Ca^{2+} and insulin secretory responses of MIN6 pseudoislets. Diabetes 1999;48:1402-1408.
21 Trivedi R, Mithal A, Chattopadhyay: Recent updates on the calcium-sensing receptor as a drug target. Curr Medic Chem 2008;15:178-186.
22 Belan P, Gardner J, Gerasimenko O, Gerasimenko J, Mills CL, Petersen OH, Tepikin AV: Isoproterenol evokes extracellular Ca^{2+}-spikes due to secretory events in salivary gland cells. J Biol Chem 1998;273:4106-4111.
23 Gerbino A, Maiellaro I, Carmore C, Caroppo R, Debellis L, Barile M, Busco G, Colella M.: Glucose increases extracellular [Ca^{2+}] in rat insulinoma (INS-1E) pseudoislets as measured with Ca^{2+}-sensitive microelectrodes. Cell Calcium 2012;51:393-401.
24 Kitsou-Mylona I, Burns CJ, Squires PE, Persaud SJ, Jones PM: A role for the extracellular calcium-sensing receptor in cell-cell communication in pancreatic islets of Langerhans. Cell Physiol Biochem 2008;22:557-566.
25 Jones PM, Kitsou-Mylona I, Gray E, Squires PE, Persaud SJ: Expression and function of the extracellular calcium-sensing receptor in pancreatic β-cells. Archives Physiol Biochem 2007;113:98-103.
26 Hills CE, Bland R, Bennett J, Ronco PM, Squires PE: TGF-β1 mediates glucose-evoked up-regulation of connexin-43 cell-to-cell communication in HCD-cells. Cell Physiol Biochem 2009;24:177-186.
27 Burns CJ, Squires PE, Persaud SJ: Signaling through the p38 and p42/44 mitogen-activated kinases in pancreatic β-cell proliferation. Biochem Biophys Res Comm 2000;268:541-546.

28 Boguslawki G, McGlynn PW, Harvey KA, Kovala AT: SU1498, an inhibitor of vascular endothelial growth factor receptror-2, causes accumulation of phosphorylated ERK kinase and inhibits their activity *in vivo* and *in vitro*. J Biol Chem 2004;279:5716-5724.

29 Hills CE, Siamantouras E, Smith SW, Cockwell P, Liu K-K, Squires PE: TGFβ modulates cell-to-cell communication in early epithelial-to-mesenchymal transition. Diabetologia 2012;55:812-824.

30 Moreno AP, Berthoud VM, Pérez-Palacios G, Pérez-Armendariz EM : Biophysical evidence that connexin-36 forms functional gap junction channels between pancreatic mouse beta-cells. Am J Physiol Endocrinol Metab 2005;288:E948-56.

31 Boggon TJ, Murray J, Chappuis-Flament S, Wong E, Gumbiner BM, Shapiro L: C-cadherin ectodomain structure and implications for cell adhesion mechanisms. Science 2002;17:1308-1313.

32 Caton D, Calabrese A, Mas C, Serre-Beiner V, Wonkman A, Meda P: Beta-cell crosstalk: a further dimension in the stimulus-secretion coupling of glucose-induced insulin release. Diabetes Metab. 2002; 28: 3S45-53.

33 Squires PE, Hauge-Evans AC, Persaud SJ, Jones PM: Synchronization of Ca^{2+}-signals within insulin-secreting pseudoislets: effects of gap-junctional uncouplers. Cell Calcium 2000;27:287-296.

34 Kanno Y, Sasaki Y, Shiba Y, Yoshida-Noro C, Takeichi M: Monoclonal antibody ECCD-1 inhibits intercellular communication in teratocarcinoma PCC3 cells. Exp Cell Res 1984;152:270-274.

35 Musil LS, Cunningham BA, Edelman GM, Goodenough DA: Differential phosphorylation of the gap junction protein connexin43 in junctional communication-competent and -deficient cell lines. J Cell Biol 1990;111:2077-2088.

36 Mege RM, Matsuzaki F, Gallin WJ, Goldberg JI, Cunningham BA, Edelman GM: Construction of epithelioid sheets by transfection of mouse sarcoma cells with cDNAs for chicken cell adhesion molecules. PNAS 1988;85:7274-7278.

37 Bhagavathula N, Hanosh AW, Nerusu KC, Appelman H, Chakrabarty S, Varani J: Regulation of E-cadherin and beta-catenin by Ca^{2+} in colon carcinoma is dependent on calcium-sensing receptor expression and function. Int J Cancer 2007;121:1455-1462.

38 Tu C-L, Chang W, Xie Z & Bikle DD: Inactivation of the calcium sensing receptor inhibits E-cadherin-mediated cell-cell adhesion and calcium-induced differentiation in human epidermal keratinocytes. J Biol Chem 2008;283:3519-3528.

39 Parkash J: Glucose-mediated spatial interactions of voltage dependent calcium channels and calcium sensing receptor in insulin producing β-cells. Life Sciences 2011;88:257-264.

40 McNeil SE, Hobson SA, Nipper V, Rodland KD: Functional calcium-sensing receptors in rat fibroblasts are required for activation of SRC kinase and mitogen-activated protein kinase in response to extracellular calcium. J Biol Chem 1998;273:1114-1120.

41 Chattopadhyay N, Ye CP, Yamaguchi T, Kerner R, Vassilev PM, Brown EM: Extracellular calcium-sensing receptor induces cellular proliferation and activation of a nonselective cation channel in U373 human astrocytoma cells. Brain Res 1999;851:116-124.

42 Huang Z, Cheng SL, Slatopolsky E: Sustained activation of the extracellular signal-regulated kinase pathway is required for extracellular calcium stimulation of human osteoblast proliferation. J Biol Chem 2001;276:21351-21358.

43 Muller D, Jones PM, Persaud SJ: Autocrine anti-apoptotic and proliferative effects of insulin in pancreatic beta-cells. FEBS Lett 2006;580:6977-6980.

44 Carvell MJ, Marsh PJ, Persaud SJ, Jones PM: E-cadherin interactions regulate β-cell proliferation in islet-like structures. Cell Physiol Biochem 2007;20:617-626.

45 Tanabe K, Okuya S, Tanizawa Y, Matsutani A, Oka Y: Leptin induces proliferation of pancreatic beta cell line MIN6 through activation of mitogen-activated protein kinase. Biochem Biophys Res Commun 1997;241:765-768.

46 Yoshitomi H, Fujii Y, Miyazaki M, Nakajima N, Inagaki N, Seino S: Involvement of MAP kinase and c-fos signaling in the inhibition of cell growth by somatostatin. Am J Physiol 1997;272:E769-774.

47 Sakwe AM, Larsson M, Rask L: Involvement of protein kinase C-alpha and -epsilon in extracellular Ca^{2+} signalling mediated by the calcium sensing receptor. Exp Cell Res 2004;297:560-573.

48 Liao J, Schneider A, Datta NS, McCauley LK: Extracellular calcium as a candidate mediator of prostate cancer skeletal metastasis. Cancer Res 2006;66:9065-9073.

OPEN ACCESS Freely available online

PLOS ONE

'Special K' and a Loss of Cell-To-Cell Adhesion in Proximal Tubule-Derived Epithelial Cells: Modulation of the Adherens Junction Complex by Ketamine

Claire E. Hills[1]*, Tianrong Jin[2], Eleftherios Siamantouras[2], Issac K-K Liu[2], Kieran P. Jefferson[3], Paul E. Squires[1]

1 School of Life Sciences, University of Warwick, Coventry, United Kingdom, **2** School of Engineering, University of Warwick, Coventry, United Kingdom, **3** University Hospital of Coventry and Warwickshire, Coventry, United Kingdom

Abstract

Ketamine, a mild hallucinogenic class C drug, is the fastest growing 'party drug' used by 16–24 year olds in the UK. As the recreational use of Ketamine increases we are beginning to see the signs of major renal and bladder complications. To date however, we know nothing of a role for Ketamine in modulating both structure and function of the human renal proximal tubule. In the current study we have used an established model cell line for human epithelial cells of the proximal tubule (HK2) to demonstrate that Ketamine evokes early changes in expression of proteins central to the adherens junction complex. Furthermore we use AFM single-cell force spectroscopy to assess if these changes functionally uncouple cells of the proximal tubule ahead of any overt loss in epithelial cell function. Our data suggests that Ketamine (24–48 hrs) produces gross changes in cell morphology and cytoskeletal architecture towards a fibrotic phenotype. These physical changes matched the concentration-dependent (0.1–1 mg/mL) cytotoxic effect of Ketamine and reflect a loss in expression of the key adherens junction proteins epithelial (E)- and neural (N)-cadherin and β-catenin. Down-regulation of protein expression does not involve the pro-fibrotic cytokine TGFβ, nor is it regulated by the usual increase in expression of Slug or Snail, the transcriptional regulators for E-cadherin. However, the loss in E-cadherin can be partially rescued pharmacologically by blocking p38 MAPK using SB203580. These data provide compelling evidence that Ketamine alters epithelial cell-to-cell adhesion and cell-coupling in the proximal kidney via a non-classical pro-fibrotic mechanism and the data provides the first indication that this illicit substance can have major implications on renal function. Understanding Ketamine-induced renal pathology may identify targets for future therapeutic intervention.

Citation: Hills CE, Jin T, Siamantouras E, Liu IK-K, Jefferson KP, et al. (2013) *'Special K'* and a Loss of Cell-To-Cell Adhesion in Proximal Tubule-Derived Epithelial Cells: Modulation of the Adherens Junction Complex by Ketamine. PLoS ONE 8(8): e71819. doi:10.1371/journal.pone.0071819

Editor: Steen Henning Hansen, Children's Hospital Boston, United States of America

Received April 4, 2013; **Accepted** July 3, 2013; **Published** August 29, 2013

Funding: This work was supported by the generous support of The Teresa Rosenbaum Golden Charitable Trust (Rosetree Trust). AFM-SCFS was made possible by the support of an equipment grant from Diabetes UK (BDA: 12/0004546). The funders had no role in study design, data collection and analysis, decision to publish, or preparation of the manuscript.

Competing Interests: The authors have declared that no competing interests exist.

* E-mail: C.Hills@warwick.ac.uk

Introduction

Ketamine is a tranquilliser that has also found use as an NMDA receptor antagonist in the treatment of human bipolar disorders [1]. However, in 2006 the UK government made Ketamine a class C drug. Possessing mild hallucinogenic properties, Ketamine is rapidly replacing heroin and methamphetamine as the recreational drug of choice [2]. Cheap to buy and easily accessible, Ketamine has several street names including "Special K", "vitamin K" and "LA Coke". In 2008, the British Crime Survey revealed that Ketamine was the fastest growing "party drug" among 16–24 year olds and it has since been dubbed the "new ecstasy" [3]. In the UK, Ketamine boasts an estimated 125,000 users, with more young people using Ketamine in England and Wales than heroin and crack cocaine combined. As the number of users rise, serious side effects are beginning to emerge. First documented in 2007, Ketamine has been shown to injure the bladder, causing ulcers (wounds) and fibrosis (stiffening of the bladder walls and shrinkage) [4]. Patients present with multiple symptoms including incontinence, bleeding, overactive bladder and bladder shrinkage, as well as damage to both the kidneys and the ureter [5]. Despite the growing presentation of these complications, there is an acute lack of understanding for the mechanisms that underlie the pathophysiological of Ketamine, and we urgently need to investigate how this mild hallucinogenic drug scars bladder and renal tissue to impair function [6].

In adults, wound repair is commonly associated with the accumulation of scar tissue (fibrosis or sclerosis). Its effects are variable and often impaired by disease or other pathophysiological insult (e.g. diabetes/drug abuse) [7]. Fibrosis involves excess accumulation of extracellular matrix (ECM), primarily composed of collagen. As normal tissue is replaced with scar tissue, a number of phenotypic and morphological changes occur and the fibrosis ultimately results in loss of function [8]. Regardless of etiology, patients subsequently exhibit a progressive decline in organ function, a largely irreversible process that, in the case of Ketamine abuse, can lead to removal of the bladder and potential end stage renal disease. In both the bladder and kidney, early changes in protein expression/function often occur before overt

fibrosis. These changes include a loss of epithelial integrity and dysregulated formation of the intercellular junction, involving, loss of epithelial E-cadherin, altered cell morphology, re-organisation of the cytoskeleton and *de-novo* expression of fibroblastic markers [9]. Cadherins have a central role in the formation of the multi-protein adherens junction, which links cell-cell contact to the actin cytoskeleton and various other signalling molecules [10]. The extracellular domain of the cell adhesion protein E-cadherin mediates ligation with neighbouring cadherins on adjacent cells [11], whilst the cytoplasmic domain binds to β-catenin linking cadherin to the actin cytoskeleton via α-catenin. The functional interaction of cadherin with F-actin, via the catenins, not only serves to increase adhesive strength of the junction but also acts as a signalling 'node' for proteins that influence adhesiveness &/or initiate intracellular signalling. The loss of E-cadherin mediated cell-to-cell adhesion represents a pivotal step in the transition of renal tubule cells from an epithelial phenotype to one more commonly associated with fibrosis [12]. Down-regulation of E-cadherin precedes changes in cell morphology, reorganisation of cell architecture and the subsequent gain in expression of phenotypic markers associated with renal pathology [12–13].

In the renal tubule, epithelial function depends on complex cell-cell interactions mediated through the adherens junction. In the current study we present data outlining early toxicological effects of Ketamine on proteins critical to formation of the adherens junction complex in the kidney. Using pharmacological manipulation, we examine potential cellular mechanisms orchestrating these changes and utilise high resolution AFM-single-cell force spectroscopy to assess the functional consequence of cell-cell tethering in Ketamine-treated cells exhibiting a loss in cadherin expression. Our data provide compelling evidence that Ketamine reduces cell-cell adhesion in epithelial cells of the proximal tubule. Translated to the *in vivo* scenario, the subsequent loss of epithelial integrity, structure and function may in part contribute to the toxicological and potential fibrotic response to Ketamine in the kidney.

Methods

Supplies for tissue culture were purchased from Invitrogen (Paisley, UK). Immobilon P membrane was from Millipore, Watford, UK and ECL from Amersham Biosciences, Buckinghamshire, UK. A Qproteome kit was obtained from Qiagen (Sussex, UK). Antibodies were obtained from Santa Cruz (CA, USA) and R&D systems (Abingdon, UK). Ketamine, TRITC-Phalloidin and Fibronectin, were obtained from Sigma (Poole, UK), as were all other general chemicals. Anti-TGF-β1 ELISA was obtained from R&D systems.

Model Cell Line

HK2 cells were obtained from the ATCC Bio-resource Centre (LGC Standards. Middlesex, UK). Cells (passages 18–30) were maintained in DMEM/Hams F12 (DMEM/F12) medium, supplemented with 10% fetal calf serum (FCS), glutamine (2 mM), and EGF (5 ng/ml) and cultured at 37°C in a humidified atmosphere of 5% CO_2. Prior to treatment, cells were transferred to DMEM/F12 low glucose (5 mM) for 48 hr as described previously [14]. Cells were serum starved overnight before applying either Ketamine (0–1 mg/mL) in the presence/absence of signalling inhibitors Wortmannin (2 μM), PD98059 (10 μM), and SB203580 (1 μM) for 24 hr. Cells were pre-incubated for 30 minutes with their corresponding inhibitors prior to Ketamine application. For assessment of Smad activity HK2 cells were incubated for 0–10 minutes with Ketamine (1 mg/mL).

MTT Assay

The 3-(4,5-Dimethylthiazol-2-yl)-2,5-diphenyltetrazolium bromide (MTT) assay is widely used for cytotoxicity assessments of pharmacological and chemical agents. Viable cells transport MTT into their mitochondria, the compound is then reduced to formazin (purple in color), and the latter is quantified colorometrically. The amount of color formed corresponds to the number of viable cells. HK2 cells were cultured in 96-well plates (5×10^3 cells/well) in 5 mM glucose containing media for 48 hrs prior to an overnight period of serum starvation. Cells were stimulated for 24 and 48 hrs with Ketamine (0.1–1 mg) and proliferation analyzed using the MTT colorimetric assay (Roche) according to manufacturers instructions. The values were presented as a percentage of the MTT uptake that was observed as compared to control cells.

Lactate Dehydrogenase Assay

Cell death or cytotoxicity is classically evaluated by the quantification of plasma membrane damage. Lactate dehydrogenase (LDH) is a stable enzyme, present in all cell types, and rapidly released into the cell culture medium upon damage of the plasma membrane. Therefore, LDH is a common marker used to determine cytotoxicity. HK2 cells were cultured in 96-well plates (5×10^3 cells/well) in 5 mM glucose containing media for 48 hrs prior to an overnight period of serum starvation. Cells were stimulated for 24 and 48 hrs with Ketamine (0.1–1 mg) and Lactate dehydrogenase levels assayed using the LDH-cytoxicity assay kit II (Abcam) according to manufacturers instructions. The values were presented as a percentage of the LDH release that was observed as compared to control cells.

Crystal Violet Assay

This is a simple assay useful for obtaining quantitative information about the relative density of cells adhering to multi-well cluster dishes. Crystal Violet stains DNA and upon solubilization, the amount of dye taken up by the monolayer can be quantitated in a plate reader. HK2 cells were cultured in 96-well plates (5×10^3 cells/well) in 5 mM glucose containing media for 48 hrs prior to an overnight period of serum starvation. Cells were stimulated for 24 and 48 hrs with Ketamine (0.1–1 mg) and cell density determined with crystal violet staining. Briefly, media was removed and cells were fixed for 10 mins with PFA. Following a brief wash with PBS, cells were incubated for 10 mins at room temperature in a 1% Crystal Violet solution. After this time interval, all traces of dye were removed with distilled water and the stain solubilized with 1% SDS. The values were presented as a percentage of cells staining in Ketamine treated cells as compared to control cells.

Quantification of TGF-β1

HK2 cells were cultured in 5 mM glucose containing media for 48 hrs prior to an overnight period of serum starvation. Cells were stimulated for 24 hrs with Ketamine (0.1–1 mg) under serum-free conditions and total TGF-β1 was measured by specific enzyme-linked immunosorbent assay (ELISA) of cell culture supernatant collected from growth-arrested HK2 cells. Active TGF-β1 is measured directly and latent TGF-β1 can be measured indirectly following acid activation of samples. This assay has <1% cross-reactivity for TGF-β2 and TGF-β3. TGF-β1 concentration was normalized to mg/ml of protein. Data were obtained as picograms of TGF-β1 per milliliter per mg of protein and are expressed as a percent as compared to control.

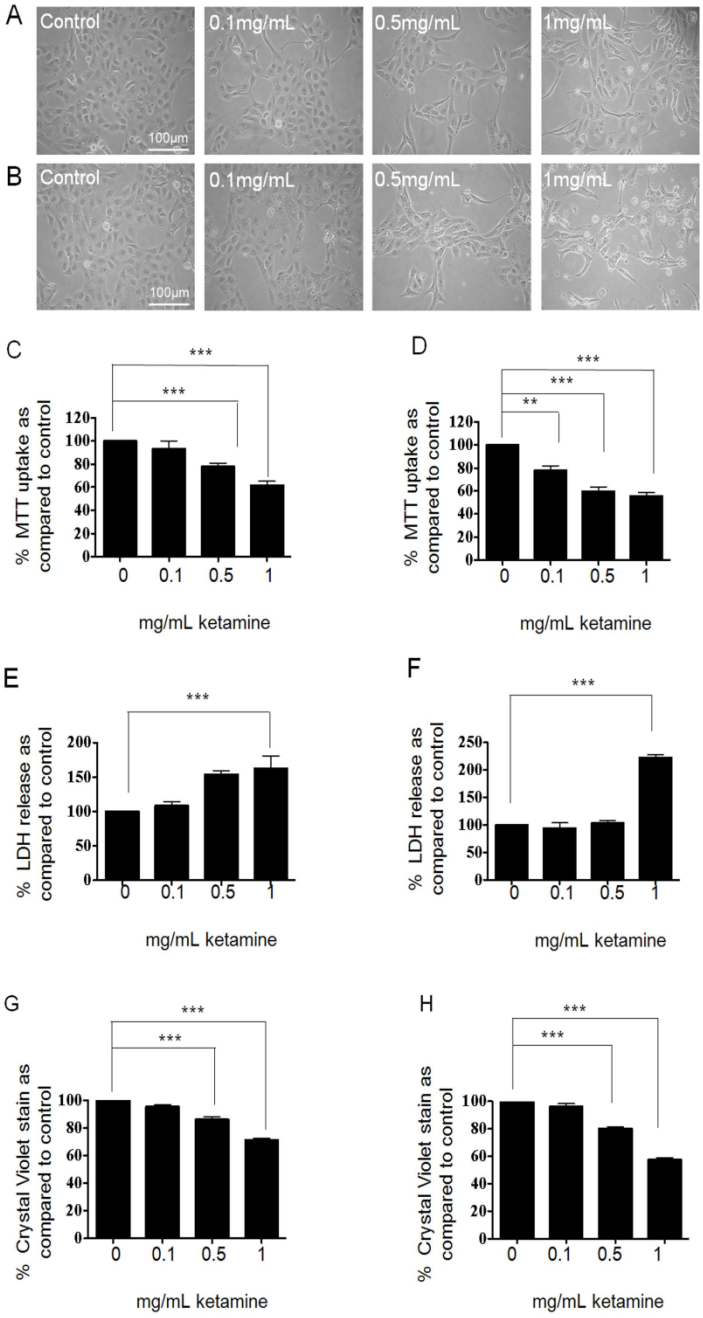

Figure 1. Impact of Ketamine on HK2 cell viability, as assessed by phase contrast microscopy, MTT uptake, Crystal Violet staining and LDH release. HK2 cells were cultured in 5 mM glucose containing media for 48 hrs prior to an overnight serum starvation. Cells were stimulated for 24–48 hrs with Ketamine (0.1–1 mg/mL) under serum-free conditions and morphological changes assessed (Panels A and B respectively). Ketamine evoked a concentration dependent change in cell morphology from a typical proximal tubular epithelial "cobblestone" appearance to an elongated fibroblast appearance. Cell viability was assessed by MTT uptake at 24 and 48 hrs (panels C and D respectively). Incubation with Ketamine at 0.5 and 1 mg/mL caused a significant decrease in viable cells as measured by MTT uptake. Cell membrane damage was assessed via LDH release at 24 and 48 hrs (panels E and F respectively). At both 24 and 48 hrs, Ketamine (1 mg/mL) caused a significant increase in LDH release. Finally cell density was determined by the Crystal violet assay. Ketamine evoked a reduction in cell density at 24 and 48 hrs (panels G and H respectively). The values obtained are expressed as a % of control (C). Results are representative of 3 separate experiments. Key significances are shown where $^{**}P<0.01$ and $^{***}P<0.001$.
doi:10.1371/journal.pone.0071819.g001

Immunoblotting

Cytosolic proteins were prepared and separated by gel electrophoresis and electro-blotting onto Immobilon P membranes as described previously [15]. For determination of protein localization, proteins were harvested using the Qproteome cell compartment kit. Membranes were probed with specific polyclonal antibodies against anti-E-cadherin (1:2000), N-Cadherin (1:1000), Snail (1:1000), Slug (1:1000), (1:2000), p-Smad 2 (1:1000), p-Smad 3(1:1000) (all R&D systems) and beta-catenin (1:1000) (Santa Cruz).

Immunocytochemistry

Cells at 80% confluence were fixed with 4% paraformaldehyde (PFA). Following blocking, the nuclear stain 4′, 6-diamidino-2-phenylindole, dihydrochloride (DAPI; 1 mM) was added for 3 mins. Cells were then incubated with TRITC-conjugated phalloidin (Sigma) diluted at 1:100 in PBS-Triton for 1 hr at 25°C. Fluorescence was visualized using an Axiovert 200 fluorescence microscope (Carl Zeiss, Welwyn Garden City, UK).

Single Cell Force Spectroscopy

Atomic Force Microscopy (AFM) Single-Cell Force Spectroscopy (CellHesion® module, JKP Instruments Germany) was used to measure cell-cell adhesion and the separation forces required to uncouple cells cultured in Ketamine as compared to control untreated cells. A single HK2 cell was bound to a cantilever using fibronectin (20 μg/ml) and poly-l-lysine (25 μg/ml) and subsequently brought into contact with an adherent cell (in a cluster of coupled cells) using a known force (1 nN). The two cells remained in contact for a defined period of time (10 sec) whilst bonding formed. The cantilever was then retracted at a constant speed (5 μm/sec) and force (nN) versus displacement (deflection of the cantilever) measured by the position of a laser beam reflected from the cantilever, until the cells were completely separated (pulling length 90 μm). Each cell-cell recording was repeated in triplicate with a 30 sec pause interval between successive measurements. Retraction recordings from multiple cells (approx. 40) in separate experiments (n = 4) were made and the maximum unbinding force (nN) and the detachment energy (fJoules) calculated.

Analysis

Autoradiographs were quantified by densitometry using TotalLab 2003 (NonLinear Dynamics, Durham, NC USA). Where data was quantified, the non-stimulated, low glucose control condition was normalized to 100% and data from all other experimental conditions compared to this. Statistical analysis of data was performed using a one-way ANOVA test with a Tukey's multiple comparison post-test. AFM data was analysed via *t*-test. Data are expressed as mean ± SEM, where 'n' denotes the number of experiments. A probability (P) <0.05 was taken to signify statistical significance.

Results

The Effect of Ketamine on Cell Viability and Cytoxicity

Cells were cultured in 5 mM glucose for 48 hrs prior to being serum starved overnight. Cells were either unstimulated (control) or stimulated for 24–48 hrs with Ketamine (0.1–1 mg/mL) under serum-free conditions. Phase contrast microscopy revealed that control HK2-cells exhibited a typical cobblestone morphology, characteristic of proximal tubular epithelial cells (Fig. 1, A and B). Exposure to increasing concentrations of Ketamine (0.1, 0.5 and 1 mg/mL) for 24 or 48 hrs evoked a concentration-dependent change in morphology towards an elongated fibrous phenotype. Furthermore, cells treated for 48 hrs at the highest concentration (1 mg/mL), appeared to exhibit cytosolic granulation and a reduction in cell number (Fig. 1B).

Cells stimulated for 24 and 48 hrs with Ketamine (0.1–1 mg/mL) under serum-free conditions were assessed for cell viability by MTT uptake (uptake directly correlates with the number of viable cells). At 24 hrs, incubation with Ketamine at 0.5 and 1 mg/mL significantly decreased viability by 22±4% and 39±5% respectively as compared to control (Fig. 1C, $P<0.001$, n = 3). At 48 hrs, Ketamine decreased cell viability by 22±4% ($P<0.01$), 41±3% ($P<0.001$) and 45±3% ($P<0.001$) as compared to control over the same range of concentrations (Fig. 1D, n = 3).

As a complimentary strategy to assess cytotoxicity, we used the Lactate Dehyrdogenase assay as a marker of LDH release into cell supernatant of control versus Ketamine-treated cells. To assess membrane damage, cells were stimulated for 24 and 48 hrs with Ketamine (0.1–1 mg/mL) under serum-free conditions prior to measuring LDH release. Results are expressed as a % of LDH release as compared to control cells. At 24 hrs, Ketamine (1 mg/mL) increased LDH levels by 62% to 162±17% of that under control (100%) conditions (Fig. 1E, $P<0.001$, n = 3), At 48 hrs Ketamine (1 mg/mL) significantly increased LDH levels by 140% to 240±18% as compared to control (Fig. 1F; $P<0.001$, n = 3). Release of LDH into the media suggests cell membrane damage and a concentration-dependent cytotoxic effect of Ketamine.

To further confirm the toxic role of Ketamine, we measured the number of adherent cells using a crystal violet assay. Cells were fixed and stained with crystal violet (1% w/v) at 24 and 48 hrs. Quantification of dye uptake was significantly reduced by 14±2% ($P<0.001$) and 29±1% ($P<0.001$) at 0.5 and 1 mg/mL respectively as compared to control at 24 hrs (Fig. 1G), and by 20±1% ($P<0.001$) and 43±2% ($P<0.001$) at 48 hrs over the same range of concentrations (Fig. 1H, n = 3). Based on our observations from all three strategies, subsequent analysis determined the effects of Ketamine (0.1–1 mg/mL) on cell-to-cell adhesion and adherens junction proteins over the more acute 24 hr time window.

The Effect of Ketamine on Expression of Adherens Junction Proteins

The transition of tubular epithelial cells from a typical, cobblestone morphology to a fibrotic phenotype is commonly associated with reorganisation of cell architecture and alterations in the expression of epithelial proteins involved in adherens and tight junction formation [12–13]. HK2 cells were cultured in 5 mM glucose containing media for 48 hrs prior to overnight serum starvation. Cells were stimulated for 24 hrs with Ketamine (0.1–1 mg/mL) under serum-free conditions and morphological and phenotypic changes assessed. At 24 hrs, Ketamine induced a concentration-dependent change in cell morphology towards an elongated fibroblast-like phenotype (Fig. 2A). These gross morphological changes were accompanied by re-organisation of the actin cytoskeleton from a diffuse transcellular network of F-actin filaments that spanned the cytosol, into more dense peripheral stress fibres (Fig. 2B).

This architectural reorganisation intimates that Ketamine causes dysregulation of the adherens junction complex and has repercussions for the integrity of the epithelial sheet. To resolve these changes, we examined the effects of Ketamine on adherens junction proteins and their transcriptional regulators. Ketamine induced a concentration-dependent decrease in whole-cell expression of E-cadherin by 28±1% ($P<0.01$), 52±12% ($P<0.001$) and 76±3% ($P<0.001$) as compared to control at 0.1, 0.5 and 1 mg/mL respectively (n = 3, Fig. 2C). The loss in expression reflected a loss in E-cadherin from all cell compartments examined (Fig. 2Hi).

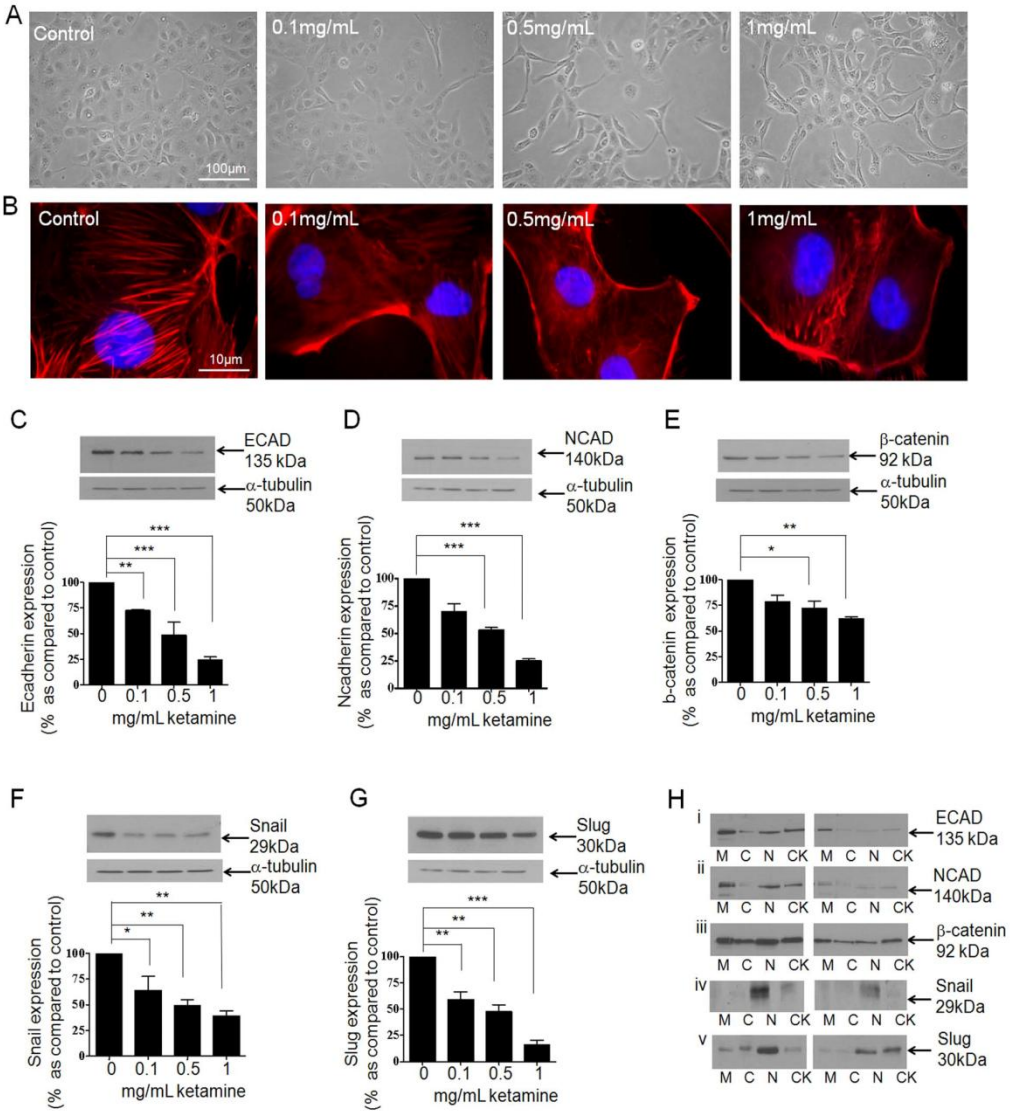

Figure 2. Ketamine evoked changes in AJ-protein expression in HK2-cells. To assess the effect of Ketamine on expression of key AJ proteins, HK2 cells were cultured in 5 mM glucose containing media for 48 hrs prior to overnight serum starvation. Cells were stimulated for 24 hrs with Ketamine (0.1–1 mg/mL) under serum-free conditions and morphological and phenotypic changes assessed. Phase contrast microscopy (panel A) and TRITC conjugated phalloidin (panel B) confirmed the dose dependent effects of Ketamine on cell morphology and cytoskeletal reorganization respectively. Whole cell expression of E-cadherin and its transcriptional co-repressor Snail were determined by western blotting. Ketamine decreased expression of E-cadherin (panel C) Snail (panel F) and Slug (panel G). Compartmental localisation of E-cadherin, Snail and Slug expression were determined for membrane (M), cytosol (C), nuclear (N) and cytoskeletal (CK) fractions +/− Ketamine (1 mg/mL). Ketamine altered the cellular localization of all three proteins, compared to control (panels Hi, Hiv and Hv respectively). Ketamine also down-regulated expression of N-cadherin (panel D) and β-catenin (panel E), with a loss in expression being apparent throughout the cell (panel Hii and Hiii respectively). Upper panels show representative blots for each protein and re-probed for α-tubulin as a loading control. Lower panels show mean (±SEM) densitometry data, normalised against the non-stimulated low glucose control (100%), from 3 or more separate experiments. Each lane in the representative blot corresponds to the associated bar in the graph. Key significances are shown, *$P<0.05$, *$P<0.01$, ***$P<0.001$.
doi:10.1371/journal.pone.0071819.g002

Previously implicated in the differentiation of epithelial cells into fibroblast, e.g. mesenchymal cells (epithelial-mesenchymal transitions), following down regulation of expression of the adhesion protein E-cadherin [16–18] we next examined the effect of Ketamine on whole cell and cell-compartment expression of the transcriptional repressors Snail (Fig. 2F) and Slug (Fig. 2G). Data suggests that Ketamine down-regulated whole cell expression of Snail by 36±13% ($P<0.05$), 51±6% ($P<0.01$) and 61±4%

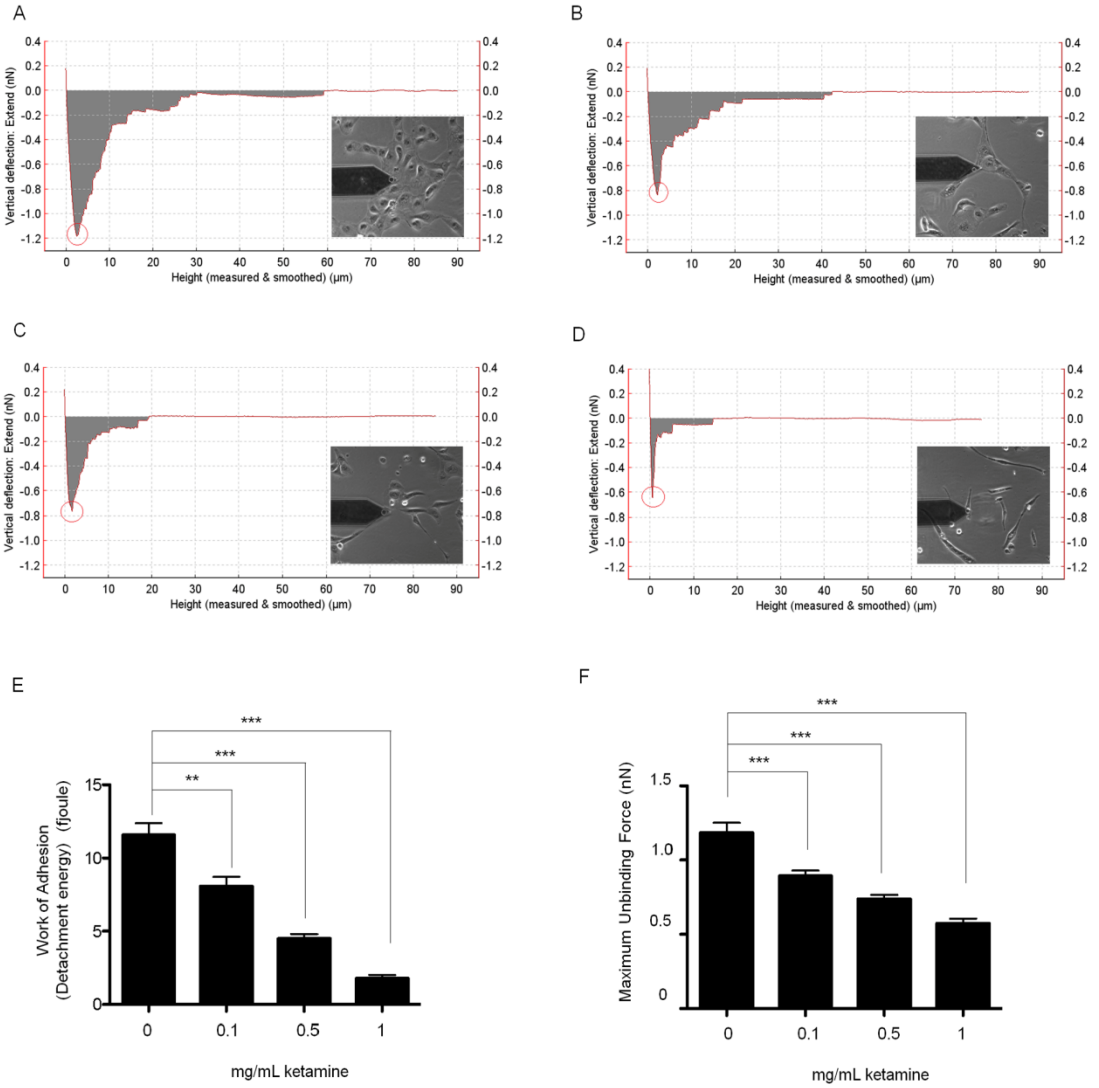

Figure 6. ***Ketamine reduces cell adhesion.*** AFM-single-cell force spectroscopy was used to measure the detachment energy (fJoules) and maximum unbinding force (nN) required to uncouple two HK2 cells. The energy required to separate the cells; grey area in panel A (control cells), panel B (0.1 mg/mL Ketamine treated cells), panel C (0.5 mg/mL Ketamine treated cells), and panel D (1 mg/mL Ketamine treated cells), and maximum force of detachment (red circle) was measured. The former is known as the "detachment energy" (panel E) and the later is "maximum unbinding force" (panel F). Ketamine decreased the maximum unbinding force and the work of adhesion in a dose dependent manner compared to control. Data is expressed as mean ± SEM. of multiple cells from 4 separate experiments, where key significances are shown, **** $P<0.0001$.
doi:10.1371/journal.pone.0071819.g006

EMT [18–19] and favouring the up-regulation of neural (N)-cadherin to replace the loss in E-cadherin, did not occur. These data suggest that the effects of Ketamine are cytotoxic, and not mediated through classic, canonical pathways usually associated with renal fibrosis.

TGF- β1 is a pro-fibrotic cytokine known to play an important role in the pathogenesis of disease-induced renal fibrosis, e.g. diabetic nephropathy [27]. Having previously shown that TGF-β1 instigates a loss in E-cadherin expression in HK2-cells, we investigated if Ketamine directly altered TGF- β1 secretion [18]. Ketamine (1 mg/mL) reduced TGF- β1 secretion to 80% of control. In renal fibrosis, TGF- β1 binds to a trans-membrane TBRII receptor and initiates several intracellular signalling cascades, including the small mothers against decapentaplegic (SMADs) and mitogen activated protein kinases (MAPK), such as extracellular regulated kinase (ERK), p38 and Jun Kinase [22]. The majority of TGF- β1 targeted genes regulated in fibrosis rely on Smad3-dependent transcriptional regulation (Brown *et al.* 2007). In the current study, Ketamine not only decreased TGF-β1 secretion but also down-regulated p-Smad2 and p-Smad3 expression at 24 hours. The failure of Ketamine to stimulate canonical TGF- β1 signalling suggests that an alternative

mechanism must mediate Ketamine-evoked effects. Co-incubation of Ketamine with inhibitors of PI3-K, p38 MAPK and ERK confirmed a partial role for all three in regulating our candidate proteins. There was a counter-intuitive relationship observed between E-cadherin and Snail in response to Ketamine treatment in the presence of the PI3-K inhibitor wortmannin. Blockade of PI3-K signalling further reduced the expression of E-cadherin, an effect most likely to reflect the dramatic up-regulation Snail under the same conditions. This suggests that Ketamine down-regulates Snail expression in a PI3-K dependent manner and that blockade of this pathway restores the reciprocal relationship between E-cadherin and its transcriptional repressor. Inhibition of p38MAPK partially restored E-cadherin expression to those of control, an effect that may, in part, be responsible for the restoration of cell morphology observed with SB203580. Co-incubation of Ketamine with wortmannin failed to negate the inhibitory effects of Ketamine on Slug, whilst the ERK inhibitor, PD98059, restored expression to approximately 50% of control, indicating a downstream involvement ERK in regulating Slug. Whilst it was evident that PI3-K and ERK have a role in regulating E-cadherin, Snail and Slug, elucidating the pathway controlling N-cadherin and β-catenin expression was not clear. Ketamine reduced the expression of both these proteins and the effect could not be restored by pharmacological inhibition.

To determine how a loss in adherens junction proteins functionally affected cell-cell adhesion, we used AFM-SCFS. The AFM-single-cell force spectroscopy used in this study has a displacement actuator of longer travelling distance (up to 100 μm) which provides an excellent capability for measuring the complete force-displacement curve of cell detachment and is essential when studying large cells such as those as found in renal tubule epithelia. Retraction force-displacement curves allow us to determine the force and energy required to uncouple cells. The former is normally referred to as "adhesion force" and the latter the "detachment energy", which can be calculated from the integration of the separation force-displacement curves, i.e. the grey area under the curve in Fig. 6A–D. Retraction force-displacement curves confirmed that 1 mg/mL Ketamine reduced the maximum unbinding force required to begin separation of two cells by 58%, whilst reducing the detachment energy required to completely separate them by 86%. The greater decrease in the detachment energy could be partly explained due to the increase in cell rigidity following Ketamine treatment, as demonstrated by re-arrangement of the cytoskeleton into peripheral stress fibres. These data suggest that it is the loss in E-cadherin expression and dissolution of the catenin/cadherin complex, which drives the detachment of cells in response to Ketamine.

In the current study, we report on Ketamine-evoked cytotoxic damage to epithelial cells of the proximal tubule. The acute effects of Ketamine are associated with early functional changes in the adherens junction complex. This loss in expression of proteins central to cell-adhesion, promotes functional disassociation of the epithelia, and is the most likely cause of early morphological and phenotypic alterations observed following Ketamine exposure. The reported changes may represent the initial basis for overt renal complications of Ketamine abuse. Whilst our studies provide novel and exciting data on the effects of this recreational drug in the proximal tubule, it is clear that this area of research demands fuller investigation. To reduce the confounding influence of the multifactorial molecular pathology that is likely to underlie Ketamine-induced renal damage within epithelia cells of the proximal tubule, we utilized the well-characterized human HK2 cell line as a minimalistic model. Despite HK2 cells having many advantages to primary tissue, the authors concede that responses are open to modification by the complexities of the *in vivo* situation. Despite this caveat, the current data provides a compelling foundation, identifying likely targets associated with early Ketamine damage, and as such, identifies future candidates for maintaining or restoring renal function in response to and from this toxic substance particularly given the catastrophic tissue damage reported for the bladder. Future work will need to extrapolate these data in to the primary scenario.

Supporting Information

Figure S1 The effect of Inhibitors alone on candidate protein expression in HK2 cells. HK2 cells were cultured in 5 mM glucose containing media for 48 hrs prior to overnight serum starvation. Cells were treated for 24 hrs with Wortmannin (2 μM), PD98059 (10 μM), and SB203580 (1 μM) under serum-free conditions and the expression levels of E-cadherin (panel A), N-cadherin (panel B), β-catenin (panel C), Snail (panel D) and Slug (panel E) determined by immuno-blotting. Upper panels show representative blots for each protein and re-probed for α-tubulin as a loading control. Lower panels show mean (±SEM) densitometry data, normalised against the non-stimulated low glucose control (100%), from 3 or more separate experiments. Each lane in the representative blot corresponds to the associated bar in the graph.
(TIFF)

Author Contributions

Conceived and designed the experiments: CEH PES. Performed the experiments: CEH TJ ES PES. Analyzed the data: CEH TJ PES. Contributed reagents/materials/analysis tools: CEH PES. Wrote the paper: CEH PES. Reviewed and edited the manuscript: IKKL KPJ.

References

1. Wright M (1982) Pharmacologic effects of ketamine and its use in veterinary medicine. J Am Vet Med Assoc. 180: 1462 71.
2. Wood D, Cottrell A, Baker SC, Southgate J, Harris M, et al. (2011) Recreational ketamine: from pleasure to pain. BJU Int. 107: 1881.
3. Morgan CJ, Muetzelfeldt L, Curran HV (2010) Consequences of chronic ketamine self-administration upon neurocognitive function and psychological wellbeing: a 1-year longitudinal study. Addiction. 105: 121 33.
4. Tsai TH, Cha TL, Lin CM, Tsao CW, Tang SH, et al. (2009) Ketamine-associated bladder dysfunction. Int J Urol. 16, 826 9.
5. Srirangam S, Mercer J (2012) Ketamine bladder syndrome: an important differential diagnosis when assessing a patient with persistent lower urinary tract symptoms. BMJ Case Rep. doi:pii: bcr2012006447. 10.1136/bcr-2012-006447.
6. Chu PS, Ma WK, Wong SC, Chu RW, Cheng CH, et al. (2008) The destruction of the lower urinary tract by ketamine abuse: a new syndrome? BJU Int 102: 1616 22.
7. Klingberg F, Hinz B, White ES (2013) The myofibroblast matrix: implications for tissue repair and fibrosis. J Pathol. 229: 298 309.
8. Guo S, DiPietro LA (2010) Factors Affecting Wound Healing. J Dent Res 89: 219 229.
9. Zeisberg M, Kalluri R (2004) The role of epithelial-to-mesenchymal transition in renal fibrosis. J Mol Med. 82: 175 181.
10. Moreno AP, Berthoud VM, Pérez-Palacios G, Pérez-Armendariz EM (2005) Biophysical evidence that connexin-36 forms functional gap junction channels between pancreatic mouse beta-cells. Am J Physiol Endocrinol Metab 288: E948 56.
11. Kanno Y, Sasaki Y, Shiba Y, Yoshida-Noro C, Takeichi M (1984) Monoclonal antibody ECCD-1 inhibits intercellular communication in teratocarcinoma PCC3 cells. Exp Cell Res. 152: 270 4.
12. Hills CE, Squires PE (2010) TGF-beta1-induced epithelial-to-mesenchymal transition and therapeutic intervention in diabetic nephropathy. Am J Nephrol 31: 68 74.

13. Hills CE, Squires PE (2011) The role of TGF-β and epithelial-to mesenchymal transition in diabetic nephropathy. Cytokine Growth Factor Rev. 22: 131 9.
14. Hills CE, Bland R, Wheelans DC, Bennett J, Ronco PM, et al. (2006) Glucose-evoked alterations in connexin43-mediated cell-to-cell communication in human collecting duct: a possible role in diabetic nephropathy. Am J Physiol Renal Physiol 291: F1045 51.
15. Hills CE, Bland R, Bennett J, Ronco PM, Squires PE (2009) TGF-beta1 mediates glucose-evoked up-regulation of connexin-43 cell-to-cell communication in HCD-cells. Cell Physiol Biochem 24: 177 86.
16. Hills CE, Al-Rasheed N, Al-Rasheed N, Willars GB, Brunskill NJ (2009) C-peptide reverses TGF-beta-1 induced changes in renal proximal tubular cells: implications for treatment of DN. Am J Physiol 296: F614 621.
17. Hills CE, Willars GB, Brunskill NJ (2010) Proinsulin C-peptide antagonizes the profibrotic effects of TGF-beta1 via up-regulation of retinoic acid and HGF-related signaling pathways. Mol Endocrinol 24: 822 31.
18. Hills CE, Siamantouras E, Smith SW, Cockwell P, Liu KK, et al. (2012) TGFβ modulates cell-to-cell communication in early epithelial-to-mesenchymal transition. Diabetologia. 55: 812 24.
19. Maeda M, Johnson K, Wheelock MJ (2005) Cadherin switching: essential for behavioural but not morphological changes during an epithelium-to-mesenchyme transition. Journal of cell Science 118: 873 887.
20. Eddy AA (1996) Molecular insights into renal interstitial fibrosis. J Am Soc Nephrol 12: 2495 2508.
21. Remuzzi G, Ruggenenti P, Benigni A (1997) Understanding the nature of renal disease progression. Kidney Int. 51: 2 15.
22. Brown KA, Pietenpol JA, Moses HL (2007) A tale of two proteins: differential roles and regulation of Smad2 and Smad3 in TGF-beta signaling. J Cell Biochem 101 9 33.
23. Hills CE, Younis MY, Bennett J, Siamantouras E, Liu K, et al. (2012) Calcium-sensing receptor activation increases cell-cell adhesion and β-cell function. Cell Physiol Biochem. 30: 575 86.
24. Selby NM (2008) Obstructive nephropathy and kidney injury associated with ketamine abuse. Clinical kidney journal. 5: 310 312.
25. Farris AB, Colvin RB (2012) Renal interstitial fibrosis: mechanisms and evaluation. Curr Opin Nephrol Hypertens 21: 289 300.
26. Kalluri R, Weinberg RA (2009) The basics of epithelial-mesenchymal transition. J Clin Invest. 119: 1420 1428.
27. Sharma K, Ziyadeh FN (1995) Hyperglycaemia and diabetic kidney disease. The case for transforming growth factor-beta as a key mediator. Diabetes 44: 1139 1146.
28. Masszi A, Fan L, Rosivall L, McCulloch CA, Rotstein OD, et al. (2004) Integrity of cell-cell contacts is a critical regulator of TGF-beta 1-induced epithelial-to-myofibroblast transition: role for beta-catenin. Am J Patho. 165: 1955 1967.
29. Angres B, Barth A, Nelson WJ (1996) Mechanism for transition from initial to stable cell-cell adhesion: kinetic analysis of E-cadherin-mediated adhesion using a quantitative adhesion assay. J Cell Biol 134: 549 57.
30. Ivanov AI (2008) Actin motors that drive formation and disassembly of epithelial apical junctions. Front Biosci. 13: 6662 81.